An evidential reasoning geospatial approach to transport corridor susceptibility zonation.

Obrike Stephen Ewomazino

BSc Geology

MSc Environment and Engineering Geology

Thesis submitted for the Degree of Doctor of Philosophy

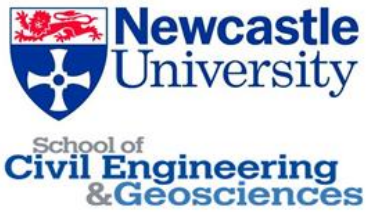

School of Civil Engineering and Geosciences

Newcastle University

October 2015

Abstract

Given the increased hazards faced by transport corridors such as climate induced extreme weather, it is essential that local spatial hot-spots of potential landslide susceptibility can be recognised. Traditionally, geotechnical survey and monitoring approaches have been used to recognise spatially landslide susceptibility zones. The increased availability of affordable very high resolution remotely-sensed datasets, such as airborne laser scanning (ALS) and multispectral aerial imagery, along with improved geospatial digital map data-sets, potentially allows the automated recognition of vulnerable earthwork slopes. However, the challenge remains to develop the analytical framework that allows such data to be integrated in an objective manner to recognise slopes potentially susceptible to failure.

In this research, an evidential reasoning multi-source geospatial integration approach for the broad-scale recognition and prediction of landslide susceptibility in transport corridors has been developed. Airborne laser scanning and Ordnance Survey DTM data is used to derive slope stability parameters (slope gradient, aspect, terrain wetness index (TWI), stream power index (SPI) and curvature), while Compact Airborne Spectrographic Imager (CASI) imagery, and existing national scale digital map data-sets are used to characterise the spatial variability of land cover, land use and soil type. A novel approach to characterisation of soil moisture distribution within transport corridors is developed that incorporates the effects of the catchment contribution to local zones of moisture concentration in earthworks. In this approach, the land cover and soil type of the wider catchment are used to estimate the spatial contribution of precipitation contributing to surface runoff, which in turn is used to parameterise a weighted terrain accumulation flow model. The derived topographic and land use properties of the transport corridor are integrated within the evidential reasoning approach to characterise numeric measures of belief, disbelief and uncertainty regarding slope instability spatially within the transport corridor. Evidential reasoning was employed as it offers the ability to derive an objective weighting of the relative importance of each derived property to the final estimation of landslide susceptibility, whilst allowing the uncertainty of the properties to be taken into account.

The developed framework was applied to railway transport earthworks located near Haltwhistle in northern England, UK. This section of the Carlisle-Newcastle rail line has a

history of instability with the occurrence of numerous minor landslides in recent years. Results on spatial distribution of soil moisture indicate considerable contribution of the surrounding wider catchment topography to the localised zones of moisture accumulation. The degrees of belief and disbelief indicated the importance of slope with gradients between 25^0 to 35^0 and concave curvature. Permeable soils with variable intercalations accounted for over 80% of slope instability with 5.1% of the earthwork cuttings identified as relatively unstable in contrast to 47.5% for the earthwork embankment. The developed approach was found to have a goodness of fit of 88.5% with respect to the failed slopes used to parametrise the evidential reasoning model and an overall predictive capability of 77.75% based on independent validation dataset.

Acknowledgment

First and foremost I wish to my express my profound thanks to my supervisors Stuart Barr and Pauline Miller for their guidance and support throughout the PhD programme. Your invaluable advice and encouragement throughout the PhD programme will always be cherished. Additional thanks goes to Stuart Barr my first supervisor who had been more than a supervisor and more of an academic mentor to me during the programme.

My sincere thanks also go to Clare Brint of Network Rail for providing access to Network Rail database and maintenance register and Martin Robertson for his assistance during the field work to Haltwhistle.

I wish to acknowledge the TETFUND Nigeria, Nasarawa State University and my family members for their financial support towards the completion of the PhD programme.

Acknowledgement is also given to Melissa Ware the academic support officer post graduate research, my PhD colleagues with whom I shared office and jokes and the entire team of the School of Civil Engineering and Geosciences.

I also wish to acknowledge the support of the members of my church, the Deeper Life Bible Church, Newcastle, for their prayers and encouragement.

Finally, I want to thank God for being gracious to me, for His gift of life, friends and the opportunity to meet with wonderful people during the course of my doctorate research. My love and thanks remains with my wife Chi and sons Ejiro and Kome to whom this work is dedicated.

Table of Contents

List of figures

List of tables

List of abbreviations and notations

AHP	Analytical hierarchy process
ALS	Airborne laser scanning
ANN	Analytical Neural Networks
AUC	Area Under the Curve
CASI	Compact Airborne Spectrographic Imaging
CFD	Cumulative Frequency Distribution
DEM	Digital Elevation Model
DTM	Digital Terrain Model
EBF	Evidential Belief Function
FOS	Factor of Safety
GIS	Geographical Information System
GNSS	Global Navigation Satellite Systems
GPS	Global Positioning System
HOST	Hydrology of Soil Types
IDW	Inverse Distance Weighted
LCM	Land use land cover map
Lidar	LIght Detection And Ranging
ln	Natural logarithm
MNF	Minimum Noise Fraction
NATMAP	National Soil Map
NDVI	Normalised Difference Vegetation Index
OWA	ordered weighted average
PCA	Principal Components Analysis
RADAR	RAdio Detection And Ranging
REP	Red Edge Position
RMSE	Root Mean Square Error
RTK	Real Time Kinematic
SAR	Synthetic Aperture Radar
SCA	Specific Catchment Area
SCS-CN	Soil Conservation Service-curve number
SPI	Stream Power Index

SPR	Standard Percentage Runoff
SSHI	Soil Slope Hazard Index
TWI	Topographic Wetness Index
USDA	United State Department of Agriculture
WLC	weighted linear combination

1 Introduction

1.1 Landslide incidence

Landslides occurrence is a natural phenomenon that gives rise to a wide variety of ground movement with gravity serving as its primary driving force (Lee and Jones, 2004). Slopes are considered stable when the shear resistance (forces available to resist movement) is greater than the normal stress (forces driving movement). Subsequently, landslide occurrences are restricted to areas where the natural equilibrium of existing slopes had experienced a change in their stability status from stable to unstable conditions (Baum *et al.*, 2005; Nichol *et al.*, 2006). Landslides or slope failures are usually a culminated effect of pre-conditioning factors that are either natural, such as groundwater variation, erosional activities, pore-water saturation (resulting from snowmelt and heavy rainfall), tremors from earthquakes and volcanic eruptions or as a result of human activities like deforestation, mining, traffic vibrations and earthworks, on existing slopes. These pre-conditioning factors build-up specific sub-surface conditions that make existing slopes prone to failure, with resulting landslide or failure occurrences often requiring a trigger before actual landslide incidence (Baum *et al.*, 2005; Lee and Pradhan, 2006).

Shallow landslides occur where the failure planes occur typically at a depth from a few centimeters to several meters within overlying weathered bedrock. This form of slope failure is often associated with slopes made up of materials of high permeability with intercalations of impervious finer materials at variable depths of the soil profile (Baum *et al.*, 2005; Bovolo and Bathurst, 2012). These intercalations allow for buildup of pore water pressures sufficient to reduce effective normal stress to a critical level and ultimately with the aid of a trigger induce failure along sliding surfaces, commonly witnessed as block glides, debris slides, debris flow or failures of road cut-slopes (Baum *et al.*, 2005). Deep seated landslides in contrast, are large slope failures associated with translational, rotational, or complex movement (Van Den Eeckhaut *et al.*, 2005). The deep seated variety typically move slowly (only several meters per year) and form along a plane of weakness such as a fault or bedding plane (Crozier *et al.*, 1995). A number of landslides may be spontaneous, fast paced and highly destructive in nature (Chen *et al.*, 2006), but the vast majority (e.g. landslide occurrences with transport corridor environment) are made up of much smaller masses,

slower displacement and considerably lower impact (Hungr *et al.*, 1999; Perry *et al.*, 2003a; Manning *et al.*, 2008; Miller *et al.*, 2012). Regardless, hazard and risk assessment of landslides has become a leading research area and subject of discussion amongst researchers, policy makers and administrators (Yesilnacar and Süzen, 2006).

1.2 Slope instability in transport corridors

Transport networks such as roads and railways are generally built along linear tracts of land commonly referred to as transport corridors (Priemus and Zonneveld, 2003). These corridors are of enormous economic importance and facilitate the movement of personnel, goods and services across regions. As such, the safety and reliability of existing transport networks are considered critically important (Perry *et al.*, 2003b; Priemus and Zonneveld, 2003). Transport corridors are by nature characterised at various sections along the network route by the existence of earthworks such as man-made soil embankment and cuttings along natural slopes. These earthworks are essential components of most rail and road networks, as the effective operation of both networks relies on the stability of the earthworks on which they are founded. Hence, slope stability and prolonged existence of earthworks are important considerations in constructing and maintaining an effective transport infrastructure (Ridley *et al.*, 2004). The presence of subsidence, flows, spreads and slides along slope margins are not uncommon along transport corridor routes (Perry *et al.*, 2003a; Jaiswal *et al.*, 2010a). Factors responsible for slope and earthwork instability, most of which are related to morphometry, geology, soil type, hydrology, geomorphology and land use (Van Westen *et al.*, 2008; Jaiswal and van Westen, 2013) are numerous and vary spatially. Moisture accumulation as result of excessive precipitation is thought to be the most frequent cause of landslide occurrences across the world (Jaiswal and van Westen, 2009).

Typically, slope instability is a common problem associated with regions known to experience seasonal heavy or prolonged rainfall such as the sub-tropics (Jaiswal *et al.*, 2010b). However recent global changes in climatic conditions, characterised by extreme weather such as high rainfall events (Ekström *et al.*, 2005) and longer winter months (Briggs *et al.*, 2013) are expected to impact negatively on the performance of existing slopes and embankments along most transport corridors (Ridley *et al.*, 2004; Briggs *et al.*, 2013). Regions where slopes were thought to be relatively stable have in recent times, as a result of increase in moisture content, been characterised by periodic occurrence of slope instability

(Clarke and Smethurst, 2010; Miller *et al.*, 2012). Relatively stable slopes in response to factors like gradual build-up of pore pressure (Smethurst *et al.*, 2006), increased permeability due to root activities (Greenwood *et al.*, 2004) and external loading are known to gradually transform into a marginally stable state (Greenwood *et al.*, 2004; Glendinning *et al.*, 2009). At this point the existence of any dynamic triggering factor exceeding certain thresholds is known to produce continuous or intermittent movements in slopes (Terlien, 1998; Berardi *et al.*, 2005). This effect is particularly pronounced in corridors with aging infrastructure sometimes characterised by obsolete engineering designs and loss of performance in existing structural supports within cuttings and on embankment (Perry *et al.*, 2003a; Perry *et al.*, 2003b). Rainfall duration and intensity are particularly important contributing factors to slope failure irrespective of climate regimes and soil types (Anderson and Kneale, 1980; Borga *et al.*, 2002; Manning *et al.*, 2008; Clarke and Smethurst, 2010).

Increased moisture concentration along sections of a transport corridor results in a gradual build-up of pore water saturation, reduction in inter-granular friction and ultimately leads to slope instability. Moisture accumulation is believed to be directly or indirectly responsible for most slope failure recorded within the transport corridor environments (Jaiswal and van Westen, 2009; Jaiswal and van Westen, 2012). Ekström *et al.* (2005) suggest an increase in the rainfall intensities as a result of climate change is expected to increase moisture content in aging transport corridors earthworks which in turn may result in a reduction in the strength of the slope materials and increased incidence of slope instability.

Equally important to slope stability is the underlying geology and the existence and extent of structural discontinuities;- faults and joints (Ayalew and Yamagishi, 2005). Soil properties such as particle size, classification and index limits, density, permeability and shear strength are known to exert great influence on slope stability. Failures are mostly localised to slopes made up of loosely cemented permeable materials with intercalations of fine grained layers, with the accompanying failure planes for most of these slides commonly situated along impervious layers that serve as temporary barriers to percolating moisture resulting in an increase in localised pore pressure (Baum *et al.*, 2005). Vegetation cover has been used to reinforce slopes (Greenwood *et al.*, 2004), with planting of trees along slope cuttings for reinforcement being a common occurrence along transport corridors (Glendinning *et al.*, 2009). Trees and shrubs are known help reduce soil moisture content through transpiration,

provide a measure of soil cohesion as a result of mechanical reinforcement by their roots and reduce the impact of interception and overland flow during rain storms (Smethurst *et al.*, 2006). Species mix, spacing of trees, age and health of vegetation have been reported as influential to the slope hydrological conductions, soil formation and cohesion due to root anchoring (Yesilnacar and Süzen, 2006; Miller, 2011).

However, a complex relationship exists between soil properties, soil horizon development, soil compaction and vegetation cover (Thompson *et al.*, 2010). Changes in land cover and land use activities along transport corridors are sometimes known to adversely impact on stability of surrounding slopes (Mattia *et al.*, 2005; Smethurst *et al.*, 2012). For example, Perry *et al.* (2003b) and Glendinning *et al.* (2009) suggest that root activities of trees and frost action may be responsible for increased permeability recorded in some cuttings and embankments.

1.3 Slope instability in the UK transport corridors

Embankments and cuttings are integral parts of transport infrastructure within the United Kingdom (Lloyd *et al.*, 2001). Many UK cuttings and embankments especially along the rail network were constructed in the mid-19th century on poorly consolidated materials, prior to the introduction of modern engineering practices (Perry *et al.*, 2003a), resulting in frequent failure due to pre-existing shear planes or groundwater movement and associated erosional processes (Perry *et al.*, 2003a; Perry *et al.*, 2003b). Subsequent remediation work often left residual rupture surfaces (Perry *et al.*, 2003b; Ridley *et al.*, 2004) leading to present day movements requiring maintenance (Perry *et al.*, 2003a).

Shallow rotational or translational slope failures have been reported by Lloyd *et al.* (2001) and Perry *et al.* (2003a) as the most common slope instability process encountered along UK transport corridors. Most of these shallow slope failures (landslides) are usually triggered by a buildup of pore water pressure as a result of elevated soil moisture content (Collins and Znidarcic, 2004; Ridley *et al.*, 2004). Other important considerations responsible for shallow slope failures along slope cuttings and embankments may include burrowing animals, embankment age, construction type, change in earth work materials, vandalism, culvert deterioration, slope geometry, slope angle and height, moisture and vegetation shrink-swell cycles (Perry *et al.*, 2003b). Failures tend to be shallow seated especially where there are no changes in the external loading conditions. According to Perry *et al.* (2003b) these failures

often occur as a series of slips along particular lengths of cuttings or embankments, in addition to other surface and near surface movements generated by erosion (by reason of surface runoff), weathering (as a result of frost) and creep (in granular or residual soils). Evaluation of records on slope stability assessment carried out on slope cuttings and embankments along transport corridors in the UK have shown that the probability of the occurrence of shallow failures on embankments are usually three times more likely in comparison with cuttings (Perry *et al.*, 2003b). As a result of the consequences associated with slope instability (landslide occurrences) there is a growing awareness for the requirement to develop proactive measures with respect to mapping zones of slope instability and the development of decision support systems that would assist in the delineation of potential hazard zones and timely follow up maintenance protocols (Sassa, 2014). Lloyd *et al.* (2001) and Perry *et al.* (2003b) are both in agreement that the cost of unplanned reactive repairs far outweighs the cost of proactive and continuous maintenance.

1.4 Slope stability assessment in the UK transport corridor

Currently, slope stability risk assessment involves a programme of regular on-site inspection (Perry *et al.*, 2003b). The routine appraisal of earthwork involves a field survey where an experienced assessor is expected to daily cover 5 km of rail track assessing the stability of earthworks. This is aimed at detecting symptoms of slope instability and prioritizing of individual earthworks with respect to the risk they possess to the operational efficiency of the entire transport network. (Miller *et al.*, 2012). Information recorded includes water ingress, noting vegetation cover types or changes in vegetation, describing drainage types and conditions and identifying areas of potential future instability (Perry *et al.*, 2003b). Earthworks are assigned a slope hazard value using a semi-quantitative approach where multiple parameters, including material composition, drainage conditions, indicators of mass movement, and presence of burrowing activity are scored by the site engineers. Based on this, earthworks are categorised as poor, marginal and serviceable (Manley and Harding, 2003; Crapper *et al.*, 2015). Poor earthworks are re-assessed at least every 2 years, marginal earthworks every 5 years and serviceable earthworks every 10 years (Manley and Harding, 2003).

These comprehensive risk assessments of potential landslide hazard are on completion meant to provide ample information on the probability and/or consequences of landslide

occurrence (Reid and Clark, 2000). This conventional approach though effective, is expensive and time consuming. Perry *et al.* (2003a) and Perry *et al.* (2003b) proposed a systematic application of a structured approach to risk analysis for all transport corridor cuttings and embankments to produce a risk profile (risk register). The assessment procedure was proposed as part of a continuous cycle of inspection, assessment and improvement. The assessment procedure is made up of strategic and tactical levels of risk assessments. The strategic level identifies the cutting and embankment performance requirements and potential hazards (risk objective). In addition, it prioritizes individual earthworks or sections of the transport corridor for further in-depth studies with respect to risk to operational efficiency of the entire corridor (Perry *et al.*, 2003a). The tactical stage of the assessment prioritizes individual earthworks and sections recognised at the strategic level of assessment where detailed assessments with respect to specific risks and mitigation measures are undertaken.

Where instability is detected, geotechnical investigation is performed to obtain information on the surface and subsurface conditions responsible for the distress to earthworks noted during field survey. Geotechnical surveys involve (1) surface exploration which may include geological and geophysical mapping, photogrammetry and the installation of displacement monitoring equipment on earthwork surfaces (Crapper *et al.*, 2015) and (2) some measure of subsurface investigation to determine the physical properties and composition of the underlying soils, strength characteristics of the soils, evidences of subsurface displacement and local hydrology, through strategic placement of instrumented boreholes (Briggs *et al.*, 2013) and/or geotechnical site investigation (Network Rail, 2005) leading to eventual remediation of the slope. In addition deterministic models have been used to evaluate the susceptibility to landslide and slope instability across sections of transport corridors (Clarke and Smethurst, 2010; Miller *et al.*, 2012; Briggs *et al.*, 2013). These process driven models are generally considered suitable for detailed scale modelling of landslide susceptibility assessment (Van Westen *et al.*, 2008). However, their high data demand may pose enormous cost on data acquisition when considered for implementation across the entire transport corridor (Miller *et al.*, 2012). These models require highly accurate physical and hydrological properties of soil, which are known to spatially vary significantly even within very short distances (Van Westen *et al.*, 2008).

1.5 Geomatic analysis in slope stability assessment

The risk based approach to prioritisation of earthworks remediation currently employed in the UK transport corridors involves an onsite assessment of potential sources of slope instability and the allocation of a "propensity to failure" score to earthworks based on field observations (Manley and Harding, 2003). As many as 30 separate parameters covering slope materials, drainage and vegetation conditions as well as indicators of potential failures, are taken into consideration in the derivation of the Soil Slope Hazard Index (SSHI); providing a measure of the propensity of failure associated with individual earthworks (Manley and Harding, 2003; Crapper *et al.*, 2015). However, important considerations such as the contributions of the broader adjoining catchment are not taken into account as computation of the SSHI values is essentially based on assessment of the individual slopes. Potentially geomatic approaches to data capture, analyses and modelling allows a greater spatial coverage of transport corridors to be investigated and the broader upland areas, which are believed to have a considerable contribution to zones of localised saturation within transport corridors (Miller *et al.*, 2012), to be considered.

The application of Geomatics in slope stability assessment of transport corridors in the UK has been primarily for routine appraisal using aerial photographs (Perry *et al.*, 2003b). However, recent advancement in remote sensing techniques and the availability of high spatial resolution digital data is gradually changing its use as a secondary source of information to use for the full characterisation of slope stability (Dai *et al.*, 2002); ranging from susceptibility zonation to post crisis management (Lloyd *et al.*, 2001; Van Westen *et al.*, 2008; Razak *et al.*, 2011; Guzzetti *et al.*, 2012). Geomatics allows for the incorporation of multi- scale, multi- temporal datasets considered as influential to incidence of slope instability and required in recognition of vulnerable earthwork slopes. The scalability and potential coverage of a wider spatial expanse of input thematic data allows for the incorporation of the broader catchment contributions and the use of a series of subset areas of the transport corridor in understanding the complex mechanisms at work in the study area. However, the challenge remains to develop the analytical framework that allows for the integration of multi scale, multi temporal datasets in an objective manner to recognise slopes potentially susceptible to failure within the transport corridor environment.

1.6 Aim and objectives

The aim of this study is to develop a geospatial model for the integration of multi-scale, multi- source Geomatic data for the broad-scale recognition and prediction of the spatial pattern of landslide susceptibility in transport corridors. To achieve this aim the following research objectives are addressed:

1. Based on a critical review on the use of Geomatics in analysis and modelling of slope hazards, develop a conceptual framework for the integration of multi-scale multi-source geospatial data for the current and future evaluation of landslide susceptibility zonation and hazard assessment within transport corridor environments.
2. To develop a terrain-based flow model that addresses the effects of catchment-scale contributions, such as run-off, on the moisture concentration of engineered slopes within transport corridor environments.
3. To develop a multi-source, multi-scale approach that is based on evidential reasoning that incorporates the catchment contributions to a linear stretch of transport corridor earthworks and spatially quantify slope stability within transport corridor environments. In addition, the developed model performance is evaluated for a substantive section of a transport corridor.

1.7 Thesis structure

The aim and objectives of the research stated in Section 1.6 are addressed over the next six chapters. A literature critique of techniques commonly employed in landslide susceptibility zonation with a view to identifying techniques suitable for application in the transport corridor environment is presented in Chapter 2. Chapter 3 provides a detailed description of the study site, the various data sets used in the construction of hydrological and landslide susceptibility models and describes the data pre-processing carried out. Chapter 4 presents the methods employed in the geodatabase development, evaluation of the catchment contribution to zones of soil moisture accumulation within the transport corridor and the development of the final integrated landslide susceptibility model. Chapter 5 presents the modelling results for the various stages of the research. The modelling results are analysed and discussed in Chapter 6 with particular emphasis on how they fit into the existing body of

knowledge and their contributions to the research field. Chapter 7 summarises the key findings in the research and also suggest directions for further studies in the future.

1.8 Summary

Moisture accumulation as a result of excessive precipitation is attributed to be the most frequent cause of landslide occurrences. In the UK, the trigger for most of the shallow landslides occurrence along transport corridor slopes is mostly weather related and confined to periods of wet weather particularly during the leaf-off wet winter months when the rate of transpiration is at its minimum and the effect of pore water pressure is at its peak. Across the UK, increase in the rainfall intensities as a result of climate change is expected. The increased moisture content experienced by aging earthworks across transport corridors may result in reduction in the strength of the slope make up materials, poor embankment and cutting performance and increased incidence of slope instability. Conditional appraisal of transport corridor earthworks is currently limited to (1) a programme of regular on-site inspection that considers multiple parameters including, material composition, drainage conditions, indicators of mass movement, and presence of burrowing activity through which earthworks are assigned a slope hazard value using a semi-quantitative approach. (2) Geotechnical investigation in locations where instability is detected. Both techniques are effective but expensive and laborious. The results are site specific and are not easily interpolated to adjoining locations. However, the application of Geomatics to susceptibility assessment allows for the incorporation of multi scale multi temporal dataset in diagnosis of vulnerable earthwork slopes and the incorporation of the broader catchment contributions.

2 Literature review

2.1 Introduction

This chapter presents a review of the key concepts of landslide susceptibility assessment and landslide susceptibility modelling with particular reference to their applicability within transport corridors. A review of landslide failure mechanisms is presented in Section 2.2. The concepts of landslide analysis and susceptibility zonation are discussed in Section 2.3. Section 2.4 highlights the spatial data requirements for landslide susceptibility assessment and methods of acquisition. Finally, Section 2.5 provides a critique of landslide modelling approaches and the considerations that govern the selection of an appropriate modelling approach.

2.2 Landslide processes

Landslides are geomorphological processes that are invariably linked to the terrain, soil characteristics, geological structures, hydrological, climatic and vegetation conditions inherent to the localities where they occur (Glade and Crozier, 2006). Landslide incidence as a physical system develops through several stages in time (Leroueil *et al.*, 2012) with its occurrences comprised of a history of pre-failure deformations, the actual failure itself and post-failure displacements (Lee and Jones, 2004). As a system, landslides exhibit a number of movement episodes separated by variable periods of inactivity (Lee and Jones, 2004) and the term failure is used to describe the development of a rupture surface (Leroueil *et al.*, 2012; Hungr *et al.*, 2014).

2.2.1 Concepts of slope stability

The principles of soil mechanics (Barnes, 2010), rock mechanics (Jaeger *et al.*, 2009) and grain flow mechanics (Takahashi, 2007) provide a framework for understanding the processes at work leading to landslide incidence in hillslopes. Slope stability is a function of the stresses acting on the slope materials and their internal strength (Iverson, 2005). A margin of stability is established as long as the internal strength of the slope material are greater than the external stresses acting on the slope (Lee and Jones, 2004). Introduction of additional external stress diminishes the existing slope equilibrium and at failure, the magnitude of shear stress (driving force) acting on the slope surpasses the total shear strength (resisting force) of the slope material (Iverson, 2000).

The assessment of shear parameters and stress-strain behaviour of geological materials are mostly derived from analysis of acquired field samples and modelling results are largely experimental, owing the technical difficulties associated with studying the process in nature (Iverson, 2005; Zhao and Zhang, 2014; Zhou *et al.*, 2014). Iverson and Reid (1992) demonstrated that increase in pore water pressure can affect shear stresses as well as normal stresses. Implemented in a two dimensional steady state poro-elastic model, the groundwater flow and effective stress fields were computed for a homogeneous hillslope. Results from the study show that saturation as a result of infiltration and groundwater flow significantly increases the Coulomb failure potential (factor of safety) in most parts of the hillslope with the locus of greatest failure potential toward the slope toe (Iverson and Reid, 1992).

However, natural hillslopes are rarely homogeneous, as some geological or pedological stratification is present in either or both the soil and underlying bedrock. Increased moisture content affects the mechanical behaviour of different soils differently (Savage and Baum, 2005). Using a layered system, Moore and Iverson (2002) demonstrated that the hydraulic properties of soil exert a greater influence on the distribution of the failure potential and the rate at which failure proceeds. The authors showed that failure in densely compacted soils tend to proceed incrementally with expansion of pore spaces accompanied by reduction in pore pressure, while loosely compacted soils were characterised by a reduction in pore spaces leading to an immediate increase in pore pressure value and eventual loss in soil strength. Follow up studies by Iverson (2005) and Cho (2014) revealed that these characteristic responses influence the spatial distribution of pore pressure on a prospective slip surface.

The presence of structural discontinuities in the form of bedding planes, schistosity, foliation, joints, cleavage, fracture, fissure, crack or fault plane can significantly influence the behaviour of slopes especially in rocky terrains (Fischer *et al.*, 2010). The orientation, roughness, persistence and nature of infilling materials can alter the strength characteristic of the soil or rock mass (Fischer *et al.*, 2010). The presence of vegetation cover on slopes may induce apparent cohesion due to the strength of interpenetrating roots of plants, inhibiting the soils natural propensity to fail or flow. The influence of vegetation cover on slope hydrology and stability is a complex interaction that is not linear in nature (Abramson, 2002). Phillips (2003) identified geomorphological processes like landslide as nonlinear in

nature, with responses to external stresses on a hillslope not proportional across the entire slope face as a result of variation in thresholds due to mineralogy and mechanical properties of soil types and storage effects such as antecedent moisture conditions. Other sources of non-linearity include multiple modes of adjustment to changes in boundary conditions as a result of multiple variables responsible for the maintenance of slope stability equilibrium and self-organisation which refers to the tendency of formation of failure patterns linked to the internal dynamics at work in the hillslope (Phillips, 2003). Nonetheless, despite the complexity associated with landslide incidence, the vast majority of the factors responsible for slope instability are identifiable and the overall system is predictable (Huang *et al.*, 2009).

Landslides are therefore as a result of complex interactions between conditioning factors responsible for progressive transformation of the slope from stable to unstable conditions and a triggering factor that initiates the development of a rupture surface, as well as associated non-linear system responses (Crozier and Glade, 2005).

2.3 Landslide investigation

Landslide analysis enables clear identification of the underlying factors responsible for the incidence of instability in slopes, including an estimation of the relative contribution of these factors to the overall process (Baum *et al.*, 2005; Lee and Pradhan, 2006). There are three main aspects to landslide assessment, namely, susceptibility, hazard, and risk (Einstein, 1988; Lee and Pradhan, 2006). Here, a brief mention is given on hazard and risk assessment components of landslide analysis as the review is essentially on landslide susceptibility assessment.

Landslide susceptibility assessment constitutes the initial stage of landslide analysis which often but not always extends into hazard assessment and risk evaluation (Aleotti and Chowdhury, 1999; Yoshimatsu and Abe, 2006; Van Westen *et al.*, 2008; Kanungo *et al.*, 2009). Landslide susceptibility zonation is employed in the prediction of spatial distribution of future landslide locations (Cascini, 2008) and depends on the identification of local conditions responsible for landslide occurrence and an inventory of past landslide locations (Aleotti and Chowdhury, 1999).

Hazard and risk assessments are challenging due many associated complexities. For example, hazard assessment deals with the probability that a landslide of a given magnitude will occur in a given time period at a particular location (Guzzetti *et al.*, 2005). The capacity to predict temporal frequency of occurrence and magnitudes of landslide differentiates landslide hazard assessment from landslide susceptibility which is simply the spatial component of hazard assessment (Guzzetti *et al.*, 2005). The probabilistic component of hazard assessment requires understanding and assessment of many uncertainties, such as the determination of the probability of failure per unit time and the quantification of expected behaviour of the failure in terms of its impact and characteristics (Aleotti and Chowdhury, 1999; Lee and Jones, 2004). These components are to a certain degree difficult to assess especially for first-time failures and in areas such as the transport corridor environment where indicators to the onset of failure are preferably mapped in contrast to actual failures (Aleotti and Chowdhury, 1999; Perry *et al.*, 2003a).

Risk assessment incorporates landslide hazard and vulnerability to estimate the levels of risk and to work out appropriate control measures to reduce risk when the level becomes unacceptable (Lee and Jones, 2004). It is a multi-stage process that essentially combines scientific investigation, expert judgment and human values (Lee and Jones, 2004). Risk is dynamic in nature and as such requires periodic updates in order to account for changes such as changes in land use policy and identification of new zones of instability (Lee and Jones, 2004; Fell *et al.*, 2008). Extensive reviews on landslide hazard and risk assessment have been produced by Dai *et al.* (2002) and Pantelidis (2011).

2.4 Landslide susceptibility assessment

Landslide occurrence is seldom without prior notice, often eventual failures are as a result of inadequate appraisal of indicators that precedes these occurrences. The acquisition of landslide information extends from an initial field survey of the conditional appraisal of landforms (Manley and Harding, 2003) to measurement of surface and subsurface displacement using field based techniques (Yin *et al.*, 2010) or from remotely sensed data (Jones, 2006; Tapete *et al.*, 2012; Drakatos *et al.*, 2013), recordings of weather related triggering factors (Caine, 1980; Crosta, 1998) and landslide susceptibility modelling (Van Westen *et al.*, 2008; Jaboyedoff *et al.*, 2012). Numerous techniques have been developed by various authors for the mapping, monitoring and modelling of landslide activities. Field

surveys enable the detection of evidence of ground movement such presence of tension cracks, leaning of trees on slope with base of each tree bowing outward in the downslope direction, offset of fence lines, slopes characterised by hummocky toe (bulging ground) and exposure of earthwork foundation resulting from soil movement (Perry *et al.*, 2003a; Perry *et al.*, 2003b). Ground movements in some cases are subtle, but can be mapped by experienced site engineers (Crapper *et al.*, 2015). The presence of indicators of potential ground movement necessitates the implementation of landslide monitoring system for periodic or continuous surface or subsurface measurement. With confirmation of slope instability, geotechnical investigation and modelling are generally employed to facilitate detailed scale assessment of slope behaviour (Miller *et al.*, 2012).

2.4.1 Field survey

Field surveys are notable sources of field data utilised in landslide susceptibility assessment. During routine mapping campaigns an assessment of the susceptibility of landforms in the study area is obtained through measurements and visual assessments aimed at identifying the presence of slope instability indicators. The nature, type and size of required data to be acquired during the repeated field campaigns are dependent on the expertise of the investigator and the field condition being investigated (Gustavsson *et al.*, 2006). The surveys help identify potential sources of failure such as zones of surface flow convergence and changes in runoff pattern due to anthropogenic modification in land use and land cover. It also help prioritise locations in need of more detailed assessments and in developing benchmarks against which conditional appraisal of landforms can be monitored (Perry *et al.*, 2003b).

Typically acquired landslide information includes inventory of failed sites, geological, hydrological, vegetation cover, geomorphological, burrowing animal activities and drainage properties. In the transport corridor environments, additional information on history of past interventions in an area is important (Perry *et al.*, 2003b). In the UK, slope hazard scores for considered slope instability causal factors are mapped against each slope using a Trimble hand held computer with inbuilt camera (Crapper *et al.*, 2015). This mode of data acquisition is highly utilised in transport corridor environments where conditional appraisal of individual earthwork is an important consideration to the overall performance integrity

and safety of the transport network. The acquired data is site specific and data size poses a challenge to data storage over time.

2.4.2 Landslide monitoring

Following the initial field survey, evidence of slope instability is usually followed up by some form of surface and subsurface monitoring. Instrumentation installed in boreholes or attached to slope surface are commonly employed to check for stability or determine the rate of ground movement along suspected or actual slip surfaces in vulnerable slopes (Perry *et al.*, 2003a). Extensometers and crack gages or telltales are used in monitoring surface displacement on earthwork cuttings (Crapper *et al.*, 2015). The instruments estimate movement normal to the slope face by measuring the separation between two stakes driven on either side of tension cracks. More sophisticated electrical models provide continuous monitoring of surface displacements. Accuracy achieved with extensometers depend on the dimensions of the crack been measured which typically is within the sub-cm range (Abramson, 2002). The approach is simple, easy to monitor and provides information on the magnitude and direction of ground movement but require protection from adverse weather conditions and burrowing animals (Crapper *et al.*, 2015). A notable setback with the use of extensometers is that as displacement progresses additional cracks potentially weaken the surrounding areas (Abramson, 2002). The driven stakes become slack introducing some measure of error into the displacement measurements.

Measurements obtained using precise surveying techniques like standard theodolite geodetic measurement (Conte and Coffman, 2013) and Global Positioning System (Mills *et al.*, 2005; Zhang *et al.*, 2008) for fixed monitoring points on slope surface are less perturbed by the ground movement. The use of total station theodolites for monitoring surface displacement requires pre-determined ground control points and repeated measurements provide a means of evaluation of the absolute movement of these points over time (Abramson, 2002). The use of theodolites in evaluating possible ground movement is both costly and tedious. Mills *et al.* (2005) showed that Global Positioning System present precision accuracy in the range of millimetres to centimetres. However, successful implementation of this technique is dependent on satellite visibility which is greatly compromised in forested areas, and narrow valleys.

Subsurface monitoring can be achieved through pitting, trenching and instrumentation installed into boreholes. Pits and trenches allow for the acquisition of undisturbed samples for geotechnical laboratory analysis and better visual assessment of the shear surfaces. Pits and trenches are usually restricted to shallow landslides (Chaplow, 1983). The use of strategically placed instrumented boreholes is preferred over pits and trenches in transport corridors owing to its lesser impact on surrounding areas and ability to probe deeper depths (Perry *et al.*, 2003a). Inclinometers installed in boreholes are used to monitor and measure subsurface movement. High precision probes provide subsurface displacement readings at regular distance down the hole (Abramson, 2002). Repeated measurements provide information on inclination changes that may have occurred, enabling the monitoring of very slow displacement movement due to slope instability (Borgatti *et al.*, 2006). Installed inclinometer tubes are fragile and prone to breakages with significant ground movement (Perry *et al.*, 2003a), making them ideal indicators for shearing processes in rapid paced landslides.

Information on subsurface hydrological conditions of the slope is usually obtained in the field with the aid of hydrological sensors installed in boreholes (Ridley *et al.*, 2004) of which piezometers are probably the most commonly used. Piezometers measure fluid pressure in saturated soils and in addition, information on the water table elevation within the soil. Seasonal groundwater fluctuation can be monitored from piezometer readings. Analysis of data obtained from strategically positioned piezometers allows for a comprehensive understanding of the overall pattern of groundwater movement (Wu *et al.*, 2008a). Data on groundwater conditions obtained from piezometers are important inputs in most process based modelling of slope instability assessments (Ridley *et al.*, 2004; Smethurst *et al.*, 2006; Briggs *et al.*, 2013).

In situ testing within boreholes allows for down-hole and across-hole geophysical surveys that provide information on internal soil structure, soil composition and conductivity (De Vita *et al.*, 2006; Carpentier *et al.*, 2012). Pressuremeter tests help determine in situ deformability characteristics of jointed rock mass (Tiwari and Rao, 2006; Sari, 2009) and permeability test (Lacerda, 2004).

2.4.3 Landslide susceptibility modelling

Landslide models are essentially simplified generalizations and approximations of naturally occurring mass movement processes (Favis-Morlock and De Boer, 2003). Landslide models provide a means for analyzing processes responsible for slope stability and the prediction of slope behaviour under certain climatic conditions or scenarios of environmental change. These models can be used for the back-analyses of previously failed slopes, in an evaluation of the effectiveness of geotechnical stabilization measures employed (Barla *et al.*, 2004) and in decision support for land use planning (Leventhal and Kotze, 2008). The choice of the most appropriate modelling approach is often governed by a number of considerations: availability of data, quality and accuracy of data, scale of zoning and required outcomes (Cascini, 2008). Landslide susceptibility zoning is either on a regional (small and medium), local (large) and site-specific (detailed scale) planning basis with outputs usually in the form of landslide susceptibility maps (Table 2.1).

Several published techniques have been proposed for evaluating landslide susceptibility (Hungr *et al.*, 2001; Van Westen *et al.*, 2008). These techniques essentially rank slope instability factors and assign different susceptibility levels (Fell *et al.*, 2008). Landslide susceptibility models are either quantitative and qualitative in nature (Cascini, 2008). Qualitative models are subjective, determine susceptibility heuristically and represent susceptibility levels using descriptive terms (Guzzetti *et al.*, 2005), while quantitative models are data driven and produce numeric estimates based on probabilities of landslide occurrence in a susceptibility zone (Fell *et al.*, 2008). On the basis of scale of study susceptibility models can either be regional or local (Crozier and Glade, 2005) and based on the nature of information used in landslide susceptibility assessment, models can be grouped as direct or indirect approaches (Van Westen *et al.*, 2003). Comprehensive reviews on the various methods of landslide susceptibility assessment can be found in Soeters and Van Westen (1996), Carrara *et al.* (1999), Guzzetti *et al.* (1999), Aleotti and Chowdhury (1999), Dai *et al.* (2002), Wang *et al.* (2005), Fell *et al.* (2008), Van Westen *et al.* (2008), and Cascini (2008).

Van Westen *et al.* (2008) categorized the various landslide susceptibility modelling approaches into four groups, namely heuristic, statistical, deterministic and probabilistic, based on the nature of their analytical framework. The classification of susceptibility

methods by various authors is to an extent fuzzy in nature. For example, Aleotti and Chowdhury (1999) and Neaupane and Piantanakulchai (2006) considered Artificial Intelligence and Expert systems as an entirely separate susceptibility modelling approach. Pradhan *et al.* (2010) emphasized soft computing techniques such as neural network analysis or fuzzy logic as modelling techniques usually subsumed into any of the four broad categories susceptibility modelling approaches as highlighted in Van Westen *et al.* (2008). Van Westen *et al.* (2008) categorized the various landslide susceptibility modelling approaches into four groups namely heuristic, statistical, deterministic and probabilistic, based on the nature of their analytical framework. Van Westen *et al.* (2008) classification of landslide susceptibility modeling approaches is widely referenced and is adopted for this review (Figure 2.2). The various methods are discussed in greater details in sections 2.4.4 and 2.4.5.

Table 2.1: Landslide susceptibility zoning showing the various mapping scales and their applications (Fell et al 2008)

Scale description	**Indicative range of scales**	**Examples of zoning application**	**Typical area of zoning**
Small	< 1:100,000	(i) Landslide inventory and susceptibility to inform policy makers and general public	>10,000 km^2 square kilometres
Medium	1:100,000 to 1:25,000	(ii) Landslide inventory and susceptibility zoning for regional development: or very large scale engineering projects. (iii) Preliminary level hazard mapping for local areas	1000-10,000 km^2 square kilometres
Large	1:25,000 to 1:5000	(i) Landslide inventory, susceptibility, hazard zoning for local areas (ii) Intermediate to advanced level hazard zoning for regional development (iii) Preliminary to intermediate level risk zoning for local areas and the advanced stages of planning for large engineering structures, roads and railways	10-1000 km2 square kilometres
Detailed	>1:5000	(i) Intermediate and advanced level hazard and risk zoning for local and site specific areas and for the design phase of large engineering structures, roads and railways	Several hectares to tens of square kilometres

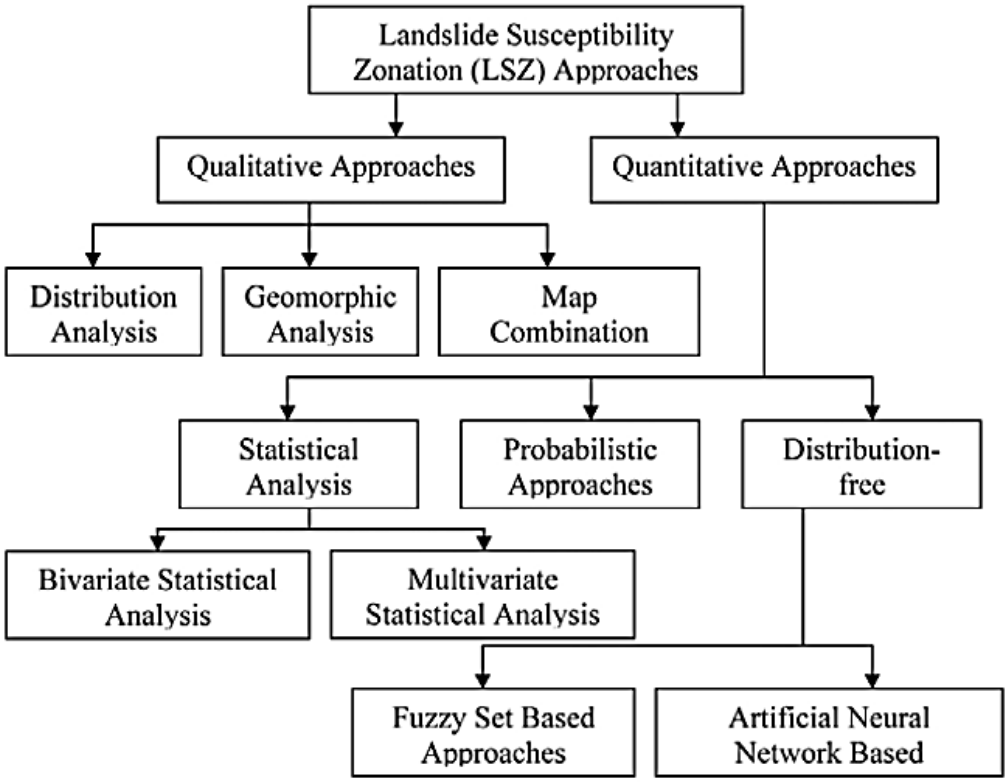

Figure 2.1: Flow chart highlighting the various landslide susceptibility assessment approaches (After van Westen et. al. 2008 and Kanungo et. al. 2009).

2.4.4 Qualitative approaches

Qualitative approaches are based on expert evaluation where field acquired evidence (input data), sometimes supported by remotely sensed (aerial photo or satellite) imagery interpretation are used in carrying out a susceptibility or hazard assessment of an area (Wati *et al.*, 2010). The assessment is based solely on the judgment of the investigator (Kanungo *et al.*, 2009). Analysis of landslide inventory, direct geomorphological mapping and heuristic or index based methods make up the qualitative methods (Kanungo *et al.*, 2009).

2.4.4.1 Analysis of landslide inventory

Landslide incidence leaves discernable features that can be classified and mapped in the field or using remote sensing techniques (Jaboyedoff *et al.*, 2012) such as hummocky terrain surfaces and disruption in land cover pattern (Guzzetti *et al.*, 2012). The determination of the frequency of landslide in an area and the analysis of landslide distribution can provide realistic estimates of landslide probability for a region that has experienced considerable

landslide occurrences (Moreiras, 2004; Chauhan *et al.*, 2010). Information on the state of activity, certainty of identification, dominant type of slope movement, estimated thickness of material involved and date(s) of known landslide activity, have been used to identify the landslide triggers and develop frequency-magnitude relationships (Dai and Lee, 2002; Guzzetti *et al.*, 2005; Jaiswal *et al.*, 2010a). Landslide density maps illustrating the number of landslide events over a region provide reasonable estimates of frequency of failure suitable for landslide susceptibility and hazard mapping (Van Den Eeckhaut *et al.*, 2009).

Cardinali *et al.* (2002) employed multi-temporal landslide map to portray the distribution of existing and past landslides and observed the evolution of new failure sites over a period of about 60 years in Umbria region, Central Italy. Analysing landslide density maps alongside the remedial procedures employed to mitigate local instability problems, the authors were able to infer the possible evolution of slopes, the most probable type of failures, and their expected frequency of occurrence and intensity (Cardinali *et al.*, 2002).

Galli *et al.* (2008) compared landslide inventory maps prepared for different parts of Italy. The study compiled a landslide distribution inventory, geomorphological landslide maps and multi-temporal landslide inventories for the different areas and compared their predictive capabilities. The results of the study revealed that comprehensive landslide inventory map performed better with an overall predictive accuracy of 85.8% as against 73.1% for the geomorphological landslide inventory maps and 72.8% for the reconnaissance landslide inventory map (Galli *et al.*, 2008).

However, there are grave suppositions on the use of inventory analysis solely to investigate the distribution, types and patterns of landslide in relation to morphological and geological characteristics have been raised by a number of authors. These authors considered the approach to be questionable or misleading due to a number of reasons: (1) that landslides are complex phenomena and the dynamics of equilibrium at a site is slightly modified with every landslide occurrence (Guzzetti *et al.*, 1996); (2) The uncertainties and errors with associated landslide inventory and estimates of the probability of spatial occurrence of slope instability based on landslide density do not adequately represent the causal factors responsible for slope instability (Galli *et al.*, 2008); (3) Most importantly, landslide inventory analysis lacks the predictive capability to identify landslide prone areas in locations where landslide is yet to occur (Dai *et al.*, 2002). However, despite these

limitations, the inventory based method is often incorporated into other methods as an important form of input data and are employed in the validation of final susceptibility map (Guzzetti *et al.,* 2012).

2.4.4.2 Direct geomorphological mapping

Geomorphological mapping is a direct qualitative assessment that relies on expert judgment drawn from field experiences and knowledge of similar studies. The approach relies on the assessor's ability to recognize and map actual or potential instability (Aleotti and Chowdhury, 1999; Cascini, 2008; Van Westen *et al.,* 2008). Its subjective nature notwithstanding, the approach has been shown to produce very reliable results when conducted by experienced investigators (Dai *et al.,* 2002).

Geomorphological mapping involves detailed identification of geomorphological features commonly responsible for slope instability where perceived significance is scored or weights are assigned (Crapper *et al.,* 2015). The sum of all assigned weights is used to rank susceptibility (Manley and Harding, 2003). The subjective nature of this approach renders it quite difficult to formalize, as the evaluation of contribution of causal factors on a given location varies with experts (Cardinali *et al.,* 2002). However, the weights assigning process to causal factors can be made less implicit when discussed among experts. For example, a consortium of experts formulated a soil slope hazard index (SSHI) algorithm which is currently used for on-site evaluation of slopes and embankments in the UK (Perry *et al.,* 2003a; Miller *et al.,* 2012). The SSHI algorithm allows for the evaluation of common slope stability parameters alongside factors such as burrowing by rodents which would be difficult to assess using remote sensing techniques (Miller *et al.,* 2009). Geomorphological mapping can be successfully applied to susceptibility assessment and zonation studies of any scale, or adapted to specific local requirements (Aleotti and Chowdhury (1999). The approach is very rigorous, time consuming and tedious in nature. On-site assessment of slope cuttings and embankments is often difficult to implement in steep hilly and heavily vegetated terrains which typify most rural sections of transport corridor routes (Perry *et al.,* 2003a; Perry *et al.,* 2003b).

2.4.4.3 Heuristic zoning

The heuristic zoning approach integrates a priori knowledge, local geomorphological and geotechnical expertise for susceptibility assessment (Wati *et al.*, 2010). The indirect to semi-direct heuristic approach employs spatial information such as digital terrain model (Ruff and Czurda, 2008), land cover maps (Castellanos Abella and Van Westen, 2008)in explaining landslide occurrence (Ives and Messerli, 1981; Rupke *et al.*, 1988; Van Westen *et al.*, 2000; Wati *et al.*, 2010). The heuristic approach is based on the assumption that the relationship between the landslide susceptibility and conditioning variables are known and specified in the models (Dai *et al.*, 2002). Conditioning factors such as topography, hydrology, geology, geotechnical conditions and vegetation cover, as well as land use are determined either by field campaign or remote sensing. The index or parameter maps obtained are classified, ranked and weighted according to their assumed relative influence on slope failure (Glade and Crozier, 2006).

Qualitative weighting under the heuristic approach is highly dependent on the experience of the individual or group of experts responsible for the analysis (Wati *et al.*, 2010). The subjective nature of the approach renders it difficult to reproduce landslide susceptibility maps for the same location by different experts (Soeters and Van Westen, 1996). The approach often requires extensive and lengthy field surveys and employs implicit rather than explicit rules (Aleotti and Chowdhury, 1999; Glade and Crozier, 2006). The subjective nature of the approach adds to the uncertainty of the model (Barredo *et al.*, 2000). However the use of GIS can produce effective combine maps using field survey and remotely sensed data, reducing the level of subjectivity (Ruff and Czurda, 2008). Ruff and Czurda (2008) using index overlay or map combination approach developed a landslide susceptibility map for study area in the Northern Calcareous Alps in Vorarlberg, Austria. Information on geological and geotechnical properties of the study area were obtained from field survey, then digitised in a GIS and developed into data layers. Data layers on geotechnical class, bedding conditions, tectonic layouts, slope angles, slope orientations, vegetation and erosion were converted into grids and spatially analysed alongside a Digital Elevation Model. Bivariate statistics was initially used to establish the relative contributions (rating) of the considered factors to slope instability in the study area. Assignment of weights to causal factors and their categories (e.g. slope classes) were achieved using expert opinion. The weighted thematic (data) layers were integrated in a GIS to generate a landslide

susceptibility map of the study area that descriptively delineation zones of instability. The index overlay approach is simple and highly adaptable as additional data layers can easily be indexed and included in the method. Which is a clear advantage over earlier discussed qualitative methods, nonetheless, the weight assignment process still remains highly subjective.

In general, the simple heuristic approach is considered useful for producing qualitative landslide susceptibility maps for regional scale assessment (Castellanos Abella and Van Westen, 2008). Decision-support tools such as analytical hierarchy process (AHP) (Mezughi *et al.*, 2012) and weighted linear combination (Akgun *et al.*, 2008) models, have been recently integrated into GIS-based heuristic approaches (Castellanos Abella and Van Westen, 2008). This new drive aimed at improving the heuristic framework, had led to (i) the incorporation of quantitative techniques like fuzzy set theory (Gorsevski *et al.*, 2005) and bivariate statistics (Ruff and Czurda, 2008) to standardise landslide predictor variables, (ii) the pairwise comparison techniques (e.g. the analytic hierarchy process-AHP (Mezughi *et al.*, 2012; Kayastha *et al.*, 2013)) and neural networks (Pradhan and Lee, 2010) to produce weights more objectively in relation to the relative importance of the variables and (iii) the use of the weighted linear combination-WLC (Ayalew *et al.*, 2004) and ordered weighted average-OWA (Feizizadeh and Blaschke, 2013) aggregation methods to compute and map landslide susceptibility. Although these methods are considered to be semi-quantitative (Ayalew and Yamagishi, 2005), they have been shown to be effective in medium-scale assessments of landslide susceptibility (Yoshimatsu and Abe, 2006). The augmented heuristic approach is however still limited by the subjective nature of the weighting of the various factors. Ruff and Czurda (2008) identified that the relative importance of factors are often very site specific, and vary with underlying geology, lithology and topography. Therefore, a degree of iterative weight adjustment is often required to describe all of the different environments. However, the most significant limitation is the inability of index overlay to incorporate the complex interactions between the multiple factors that control slope instability into the susceptibility assessment framework (Castellanos Abella and Van Westen, 2008). The heuristic approach is therefore more suitable for regional susceptibility studies, as its subjective nature limits its applicability to detailed scale slope stability assessment.

2.4.5 Quantitative approaches

The quantitative methods (statistical, deterministic and probabilistic) were developed to address the subjective nature of the attribute weighted values normally assigned to the various factors that are assumed to influence slope stability in heuristic studies (Aleotti and Chowdhury, 1999). The quantitative techniques can be considered as more objective due to their data-dependent character. However, the success of these techniques is often affected by the number, quality and reliability of data (Aleotti and Chowdhury, 1999; Van Westen *et al.*, 2008)

2.4.5.1 Statistical approaches

Statistical techniques for modeling landslide susceptibility zonation have been successfully applied at various scales, where conditions responsible for past slope failure are considered as landslide incidence thresholds representing local terrain conditions necessary for landslide occurrences (Santacana *et al.*, 2003; Nandi and Shakoor, 2010; Van Den Eeckhaut *et al.*, 2012). Landslide inventories of past landslides, topographic information and thematic maps on local factors responsible for slope instability are the essential components necessary to statistically model landslide probability in space and time (Vorpahl *et al.*, 2012). The statistical approach compares the spatial distribution of landslides with the various causal factors that are considered influential to slope stability (Nandi and Shakoor, 2010). The approach allows for the validation of the importance of each of the causal factors considered and often employs the use of GIS. As a result of the flexibility of the statistical approach, there are several scientific publications on studies that have successfully explored the combination of fuzzy membership in GIS based landslide hazard mapping (Binaghi *et al.*, 1998; Lee *et al.*, 2002; Van Westen *et al.*, 2003), logistic regression (Dai and Lee, 2003; Santacana *et al.*, 2003) and artificial neural network (ANN) classification (Lee *et al.*, 2003; Pradhan and Lee, 2010). The statistical approach can be broadly divided into bivariate statistical analysis, multivariate methods, and advance machine learning techniques (Van Westen *et al.*, 2008).

In a bivariate statistical analysis, thematic maps for each of the considered landslide causal factor (terrain factors, land cover/land use, soil types/depth, rainfall etc.) is combined with the landslide inventory map, and weight values (based on landslide densities) are calculated for each factor class (e.g. slope class 10^{o}-20^{o}) (Nandi and Shakoor, 2010; Yalcin *et al.*,

2011). Using normalised values (landslide density per factor class in relation to the landslide density over the whole area), a landslide susceptibility map is created by summation of the derived weights for the considered individual parameters (Yalcin, 2008). Several weight computing techniques such as the information value method (Shahabi *et al.*, 2013), weights of evidence (Lee and Choi, 2004), likelihood ratio (Akgun *et al.*, 2008), and Bayesian statistics (Lee *et al.*, 2002) have been implemented in bivariate landslide susceptibility mapping. Bivariate models are convenient for quantifying the contribution of variables (Kanungo *et al.*, 2009), they also serve as good learning tools for deciphering which factors or combination of factors plays a role in the initiation of landslides (Akgun *et al.*, 2008; Yalcin, 2008). Bivariate models are semi-quantitative in nature, as some measure of subjectivity is associated with assigned weights to factor maps (Aleotti and Chowdhury, 1999). Commonly employed bivariate models include statistical index method (Yalcin, 2008), weighting factor method (Çevik and Topal, 2003) and frequency ratio (Yilmaz, 2009).

Multivariate statistical models evaluate the relationship between a dependent variable (landslide occurrence) and a series of independent variables (landslide controlling factors). Multivariate statistics are used to model and quantify the relationship between landslide susceptibility and causal factors (Dai *et al.*, 2002). Considered factors are sampled and the presence or absence of landslides is determined for each of the sampling units and the result analysed using multivariate statistics (Dai and Lee, 2003). Multivariate statistical models are perhaps the most commonly featured in literature. These include: linear regression analysis (Carrara *et al.*, 1991), multiple regression analysis (Carrara, 1983), logistic regression analysis (Ayalew and Yamagishi, 2005) and discriminant analysis (Van Den Eeckhaut *et al.*, 2009). However, logistic regression and discriminant analysis are the two most featured multivariate statistical methods in landslide susceptibility assessment.

Logistic regression (a generalized linear model) establishes relationship between casual factors (terrain factors, land cover/land use, soil types/depth, rainfall etc.) with the stability or susceptibility of an area to landslide activities (Dai and Lee, 2003). Logistic regression analysis involves the fitting of a regression equation to data and then expressing the probability of the presence/absence of landslides in each grid cell. The relative contribution of grid cell to the logistic function can be obtained by looking at the significance of each

regression parameter (Ayalew and Yamagishi, 2005). Logistic regression is one of the most frequently used multivariate modeling techniques in landslide susceptibility studies (Lee, 2005; Felicísimo *et al.*, 2012). In landslide susceptibility assessment, the dependent variable is binary (representing presence or absence of a landslide) in nature. The added logistic link function to the usual linear regression model enables binary dependent variables to be modelled as continuous variables. Thus, explanatory variables may be either continuous or discrete, or a combination of both, and do not necessarily require the explanatory variables to be normally distribution (Lee, 2005). The logistic regression model is given by:

$$p = \frac{\exp(Y)}{(1 + \exp(Y))} \quad 0 \leq Y \leq 1 \qquad \text{Equation 2.4}$$

Where p is the probability of an event (landslide) occurrence, Y is a linear logistic model:

$$Y = \beta_0 + \beta_1 X_1 + \beta_2 X_2 + \beta_3 X_3 + \ldots + \beta_n X_n + \varepsilon \qquad \text{Equation 2.5}$$

Where β_0 represents the intercept on the model, β_1, β_2 … β_n, are the partial regression coefficients estimated from training data using the maximum likelihood method (Lee, 2005) and $X_1, X_2, \ldots X_n$ represents the independent variables (Lee, 2005; Guzzetti *et al.*, 2006). The logistic regression model was employed for the assessment of landslides initiating from cut slopes along transportation corridors (Ayalew and Yamagishi, 2005). Using an inventory map of 87 landslides locations as dependent variable and lithology, bed rock-slope relationship, lineaments, slope gradient, aspect, elevation and road network as independent variables, Ayalew and Yamagishi (2005) developed a landslide susceptibility map of a section of transport corridor in map in the Kakuda-Yahiko Mountains of Central Japan using logistic regression. The approach proved useful in predicting actual and potential failure locations. The model identified aspect and slope gradient as having more significant contribution to in stability than elevation, although field observations support the contrary. The developed susceptibility map had an overall accuracy of 84%, classifying 8.87% of the total study area as medium to high susceptibility zones. The study was able to demonstrate the ability of logistic regression as an effective means of mapping instability in the transport corridor, however some derived coefficients were found to be misleading. This was attributed to the curvilinear property of the model and mountainous terrain. Jaiswal *et al.*

(2010b) also reported that, most of the landslides were found to be shallow translational debris slides and debris flow-slides on natural and engineered slopes triggered by rainfall. Many of which occurred as first-time failures. The results of both studies showed that logistic regression provides reasonable assessment for landslide susceptibility of transport corridor slopes. The choice of model in Jaiswal *et al.* (2010b) was informed by the nature of failure observed (shallow translational debris slides in a largely homogenous overburden) during the assessment stage.

Perry *et al.* (2003a) have reported the existence of non-linear slow rotational slide in some sections of the UK transport corridor for which linear regression models are unsuitable. Das *et al.* (2011) emphasised the need for a sufficiently robust data driven susceptibility model that can accommodate the complexities often associated with landslide incidence when modelling susceptibility along transport corridor slopes so as to better represent complex terrain conditions. The findings of the study show that landslides within the transport corridor environment are highly discrete events and the landslide controlling factors are not entirely independent. Logistic models are characterised by high predictive capabilities, but these models may not be the most appropriate for detailed scale assessment of slope instability.

Discriminant analysis and the logistic regression approaches are two of the most popular multivariate landslide susceptibility modelling techniques (Ayalew and Yamagishi, 2005). Discriminant analysis models classify cases into one of several mutually exclusive groups based on their values for a set of predictor variables. For landslide susceptibility assessment, two groups are typically established: pixel identifying areas free of landslides incidence (S_0, stable slopes), and pixels of areas with landslide (S_1, unstable slopes). The discriminant function analysis is based on the assumption that the two groups (S_0 and S_1) are mutually exclusive and slope instability (t) is restricted only to one of the groups (i.e. t (0, 1)).
The goal of DA is to determine the group membership of each pixel by definition of a linear relationship between the landslide causal factors considered, which effectively segregates between the populations of stable and unstable slopes (Guzzetti *et al.*, 2005), thus, enabling the mapping of individual pixels into their appropriate groups with minimal error. Discriminant analysis models are linear in nature (Guzzetti *et al.*, 2006) and assume the form:

$$L = \beta_0 + \beta_1 X_1(t) + \beta_2 X_2(t) + \beta_3 X_3(t) + \cdots + \beta_n X_n(t) \quad \text{Equation 2.3}$$

Where L is the index or a point on the equation line differentiating stable from unstable locations; $X_i(i = 1,2,3, \ldots, n)$ are the input causal factors; $\beta_i(i = 1,2,3, \ldots, n)$ are coefficients estimated from the training data through discriminant analysis.

Both logistic regression and discriminant analysis establish linear or log-linear relationships between landslide susceptibility and causal factors. While the relationship between landslides and causal factors can be extremely complex and inherently highly nonlinear. As such, the linear and generalized linear models commonly fail to reflect the nonlinear nature inherent in landslides (Zhou *et al.*, 2002; Zhu *et al.*, 2014). Furthermore, these models are known to poorly handle multi-scale data, as all causal factors are combined with little considerations to the difference in scale at which the thematic data were acquired (Dai *et al.*, 2002). Generally, bivariate and multivariate approaches are characterized by a tendency to over simplify the factors that condition landslides (Carrara, 1983; Carrara *et al.*, 1991). Thus, both approaches are commonly considered best for regional or large scale studies where the effects of local variation terrain properties are minimal (Dai *et al.*, 2002; Fell *et al.*, 2008).

2.4.5.2 Machine learning approaches

There are also nonlinear regression models and machine learning techniques that address modelling nonlinearity in landslides (Goetz *et al.*, 2011). Advances in machine learning have provided new techniques such as classification tree analysis, generalized additive models, boosted regression tree analysis and maximum entropy (Wan *et al.*, 2010; Goetz *et al.*, 2011; Felicísimo *et al.*, 2012; Vorpahl *et al.*, 2012). The application of modelling techniques such as classification tree analysis, boosted regression tree analysis and maximum entropy to landslide assessment has only been recently reported (Felicísimo *et al.*, 2012; Vorpahl *et al.*, 2012) and are yet to be fully explored with regards to their suitability in landslide susceptibility modelling. (Vorpahl *et al.*, 2012). Developments in statistical software (SPSS and MATLAB) and computer programming languages like R, Python and MATLAB have facilitated the applicability of these machine learning techniques.

The generalized additive model (GAMS) is a semi-parametric extension of the logistic and linear regression models that combines linear and nonlinear relationships between predictor and response variables (Brenning, 2008; Goetz *et al.*, 2011). The nonlinear term of the model employs smoothing functions for the nonlinear transformation of predictor variables, hence its ability to effectively model complex geomorphological distributions (Goetz *et al.*, 2015). The linear term which employs the logistic additive model for binary (presence/absence) response variables typically employed in landslide assessment, discriminates between mapping units (stable and unstable slopes) using the logit of the occurrence probability (Petschko *et al.*, 2014). GAMS has only recently been introduced into landslide susceptibility (Brenning, 2008; Petschko *et al.*, 2014; Goetz *et al.*, 2015). The model handles large datasets poorly (Goetz *et al.*, 2011), as smaller models were identified to be associated with lesser errors (Petschko *et al.*, 2014). This was attributed to the smaller sample size which prevented model overfitting (Petschko *et al.*, 2014). Overfitting refers to a model's tendency to produce excellent predictions for training data employed in the model's parameterisation, but perform poorly when new test data not considered during model training are introduced. This is a major setback with use of GAMS in landslide susceptibility assessment as data size is typically large and model predictions maybe unreliable. Goetz *et al.* (2011) and Petschko *et al.* (2014) suggested the division of the entire study area into smaller lithological domains that can be modelled separately and the final susceptibility map of the study area derived by merging the individual susceptibility maps of the domains. Goetz *et al.* (2011) reported an overall performance accuracy of 83.4% for GAMS in the study area. The result suggests that GAMS can be considered for detailed scale susceptibility analysis, however, investigators should be mindful of the model's tendency of overfitting.

Classification tree analysis possesses the capacity to capture existing non-linearity and interactions that may exist within a complex landslide system by evaluating parameter interfaces and producing step-like response functions between the considered variables and the model outcome (Vorpahl *et al.*, 2012). The approach uses recursive partitioning of multidimensional space of a single variable based on sets of simple rules generated at each step to minimize variability within each resulting subset and maximize class purity (Elith *et al.*, 2008; Felicísimo *et al.*, 2012; Vorpahl *et al.*, 2012). A pruning procedure is usually required at the end of the recursive partitioning process through internal cross-validation to

reduce the existence of data deviance at the terminal nodes (Felicísimo *et al.*, 2012). Under this approach, the predictor variables can be numeric, binary or categorical in nature and the model outcomes are usually unaffected by the monotonous transformations and differences in scale of measurement amongst predictor variables (Elith *et al.*, 2008). The classification tree models are insensitive to outliers and possess the ability to accommodate missing data within the predictor variables by the use of surrogates (Breiman *et al.*, 1984; Elith *et al.*, 2008). Comparative studies show that classification tree models are usually not as accurate as other regression models like generalized additive models (Elith *et al.*, 2008; Felicísimo *et al.*, 2012; Vorpahl *et al.*, 2012). Model sensitivity is another limiting factor. Vorpahl *et al.*, (2012) noted that the resultant tree structure is heavily dependent on the data samples, where small adjustments in the training data commonly result in very different series of splits. This lack in robustness introduces uncertainty into the model interpretation and predictive performance of the approach (Elith *et al.*, 2008).

Fuzzy logic has been applied in landslide susceptibility assessment (Ercanoglu and Gokceoglu, 2004; Gorsevski *et al.*, 2005; Marjanović and Caha, 2011). This approach stems from the fact that the threshold for landslide incidence is naturally not discrete but exists within a range(Gorsevski *et al.*, 2005). The fuzzy set theory allows a varying degree of membership for elements in relation to a set in the range 0 - 1 (Gorsevski *et al.*, 2005; Muthu *et al.*, 2008). When applied to landslide susceptibility, a membership degree is established between the presence/absence of landslides and the parameter class (e.g., the presence of landslides in the 0 - 22.5 aspect category) for each class of an environmental variable (e.g., for each aspect category) (Gorsevski *et al.*, 2005; Marjanović and Caha, 2011).

Membership values are computed using either frequency ratio (which is the ratio of landslide cells in an attribute class to the total landslide cells in the area) or cosine amplitude computed as the ratio of the number of landslide cells in an attribute class to the square root of its product of the total number of cells in an attribute class and the total number of landslide cells (Marjanović and Caha, 2011). A fuzzy set is constructed for each environmental variable (Muthu *et al.*, 2008). Fuzzy sets for different environmental factors are then combined using rules commonly referred to as fuzzy operators to estimate of landslide susceptibility (Ercanoglu and Gokceoglu, 2002). Several fuzzy operators exist for

combining membership functions with the AND and OR operators being the most popular (Gorsevski *et al.*, 2003). Fuzzy logic has been employed in landslide susceptibility assessment on regional scale by many authors (Ercanoglu and Gokceoglu, 2002; Gorsevski *et al.*, 2003; Muthu *et al.*, 2008; Kanungo *et al.*, 2011; Pradhan, 2011). The fuzzy set theory enables the quantitative processing of multiple datasets and allocates objective weights (Ercanoglu and Gokceoglu, 2004). The fuzzy logic approach is flexible and effectively models complex geomorphological processes (Pradhan *et al.*, 2010), and copes well with a non-parametric dataset (Kanungo *et al.*, 2006).

Expert opinion is important in weight determination under the fuzzy logic approach (Zhu *et al.*, 2014), as models developed by experts with detailed knowledge of landslide characteristics and of their relation with the landslide conditioning factors have been shown to perform better (Pradhan, 2011; Zhu *et al.*, 2014). Pradhan (2011) showed that landslide susceptibility maps developed using different fuzzy algebraic functions resulted in different prediction accuracies. Validation results show an overall accuracy of 94.73% for gamma operator, 84.76% for the fuzzy algebraic "Or" operator and 84.82% for the fuzzy "And" operator. Most importantly, the results show that that the data driven fuzzy logic model performed only marginally better in comparison with the logistic regression model (Pradhan, 2011).

Another approach based on machine learning is the artificial neural networks (ANN). ANN is a computational framework modelled after the human behaviour and is capable of resolving complex problems (Lee *et al.*, 2003; Pradhan and Lee, 2010). Made up of highly interconnected neural, ANNs possess the ability to respond to external inputs and learn structures and patterns of the new environment. Hence model calibration is required to define the functionality of the network (Pradhan and Lee, 2010). In addition, neural networks require less data for training than other statistical methods as a result of the network's iterative learning process (Lee *et al.*, 2004). ANNs are good at establishing rules between input and output but the rationale behind why they work in a particular manner for any given calibration set is almost impossible to explain. The back propagation learning algorithm is most commonly adopted in ANN simulation for landslide susceptibility (Lee *et al.*, 2003).

ANN consist of multiple layers of individual processing nodes (commonly referred to as neurons), comprising an input and an output layer and one or more hidden layers. A neural network takes the input information and learns how to predict the output by establishing and adjusting weights between neurons on the same or on different layers, in response to errors between predicted and known output values. At each processing node, adjustments are made through weighting summations and nonlinear functions. On conclusion of the training phase, the ANN is able to predict the output values (e.g., landslide susceptibility) given a set of inputs (e.g., the environmental factors). The difficulty associated with understanding how the decisions were reached restrains the possibility of using findings obtained with a neural network prepared for an area in a neighbouring area. Also, the role, functionality and significance of the weights and of the nonlinear calibration functions are difficult to interpret. Artificial neural networks have been successfully applied to regional scale landslide susceptibility mapping (Lee *et al.*, 2003; Pradhan and Lee, 2010 and Wang *et al.* 2005).

2.4.5.3 Deterministic (process based) approaches

Deterministic approaches are generally regarded as best suited for analysis of site specific engineering slope studies (Miller *et al.*, 2012). and the quantitative information derived from these models on landslide analysis can be used directly in the design of engineering works (Perry *et al.*, 2003a) or in the quantification of risk (Van Westen *et al.*, 2006). Susceptibility assessment is determined using slope stability models and factor of safety computation(Lu and Godt, 2008). This approach requires a huge quantity of detailed input data, usually derived from laboratory tests and detailed field measurements (Van Asch *et al.*, 2007). An index expressing the ratio between the local stabilizing and driving forces (factor of safety) is computed using parameters such as the geotechnical properties of soil, meteorological data, external stresses and seismic acceleration (Harp *et al.*, 2009). In theory, values of the index greater than 1.0 indicate stability of the slope, while values less than 1.0 flag off unstable conditions (Harp *et al.*, 2009; Miller *et al.*, 2012). A marginally stable slope is achieved at a safety factor of exactly 1.0 indicative of a threshold condition produced by equivalence of the stabilizing and driving forces (Glade and Crozier, 2006). An overview of deterministic models and their application for landslide susceptibility assessment is given in Casadei *et al.* (2003), Van Asch *et al.* (2007) and Simoni *et al.* (2008).

Deterministic models are developed based on an understanding of the physical laws regulating to slope stability and attempt to extend spatially the simplified stability models commonly utilised in geotechnical engineering studies (Van Asch *et al.*, 2007). Most of the deterministic models employed in susceptibility assessment make use of a 1- dimensional or 2-dimensional model describing slope stability of slopes with an infinitively large failure plane, commonly referred to as an infinite slope model and are therefore only applicable to modelling shallow translational landslides (Savage *et al.*, 2004; Harp *et al.*, 2009). Infinite-slope stability models are a first-order approximation that provide close representation of surface and near surface terrain processes, as such can be used in a grid-based GIS framework to assess the spatial distribution of relative landslide susceptibility (Haneberg, 2004). The 1-D infinite slope models are typically comprised of a coupled hydrological model (for soil moisture and pore water pressure under different simplification and assumption) and a slope stability model. In some cases an impact model, such as basin sediment yield can also be coupled (Bathurst *et al.*, 2006; Bovolo and Bathurst, 2012). These incorporate the effects of groundwater response to rainfall on slopes for modelling shallow translational landslides. The incorporated hydrology component assumes a slope parallel flow either as a steady state function of slope and drainage area (steady-state models)(Montgomery and Dietrich, 1994) or by dynamically evaluating the entire process from rainfall to the transient response of the groundwater (dynamic models). For simplicity, the slip surface is assumed to be planar, at a fixed depth, and most commonly parallel to the topographic surface (Godt *et al.*, 2008). Additional assumptions are made with regards selection of values for pore fluid pressure (Lu and Godt, 2008). Harp *et al.* (2009) asserted that steady state models are easier to administer over large areas, as the estimation of the distribution of groundwater at that scale is subject to large uncertainties. However, for large scale studies, results from steady state model were a bit conservative in comparison to those obtained from dynamic models.

Dynamic 1-D infinite slope model are capable of simulating temporal changes in the landscape. The models are able to addresses the spatial and temporal variation of landslide occurrence. Dynamic models compute values of factor of safety for each grid for a given scenario and by grouping pixels with the same low Factor of Safety into potential landslide polygons, the possible landslide size is determined (Van Asch *et al.*, 2007). A number of deterministic models are dynamic in nature with capacity for futuristic instability predictions

and use for back analysis (Harp *et al.*, 2009). When implemented in a GIS, the models are able to calculate the changes in the values with time per grid cell (Harp *et al.*, 2009).

Notable examples of physically based models are TRIGRS (Transient Rainfall Infiltration and Grid-based Regional Slope-stability analysis) (Baum *et al.*, 2005), SINMAP (Stability Index Mapping) (Pack *et al.*, 1999), SHALSTAB (Shallow Landsliding Stability model) (Rosso *et al.*, 2006), SHETRAN (Shallow Landslide and Sediment yield model) (Bovolo and Bathurst, 2012), LISA (Level 1 stability analysis) (Formetta *et al.*, 2014), SMOPH (Slope morphology) and dSLAM/IDSSM (Distributed shallow landslide model/integrated dynamic slope stability shallow landslide model). A few selected models that have frequently featured in scientific literatures on deterministic modeling of landslide susceptibility zonation are briefly discussed.

TRIGRS is a simple GIS based deterministic slope stability model that runs on FORTRAN and is designed to model the potential occurrence of shallow landslides by incorporating the transient pressure response to rainfall and infiltration (Baum *et al.*, 2005). This model combines an infinite slope stability calculation with an analytic one-dimension solution for pore-pressure transmission in a soil layer of finite depth in response to time varying rainfall and could be superimposed on any steady-state groundwater flow field that is consistent with the model assumptions (Baum *et al.*, 2005). The TRIGRS model uses a coupled infinite slope models to compute the factor of safety for each grid cell. The model accounts for slope heterogeneity, tolerates flexible variation in input values of material properties and other parameters like rainfall intensity and duration from cell to cell (Godt *et al.*, 2008). The slope cells within the model are considered as units with constant thickness. The susceptibility to slide for each saturated slope cell is generally computed based on the slope cell inclination and the computed shear strength for each cell and stored as factor of safety (Figure 2.3). This modelling approach has been utilized in a number of studies (Baum *et al.*, 2005; Godt *et al.*, 2008). However, a number of studies have reported inconsistencies in the model predictions stating that these predictions sometimes delineate larger areas of failure than actually exist (Chang and Kim, 2004; Safaei *et al.*, 2011). Uncertainty in soil thickness, local variation in soil properties and DEM errors are some of the reasons provided as being the main causes of this problem (Baum *et al.*, 2005).

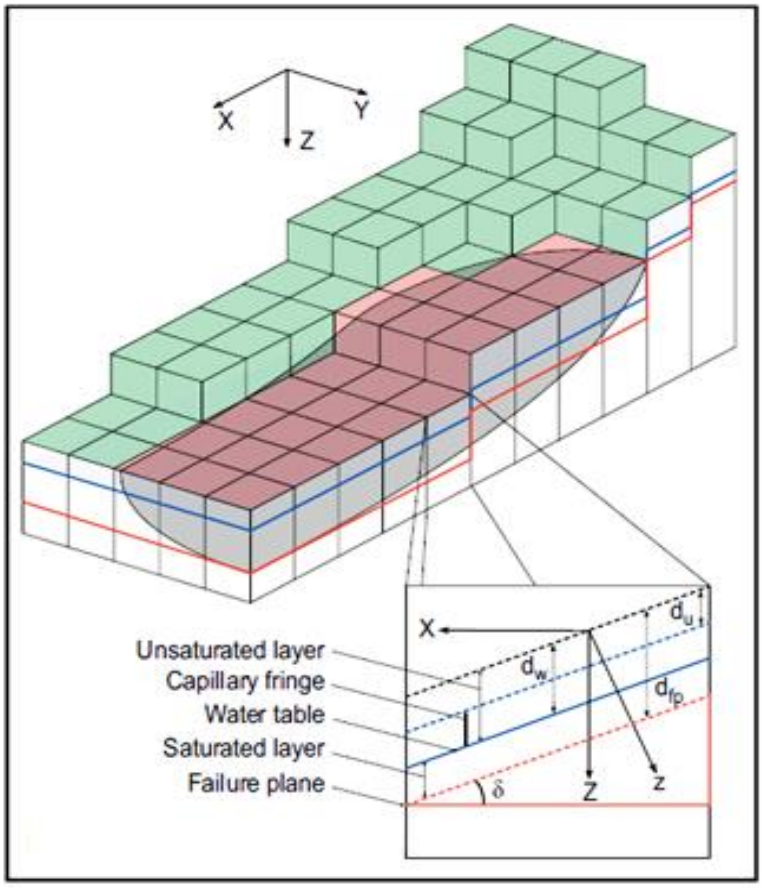

Figure 2.3 The TRIGR model showing unit cell coupled infinite slope model for computing factor of safety for each grid cell. Key: d_w, depth to water table, d_{fp}, depth to sliding plane, d_u, depth to capillary fringe. (After, Raia et al 2014)

SHALSTAB is an infinite slope stability model coupled with a hydrologic model (Rosso *et al.*, 2006). The model incorporates the influence of rainfall on slope stability assessment. Thus model predictions are based on the minimum amount of steady state rainfall required to trigger a landslide occurrence (Rosso *et al.*, 2006). Like the TRIGRS model, the required morphometric input data are usually DEM derived, in addition to other geotechnical parameters such as bulk density, angle of internal friction and depth to water table. The SHALSTAB model assumes the local surface topography as a dominant control of landslide occurrence and estimates pore-pressure for steady state saturated water flow parallel to slope plane (Montgomery and Dietrich, 1994; Rosso *et al.*, 2006). The critical relative wetness (the ratio of steady state rainfall and soil transmissivity) is based on steady state saturated water flow parallel to slope plane that potentially triggers slope failure (Figure 2.4a). The

ratio relationship between the steady state rainfall and soil transmissivity defines the susceptibility of a location to landslide (with lower critical relative wetness translating to higher susceptible to failure occurrence for a given location) (Montgomery and Dietrich, 1994; Goetz *et al.*, 2011). The SHALSTAB model categorizes slope stability into any one of three classes, namely unconditionally stable, conditionally stable and unconditionally unstable (Figure 2.4b&c).

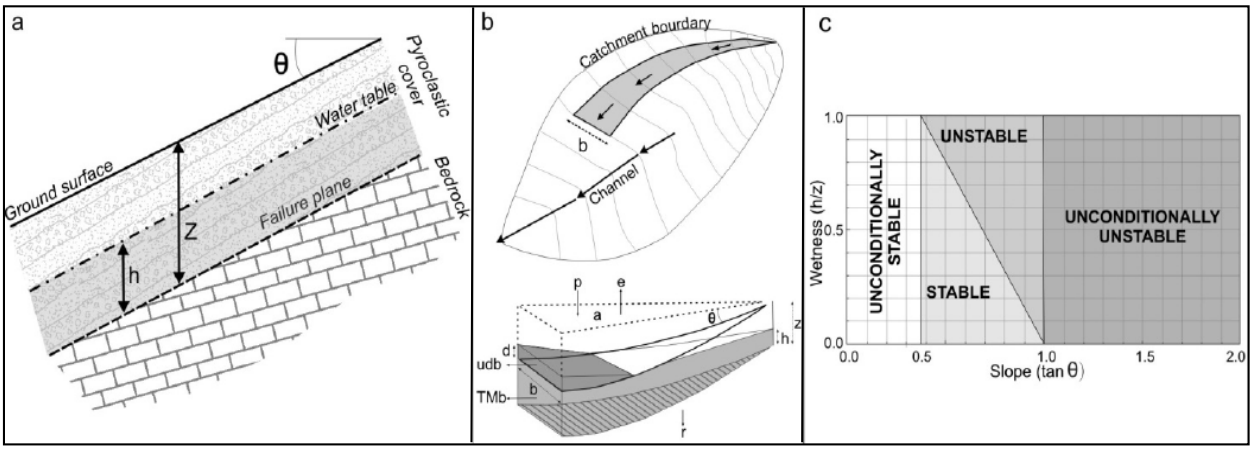

Figure 2.4: The conceptual components of the SHALSTAB model (after Montgomery and Dietrich, 1994). Key: a) infinite-slope conceptual scheme; b) hydrological model (p, precipitation; e, evapotranspiration; r, deep drainage; a, drainage area; h, the height of the water table; z, soil thickness; u, mean subsurface flow velocity; h, water level of surface flow; T, transmissivity; θ, slope angle; M, sinθ ; b, contour length); and c) definition of stability fields.

SHALSTAB assumes zero soil cohesion to compensate for spatial and temporal heterogeneity of soil cohesion and as a result is thought to produce the most conservative slope stability estimates (Dietrich *et al.*, 2001). Goetz *et al.* (2011) demostrated that this can be overcome by model optimization performed by increasing the frictional angle appropriately. However, this does not fully capture the effects of cohesion, but does compensate for cohesion in the friction angle, hence allowing for the application of SHALSTAB in area where cohesion is an important consideration (Rosso *et al.*, 2006).

SHETRAN is a physically based distributed model (PBDM) that is written in FORTRAN and runs on Microsoft windows. This model was developed for water flow, sediment and solute transport in river catchment (Figure 2.5). The model can be integrated into slope

stability studies as it includes a hydrological component for simulating: rainfall, evapo-transpiration, overland flow (run-offs) and channel flows and variably surface flow (Birkinshaw *et al.*, 2010). The model essentially requires information on the spatial distribution of vegetation cover, soil, topography, geotechnical properties and time-series data for precipitation and evaporation (Birkinshaw *et al.*, 2010; Bovolo and Bathurst, 2012). The precipitation and evaporation data are simulated to provide information on the temporal variation in soil moisture content (pore-water pressure) for each grid cell. The resulting pore-water pressures are then fed into a coupled slope stability model to derive the factor of safety for each cell is computed (Miller *et al.*, 2012).

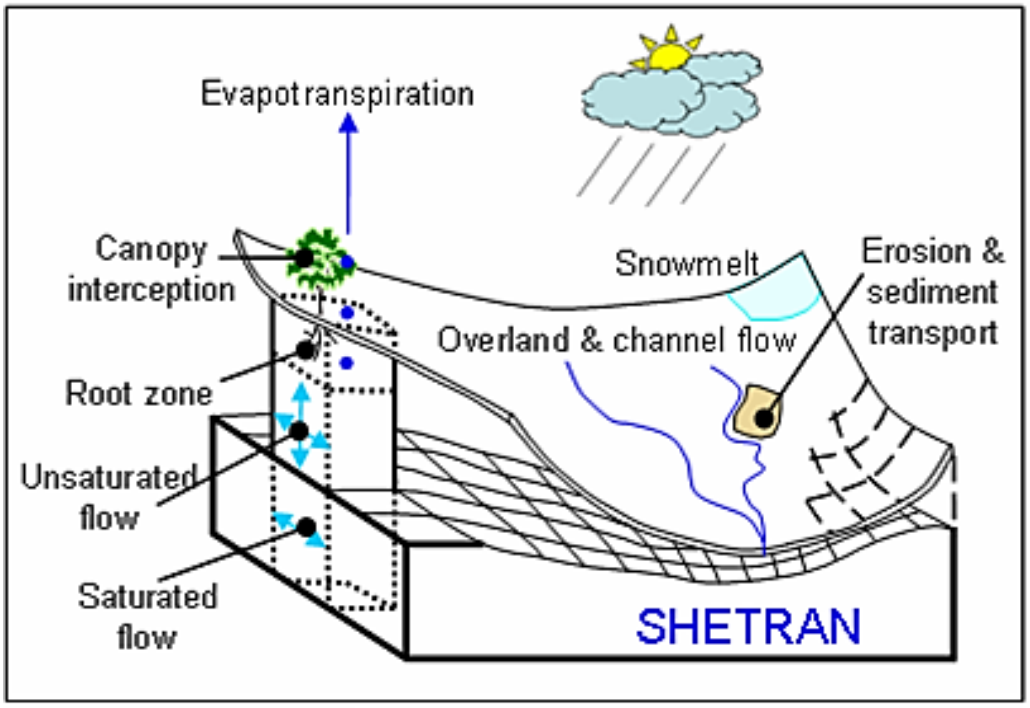

Figure 2.5: Schematic illustration showing Conceptual structure (stream links and columns) in the SHETRAN model. Each column comprises many finite-difference cells, stacked one above the other with lateral transport between cells in neighbouring columns (After Ewen et al 2000).

Slope susceptibility to failure within the slope stability model is determined as a function of the spatial and temporal variation of soil saturation conditions, derived from simulations using the hydrological model and the standard geotechnical infinite slope factor of safety analysis (Bovolo and Bathurst, 2012). Miller *et al.* (2012) employed the SHETRAN model in a hazard assessment study of engineered slopes along a transport corridor. The

hydrological component of the model was used to simulate, from rainfall data, the pore-water pressure for all the grid cells. These were subsequently input into a finite difference model FLAC from which the geotechnical aspects were modeled. A factor of safety for each grid cell was computed and used to model the susceptibility to failure for the engineered slopes under investigation (Miller *et al.*, 2012). SHETRAN has been shown to be an important hydrological modeling tool for detailed scale slope stability assessment within transport corridor environment (Miller *et al.*, 2012). However, like other infinite slope deterministic modelling approaches, its large data requirement limits its applicability over extensive transport corridor cuttings and embankments.

In addition to the GIS-based models for slope stability assessment, there is also a range of detailed 2-D and 3-D numerical models normally employed in cross sectional or single slope analysis (e.g. Slope/W, SLIDE, CLARA etc.) (Krahn, 2004). Numerical models can be grouped as continuum based (e.g. finite element, finite difference, with software such as FLAC3D, PLAXIS, and VISAGE) or discontinuum based (e.g. distinct element, discrete element, with software such as UDEC) models (Eberhardt, 2003).

In continuum modelling, the entire slope mass is divided into finite number of elements and represented as a mesh (Krahn, 2004). The Finite-difference methods provide numerical approximations based on differential equations of equilibrium, strain displacement relations or the stress-strain equation (Eberhardt, 2003). While the finite element technique explores solutions based on numerical approximations of the connectivity of elements, continuity of displacement and stresses between elements (Eberhardt, 2003). Both methods are capable of modelling material heterogeneity, non-linearity and boundary conditions, but incapable of simulating infinitely large domains due to their internal discretization (Dai and Lee, 2003; Van Asch *et al.*, 2007). Boundary Element Methods require discretization at the boundaries of the solution domains only, which simplifies the input requirements, but becomes impractical when more than one material must be taken into account. It is the most efficient technique for fracture propagation analysis (Eberhardt, 2003).

In discontinuum modelling, slopes are represented as discontinuous medium or as assemblages of blocks formed by connected fractures in the problem domain (Van Asch *et al.*, 2007). The distinct element method is an example of discontinuum modelling(Van Asch *et al.*, 2007). The underlying concept behind discontinuum modelling is the repeated

computation of limit equilibrium (the ratio of shear strength to shear stress) for each block. Thus, modelling large displacements including fracture opening and complete detachments is straightforward using the distinct element method (Krahn, 2004), but less suitable when modelling plastic deformation (He *et al.*, 2014). The distinct element method is mostly applied to rock slope where the prevalence of joints and fractures are widespread.

In general, the deterministic models cover attempts to describe the underlying physical processes leading to slope failure. As such, the results obtained are often considered to be a closer representation of reality than the heuristic and statistical models. When properly calibrated with an accurate landslide inventory deterministic slope stability assessments are generally assume to have a distinct advantage over the heuristic and statistical models which exhibit greater tendency towards epistemic and aleatory uncertainties (Carrara *et al.*, 1999; Brenning, 2005; Petschko *et al.*, 2014). However, their large data requirement and parameterization challenges have limited their use for detailed scale assessment of slope over large areas. In addition, the conventional factor of safety computed for individual slope and used in the development of the hazard map of the study area does not reflect the spatial and temporal variability of pore water pressures, angle of internal friction, cohesion and undrained shear strength. The models are also not suitable in predicting the development of complex landslides within complex hydrological systems, as in more complex models the factor of safety becomes a random variable (Van Asch *et al.*, 1999). However the greatest limitation is the models inability to effectively handle uncertainty and parameter variability (Van Asch *et al.*, 2007), which is common place with transport corridor environment , where land cover type and geotechnical properties of slopes in cuttings can vary drastically over short distances (Miller *et al.*, 2012).

2.4.5.4 Probabilistic modelling.

Probabilistic landslide susceptibility modelling uses presumed probability distributions of input variables to calculate probability distribution for stable and unstable locations (Lee and Pradhan, 2006). Probabilistic models estimate on the basis of past historical data ("*a priori"*) the probability of the reoccurrence of an event. Unlike the deterministic approach, which establishes invariant or spatially explicit parameter values and lack an element of uncertainty , the probabilistic approaches allow for uncertainty by assigning probability distributions to model parameters (Aleotti and Chowdhury, 1999). Given the uncertainty

associated with landslide phenomena and their relationships with the landscape, the approach has been widely employed in landslide susceptibility assessment (Chung and Fabbri, 1999; Park, 2011). Generally, within the probabilistic framework, the collected data layers are represented by conditional probabilities or likelihood ratio functions. Then the individual variable probabilities are combined using combination rules such as Bayesian combination rule (Lee *et al.*, 2002) and fuzzy membership functions (Zhu *et al.*, 2014) according to the theoretical backgrounds adopted.

The probabilistic framework recognizes key issues usually generalised in deterministic modelling (Aleotti and Chowdhury, 1999), such as important considerations like parameter variability and uncertainties associated with the mechanism of failure, occurrence of failure and its impact on the surrounding environment which are seen to exhibit complex relationships (Van Westen *et al.*, 2008). The earliest applications of the probabilistic approach in slope stability assessments were essentially within the context of traditional soil mechanics and geotechnical slope evaluation (Chowdhury and Zhang, 1993; Chowdhury and Xu, 1995). The incorporation of GIS into the probabilistic framework had enhanced better visualization and the ability to compare spatial distribution of landslides with respect to the various conditioning and triggering factors (Aleotti and Chowdhury, 1999). The robustness and versatility of the probabilistic framework allows for the integration of innovative approaches for simulation of failure progression using process based techniques (Raia *et al.*, 2014), as well as the development of decision support systems that are not only based on performance indicators but also on consequence of failure (Aleotti and Chowdhury, 1999). Probabilistic models are known to potentially handle better the process of combining different data layers of information required in slope stability assessment which are usually multi-scale and multi-source in nature (Chung and Fabbri, 1993; Binaghi *et al.*, 1998; Park, 2011).

In a probabilistic assessment of landslide susceptibility by Binaghi *et al.* (1998) , a Certainty factor approach was used as Favourability Functions (FF) to handle the problem of combining heterogeneous data. A Certainty factor is somewhat similar to a conditional probability but rather presenting the degree of probability of an outcome, a Certainty factor represents a measure of belief in an outcome (Roventa and Spircu, 2009). The variations in the measures of belief are assessed in relation to the probability of occurrence of an event

under certain conditions with respect to the overall prevalence of the event (i.e. favourbility function) (Acevedo and Real, 2012). In the study by Binaghi *et al.* (1998), multi source data (discrete and continuous data) were initially transformed, normalised and then afterwards combined in a pairwise manner to enable the assessment of the contributions of individual causal factors to slope instability zonation. The application of the probabilistic approach to landslide hazard zonation is always performed under the assumption that landslide susceptibility can be determined by the statistical relationships between historic landslide locations and the identified causal factors represented as thematic spatial datasets (Binaghi *et al.*, 1998). In Binaghi *et al.* (1998), the Certainty factor at each grid cell was defined by the conditional probability of landslide occurrence based on an evidential threshold defined by the spatial interactions between various thematic datasets. The range of variation of the Certainty factor is [-1, 1], making it easier to understand the effect of each category of a thematic layer on landslides (Chung and Fabbri, 1993). Positive numbers are indicative of an increase in certainty after the threshold evidence is observed, while negative numbers correspond to decrease in certainty; a zero value usually indicates that the prior probability is very similar to the conditional one (Roventa and Spircu, 2009). A Certainty factor is calculated for each layer and the layers combined using a pairwise combination rule (Heckerman, 1986). Susceptibility to failure can easily be inferred from the degrees of belief generated, as the intervals remain consistent on application to other areas (Binaghi *et al.*, 1998; Sujatha *et al.*, 2012). Binaghi *et al.* (1998) revealed that the level of confidence in the use of Certainty factor in hazard zonation and assessment using data driven techniques was higher in comparison with zonation assessments derived from expert weightings. In addition the appropriate selection and classification of thematic layers were identified as key considerations when employing the use of this method. The primary advantage of this method lies in the expression of degrees of belief, but does not reflect the associated uncertainty (Sujatha *et al.*, 2012).

A number of authors (Lee *et al.*, 2002; Van Westen *et al.*, 2003) have utilized the weight of evidence approach in landslide susceptibility modelling. Weight of evidence is a quantitative data driven approach used in the determination of weight of causal factors (evidences) and in the combination of generated weights (Lee and Choi, 2004). The approach utilises the log-linear form of Bayesian probability in estimating the relative importance of the evidences (Van Westen *et al.*, 2003). An overlay of the various thematic maps on the

landslide inventory of study area allows for the computation of weights. Weights are estimated according to the landslide density for each class of the evidence layer. Derived weights can be positive or negative. Positive contrasts are indicative of higher influences of the causal factor for on landslide occurrence and vice versa(Lee and Choi, 2004). The weights are in turn used as rating for each of the category of causal factors (usually represented as thematic layers) (Van Westen *et al.*, 2003). A landslide susceptibility index usually used in categorizing the area into the different susceptibility zones is computed from the summation of the ratings of the various thematic data layers (Lee *et al.*, 2002; Van Westen *et al.*, 2003; Lee and Choi, 2004). A number of studies have reported the use of weight of evidence approach as an effective means of weight generation and combination for the development of landslide susceptibility maps (Lee *et al.*, 2002; Van Westen *et al.*, 2003). Regmi *et al.* (2010) evaluated seventeen causal factors considered as influential to landslide incidence in the study area. Weight maps of the seventeen measured causal factors covering topography, hydrology, geology, land cover, and human influences were generated using weight of evidence. A susceptibility map of the study area was derived from the summation of weighted factors summed on a pixel-by pixel basis and had a prediction accuracy of 78% on validation. The study identified that the application of the weight of evidence approach is most suitable for locations with compressive landslide inventory as it played a significant role in the accuracy of the final map developed. The methodology provides an ample means of selecting the most appropriate causal factor to be consider for a susceptibility assessment based on weights generated (Van Westen *et al.*, 2003; Regmi *et al.*, 2010). However, the approach does not reflect the uncertainty associated with the predicted spatial zones of instability (Regmi *et al.*, 2010).

Probabilistic framework in contrast to the other quantitative methods are more objective by the reason of its data dependent character (Aleotti and Chowdhury, 1999; Ercanoglu and Gokceoglu, 2004) and unlike deterministic models, the probabilistic methods required less quantity of data, though their predictive accuracy is invariably dependent on the number, quality and reliability of the data. The integration of soft-computing techniques such as fuzzy logic, neural networks and generic algorithms with machine learning capability reduces the data quantity dependency for assessment and enables the capacity to process both parametric and non-linearity (Binaghi *et al.*, 1998; Tangestani, 2009). These techniques

are usually free of any distribution assumptions or bias of data and their weights are objectively computed (Ercanoglu and Gokceoglu, 2004).

Another approach that has been recently applied (Tangestani, 2009) to landslide susceptibility prediction is evidential reasoning. The technique is based on Dempster-Shafer theory of evidence, a general framework for modelling probability with the assignment of uncertainty (Yager *et al.*, 1994). The Dempster-Shafer theory of evidence was first proposed by Dempster (1968) and was formalised by Shafer (1976). The Dempster-Shafer theory of evidence (evidential reasoning) estimates probabilities based on how close the evidence proves the truth of the hypothesis been considered, thus providing a mathematical framework for the estimation of uncertainties (Pearl, 1990). The strength of the Dempster-Shafer theory of evidence approach is in its ability to utilise multi-source, multi-scale data and relative flexibility to deal with varying degrees of uncertainty (Carranza *et al.,* 2009; Park, 2011). The approach represents the partial information provided by various independent sources as numeric measures and combines these measures using a combination rule to produce an overall assessment of the total evidence in support of the existence or absence of a phenomenon, which in this case is slope instability. The ability to assign uncertainty to probability distribution is the main distinction between traditional Bayesian probability and the Dempster –Shafer theory of evidence (Gorsevski *et al.,* 2005). In Bayesian probability two probability states exist (i.e. positive and negative) (Gorsevski *et al.,* 2005). These two states are assumed to be mutually exclusive (existence of one is not influence or caused by the other) and collectively exhaustive (constitute the entire range of possible outcome) (Yager *et al.,* 1994). In the Dempster –Shafer theory of evidence, uncertainties are not just assigned to each state of nature, but also exists as a subset (Gorsevski *et al.,* 2005). Thus allowing associated uncertainty to be modelled alongside probability predictions.

The Evidential reasoning approach also allows for the definition of a frame of discernment (Park, 2011), which is a set of causal propositions (factors or evidences) assessed as influential to the occurrence of terrain instability and a target proposition (e.g. landslide occurrences) in the study (Park, 2011; Tien Bui *et al.,* 2012). The frame of discernment permits a collection of proposition from various sources and type (multi source), different time (multi temporal) and not necessarily of the same scale (multi scale) (Althuwaynee *et*

al., 2012; Lee *et al.*, 2013). This enables the assessment of the impact and influence of a variety of factors on what is a complex system. The propositions are mutually exclusive and collectively exhaustive (Park, 2011). Basic probability assignments (weights) are developed for each proposition. The basic probability assignment or mass function assigns a belief function to each proposition. The belief function is the measure of the total amount of belief committed (a number from 0 -1) to every attribute in a proposition with relations to the presence or absence of a target proposition and plausibility function (a measure of ignorance or uncertainty) (Park, 2011; Tien Bui *et al.*, 2012). Belief intervals, alongside mass functions are used for information representation (evidential layers) and unlike in the traditional probability theory, the interval between belief and plausibility gives an indication on the uncertainty associated with a target proposition (Figure 2.6).

The evidential layers (thematic maps of propositions with assigned belief values) are then aggregated using the Dempster's rule of combination. The combination rule results in a final belief function based on conjunctive pooled evidence, where the influences of all the evidences represented (Yager *et al.*, 1994). The Dempster-Shafer evidential belief model possesses the capacity to capture existing non-linearity and interactions that may exist within a complex landslide system. Its capacity for aggregation of evidence provided by incongruent sources (Lee *et al.*, 2013) strengthens its appropriateness for the transport corridor environment where important datasets required for slope stability assessment are often from diverse sources and at different scales.

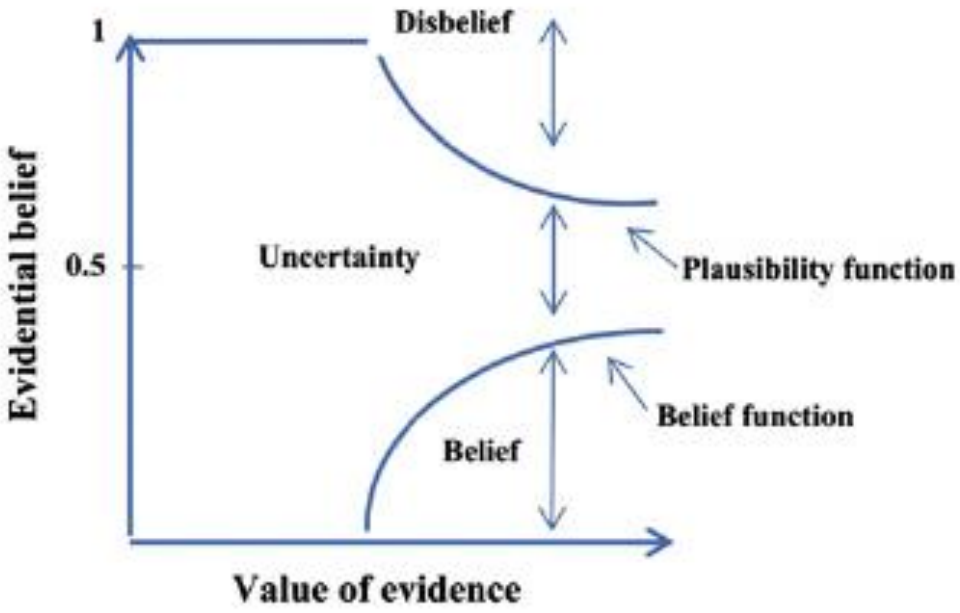

Figure 2.6 Schematic representation of the basic probability assignment functions of the Dempster-Shafer theory of evidence approach. (After Carranza et al 2005 and Althuwaynee et al 2012)

One of the earliest attempts at integration of a data driven Dempster-Shafer theory of evidence approach to landslide studies was by Tangestani (2009). The study compared the Dempster-Shafer evidential belief model and fuzzy logic models for landslide modelling in the Zagros Mountains in Iran. The results of the study suggested better predictive performance for the fuzzy model. The results show that the fuzzy logic map had a classification of 94%, while the evidential belief function model had a classification accuracy of 73%. The study attributed the difference in classification accuracy to the degree of conflict between considered factors in the evident belief function model as a result of the combination rule employed. However the methodology adopted for comparison of the performance of the fuzzy logic and evidential belief models was flawed in that the fuzzy membership was determined based on expert opinion while the evidential belief function model was essentially data driven. Based on the reported results the evidential belief model identified concern with the choice of causal factors used in the study as report in the almost uniform uncertainty values (0.2 -0.3) for 99.7% of the study area (Tangestani, 2009). This

concerns may have been rightly adjusted in the fuzzy model through expert opinion (Porwal *et al.*, 2003). Tien Bui *et al.* (2012) in a later comparative study also compared the predictive performance between the evidential belief and three other fuzzy models (fuzzy SUM, fuzzy PRODUCT and fuzzy GAMMA). In the study, the models were essentially data driven. The study identified the evidential belief model as exhibiting the highest prediction capabilities amongst all considered models.

Park (2011) applied evidential belief model for landslide susceptibility mapping in Jangheung in Korea and compared the performance of the model with Logistic Regression. The study reported better predictive capability for the evidential belief model, as the approach is not restricted to establishing correlation based only on log-linear relations between variables. The Evidential reasoning approach quantitatively models parameter uncertainties, exhibit robustness and scale well to large data sets (Park, 2011; Althuwaynee *et al.*, 2012; Lee *et al.*, 2013). Various studies (Park, 2011; Althuwaynee *et al.*, 2012; Tien Bui *et al.*, 2012; Lee *et al.*, 2013) have demonstrated the potential of the data driven Dempster-Shafer theory of evidence approach to adequately represent quantitative relationship between landslide occurrences using multi-source, multi scaled spatial data layers in addition to modelling the degree of uncertainty. These elements are important in the consideration of model selection for detailed scale susceptibility zonation of slopes over extensive linear expanse as is the case with the transport corridor environment. There is no record on the application of the evidential reasoning approach to detailed scale slope stability assessment, reasons may be the demand for very high resolution dataset required to ensure minimal degree of uncertainty necessary for detailed scale slope stability assessment (Brenning, 2005; Althuwaynee *et al.*, 2012; Miller *et al.*, 2012).

2.5 DEM generation

The use of digital representations of the topographic surface in landslides analysis is common practise (Jaboyedoff *et al.*, 2012). DEMs in addition to providing a continuous elevation value over a topographic surface also enable the easy extraction of terrain attributes like slope gradient, slope aspect, altitude, internal relief, slope curvature and roughness that serve as important input data in landslide analysis (Jaboyedoff *et al.*, 2012). DEMs also provide a means for effective visualization and semi-automatic classification of landslide domains during inventory mapping (Guzzetti *et al.*, 2012). Surface topography

also influences flow sources, flow direction and zones of moisture accumulation, all of which are easily derived from DEM (Sørensen and Seibert, 2007). These terrain derivatives are important hydrological components of quantitative landslide analysis (Montgomery and Dietrich, 1994; Goetz *et al.*, 2011), that help simplify complex surface and subsurface processes and providing indirect means of evaluating these processes for a given location (Goetz *et al.*, 2011).

DEM generation can be accomplished from a variety of sources, which include, digitizing contours from existing contour maps, differential Global Navigation Satellite Systems (GNSS) measurements, Light Detection and Ranging (LiDAR), digital photogrammetry, interferometric synthetic aperture radar (InSAR) and high resolution satellite images (Hsing-Chung *et al.*, 2004; Jaboyedoff *et al.*, 2012). The classic field survey for spot height measurement using portable RTK (Real Time Kinetic) GPS is conceivable only for small areas (Schmidt and Persson, 2003), the procedure is labour intensive over large areas. Spot elevation values can be derived over wide areas from aerial photography and photogrammetric techniques (Schmidt and Persson, 2003). Aerial photographs provide fairly high resolution DEMs for landslide inventory mapping (Guzzetti *et al.*, 2012) but are considered not adequate to represent hydrological features, particularly in complex urban environments, or where dense vegetation is prevalent (Haugerud and Harding, 2001; Tenenbaum *et al.*, 2006). This calls to question its application in a transport corridor environment. Spot height values derived from SAR sensors can also be used in generating high resolution DEMs using SAR interferometry (also known as InSAR) where the difference in the signal from two separate SAR antennae are used to construct a map of surface elevation (Rosen *et al.*, 2000; Mather and Koch, 2011a). However, InSAR signals can be perturbed by different land covers, particularly vegetation (Rosen *et al.*, 2000) and as a result is not as accurate as airborne laser scanning (ALS) systems for generating DEM (Hsing-Chung *et al.*, 2004). The ALS technique (also referred to as LiDAR) enables the acquisition of high-resolution elevation point clouds of the topography from which accurate and precise high resolution digital representations of the topographic surface can be obtained for areas (Shan and Toth, 2008). Terrain data derived from ALS has been shown to be useful for depicting fine scale features such as roads and culverts (Hollaus *et al.*, 2005), which are known to influence the accuracy of terrain derived indices such as the terrain wetness index (Tenenbaum *et al.*, 2006).

The ALS system is an active measurement technique that transmits discrete pulses towards the earth while flying specific survey routes (Petrie and Toth, 2008). Aircraft or helicopter mounted ALS systems allow for timely acquisition of high density elevation data over large areas, with its relative cost effectiveness in terms of the quality and quantity of data generated making it a popular source of elevation data for high resolution terrain mapping (Jaboyedoff *et al.*, 2012). The ALS system is an active measurement technique that transmits discrete pulses towards the earth while flying specific survey routes (Petrie and Toth, 2008). Under favourable weather conditions, very high resolution DEMs of less than 1 m, with errors better than 25 cm can be derived from the ALS point cloud (Hollaus *et al.*, 2005). In forested areas, the ALS's capability of canopy penetration as a result of actual ground hits by some of the emitted discrete pulses enables quantitative descriptions of the topographic surface in these areas (Maune, 2008). To ensure maximum capture of returns representing actual ground hits, automatic and semi-automatic procedures using filtering algorithms are employed to eliminate the topographic return from the returns due to vegetation canopy and other surface obstructions (Haugerud and Harding, 2001). ALS DEMs have been reported as providing suitable representation of topography for detailed scale slope stability assessments (Baum *et al.*, 2005; Schulz, 2007; Hardy *et al.*, 2012).

2.6 Soil moisture characterisation using terrain analysis

Shallow translational failures along slope faces are often associated with short and intense rain storms (Jaiswal *et al.*, 2010b). These storms build up antecedent soil moisture largely related to soil's physical properties and generate surface runoff that flow to zones of moisture accumulation mostly controlled by topography (Jaiswal *et al.*, 2010a). Antecedent soil (Tarboton *et al.*, 2009) moisture and flow accumulation are two important factors that greatly influence instability in natural slopes (Fourie, 1996) and their importance become more pronounced in detailed scale analysis (Van Westen *et al.*, 2008). Difficult terrain and the labour intensive nature of mapping soil moisture using traditional techniques tend to limit the spatial coverage of available soil moisture data (Hardy *et al.*, 2012). Remote sensing techniques employing both passive and active microwave systems have been developed and applied to characterise soil moisture in different environment (Lobell and Asner, 2002; Baghdadi *et al.*, 2005; Zheng *et al.*, 2005; Pierdicca *et al.*, 2010). However, these techniques are constrained by poor spatial resolution and the presence of dense vegetation (Schmugge *et al.*, 2002; Hardy *et al.*, 2012).

Topography is known to exert significant influence on local and regional hydrology, as such DEMs are widely used to derive information for modelling of hydrological processes (Tarboton *et al.*, 2009). Terrain-based flow models are built on a basic underlying assumption that surface and near surface water essentially move downslope draining steeper terrain and converging in plains (Sørensen *et al.*, 2006). The development of a digital flow field and computation of upland contributing area draining through each grid cell within the flow field provides the basis for the computation of a range of flow related indices (Tarboton *et al.*, 2009). Topography wetness index (TWI) is perhaps the most popular DEM derived index used to describe the spatial pattern of soil moisture (Sørensen *et al.*, 2006). The TWI takes into account the local slope geometry and local upslope contributing area in quantifying the topographic control on hydrological processes. The concept of TWI was first presented by Beven and Kirkby (1979) within the runoff model TOPMODEL. Traditional TWI which hereafter will be referred to as classic TWI can be expressed by:

$$TWI = \ln\left(\frac{a}{\tan\beta}\right) \qquad \text{Equation 2.6}$$

Where a is the local upslope area draining through a specific pixel per unit contour length and β is the local slope (Sørensen *et al.*, 2006). The tangent curvature of the slope provides a measure of flow convergence or divergence, while the upslope area is indicative of the potential area contributing to flow draining through a unit contour length (Western *et al.*, 1999). Intrinsically, as the upslope area increases and slope steepness decreases, classic TWI and soil moisture content increase (Sørensen *et al.*, 2006). The application of classic TWI in slope stability studies stems from this unique relationship, as high soil moisture content is often confined to areas of topographic convergence which in turn are associated with higher occurrence of slope failure (Sørensen *et al.*, 2006; Sørensen and Seibert, 2007). As a result, classic TWI has been used to model spatial scale effects on hydrological processes (Wood *et al.*, 1988; Penna *et al.*, 2009), analysing soil moisture pattern in forested areas (Tenenbaum *et al.*, 2006), characterisation of soil moisture in transport corridor environment (Hardy *et al.*, 2012) as well as in evaluating moisture contribution to slope stability assessment (Borga *et al.*, 2002; Baum *et al.*, 2005; Miller *et al.*, 2012). Tenenbaum *et al.* (2006) explained that the classic TWI values are expressions of subsurface flows and propensity to wetness and as such, not to be considered as direct prediction of soil moisture content.

Classic TWI computations are normally derived from gridded elevation data and the best results have been obtained over undulating terrains (Schmidt and Persson, 2003). Schmidt and Persson (2003) reported good correlation between measured surface moisture and generated classic TWI values obtained from a 3 m DEM. The study sites located in Central Sweden and North East Germany revealed best results over undulating terrain where the effects of topography on overland flow is more evident, while low relief areas typically characterized by flow convergence performed rather poorly (Tenenbaum *et al.*, 2006). Barling *et al.* (1994) in an earlier study had established that topography plays no significant contribution to soil moisture distribution in areas characterized by an overall shallow slope angle of six degrees or less. Studies by Tenenbaum *et al.* (2006) showed that in addition to undulating terrain, higher correlation between measured soil moisture and DEM derived classic TWI values are attained under wetter conditions. The study compared soil moisture measurements to classic TWI calculations derived from DEMs with spatial resolutions ranging from 0.5 m to 30 m, over a forested area with undulating terrain, and a relatively low relief suburban area in Baltimore, USA.`

A number of other studies have established classic TWI as a useful predictor for the spatial distribution of surface moisture (Western *et al.*, 1999; Sørensen *et al.*, 2006). Classic TWI is mainly used to characterize long-term terrain moisture status in relation to landscape processes (Hardy *et al.*, 2012). Several studies have focused on improving classic TWI to simulate soil moisture more accurately (Sørensen *et al.*, 2006; Ma *et al.*, 2010). The various approaches have essentially entailed (1) integration of other topographic parameters such as curvature, aspect, potential solar radiation and relative terrain position to improve the index's prediction capability (Western *et al.*, 1999; Tenenbaum *et al.*, 2006; Ma *et al.*, 2010; Hardy *et al.*, 2012), (2) the measure of local terrain slope to be used in the estimation of local hydrological gradient (Sørensen *et al.*, 2006) and more importantly (3) the improvement of flow direction algorithms (O'Callaghan and Mark, 1984; Quinn *et al.*, 1995; Tarboton, 1997).

Traditionally, individual upstream cell contributions are transferred along steepest downslope direction to one or more of the eight neighbouring cells. The most common procedure for routing flow over a terrain surface represented by a grid DEM is the eight-directional method commonly referred to as the deterministic eight-node (D8) algorithm

(O'Callaghan and Mark, 1984). The single flow direction method (D8) works well in valleys but is known to introduce grid bias, produces parallel flow lines and is problematic near catchment boundaries (Tarboton, 1997). In cases where the steepest descent cannot be established, a broader search radius or random selection from among grid tiles is used. The D8 approach is limited because it can assign flow to only one of eight possible directions; each separated by 45^{o} in a square grid. In addition the D8 handles poorly flow routing in relatively flat terrain. The method developed by Garbrecht and Martz (1997) presented a means for routing flow across plains. The approach improves on the D8 by routing flow both away from higher terrain and towards lower terrain thus overcoming the limitations associated with routing flow across plains (Costa-Cabral and Burges, 1994).

Multiple flow direction methods have also been proposed by various authors (Freeman, 1991; Quinn *et al.*, 1991; Tarboton, 1997; Seibert and McGlynn, 2007). These approaches proportion the outflow from each element between one or more downslope elements, introducing dispersion (spreading out) of the flow with the goal to represent downslope flow in an average sense (Figure 2.6). Wolock and McCabe (1995) showed that smoother classic TWI patterns and higher classic TWI values are generated using multiple flow direction (MFD) algorithms in contrast to single flow routing (SFD) algorithms which are more sensitive to small errors in elevation. In addition, MFD algorithms produce more realistic representations of contributing areas in upslope area calculation and are able to resolve the problem of flow dispersion overestimation (parallel unrealistic flow paths) (Quinn *et al.*, 1991; Gallant and Wilson, 1996).

The D-infinity (D∞) multiple flow direction model (Tarboton, 1997) represents flow direction as a vector along the direction of steepest downward slope on eight triangular facets centred at each grid cell. Flow from a grid cell is shared between the two downslope grid cells closest to the vector flow angle based on angle proportioning (Tarboton, 1997). Siebert and McGlynn (2007) introduced MD∞ (an extension to D∞) that combines ideas from Tarboton (1997) with Quinn et al. (1991). The MD∞ approach calculates slopes on triangular facets, but then proportions the flow between multiple downslope directions on triangular facets, thereby accounting for divergent situations where flow between more than two downslope grid cells is likely.

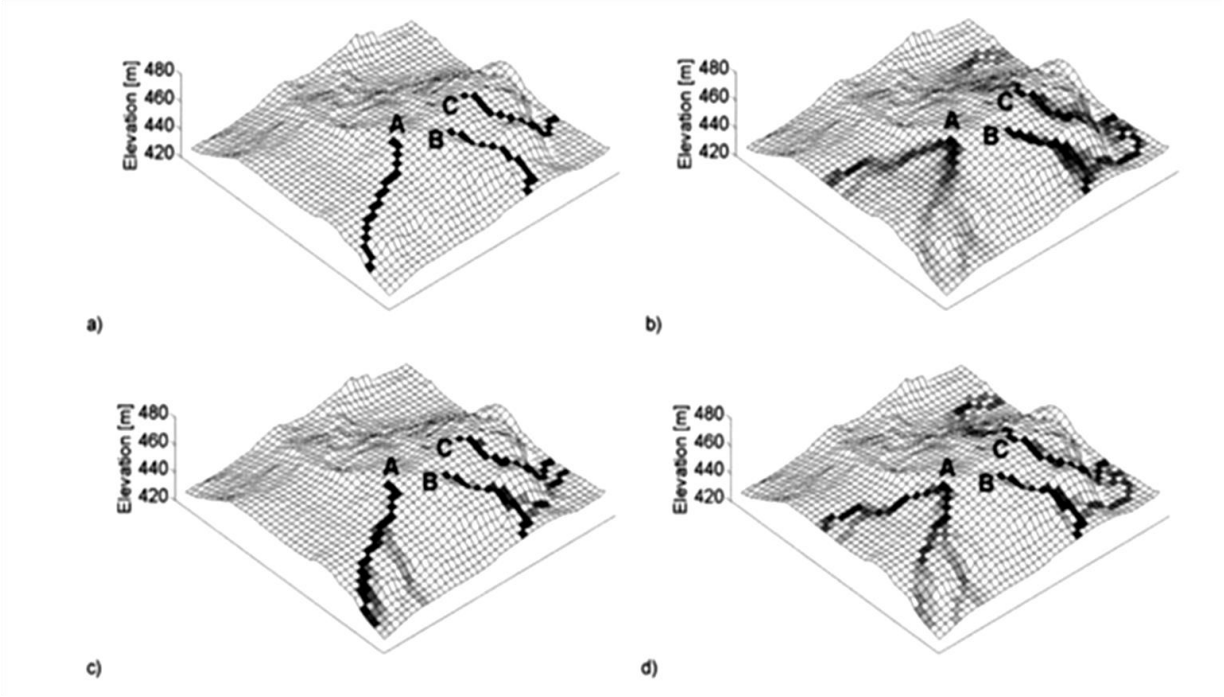

Figure 2.6: Effects of different flow algorithms on downslope routing of flow from three cells (A,B and C) on a 20m DEM for an area in Central Sweden using: (a) single flow routing D8 (O'Callaghan and Mark 1984), (b) Multiple flow direction MD8 (Quinn et al 1991), (c) D∞ (Tarboton 1999) (d) MD∞ (Siebert and McGlynn 2007). From Siebert and McGlynn (2007)

A major criticism on the use of classic TWI is that the TWI computation is deemed to oversimplify overland flow as it assumes homogeneity for soil types, no vegetation cover and that the entire upslope contributing area flow accumulation is relatively unaffected by processes of infiltration and evapotranspiration (Barling *et al.*, 1994). This limitation in classic TWI computation has led to the development of quasi and fully dynamic wetness indices that better reflected the contributions of the spatial variability in soil types and the incorporation of temporal dimensions, taking into account hydraulic functions such as saturated hydraulic conductivity (Cho and Lee, 2001), subsurface flow (Reid and Iverson, 1992), discharge rates and drainage porosity (Iverson, 2000) to calculate the effective upslope contributing areas per unit width of contour (Barling *et al.*, 1994; Borga *et al.*, 2002)

The approach of Barling *et al.* (1994) and Borga *et al.* (2002) does not differ greatly from the physical based models in Section 2.4.5.3, in terms of the significant amount of input data required, hence detracting from the original advantage of the use of classic TWI as a

surrogate measure for characterising soil moisture distribution with less reliance on field measured data (Sørensen and Seibert, 2007; Hardy *et al.*, 2012). More recently, Tarboton *et al.* (2009) proposed a weighted flow grid approach (incorporated into a terrain based flow data model) that extends the influence of integration of multiple data through flow accumulation propagation. This enables the inclusions of soil and vegetation information into the calculations of flow related quantities. The approach allows for the definition of flow algebraic functions that enable the evaluation of the contributions of the individual input data (vegetation and soil) in extending the concepts (flow accumulation) captured by recursive calculations of a weighted contributing area. For example, runoff from upstream grid cells can be computed taking into consideration the opportunity for infiltration downslope, as runoff is generated only when the downslope infiltration capacity has been exceeded. However, such an approach requires knowledge of the hydraulic properties of the soils in the study area (Tarboton *et al.*, 2009).

2.7 Issues of DEM resolution and grid sizes

The scale of study, the characteristic area and terrain element to be extracted are often the most important considerations in the choice of DEM resolution (Wu *et al.*, 2008b). An appropriate DEM resolution is one that sufficiently represents the interested features within the area of interest (Gritzner *et al.*, 2001). High resolution topographic information has been shown to better represent topographic influences on surface flow routing and susceptibility of a slope to landsliding (Dai and Lee, 2002; Ma *et al.*, 2010). Important thresholds illustrating slope gradients and morphology that have the most influence on the occurrence of landslide within a study area are easily identifiable at finer grid resolution. However, this information becomes blurred with reduction in grid resolution (Van Westen *et al.*, 2008). The selection of the optimal spatial resolution is central to all environmental related analysis involving the use of digital elevation data (Aryal and Bates, 2008). For example detailed studies generally require higher spatial resolution data for more detailed information, as terrain elements in lower resolutions are comparatively more generalised and derived terrain indices less meaningful (Gritzner *et al.*, 2001; Wu *et al.*, 2008b; Li *et al.*, 2011).

The use of high resolution data in hydrological modelling in addition to being often computationally intensive can also result in the introduction of unwanted perturbations to flow direction and slope angles (Sørensen and Seibert, 2007; Chen and Li, 2012). Thus the

selection of an appropriate grid resolution for hydrological modelling is often a trade-off between minimised computational requirement and retention of realistic model performance (Gritzner *et al.*, 2001; Tenenbaum *et al.*, 2006). Lower resolution DEM generally exhibit smoother terrains and shorter flow paths (Zhang and Montgomery, 1994), with maximum and mean slope values significantly decreasing with decrease in DEM resolution (Vaze and Teng, 2007). As such terrain derived hydrological indices are often less perturbed due to relatively reduction in the presence of micro-topography with reduction in DEM resolution. Endreny and Wood (2003) showed that there is considerable spatial variability in generated runoff flow path with varying spatial resolution.

2.8 Conclusion

This chapter has provided a critique of the various qualitative and quantitative techniques for modelling landslide susceptibility. The strength and weakness of the various techniques were enumerated with a view to ascertaining their suitability for landslide susceptibility in a transport corridor environment. The qualitative methods have been shown to produce highly accurate results when executed by experienced experts (Van Westen *et al.*, 2008). The field based approaches allow for susceptibility assessment of every locality separately without the need to incorporate a simplification of causal relationships typically required for most of the other methods. Assignment of weights and ratings to factors and their categories respectively is usually at the discretion of the investigator (Ruff and Czurda, 2008). This subjective nature is considered as a major setback and limits its application in engineering scale studies as a result of its associated level of uncertainties (Kanungo *et al.*, 2009).

Quantitative methods (statistical, deterministic and probabilistic) are more objective due to their data-dependent character and the fact that the analysis is less reliant on expert judgement. The deterministic approach has a strong theoretic base and uses physical laws to clearly describe the underlying processes responsible for instability (Harp *et al.*, 2009). The results obtained are considered to be a closer representation of reality and more consistent in comparison with those of the heuristic and statistical models (Van Westen *et al.*, 2008). When properly calibrated, deterministic slope stability assessments are generally assumed to have distinct advantages over the heuristic and statistical models which are more prone to epistemic and aleatory uncertainties. However, concerns of its high data demand, challenges with parameterization of heterogeneous variables and extrapolation of results render the

technique prohibitive when considered for detailed scale assessment of slope over considerable expanse as is the case with transport corridors (Aleotti and Chowdhury, 1999; Cascini, 2008).

The statistical approach compares spatial distribution of landslides with the various causal factors that are considered influential to slope stability. Quantitative or semi-quantitative estimates are then made for areas currently free of landslides, but where similar conditions exist. Statistical approaches are based on the observed relationships between each factor and distribution of landslides. The approach is robust and versatile as evident by the vast number techniques proposed within the statistical framework. Regression models are effective in establishing linear and log-linear relationships between the causal factors but perform poorly in areas characterized by complex landslides. The use of models employing advanced statistical and machine learning techniques have been shown to sufficiently capture non-linear relationships between causal factors. Generally, being essentially data-driven, statistical models are not readily extrapolated to the neighbouring areas and are encumbered by issues of over-simplification. As such, statistical methods are considered best suited for regional to large area studies (Carrara *et al.*, 1991).

The use of probabilistic models in slope stability assessment is frequently encountered in literature and has been successfully applied to detailed and regional scale studies. These models effectively handle the natural variability of geotechnical parameters and the uncertainties associated with boundary conditions. The probabilistic method is flexible, robust and permits the integration of soft computing techniques like fuzzy logic, neural networks and evidential reasoning. Fuzzy logic and evidential belief function approaches have the capability of dealing with data incompleteness (ignorance) and vagueness (fuzziness) which are among the most common uncertainties associated with landslide modelling. The evidential belief function approach exhibits higher predictive capability in comparison with the fuzzy logic approach (Tien Bui *et al.*, 2012).

3 Study Area and Datasets

3.1 Study area

The study area comprised an eight kilometre stretch of road and rail network within the Newcastle-Carlisle transport corridor located around Haltwhistle in the North East of England. The section consists of the A69 trunk road, the Haltwhistle by-pass, a number of highway embankments, an extensive stretch of railway embankments and cuttings. The railway section comprised a double track rail line which is associated with a history of persistent instability in recent years and has been the focus of a number of studies (Hardy *et al.*, 2012; Miller *et al.*, 2012). Occurrences of numerous minor landslides after episodes of prolonged rainfall are common within the aging railway infrastructure constructed over a century ago (Perry *et al.*, 2003a).

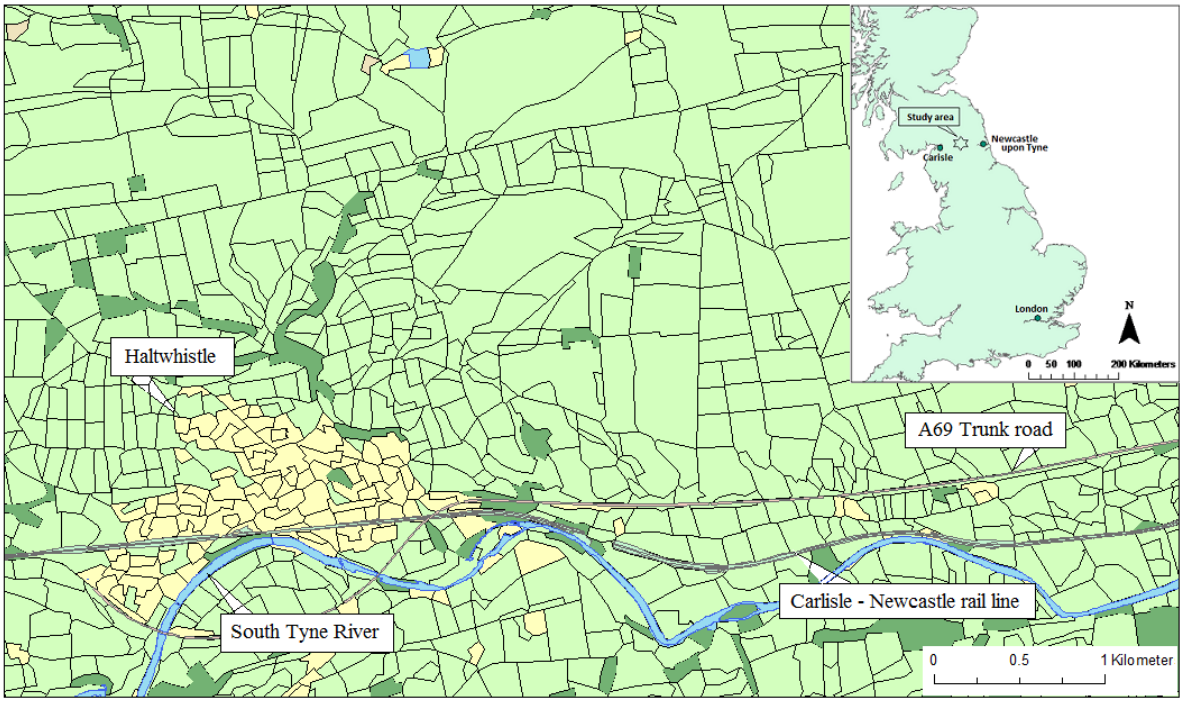

Figure 3.1: Location of Carisle-Newcastle transport corridor around Haltwhistle, illustrating proximity to the South Tyne River. © Crown copyright 2014. An Ordnance Survey EDINA supplied service.

3.2 Land use and vegetation

The transport corridor lies within a glacial trough valley floor characterised by the relatively flat floodplains of the South Tyne River, with sections of the railway embankments situated

in close proximity to the river (approximately 15 m). The surrounding landscape supports considerable nucleated settlements that have expanded up the valley sides. The valley floor is generally open ranged grassland with tree cover concentrated along tributary routes. The land use of the surrounding agricultural areas is mainly pasture with well-defined field boundaries made up of a mixture of hawthorn hedges with hedgerow trees and stone walls. The agricultural fields within the valley floor support a mixture of arable and dairy farming. Some portions of these pasture lands are poorly drained and as such, characterised by high antecedent moisture content which often results in the periodic waterlogging of such areas (see Figure 3.2). The adjoining upland agricultural areas that form the broader catchment are situated on the valley sides of the glacial trough (the Tyne gap) between the North Pennies and the Northumberland Uplands. Comprising mainly pasture land used for sheep and dairy farming, the valley sides are characterised by mixed scale field pattern defined by hedges, wire fencing and, at some locations, stone walls (see Figure 3.3).

Typical vegetation conditions within the study area are representative of those found across Northern England (Lim *et al.*, 2007; Miller *et al.*, 2009). The study area is predominantly made up of a mixture of grasses, agricultural weeds, shrubs and semi-matured trees and bare earth slopes interspaced by stretches of dense deciduous woodlands. The woodlands exist as semi-natural and mixed conifer plantations confined to tributary valleys or within semi-natural woodland estates. Improved pasture lands are more prevalent to the west of the valley sides typically characterised by steeper slopes with increasing arable component in the east where shallower slopes dominate. The hill slopes are reasonably wooded with small to medium sized broadleaf and coniferous woods providing a network of tree cover (see Figure 3.4). The northern slopes have in places, semi-natural woodland, areas of coniferous plantation situated within large estates and shelterbelts extending into surrounding farmland. At higher elevations, notably towards the north, rough grazing and moorland dominate, while the southern slopes are characterised by large coniferous forests south of the River Tyne.

Figure 3.2: Seasonally water logged fields situated on the valley floor, with considerable upland contribution from adjoining agricultural fields.

Figure 3.3: South facing earthwork cutting at Whitchester, showing the general undulating terrain. Adjoining fields are used for pasture farming.

Figure 3.4: A cutting earthwork approximately 2.6 km east of Haltwhistle. The adjoining fields indicate the heterogeneous nature of the vegetation cover in the study area.

3.3 Geology

The Tyne gap is underlain by Carboniferous rocks (345 to 280-million-years-old) which dominate the bedrock geology of northern England (Bott, 1987). The Yoledale group is the dominant lithological unit in the southern Northumberland trough where the study area is situated. The Yoredale group (Lower and Middle Coal Measures) consists of a cyclic succession of bioclastic limestones, sandstones, mudstones, siltstones and coals (Johnson *et al.*, 1995). The coal measures represent the fossilised remains of swamp vegetation which grew as luxuriant forests on the deltas, while the mudstones were deposited under shallow marine conditions (Johnson *et al.*, 1995). The Yoredale group is interpreted as being the result of alternating periods of relatively slow and rapid subsidence of the area, a reflection of a complex marine and non-marine deltaic conditions that existed during the deposition of the Group (Johnson *et al.*, 1995; Waters and Davis, 2006; Waters *et al.*, 2007). The Group outcrops as the Tyne Limestone Formation, the Alston Formation and the Stainmore

Formation at different locations of the study area. (Waters *et al.*, 2007). The underlying bedrock geology significantly influences the physical and hydrological properties of the soils across the study area (Mackney *et al.*, 1983). At the end of the Carboniferous period, volcanic activity resulted in the emplacement of wide spread igneous intrusions in a number of locations across Northumberland basin; an example of which is the Great Whin Sill, a doleritic outcrop that runs as a narrow, rolling east-west ridge north of the Tyne valley and is well exposed near Haltwhistle (Johnson *et al.*, 1995). The bedrock geology of the study area and adjoining catchment is presented in Figure 3.5.

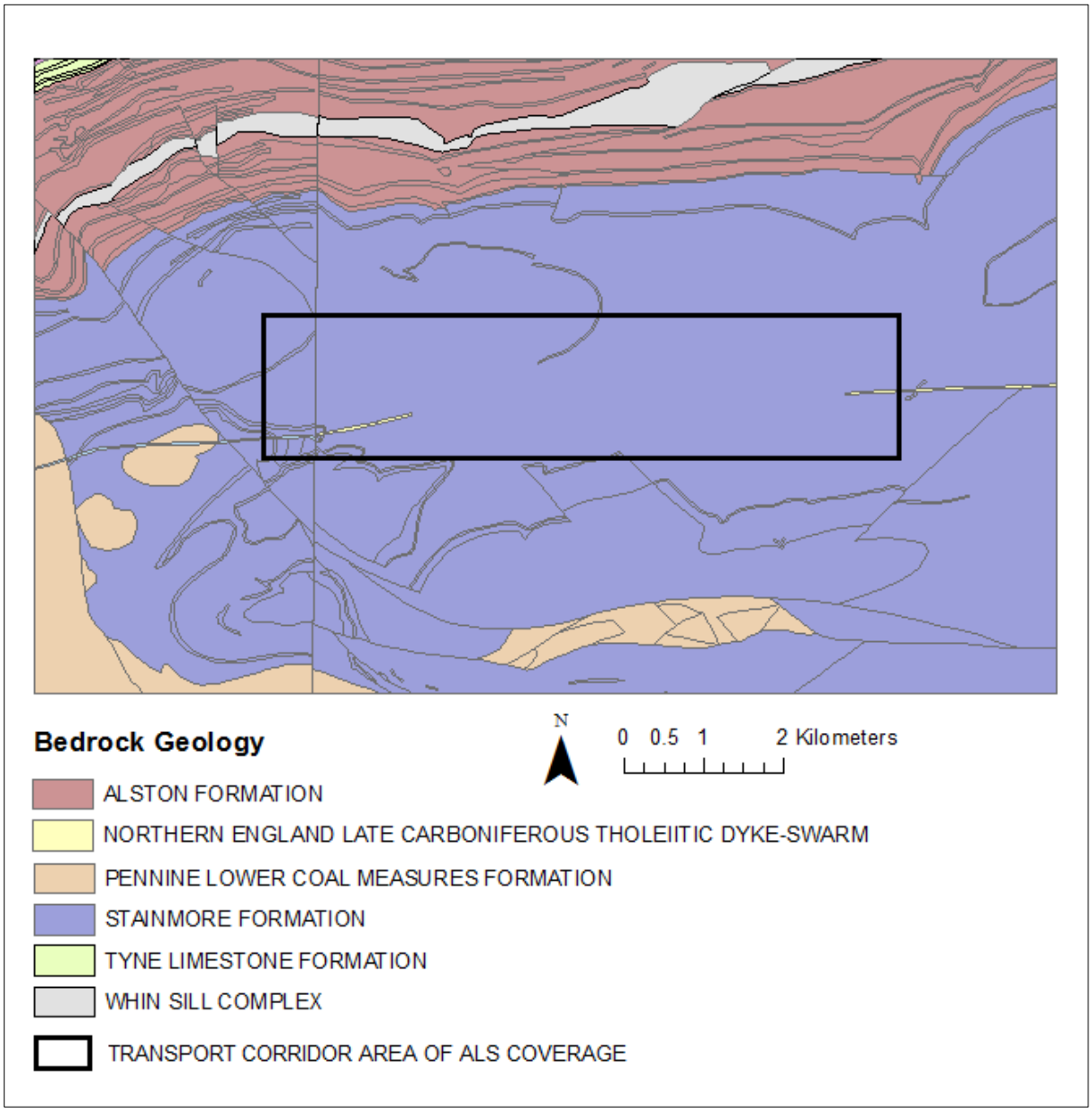

Figure 3.5: Bedrock geology of the study area and adjoining catchment, highlighting the area covered by the Airborne Laser Scanning dataset. © Crown copyright 2014. An Ordnance Survey EDINA supplied service.

On top of the Bedrock Geology lies a Quaternary drift geology resulting from temperate climate periods interrupted by repeated advances and retreats of glaciers and ice sheets. The resulting drift geology is a basin covered by a thick layer of sediments deposited during the last main glacial period of the Ice years. The drift geology is essentially made up unsorted glacial tills (boulder clay), peat, with small areas of glacio-fluvial sands and gravels lining

the wider floodplains of the South Tyne River and tributaries, with alluvial silts along the river courses (Johnson *et al.,* 1995).

3.4 Previous studies

The study area is characterised by incessant failures and had been the focus of many studies. Numerous detailed geotechnical investigations have been carried out on failed slopes in the transport corridor (Network Rail, 2005). These investigations provided information on the physical and geotechnical properties of the earthwork cuttings and the underlying soil formations. Results from instrumented boreholes revealed the geotechnical properties of subsurface soils and the hydrological conditions around the earthworks. A series of studies on the application of remotely sensed data for the characterisation of soil moisture and prediction of zones of instability along this section of transport corridor commenced with the acquisition of the airborne laser scanning (ALS) dataset in October 2006, July 2007 and April 2008 and the compact airborne spectrographic imaging (CASI) imagery in September 2007. Lim *et al.* (2007) assessed the positional accuracy of the acquired ALS dataset using check point analysis and found its positional accuracy to be within 10 cm in both plan and elevation. Hardy *et al.* (2012) used terrain analysis calculations and Ellenberg values computed for the different vegetation cover to mapped soil moisture on the transport corridor earthwork embankments. The study developed a reliable and inexpensive means of characterising soil moisture in transport corridor earthworks.

Miller *et al.* (2012) developed a deterministic model for the prediction of zones of instability in the transport corridor. The study utilised the enormous geotechnical data generated during the detailed scale geotechnical assessment of failed earthworks to parameterise the process based model. All of these studies were however limited to the transport corridor with little consideration given to catchment contributions.

3.5 Datasets

A significant component of performing a landslide zonation regardless of the approach adopted for the landslide analysis, involves collection and management of study area data on past landslides, environmental conditions, triggering factors and the potential risk at occurrence. The choice of datasets for this study was guided by a comprehensive reconnaissance survey, numerous field visits, discussions with engineers at Network Rail, the company responsible for earthwork condition appraisals, and previous studies on the

study area. The datasets used in this study are primarily a collection of spatial data layers representing factors considered relevant for landslide susceptibility assessment across the transport corridor. These datasets can be broadly grouped into two types. (1) high spatial resolution datasets limited to the transport corridor, and (2) datasets of coarser spatial resolution covering the adjoining catchment area. The need to incorporate the contributions of the broader catchment within the slope stability assessment stems from the fact that the influence of the broader scale topography (adjoining upland terrain which rises to the north and south of the corridor) is expected to significantly contribute to zones of localised saturation within the transport corridor slope and embankments. This section details the various datasets employed in the study and the nature of data pre-processing employed. A compilation of all the datasets, their characteristics and sources is presented in Table 3.1.

3.5.1 Topography

3.5.1.1 Lidar data acquisition and pre-processing

Airborne laser scanning (ALS) data were acquired over 8 km stretch of road and rail network between Newcastle and Carlisle in July 2007 from a helicopter mounted Optech ALTM discrete return sensor. The sensor with a pulse frequency of 50 kHz produced high spatial resolution coverage with a nominal point spacing of 20 points/m^2 . Small format colour and near infra-red digital aerial imagery at a resolution of 5 cm was also acquired contemporaneously alongside the ALS data for the purpose of providing supplementary information during the interpretation of the ALS data. The position, orientation and timing information for captured images were recorded with a separate IMU. These information in addition to the camera calibration files were used to generate orthorectified images of the transport corridor. The ALS data extends for 100m on both sides of the A69 trunk road and rail route.

Table 3.1: Overview of dataset used in the study

	Data type	Information	Format	Dataset Resolution	Source
1	Topography				
	Digital terrain model	A. Airborne laser scanning data acquired in July 2007	ESRI grid	20 points/m^2	Geomatics Group UK
		B. Land-Form PROFILE 10m DTM acquired from MasterMap dataset	ESRI grid	1:10,000	Ordnance Survey
	Map data	C. Vector mapping data	ESRI Shape file (polylines and polygons)	1:2,500	Ordnance Survey
2	Land cover				
	Multispectral imagery	A. Compact Airborne Spectrographic imagery acquired in September 2007	ERDAS Imagine Grid	1:600	Geomatics Group UK
	Vector	B. Land cover map (LCM 2007)	ESRI Shape file (polygons)	1:25,000	Centre for Ecology and Hydrology UK
3	Geology				
	Vector	Geological map	ESRI Shape file (polygons)	1:50,000	British Geological Survey UK
4	Soil				
	Vector	A. National Soil map NATMAP	ESRI Shape file (polygon)	1:250,000	National Soil Resources Institute (NSRI) Cranfield University UK
		B. Hydrology Of Soil Types (HOST) data	ESRI Shape file (polygon)	1:100,000	National Soil Resources Institute (NSRI) Cranfield University UK
5	Precipitation				
	MIDAS dataset	Mean daily rainfall values from 2000 - 2010 (Haltwhistle weather station)	Excel tables		British Atmospheric Data centre UK
6	Landslide Inventory				
	Merlin dataset	Frequently maintained cutting and embankment locations	ESRI Shape file		Network Rail UK

During the ALS data acquisition, some specially built checkpoint targets were purposefully distributed on either side of the transport corridor and throughout the areas to be covered by the ALS (Lim *et al.*, 2007; Miller *et al.*, 2009). Conventional photogrammetric targets were also evenly distributed across the ALS surveyed area. This was done to further increase redundancy and obtain representative coverage of locations against which the positional accuracy of the acquired ALS data could be assessed. All checkpoints were surveyed using rapid-static GPS prior to the survey flights. A detailed overview of the checkpoint analysis and error assessment procedures is presented in Lim *et al.* (2007). The ALS data were processed in TerraScan software, with nonground points classified and removed following the procedures presented in Soininen (2014). The ALS point cloud was imported into TerraScan and filtered for noise, pits and birds by screening for absolute elevation limits, isolated points and height above ground (Brovelli and Lucca, 2012; Soininen, 2014).

Terrascan employs the Axelsson's algorithm (Soininen, 2014) that derives a TIN network from neighbouring minima as a first approximation of the bare ground and then utilises a cost function based on the second derivatives of elevation difference to classify vegetation cover and buildings (Brovelli and Lucca, 2012). The classification procedure allows user defined parameters such as the maximum building size (edge length of the largest building), the iteration angle (maximum angle between points), the terrain angle (steepest terrain slope) and the iteration distance (maximum distance from a point to a triangle plane during iteration). The routine builds an initial model from selected low points, and then models upwards by iteratively adding a new point to the classified ground hits. The predefined iteration parameters determine how close a point must be to a triangular plane to be accepted by the model. A maximum building size of 30m was used to ensure that the filtering routine selects local low points that are confident ground hits around a 30 by 30 m area (Brovelli and Lucca, 2012; Soininen, 2014). An iteration angle of 6^{o} was selected as a compromise between higher values (typically used for hilly terrain) that permit considerable spacing between points thus reducing the addition of unnecessary point density and the low values that allow for higher point density to better represent topography variation in flat areas (Soininen, 2014). A terrain angle of 60^{o} and iteration distance of 1.40 m ensured the avoidance of unnecessary point density being added to the ground model. The resulting digital terrain model (DTM) was then imported to ArcGIS and resampled to a regular 0.5 m grid.

Artificial pools resulting from false digital dams due to the DTM's inability to recognise the presence of culverts, storm sewer, flood control structures and other draining structures along flow routes intersected by roads and bridges are common defects when computing flow accumulation from high resolution DTMs. A measure of DTM correction was carried out on the resultant ALS DTM to ensure that overland flow is in no way inhibited due to the presence of digital dams. Conventional breaching techniques can artificially lower the DTM along the alignment of the subsurface drainage structure to allow flow accumulation through the digital dam during terrain processing (Hutchinson, 2013). One particular implementation of this is the drainage enforcement option in the topo-to-raster tool in ArcGIS which recalculates elevation data at digital dam locations identified by dam breaks. The dam breaks are digitised sections of the drainage network that intercept the digital dams. The drainage sections (short breach arcs) are normally digitised in the downstream direction as specified by the topo-to-raster tool in ArcGIS. This approach was however considered inadequate for bridge sections that span considerable distances. Consequently, a semi-automatic procedure in TerraScan was utilised to recognise ground points representing sections of bridge structures responsible for digital dam formation. The spot heights at these locations were further refined to reflect the surrounding ground terrain by manually editing. The reconditioned DTM is presented in Figure 3.6.

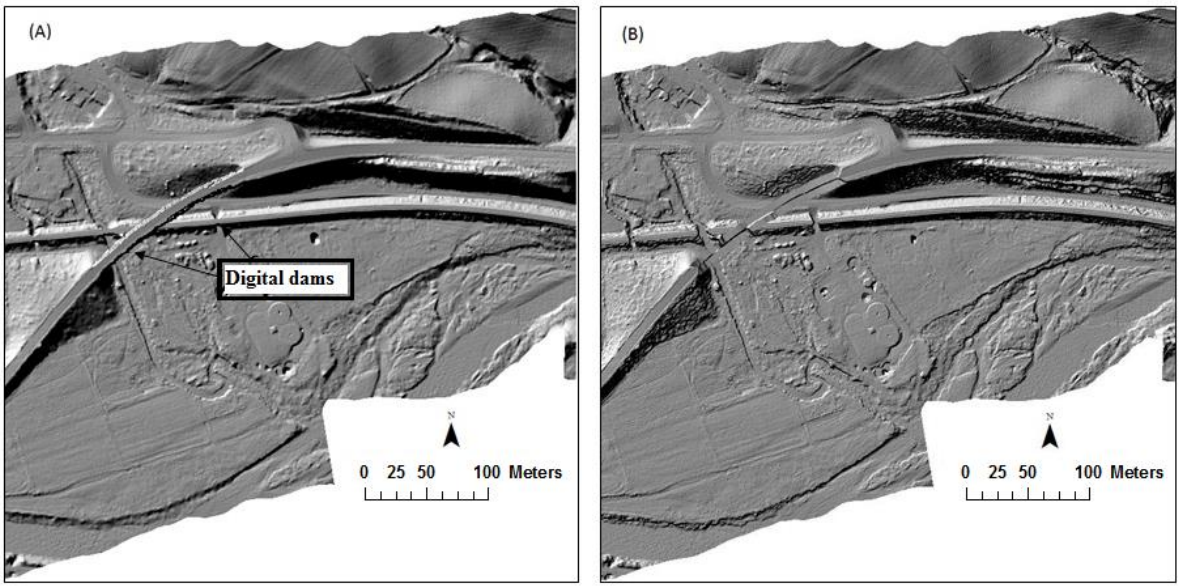

Figure 3.6: Results of removal of digital dams from the ALS digital terrain model of transport corridor. (A) DTM with digital dam, (B) Corrected DTM

3.5.1.2 Land-Form PROFILE 10m DTM

A total catchment area of 72 km^2 was employed for the evaluation of catchment contribution to moisture accumulation in the transport corridor. The area covers a little more than the entire stretch of the section of the Newcastle – Carlisle transport corridor investigated and 4 km on either side (north and south) of the transport corridor (see Figure 3.7). Hence, additional elevation information on the broader catchment adjoining the transport corridor was derived from the Ordnance Survey (OS) Land-Form PROFILE 10m DTM. The Land-Form PROFILE 10m DTM is a terrain height dataset with the highest resolution available nationwide, providing height data at a scale of 1:10,000 for the entire United Kingdom. The Land-Form PROFILE 10m DTM data was derived from the Land-Form PROFILE contour lines product and supplied in 5km by 5km tiles, with a grid size of 10m. The Land-Form PROFILE contour data from which height information utilised for the DTM generation was derived were produced from aerial photography and ground surveyed methods for densely forested areas or locations not clearly visible on the photography (Ordnance Survey, 2012). The vertical accuracy of the DTMs varies with location, as it is dependent on the density of the height data contained in the contour file. Flat areas with relatively few contour lines (widely spaced) are characterised by minor

irregularities often evident as slight terracing of the terrain, in contrast to hillier areas with more contours and more accurate DTM. The Land-Form PROFILE DTM product has a vertical accuracy of 0.3 m (Ordnance Survey, 2012). Height data of the adjoining catchment area around the transport corridor was downloaded from EDINA Digimap site at the University of Edinburgh.

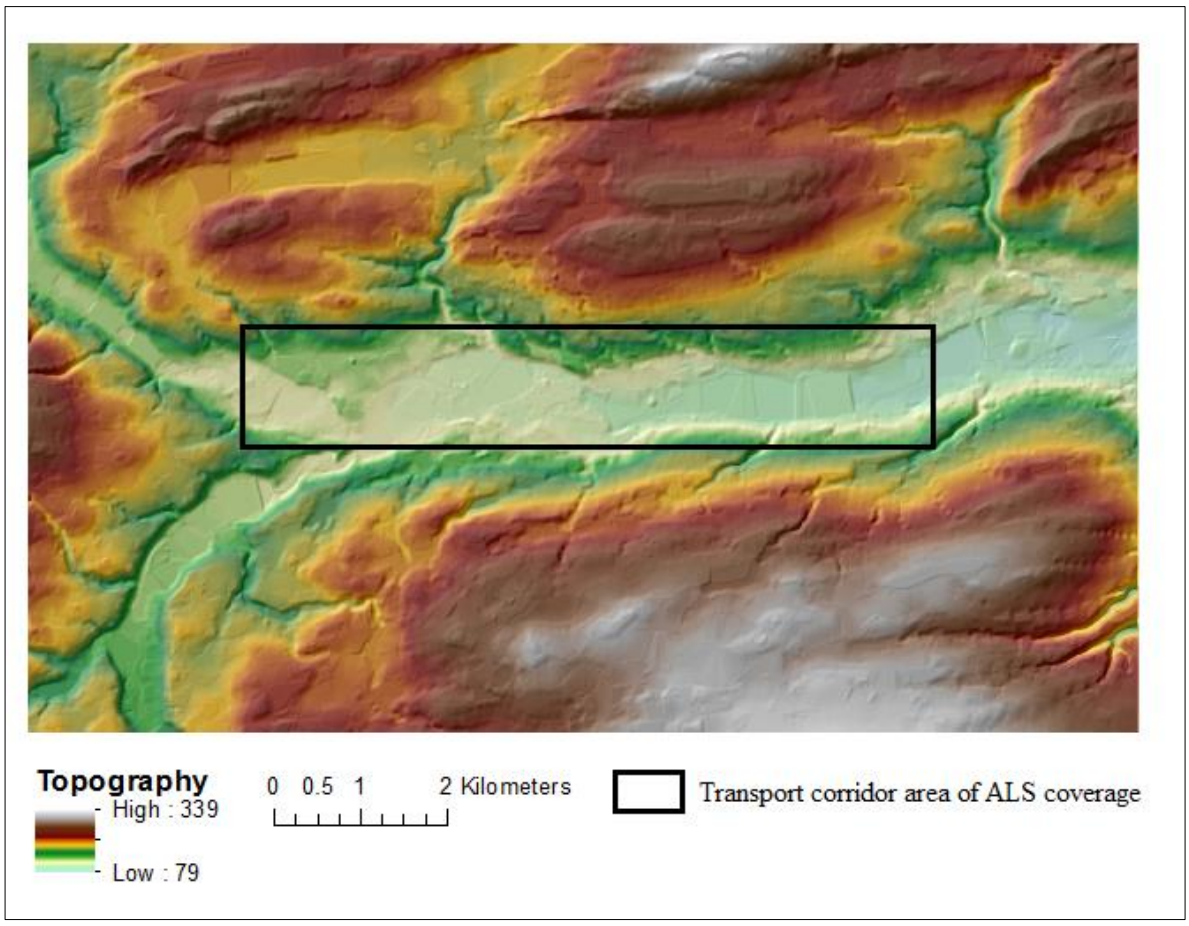

Figure 3.7: The catchment area with the east-west trending floodplain of the South Tyne River surrounded by upland terrains rising to the north and south.

3.5.2 Vector mapping data

The 1:2500 Ordnance Survey vector mapping data with an absolute positional accuracy of 2.4m was also utilised in the study. The dataset extensively covers a range of both man-made and natural features in the UK. Hence, this dataset affords detailed representation of a range of topographic features such as steep slopes, rail lines and associated earthwork landforms, providing a means of confining analysis to the earthwork landforms. The dataset

for the study area was downloaded from the OS-MasterMap hosted on the EDINA Digimap site at the University of Edinburgh.

3.5.3 Land cover

3.5.3.1 Airborne spectrographic imagery and processing

Information on the spatial distribution of vegetation within the transport corridor was obtained from very high spatial resolution multispectral aerial imagery captured using a Compact Airborne Spectrographic Imaging (CASI) sensor. The CASI dataset was acquired over a slightly larger spatial extent of the transport corridor than the ALS data. A 32-band multispectral pushbroom sensor mounted on a fixed wing aircraft recorded data in 32 bands over the visible and near-infrared regions of the electromagnetic spectrum (397-988 nm). The CASI sensor is adjustable thus enabling bands to be centred over different wavelengths. The CASI image employed in the study was acquired by the Geomatics Group and default bandsets as defined by the Geomatics Group for vegetation analysis was used in this study. The CASI data were acquired in September 2007 from a flying height of 1100m with a resultant imagery of 60 cm pixel resolution.

Radiometric calibration of the imagery was performed using field spectroscopy measurement taken over three 6 x 6 tarpaulin targets acquired contemporaneously with the CASI data. The reflectance spectra of each of the calibration targets were measured on the ground using a field spectrometer and the reflectances in the wavebands used by the sensor were derived. The recorded radiances of the calibration targets were extracted from the CASI image. Using the empirical line method following the procedure outlined in Smith and Milton (1999), the recorded radiance and reflectances for the three tarpaulin targets were compared and a linear regression equation that predicts reflectance from radiance calculated. An example of the radiometric calibration for band 1 using the empirical line method is presented in Figure 3.8. A separate linear regression equation was developed for each of the 32 wavebands (see Appendix 2). These equations attempt to remove both illumination and atmospheric effects (Smith and Milton, 1999). Prior to the CASI data acquisition, the calibration target locations were sufficiently spaced at least twelve metres apart, so as to eliminate signal interference from neighbouring targets (Smith and Milton, 1999).

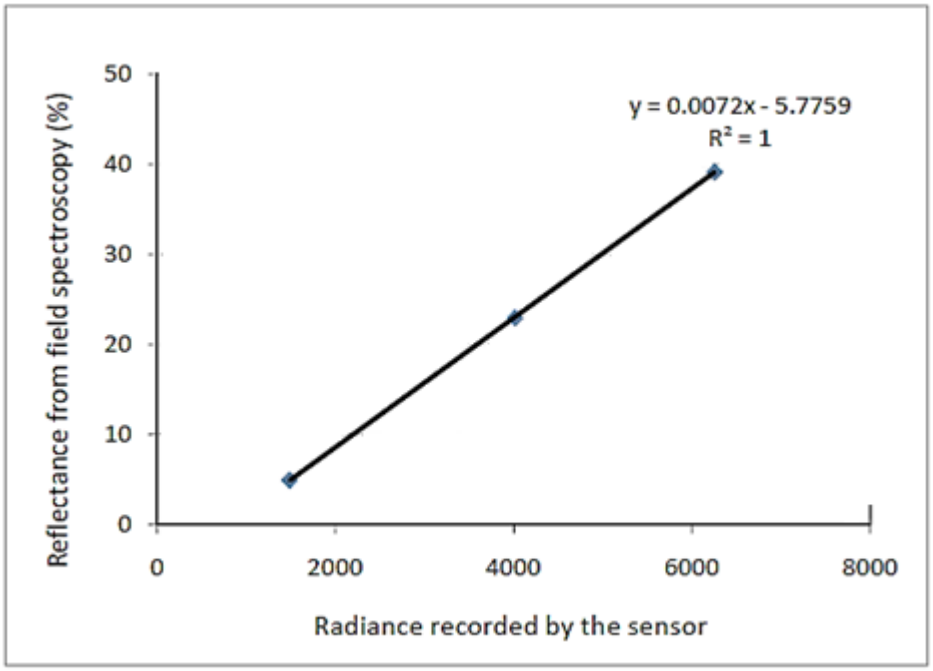

Figure 3.8: Radiometric calibration of CASI band 1 with regression equation and correlation coefficient.

Geometric calibration was carried out by Geomatics Group the dataset supplier, in line with procedures outlined in Brown *et al.* (2003). The CASI imagery is synchronised with the onboard navigation system and geocorrected using navigation data by means of bespoke software from Itres (www.itres.com). The software allows for geocorrection using a fixed elevation surface. Positional data from the navigation system is post-processed using ground GPS data referenced to the Ordnance Survey passive and active networks in the UK. The positional accuracy of the CASI imagery was often rudimentarily assessed during the data acquisition campaign by comparing the imagery to map overlays from Ordnance Survey data control points. The system was calibrated each time the instrument was replaced and as a precautional measure, periodic test flights were flown to ascertain the validity of the calibration. The CASI imagery acquired over the transport corridor was delivered in two strips. Geometric validation of the CASI imagery against independent ground control points obtained in the using RTK GPS was carried out on the imagery on delivery. The checkpoint analysis for the two CASI strips revealed maximum RMSE of 1.1 and 0.98 pixels respectively. A detailed account of the checkpoint analysis and error assessment procedures is presented in Hardy *et al.* (2012).

The two strips covering the transport corridor and adjoining fields were merged using the ERDAS IMAGINE software. The CASI image is a collection of image data in 32 narrow adjacent spectral bands. As a result of its densely sampled spectral signature of land cover, the CASI image provides apt discrimination for intra and inter-class heterogeneity within the transport corridor and is easily adaptable to specific applications. However, its use in spectral analysis is known to be encumbered by the high dimensionality nature of the data. To prepare the imagery for subsequent analysis, a degree of pre-processing was carried out to reduce the amount of noise within the data and the data dimensionality. Attempts to analyse vegetation using multispectral imagery has largely been by means of developed indices that employ spectral information from the red and infra region of the electromagnetic spectrum which have particularly defined response to plant leaves (Bannari *et al.*, 1995). Most traditional approaches to multispectral data analysis were developed for relatively few broad wavelength bands and as such are not as effective with image data of high dimensionality (Mather and Koch, 2011b).

Earlier studies on the transport corridor using the CASI imagery (Hardy *et al.*, 2012; Miller *et al.*, 2012) had employed the minimum noise fraction transformation (MNF) technique as means of reducing noise and data dimensionality. The MNF transforms the original image into a cascaded principal components of varying quality but with the same dimensions (Van der Meer *et al.*, 2006). However, studies by Tsai and Philpot (2002) and Cen *et al.* (2013) have shown that there is high likelihood of losing important low variance, largely uncorrelated data often classified as random noise in techniques that employ spectral data transformation.

In this study, data dimensionality reduction was achieved by using simple band selection. The approach uses selected band of the original image and allows for the retention of the important low variance, largely uncorrelated data often lost in techniques employing image transformation (Tsai and Philpot, 2002). The main critique of this technique is the possibility of leaving out subtle but useful information in the original data during band selection (Tsai and Philpot, 2002; Cen et al 2013). Therefore, careful considerations of the material properties being investigated are essential during the band selection process. The band selection process in this study was guided by findings from studies by Bajwa *et al.*

(2004) and Perry and Roberts (2008) that evaluated the use of reflectance measurement at key wavelengths in the characterisation of biomass, leaf area, stress and species type.

The first stage of the processing aimed to reduce the amount of noise within the data, involved the exclusion of wavelengths representing data covering the blue region (397-500nm) of the spectrum characterised a low signal-to-noise ratio (Grogan and Fensholt, 2013). Surface reflectance values within this region are often significantly affected by the presence of atmospheric aerosols and water vapour during data acquisition (Grogan and Fensholt, 2013). The process of exclusion of the wavelengths in the blue band from spectral information used for land cover characterisation has been reported by various authors (Tsai and Philpot, 2002; Pu *et al.*, 2008). A subset image from the primary study image (32-band CASI) was created in Erdas Imagine with the exclusion of wavelengths covering 397-500nm representing the blue region of the electromagnetic spectrum. The resulting 19-band image then served as the initial Base image for subsequent reduction in data dimensionality.

A considerable level of redundancy exists within the CASI data set as a result of the high correlation between certain bands (Tsai and Philpot, 2002). The reduction in data dimensions by band selection was investigated. The choice of bands was predicated on the fact that the image is to be used for the classification and assessment of the contribution of land cover classes to overland water flow and slope stability assessment across the study area. As such, bandwidths representing regions of the electromagnetic spectrum that are extremely sensitive to vegetation and known to reveal subtle vegetation characteristics such biomass, leaf area, stress and species types were of particular interest and thus selected alongside other bandwidths. The subset tool in ERDAS IMAGINE software was employed for the extraction of selected of bands. A total of 8 bands were selected. Two bands were selected from the green (530nm, 575nm), three bands from the red edge region of the reflectance spectrum (675nm, 728nm, 758nm) and the last three bands from the near infra-red region (824nm, 864nm, 988nm). However, the green and red bands cover the visible range of the spectrum and these bandwidths are known to be commonly high correlated (Mather and Koch, 2011a). The processed image is presented in Figure 3.9.

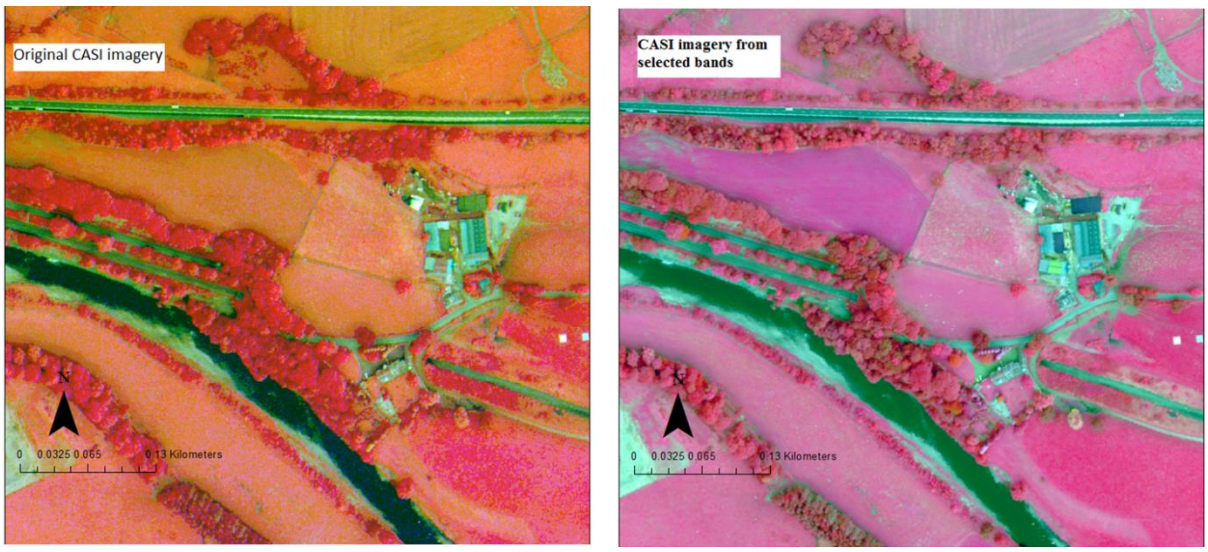

Figure 3.9: CASI imageries of the transport corridor showing the imagery derived from simple band selection technique.

3.5.3.2 Land cover maps (LCM 2007)

Additional land cover information on the adjoining catchment area was acquired from the Land use land cover map (LCM 2007) from the Centre for Ecology and Hydrology UK. The LCM 2007 map of adjoining catchment around the transport corridor test site has a spatial coverage of 100 km^2 and is presented in Figure 3.10. The vector based LCM 2007 is a parcel based classification of UK land cover. Each parcel is represented as a polygon with a rich set of metadata attached. The LCM2007 data of the UK is derived from a supervised maximum likelihood thematic classification of spectral data derived from multi-temporal summer-winter composite images captured by satellite sensors with a spatial resolution of 20-30m. The LCM2007 data set was produced using the object based image analysis (OBIA) technique which considers land surface as a collection of discrete irregular objects and partitions an image into objects (lakes, forest, urban areas, fields, etc.) based on the conceptual relationship that may exist between the various objects. This technique is acknowledged to produce more accurate thematic land cover maps in contrast with traditional pixel based image analysis (Gao and Mas, 2008).

Land cover objects for the LCM2007 were derived from generalised digital cartography obtained from the Ordnance Survey MasterMap(OSMM) topographic layer. Parcel boundaries were further refined by image segmentation, contextual and ancillary information from independent ground reference data to derive land cover objects which

accurately delineated cartographic boundaries (Morton *et al.*, 2011). This ensured that the parcel based classification constructed from generalised OSMM polygons clearly represent real-world objects, such as fields and clusters of woodland and further enhances its compatibility with other available GIS datasets for the UK. The LCM2007 classifies the land cover in the UK into 23 sub-classes and represents the highest thematic resolution available with suitable coverage in the UK (Morton *et al.*, 2011). The LCM 2007 has its minimum mappable area set at greater than 0.5 hectares; as such parcels less than 0.5 hectares and linear features less than 20m in width are generally dissolved into the surrounding landscape during the production process. Parcels are classified based on the dominant land cover in accordance with the Broad Habitat land cover categorisation (Jackson, 2000; Morton *et al.*, 2011).

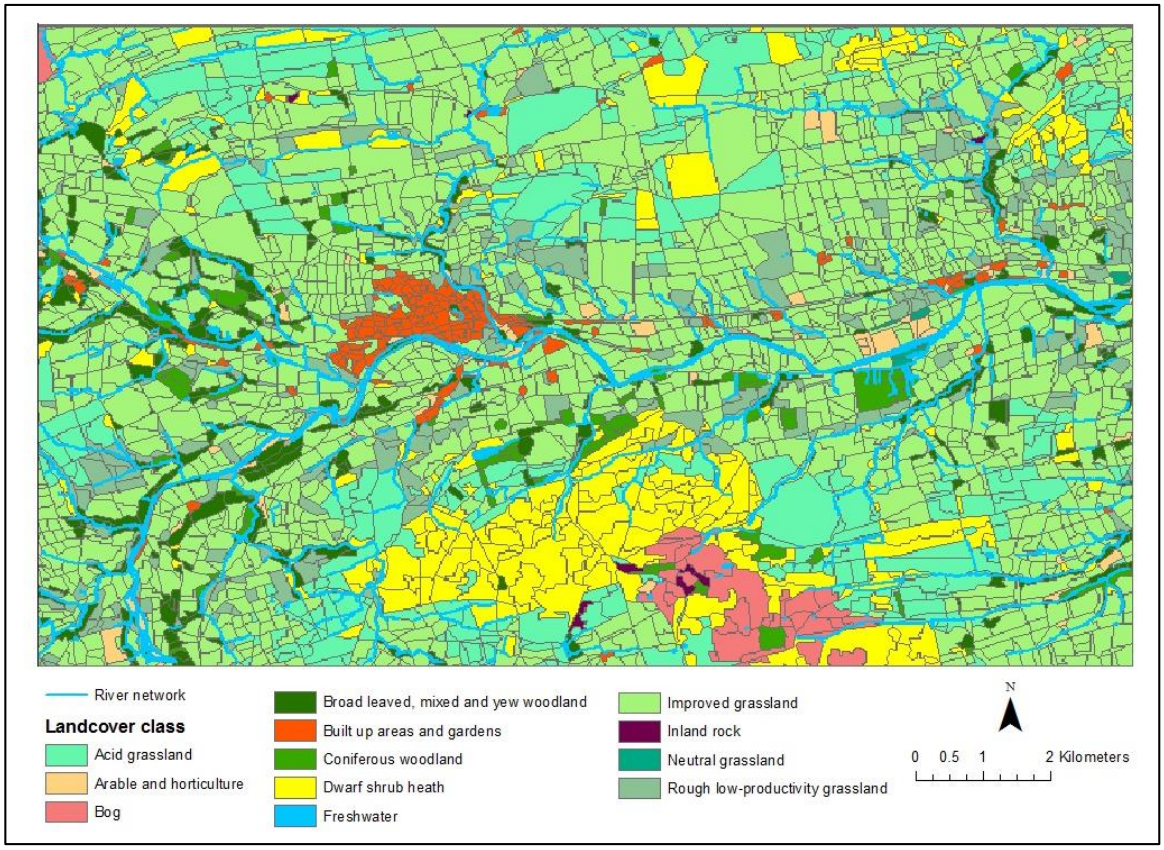

Figure 3.10: Land cover map of adjoining upland agricultural area.

The LCM 2007 data of the broader catchment comprised 21 classes.Table 3.2. These sub-classes were further refined for the purpose of this research by the merging of sub-classes with similar hydrological responses together in ARCGIS to give the five predominant

classes namely bare ground, grassland, manmade, water bodies and woodland within the broader catchment as indicated in Table 3.3.

Table 3.2: The relation between the aggregated land cover classes employed in the study for the land cover categorisation of the adjoining broader catchment areas and broad habitat classification and the LCM2007 classes.

Broad Habitat class (Jackson 2000)	LCM 2007 class (Morton et al 2011)	Aggregated Land-cover Class
Freshwater	River	Water
	Lake	Water
Bog	Bog, grass dominated	Water
	Bog, heather dominated	Water
Improved grassland	Improved	Grassland
Dwarf shrub heath	Heather grass	Grassland
Acid grassland	Acid grassland	Grassland
Improved grassland	Hay	Grassland
Dwarf shrub heath	Heather and dwarf shrub	Grassland
Rough low-productivity grassland	Rough low-productivity grassland	Grassland
Arable and horticulture	Arable unknown	Grassland
Built up areas and gardens	Suburban	Manmade
	Urban	Manmade
	Urban industrial	Manmade
Broad leaved, mixed and yew woodland	Mixed	Woodland
	Deciduous	Woodland
	Scrub	Woodland
Coniferous woodland	Conifer	Woodland
	Recent (<10 years)	Woodland
	Felled	Woodland
Inland rock	Inland rock	Bare ground

Grassland makes up the predominant land cover, covering 87.9% of the total area. This class is the amalgamation of the various grassland types and horticultural lands and dwarf shrub heath. The broader catchment is typically well vegetated with the bare ground accounting for only 0.2% of the total area. The grass and heather dominated bog vegetation are located in the uplands of the North Pennines south of the study area and are often waterlogged.

Table 3.3: Parcel and Land use distribution within the study area

ID	Name	Area (km^2)	Total area (%)	Total number of parcels	Largest parcel area (km^2)	Mean parcel area (km^2)
1	Bare ground	0.15	0.2	9	0.0270	0.017
2	Manmade	2.14	2	3033	0.0800	0.012
3	Grassland	90.89	87.9	177	0.6180	0.030
4	Water body	2.29	2.2	56	0.2970	0.041
5	Woodland	7.93	7.7	514	0.1734	0.015

3.5.4 Soils

The soil map comprised the transport corridor and the adjoining catchment (100 km^2) was obtained from the National Soil Map Resource Institute (NSRI) at Cranfield University, UK and NATMAP vector data set (Avery, 1980). The NATMAP vector dataset is the most detailed of four version of the National Soil Map and includes information on 300 mapped soil associations at a scale of 1:250,000. Within each map unit (soil association) multiple soil series are represented as a hierarchical structure which enables easy integration with other soil data (Mackney *et al.*, 1983). The description of the dominant soils and their distribution is presented in Table 3.4.

The NATMAP vector data for the study area reveals a general distribution of soils that is patchy in nature and that a vast majority of upland agricultural terrains adjoining the transport corridor are essentially underlain by slowly permeable soils made up of fine loamy soils overlying clays and are seasonally waterlogged. These soils that make up about 96% of the area and are characterised by high surface runoff during storms and lateral flow at shallow depths. The slowly permeable subsurface horizons results in prolonged moisture retention and seasonal waterlogging (National Soil Resources Institute, 2008). Well drained soils are typically localised along drainage course of the South Tyne River and only constitute 1.04% of the catchment area. The river terrace soils that line the drainage courses are essentially made up of sands and gravelly soils are well drained and only constitute 1.04% of the area of the adjoining catchment.

Table 3.4: Description and distribution of Soil Map Units in the study area

Map unit name	Simple description	Dominant soils	% Area
BANGOR	shallow peat over hard rock	Very shallow very acid peaty-topped upland soils. Often on steep slopes.	0.08
ELLERBECK	stony loam over gravel	Very stony well drained loamy soils locally on hummocky ground.	1.04
NERCWYS	deep loam	Deep fine loamy soils with slowly permeable sub-soils and slight seasonal waterlogging.	0.26
WHARFE	deep loam	Deep stone-less permeable fine loamy soils.	0.40
ALUN	deep loam	Deep stone-less permeable coarse loamy soils.	0.32
ANGLEZARKE	loam over sandstone	Well drained very acid coarse loamy soils over sandstone with a bleached subsurface horizon.	0.07
SALOP	seasonally wet deep red loam to clay	Slowly permeable seasonally waterlogged reddish fine loamy over clayey, fine loamy and clayey soils	0.23
CLIFTON	seasonally wet deep red loam	Slowly permeable seasonally waterlogged reddish fine and coarse loamy soils and similar soils with slight seasonal waterlogging.	0.13
DUNKESWICK	seasonally wet deep loam to clay	Slowly permeable seasonally waterlogged fine loamy and fine loamy over clayey soils	0.35
BRICKFIELD 3	seasonally wet deep loam	Slowly permeable seasonally waterlogged fine loamy fine loamy over clayey and clayey soils.	60.40
WILCOCKS 1	seasonally wet deep peat to loam	Slowly permeable seasonally waterlogged fine loamy and fine loamy over clayey upland soils with a peaty surface horizon.	35.59
ENBORNE	seasonally wet deep loam	Deep stone-less fine loamy and clayey soils variably affected by groundwater.	0.07
LONGMOSS	peat	Thick very acid peat soils. Largely un-drained and perennially wet.	0.76
WINTER HILL	blanket peat	Thick very acid raw peat soils. Perennially wet.	0.19

Also acquired alongside NATMAP vector dataset, was the Hydrology of Soil Types (HOST) dataset. The HOST dataset is a hydrologically based classification of UK soils (Boorman *et al.*, 1995). The classification is based on the physical properties and the effects on storage and transmission of water as exhibited by each soil series in the 1:250,000 England and Wales soil map and corresponding NATMAP data. The HOST classification recognises the influence of different soil types on the hydrological responses at both local and regional levels. The HOST classification is largely independent of scale and was

derived by assessing the hydrological difference between soil classes using regression analysis against long-term flow data in 800 catchments in the UK (Boorman *et al.*, 1995). Following this, conceptual models of the process that occur in the soil and where appropriate, the substrate, were developed. The resulting scheme has 29 classes based on 11 response models that describe the dominant pathways of water movement through the soil and substrate (Hess *et al.*, 2010). The HOST classification permits direct computation of the important hydrological indices like the Standard Percentage Runoff (SPR). The SPR provides an indication of the propensity of soils to generate overland flow to nearby streams in a catchment. SPR is based on the examination of the response of streams to rainfall events occurring in the catchment (Boorman *et al.*, 1995). The HOST map of the study area is presented in Figure 3.11

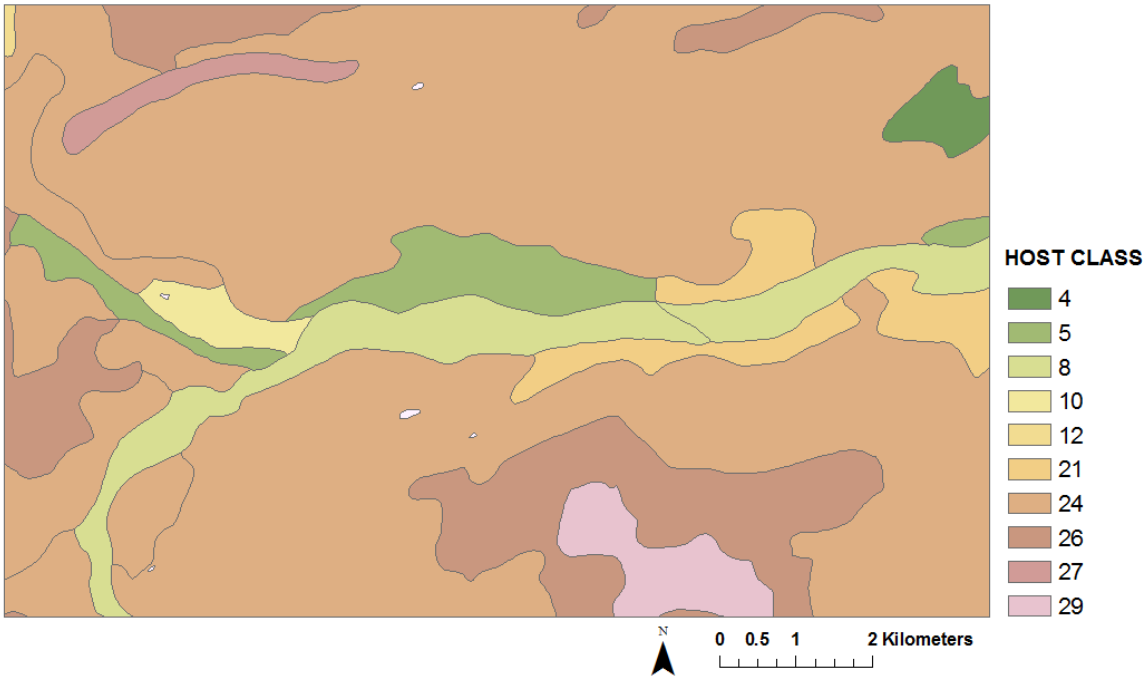

Figure 3.11: HOST map showing the spatial distribution of the various HOST classes in the study area. Description of various HOST class is given in Table 3.5.

Table 3.5: Characteristics of HOST classes and percentage areas in the study location

Map unit name	Host class	Description	% Area	SPR value (%)
ANGLEZARKE	4	Free draining permeable soils on hard but fissured rocks with high permeability but low to moderate storage capacity.	0.94	2.0
ELLERBECK	5	Free draining permeable soils in unconsolidated sands or gravels with relatively high permeability and high storage capacity.	4.16	14.5
WHARFE ALUN	8	Free draining permeable soils in unconsolidated loams or clays with groundwater at less than 2m from the surface.	6.70	44.3
ENBORNE	10	Soils seasonally waterlogged by fluctuating groundwater and with relatively rapid lateral saturated conductivity.	1.05	25.3
LONGMOSS	12	Un-drained lowland peaty soils waterlogged by groundwater.	0.09	60.0
NERCWYS	21	Slowly permeable soils with slight seasonal waterlogging and low storage capacity over slowly permeable substrates with negligible storage capacity.	3.84	47.2
SALOP CLIFTON DUNKESWICK BRICKFIELD 3	24	Slowly permeable seasonally waterlogged soils over slowly permeable substrates with negligible storage capacity.	68.02	39.7
WILCOCKS 1	26	Permanently wet peaty topped upland soils over slowly permeable substrates with negligible storage capacity.	11.67	58.7
BANGOR	27	Permanently wet peaty topped upland soils over hard impermeable rocks with no storage capacity.	1.15	60
WINTER HILL	29	Permanently wet upland blanket peat.	2.39	60

3.5.5 Landslide inventory

Inventory acquisition by means of classic landslide mapping from remotely sensed data has limited applicability in transport corridor environments as landslide locations are often cleared and remedied soon after landslide occurrences (Miller *et al.,* 2012). The remedial activities often obscure evidence of landslide occurrence revealed in the morphology, vegetation and/or drainage conditions of the slope. Consequently, maintenance records and geotechnical reports on slope instability investigation are often the most reputable sources of information on location, magnitude and frequency of slope instability along the transport corridor (Jaiswal *et al.*, 2011). In the UK, there are guidelines in place that stringently enforce conditional appraisal of the earthworks within transport corridors (Perry *et al.*, 2003a). The landslide inventory used in the susceptibility assessment was obtained from the MERLIN database compiled by Network Rail, the owners and operators of rail infrastructure in the UK (Perry *et al.*, 2003a). The inventory highlights locations along the transport corridor that have been identified during statutory routine inspection of slope cuttings and embankments and assessed as being prone to loss of performance as a result of minor landslide events. The Network Rail inspection data divides the transport corridor into 110- yard linear sections and based on a semi-quantitative slope stability assessment scheme, assigns slope hazard values by scoring keys parameters responsible for slope stability. These parameters include material composition, animal burrowing activities, drainage conditions, indicators of landslide initiation and earthwork height. Based on the total hazard value assigned, the evaluated soil embankments, soil cuttings and natural soil slopes conditions are classified into serviceable, marginal or poor. Locations within the 110-yard linear sections classified as poor represent sections with least slope stability. These locations are typically characterised by incessant failures during heavy rainstorms and are known to require some level of periodic maintenance. Majority of the Network Rail inspection data were acquired in 2008 and have been periodically updated over the years. Eight inventory locations with varying spatial areal coverage ranging from 337.5m^2 to 1769m^2 were identified by Network Rail along the 8 km stretch of Newcastle-Carlisle transport corridor route considered in this study. These locations were digitised and stored as a feature class in the project geodatabase.

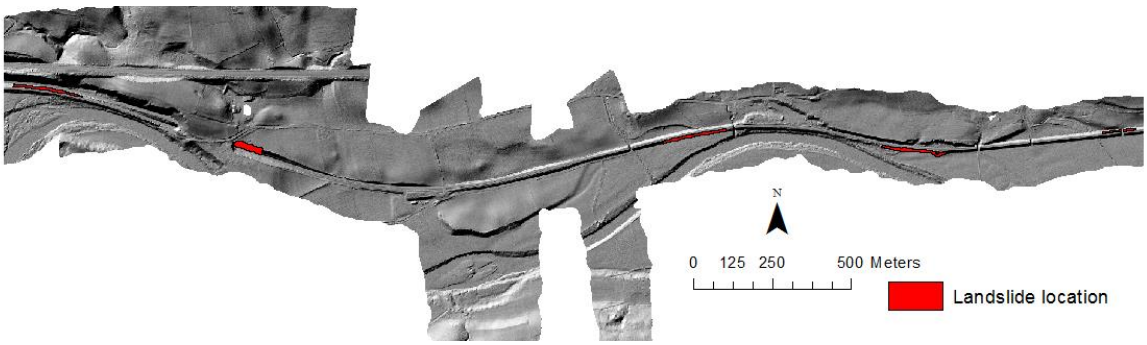

Figure 3.12: Locations of failed earthwork cutting and embankment derived from the Melin dataset compiled by Network Rail

3.5.6 Precipitation

Precipitation that has occurred prior to a storm event can have a significant impact on the subsequent runoff response during rainfall event and partly accounts for the non-linearity in runoff response to similar storm rainfalls under different antecedent soil moisture conditions (Hughes, 1998). Permeable saturated soils generate runoff quite readily due to reduced infiltration rates. Same soil under drier conditions is characterised by infiltration and low infiltration excess runoffs. This is particularly true in sub-catchments where soil moisture plays an important role in the generation of runoff. Daily rainfall data from 2000 to 2010 recorded at the Haltwhistle weather station was acquired from the Met Office Integrated Data Archive System (MIDAS) database hosted by the Centre for Environmental Data Archival of the Natural Environmental Research Council (NERC), UK. Daily rainfall values from the Haltwhistle weather station were assumed to be equivalent and applicable to the entire study area. This approach is consistent with other studies where precipitation data over a small catchment has been used (Mishra and Singh, 2003). The daily records were averaged and plotted on a line chart on monthly basis. Days with significant rainfall depth noted and storms were identified. Equally important were precipitation values for the pre-storm days, five and seven pre-storm rainfall data were computed for each storm. The depth of precipitation prior to the actual storm is responsible for the build-up of antecedent moisture in the soils which is an important consideration in runoff generation (Hess *et al.*, 2010).

3.6 Summary

This chapter presented a description of the transport corridor and the adjoining agricultural fields. The chapter also outlined the various datasets employed in the study covering

topography, land cover land use, soil and geology, precipitation and landslide inventory. A summary of data type, extent and source is provided in Table 3.1. Two broad groups of datasets were identified; the high spatial resolution data limited to the transport corridor and coarser dataset on the adjoining catchment. The incorporation of both data is expected to provide the contribution of the broader catchment on the slope stability assessment of earthwork slopes in the transport corridor.

In addition, the nature of pre-processing carried out on each of the datasets was discussed. This included the removal of noise data that would have otherwise introduced errors into the assessment (classification of the ALS point cloud), feature selection to further reduce data redundancy (simple band selection in CASI data) and categorisation of the various data to common indices for ease of data integration. The pre-processed data developed in this chapter were integrated into the developed methodology discussed in Chapter Four.

4 Methodology

4.1 Introduction

Chapter 2 showed that landslide occurrence is seldom simple in nature even in engineered slopes such as transport corridors (Lee and Jones, 2004). The processes responsible for instability in slopes are invariably linked to the terrain, soil characteristics, geological structures, hydrological, climatic and vegetation conditions inherent to the localities where they occur (Glade and Crozier, 2006). Failures are generally products of existing slope instability and a careful evaluation of the interrelationships between the various intricate factors that potentially influence landslide occurrences usually reveal patterns and thresholds which can be used to perform landslide susceptibility zonation (Van Westen *et al.*, 2008; Jaiswal and van Westen, 2013). The overarching aim of this research work is the development of a geospatial Data driven approach for the broad-scale recognition and prediction of the spatial landslide susceptibility within transport corridors, to enable timely and robust prioritization of further detailed levels of risk evaluation.

4.2 Methodological framework

The stability of a slope depends on the relationship between the external stresses acting on the slope and the internal strength characteristic of the materials that make up the slope (Iverson, 2005). Rainfall-induced failures in engineered and natural slopes are typically initiated by a reduction of confining stress as a result of a build-up of pore water pressure during or following periods of intense rainfall (Iverson, 2000). At relatively fine spatial scales, surface and near surface processes such as infiltration, evapotranspiration and flow accumulation are vital to slope stability (Reid, 1997) and the influence of local topography, underlying soil properties, land cover type on these surface processes is often significant.

Numerous parameters that explain the influence of these surface and near surface processes on slope instability have been identified and the relative importance of these parameters is known to vary with location and the scale of study (Fell *et al.*, 2008). Among the most widely applied parameters for detailed scale assessment of slope stability are those that relate to slope (gradient, shape and direction), soil properties, soil moisture/rainfall and land cover type (Harp *et al.*, 2009; Miller *et al.*, 2012). Landslides are the results of complex interactions between surface and near surface processes which need to be conceptually understood. In this regard, a conceptual framework was developed pulling together the

various processes and parameters identified from literature and during field visits. A flowchart of the methodological framework developed for this study is presented in Figure 4.1. The flow chart highlights the stages of integration of multi-scale geospatial data and landslide susceptibility assessment for fine scale natural slope application. The methods can be broadly divided into three parts.

The first part addresses the development of an integrated and scalable spatial geodatabase for the incorporation of information on the condition and triggering factors responsible for landslide incidence on slope cuttings and embankments along transport corridors; developed review of the scientific literature (chapter 2), Network Rail reports and numerous field visits. The field visits involved inspection of the earthworks for assessment of the various slope instability processes, collection of training and validation data employed in a supervised classification and development of a land cover map of the study area. Pre-processed geological, topographical, land use, land cover and meteorological datasets constitute the primary data layers incorporated into the spatial geodatabase developed in ArcGIS.

Secondary datasets of derived slope stability parameters such as slope gradient, aspect curvature, land-cover, soil type, precipitation and drainage were extracted from the primary datasets. Two categories of terrain and land cover data were acquired; very high resolution datasets spatially limited to the transport corridor from which slope stability parameters were extracted and a coarser resolution data covering the adjoining catchment area employed in the evaluation of catchment contribution. A landslide inventory of recorded slope failures along the transport corridor and maintained areas due to subsidence was obtained from the routine maintenance register hosted by Network Rail.

The second part of the methodology relates to objective 3: the development of a surface runoff model that evaluates the upslope contribution of the adjoining broader catchment to zones of moisture accumulation along slope cuttings and embankments within the corridor. The location of the transport corridor within the South Tyne River floodplain, bounded to the north and south by valley walls of the Tyne Gap, suggests that overland flow from adjoining land may occur. The depth and velocity of surface runoff generated in temperate areas is a function of local terrain, underlying soil properties and vegetation cover type (Archer *et al.*, 2013). Thus, at this stage, a new method was developed to enable the

transfer of the contribution of surrounding upland areas of the larger catchment to the spatial distribution of soil moisture within the transport corridor itself. A novel approach was developed that incorporates the influence of infiltration, interception and modulation of overland flow due to the presence of land cover types in the computation of soil moisture accumulation. Using this, modified terrain wetness index was derived.

The preceding two methodological stages provide data for the third part of the methodology and objective 4, which is the development of a multi-source multi-scale slope stability within transport corridor environments accounting for data uncertainty and vagueness. This was achieved by employing an evidential reasoning framework based around Dempster/Shafter theory (Dempster, 1967); the first known application of this approach to such a fine scale engineered earthworks environment for landslide susceptibility analysis.

In addition to Figure 4.1, Appendix 1 presents a series of separate flow charts for each major stage of the methods which are presented in greater detail in the following sections.

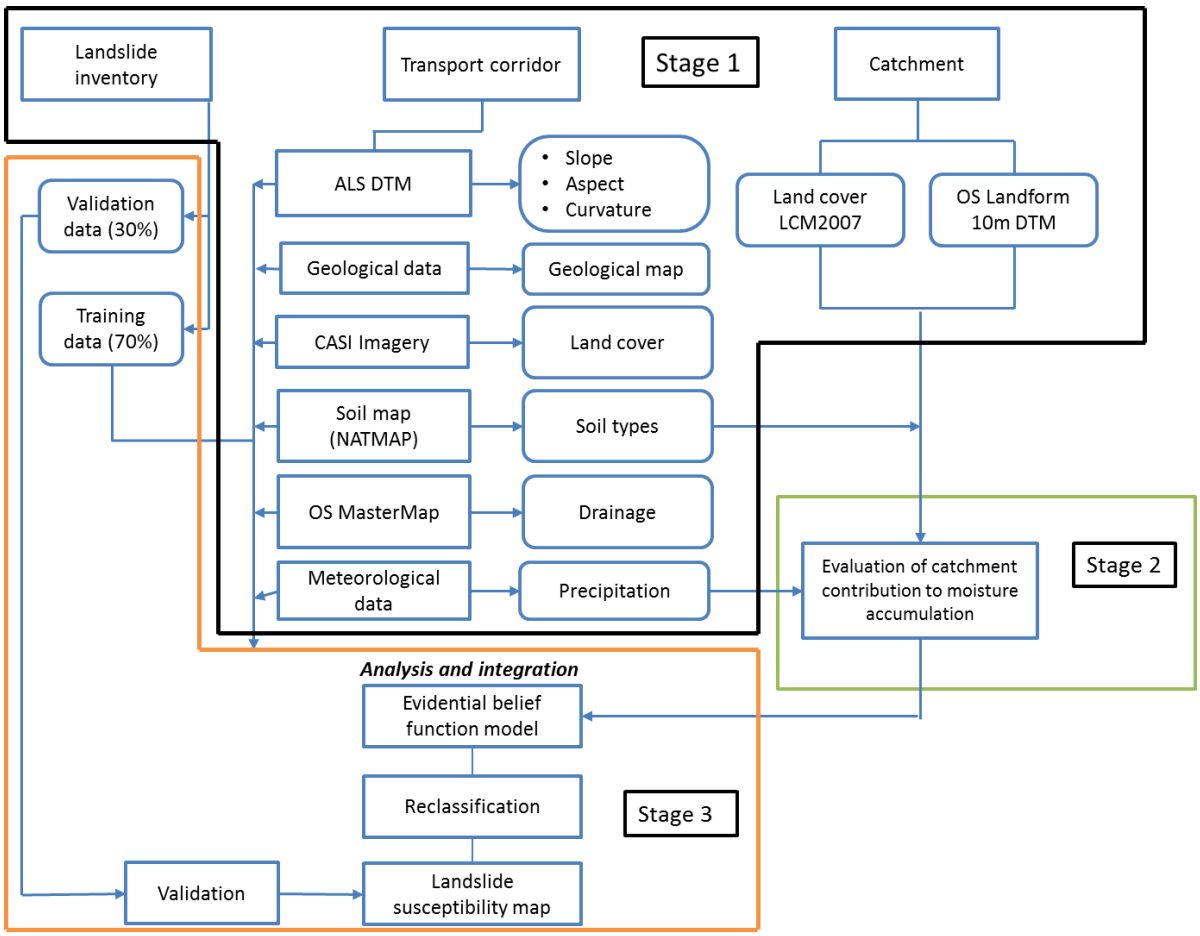

Figure 4.1: Flow diagram summarising the methods described in this chapter. A more comprehensive sets of flow diagrams detailing the methods is presented in Appendix 1.

4.3 Data preparation

Chapter 3 specifies the spatial data layers representing factors considered relevant for landslide susceptibility assessment across transport corridors. The previous chapter also presents the rationale for their selection and the data pre-processing carried out. This section presents the data processing carried out for the extraction of relevant slope stability parameters from these datasets for the construction of a geospatial database.

4.3.1 DTM generation

Two sets of elevation data were employed in the DTM generation. These include the high resolution ALS data of the transport corridor and the coarser OS Land-Form PROFILE 10 m DTM.

The ALS classified ground points was exported into ESRI ArcGIS. Two separate DTMs (regular 0.5 m grid) were generated from the ALS classified ground points. The first served as a standard interpolation technique for ample representation of the topographic complexity of the transport corridor while the second DTM was used for hydrological modelling of flow within the study area. The inverse distance weighting (IDW) technique was used to the represent a standard interpolation technique. The IDW routine interpolates between points to generate a raster surface. IDW is a deterministic approach that assumes for each input point a local influence (which diminishes with increasing distance) on the point being estimated. The IDW interpolation estimates grid elevation for an un-sampled location by averaging the measured values around the prediction location and assigning a weighting factor that diminishes as a function of distance from each input point within a search neighbourhood and the estimated location (Anderson *et al.*, 2005). The assigned weighted average takes into consideration only the influence of proximity over spatial correlation. The IDW interpolation can be mathematically represented as:

$$\tilde{\mathrm{Z}}(s_0) = \sum_{i=1}^{N} \lambda_i \mathrm{Z}(s_i) \qquad \text{Equation 4.1}$$

Where: $\tilde{\mathrm{Z}}(s_0)$ is the estimated value at the un-sampled location s_0, N is the number of measured sample points surrounding the predicted location that was used for the prediction. λ_i are the weights assigned to each measured point used in the estimation which decreases with distance. $\mathrm{Z}(s_i)$ is the observed value at location s_i.
The formula for determining the weights (λ_i) is as follows:

$$\lambda_i = \frac{d_{i0}^{-p}}{\sum_{i=1}^{N} d_{i0}^{-p}}, \qquad \sum_{i=1}^{N} \lambda_i = 1 \qquad \text{Equation 4.2}$$

Where d_{i0} is the distance between the prediction location (s_0), and each of the measured locations (s_i). As the distance becomes larger the weight is reduced by a factor of p. The weights are proportional to the inverse distance raised to the power p. The weighting values range from 0 to 1 and can be altered by varying the type of search and the number of input points within search neighbourhood or by changing p. A defined search neighbourhood

determines the number of input sample points (N) to be included in the inverse distance weighting interpolation of each location.

The IDW routine was applied with the ArcGIS default power of 2 using a variable radius distance set to take an average 20 points. Various studies (Yue *et al.*, 2007; Bater and Coops, 2009) have shown this value to be an acceptable compromise between the higher power values that generally assign greater influences to points closer to interpreted location, typically resulting in an increase in topographic detail and the lower power values that result in smoother interpreted surfaces and a loss of high frequency variability due to the allocation of higher weights to points further from the interpolated locations. A variable search radius was used in calculating the values of the interpolated cells as the density of ALS data was not evenly distributed across the scene. An average of the nearest 20 points was specified to match the minimum density of the ALS data and to ensure that there were at least 20 points per grid square to interpolate from.

The IDW routine is relatively quick and simple to compute for dense sample points such as the ALS data of the transport corridor (ERSRI, 2010). Potential alternatives such as kriging suffer from significant computational overheads such as calculating the exponential semi-variogram that often result in them being inappropriate for large volume spatially dense data such as ALS data (Rees, 2000). The kriging technique is based on the assumption that the distance or direction between sample points reflects a regionalised spatial correlation that can be used to explain variation in the surface. Weights in the kriging approach take into account both distance and degree of variation between sampled points. (Childs, 2004). Kriging tends to produce better terrain representation with sparse and uneven distributed sample points (Rees, 2000), with kriging having minimal benefit over IDW when applied to spatially dense data (Lloyd and Atkinson, 2002).

In addition to the IDW interpolation technique, thin plate spline interpolation is often employed and for the creation of hydrologically correct digital elevation models was also employed. The thin plate spline interpolation technique is based on the ANUDEM program developed by Hutchinson (1989). The method is iterative, employing a finite difference interpolation algorithm that maintains a realistic drainage network using a small number of well-chosen elevation and stream line data sets (Kienzle, 2004; Hutchinson, 2008). The ANUDEM algorithm constructs relatively smooth surfaces from irregularly spaced

elevation data by the application of a spatially variable smoothing function, which is dependent on a measure of roughness (roughness penalty) exhibited by the input elevation values. The routine has the option for the enforcement of drainage constrains which attempt to remove all sink, or depression, in the output DTM. The use of ANUDEM for DTM modelling in hydrology is well documented (Bater and Coops, 2009; Chen *et al.*, 2012). During interpolation constraints such as connectivity of drainage structure and accurate representation of ridges and streams from input elevation data are usually imposed by default, (ERSRI, 2010), as was the case for the generation of a 0.5m DTM from the ALS data. The relatively smooth surfaces produced by the ANUDEM interpolation technique, enhanced the computation of continuous flow across the transport corridor terrain devoid of spurious pits (Bater and Coops, 2009; Hutchinson, 2013). However, the main concern with this method as is the case with all other spline techniques is that it provides unrealistically smooth view of reality such that the estimation of attribute values from first (slope and aspect) and second order derivatives (curvature) for terrain related modelling may be misleading (Chen *et al.*, 2012).

4.3.1.1 DTM accuracy assessment and sensitivity

Normally DTM accuracy would be evaluated using an independent sample of measurements surveyed in the field. However in the case of this study, such contemporary field data did not exist. To overcome this, the ALS ground return points were randomly subsetted into training and validation datasets consisting of 1,564,411 (97%) and 48383 (3%) points respectively. This proportion of training to test data afforded the assessment of error associated with the height predictions of the interpolation techniques at locations lacking measured points in the dataset without compromising the integrity of the ALS data. This approach is consistent with similar studies such as (Bater and Coops, 2009). To ensure adequate representations of existing topographic variation in the study area in the validation dataset, the study area was classified to reflect the three dominant terrains (described in section 3.2) using independent elevation data (OS Land-Form PROFILE 10m DTM); namely the plains, gentle valley slopes and the upland areas. 3% of the total ALS point data in each of the stratified bin were randomly partitioned to generate the validation dataset.

Sensitivity testing was carried out to evaluate the impact changes in input DTM spatial resolution has on terrain analysis calculations with a view to selecting an optimum grid

resolution that would provide an adequate representation of the earthwork topography and minimise the inclusion of micro-topographic effects during hydrological modelling (Miller *et al.*, 2012). In total, 10 DTMs were produced using the IDW and ANUDEM interpolation techniques using ArcGIS. For each interpolator, DTMs were generated with spatial resolutions of 0.5, 1, 1.5, 2, 2.5, 3, 3.5, 4, 4.5 and 5 m. Simple visual interpretation was used to assess visible changes such as the introduction of artefacts as a result of changes in DTM resolution. The effects of resolution on surface roughness was assessed by comparing elevation values derived from transects across the earthwork. The quality of the resulting DTM was assessed using the validation data to compare the biases and accuracies of the surfaces. For each DTM, vertical errors were calculated for every point in the validation data as the differential between the predicted value of the DTM and measured value from the ALS data at the same location. Global statistics was calculated to assess the overall performance of the interpolation routines. The mean error provided a measure of bias, with positive values indicating the interpolation algorithm as over estimating the actual data values (Bater and Coops, 2009). The Root Mean Square error (RMSE) and mean absolute error provide measures of the global accuracies of the interpolated surfaces (Bater and Coops, 2009). In addition slope and aspect grids were also generated using the slope and aspect tools in ArcGIS and assessed by comparing the generate slope and aspect values of higher resolutions against the 0.5 m DTM set as a benchmark.

4.3.2 Land cover map classification

The CASI imagery was used to derive the land cover classification used to assess vegetation influence on instability in the transport corridor. Careful consideration was given to the choice of the possible number of land cover classes, sample size, location and field collection of training data and the collection of validation data to be used for accuracy assessment Reconnaissance field visits and review of literature on past land cover studies of the study area and environs provided insights into the possible number of land cover classes that existed within the transport corridor. Nine main land cover types were identified during the reconnaissance field visit; pasture, managed pasture, shrubs, deciduous woodland, river, bare earth and man-made structures (roads, rail and buildings). An unsupervised classification of the CASI image of the transport corridor was performed in Erdars Imagine using the ISODATA classifier into 50 spectral classes. A large number of clusters was chosen to ensure adequate separation of the various land cover classes. The spectral classes

were matched with land cover information from a 5cm aerial photograph acquired contemporaneously with the data of the transport corridor. The spectral classes representing a particular land cover type were merged to arrive at the earlier identified nine main land cover classes. The unsupervised classification of the transport corridor derived from the 8 band CASI image, alongside the 5cm aerial photograph provided a basis for the positioning of stratified random sampling points for the collection of training data used in the supervised classification of a land cover map of the study area. The stratified random sampling technique was adopted to ensure adequate sampling of the various land cover classes (Congalton, 1991). A total of 438 validation points and 200 training points were randomly located throughout the study area. The training and validation sets for each of the classes were established using a field mapping exercise and from the 5cm aerial photograph of the transport corridor.

Supervised classification was carried out on the processed 8-band CASI image using the maximum likelihood classifier routine in Erdas Imagine software. The field work established nine main land cover classes for the transport corridor, this includes pasture, managed pasture, shrubs, deciduous woodland, water, bare earth and man-made structures like roads, rail and buildings. Training sets were digitized using visual interpretation of the image in different band combinations alongside in-situ land cover information acquired during the field survey. Visual interpretation of sets of image characteristics such as shape, size, structure, texture, tone and pattern of objects was also employed in the identification of digitized boundaries for each of the training sets for the various land cover classes. The spectral signature for the various land cover classes were derived from the training sets and evaluated to assess their degree of separability using the transformed divergence algorithm in Erdas Imagine (Jensen, 2004). Using maximum likelihood supervised classification based on a total of 200 randomly distributed training sites, the various land cover within the transport corridor were classified into one of the nine categories. A fuzzy convolution filter was applied to the resulting classification to optimise the classification results (ERDAS, 2008). The fuzzy convolution filter creates a single classification band by removing isolated pixels and smoothening boundaries between classes (Jensen, 2004). This context-based classification reduces the speckle effect and improves overall interpretation (Jensen, 2004). The classification accuracy was then assessed at 438 validation points randomly located throughout the study area. An overall classification accuracy of 80.37%. % with a

kappa statistic of 0.85 was obtained for the simple band selection CASI image. While the classification result may suggest a high overall accuracy, closer inspection revealed the existence of misclassified pixels between land cover classes that lack significant spectral distance between the mean vectors and covariance of class signatures, hence these classes were subsequently merged into a single class. For example, there was significant overlap of the ballast-lain rail bed, roads and building land cover classes. Consequently these classes were merged to form the manmade land cover class. The pasture, managed pasture and shrub land cover classes were also combined into a single land cover class (pasture) as a result of their similar hydrological characteristics and the misclassified pixels that existed between these classes. A final land cover classification that identified (1) mixture of pasture grassland, agricultural weeds, wild flowers and shrubs (2) bare earth, (3) woodland comprised of a mixture of coniferous and deciduous woodland majorly aligning flow routes of tributaries or situated within woodland estates (4) water and (5) manmade with an overall accuracy of 90.15% with a kappa statistics of 0.85 (Table 4.1) was obtained for the simple band selection CASI image of the transport corridor. The contingency matrices and separability table tables are presented and discussed in detail in chapter five.

For a comparative assessment, the minimum noise fraction transformation technique was also applied to the primary image (19 band CASI image) which was introduced in section 3.4.2.1. The Minimum Noise Fraction (MNF) transform algorithm employs two consecutive data reduction operations (Green *et al.*, 1988; Van der Meer *et al.*, 2006). The first is based on an estimation of noise in the data as represented by a correlation matrix. This transformation decorrelates and rescales the noise in the data by variance to improve the overall signal from vegetation (Green *et al.*, 1988). The second operation creates a cascade of principal components that contain weighted information about the variance across all bands in the raw dataset. (Van der Meer *et al.*, 2006). The dominant components were selected and used in an inverse MNF transform to convert the data back to its original spectral space, resulting in the same number of transformed channels as the original image (19 CASI bands). The spectral subset chosen for the transport corridor data were bands one to eight, which were determined to contain over 99% of the total variance in the data. The MNF transform is usually better than the Principal Components (PC) transform at compressing and ordering multispectral and hyperspectral images in terms of image quality (Berman *et al.*, 2012). The MNF transform is also invariant to invertible (i.e. non-singular)

linear transformations of multispectral or hyperspectral data, a property not shared by the PC transform (Berman *et al.*, 2012).

A maximum likelihood supervised classification was also implemented on the spectral transformed (MNF) CASI), using the same training areas that were employed for the simple band selection approach. A classification accuracy of 74.43 % and with a kappa statistics of 0.68 was obtained for the MNF transform CASI image of nine land cover classes. The overall classification accuracy was improved by merging land cover classes with overlapping spectral signatures. Consequently the rail, road and building classes were combined to achieve the manmade class. A merged land cover class (pasture) made up pasture, managed pasture and shrub land cover classes was also derived. A final land cover classification that identified pasture, bare earth, woodland, water and manmade with an overall accuracy of 83.59 % with a kappa statistics of 0.76 (Table 4.2) was obtained for the MNF transform CASI image of the transport corridor.

The supervised classification map obtained from simple band selection was used as the land-cover map for the transport corridor as it provided a higher overall accuracy.

Table 4.1 Contingency matrix showing the classification accuracy of the maximum classification routine carried out on the CASI imagery derived from simple band selection.

	Woodland	**Pasture**	**Bare earth**	**Manmade**	**Total**	**Producer's accuracy (%)**	**User's accuracy (%)**
Woodland	41	20	0	2	64	100.0	65.08
Pasture	0	181	8	3	189	87.86	94.27
Bare earth	0	6	17	0	25	68.0	73.91
Manmade	0	0	0	118	118	95.93	100.0
Total	41	207	25	123			
Overall accuracy = 90.15%				Overall Kappa statistics = 0.85			

Table 4.2: Contingency matrix showing the classification accuracy of the maximum classification routine carried out on the MNF transform CASI image.

	Woodland	**Pasture**	**Bare earth**	**Manmade**	**Total**	**Producer's accuracy (%)**	**User's accuracy (%)**
Woodland	39	13	0	3	55	95.12	70.91
Pasture	2	152	4	0	158	73.43	96.20
Bare earth	0	42	21	1	64	84.0	32.81
Manmade	0	0	0	119	119	96.75	100.0
Total	41	207	25	123			
Overall accuracy = 83.59%				Overall Kappa statistics = 0.76			

4.4 Characterisation of hydrological spatial variability

Flow accumulation and soil moisture distribution were important considerations in the assessment of slope instability in the transport corridor. Moisture accumulation has been identified as the main trigger of failure in UK slopes (Perry *et al.*, 2003a; Ridley *et al.*, 2004). Terrain-based flow models are particularly useful in the delineation of zones of saturation. These models are built on a basic underlying assumption that water and its constituents essentially move downhill draining steeper terrains and concentrating in areas of topographic convergence. Terrain based flow models provide the basis for the derivation of many hydrological parameters used in hydrological terrain analysis (Tarboton *et al.*, 2009). The classic TWI is perhaps the most popular terrain-based flow model derived indices used to describe the spatial pattern of soil moisture (Sørensen *et al.*, 2006). The classic TWI takes into account the local slope geometry and local upslope contributing area in quantifying topographic control on hydrological processes (Sørensen *et al.*, 2006; Ma *et al.*, 2010). However, the classic TWI has a number of limitations (Wilson and Gallant, 2000) such as an absence of land-cover information and the assumption of uniform soil properties (Borga *et al.*, 2002).

In order to address these deficiencies, this study developed a novel approach to TWI computation that integrates the contribution of land cover and soil properties to surface runoff characterisation. The developed approach incorporates two key components; (i) the

development of a weight grid that quantifies the contribution of the soil-land cover interface to surface runoff generation, and (ii) the propagation of soil–land-cover interactions to downslope flow accumulation.

4.4.1.1 Theoretical framework

There are a number of models that provide a means of evaluating the interaction between land cover and soil based on empirical relationships with respect to runoff generation. These models use approaches ranging from fully empirical lumped models (Beven and Kirkby, 1979) to spatially distributed mechanistic approaches (Beven, 2000; Bovolo and Bathurst, 2012), each with its limitations and advantages (O'Connell *et al.*, 2007). The Soil Conservation Service-curve number (SCS-CN) model is an event model to predict direct runoff volumes for individual storm events. The approach utilises a quantified conceptual framework linking soils, land cover, land management and weather to runoff generation (Hess et al 2012), and can be applied to rural and urban areas without the need for calibration. The method was developed from many years of storm flow records in catchments in the USA and is applicable to small catchments. This approach unlike the classic TWI, incorporates the influence of land cover and underlying soil contribution to the computation of generated overland flow (Soulis and Valiantzas, 2012).

With the aid of a set of empirical equations that relate direct runoff volume to the rainfall amount catchment characteristics and antecedent wetness (USDA, 2004), the Soil Conservation Service (SCS-CN) curve number method models the interaction between land cover and soil type based on a single storm event and computes runoff depth (Mishra and Singh, 2003). The SCS curve number method accounts for the contributions of important catchment characteristics such as land cover, soil hydrological group and soil hydrological condition in the computation of direct runoff as a consequence of rain storms (Hess *et al.*, 2010; Soulis and Valiantzas, 2012). The advantage of the SCS curve number method is its relatively simple data requirements and ability to compute runoff depth for each location thus providing a measure of runoff modulation from infiltration, interception and relative flow velocity on the basis of soil type and land cover.

The SCS curve number method is based on the water balance equation and two fundamental assumptions (Mishra and Singh, 2003; Soulis and Valiantzas, 2012). The water balance equation states that

$$P = I_a + F + Q \qquad \text{Equation 4.3}$$

Based on the water balance equation, it is theorised that the actual amount of direct runoff to potential runoff (effective rainfall) is the same as the ratio of actual infiltration to the potential maximum retention:

$$\frac{Q}{P - I_a} = \frac{F}{S} \qquad \text{Equation 4.4}$$

Where Q is the amount of runoff generated, P is the total rainfall in millimetres, I_a is the initial abstraction (mm) which represents all the losses due prior to runoff generation, which include water retained in surface depressions, interception by vegetation, infiltration and evaporation. S is the potential maximum water retention by soil and vegetation (mm) after the commencement of runoff and F is the actual retention or cumulative infiltration less the initial abstraction (mm).

The combination of equations 4.3 and 4.4 forms the basis for the SCS curve number method

$$Q = \frac{(P - I_a)^2}{(P - I_a + S)} \qquad \text{Equation 4.5}$$

This equation is valid for P $\geq I_a$; otherwise Q = 0.

The second assumption is based on the idea that the amount of initial abstraction is a fraction of the potential maximum retention (Soulis and Valiantzas, 2012).

$$I_a = \lambda S \qquad \text{Equation 4.6}$$

Where λ is the ratio of initial abstraction to the potential maximum water retention by soil and vegetation, developed from an empirical relationship between I_a and S based on long term observation of small watersheds (Mishra and Singh, 2003).

The SCS curve number method as presented in the National Engineering Handbook - NEH4 by the USDA Soil Conservation Service (SCS) considers λ to be equal to 0.2 for

normal practical applications (Mishra and Singh, 2003). Incorporating equation 4.6 with λ set to 0.2 into equation 4.5, an equation with only two parameters is obtained.

$$Q = \frac{(P - 0.2 \cdot S)^2}{(P + 0.8 \cdot S)} \qquad \text{Equation 4.7}$$

The potential maximum retention, S, is expressed in in terms of the dimensionless curve number through the relationship:

$$S = \frac{25400}{CN} - 254 \qquad \text{Equation 4.8}$$

The SCS curve number method enables the computation of the runoff volume for each grid cell, based on the weighted relationship between soil types, antecedent moisture and land cover combinations. However, these values are independent of contribution from upslope adjacent grids. The calculation of runoff depth in mm (Q) for the study area requires information on the various land cover, hydrological soil groups DEM and 5-day antecedent rainfall as input data. A runoff coefficient grid is computed for each grid cell using the following equation;

$$\alpha = \frac{Q}{P} \qquad \text{Equation 4.9}$$

Where α is runoff coefficient and is the proportion of rainfall that actually results in overland flow during an event. This coefficient takes into account initial losses (water stored in depressions), the continuous losses (infiltration) and the hydrodynamic effects encountered while surface water flows overland (Butler, 2011). Thus, the value represents the lumped effect of a number of catchment processes (Viglione *et al.*, 2009). The runoff coefficient value for a location typically varies with time during storms with lower coefficient values at the start of rainfall and higher after soil saturation. However for this study only the overall runoff coefficient for the entire rainfall duration is computed. The runoff coefficient grid serves as a weighted grid to incorporate the lumped catchment characteristics into the calculation of flow accumulation and modified TWI. In SCS CN

method, runoff depth is computed for each grid cell irrespective of the upstream contributing area draining into the cell (Mishra and Singh, 2003).

The flow accumulation operation enables the integration of upslope contribution to be modelled downstream. The runoff depth at a particular cells of interest is the runoff depth computed for that cell and the sum of the all the upstream cells draining through the cell of interest. Hence an additional weight grid such as the runoff coefficient generated using the SCS CN approach can be introduced into the flow accumulation calculation to reflect the local influence of rainfall, amount water loss to interception vegetation, evapotranspiration and infiltration. However the calculation of the upslope contributing area is dependent on the manner at which the accumulated area of upstream cells is routed downstream (Sørensen *et al.*, 2006). The D∞ flow distribution algorithm by Tarboton (1997) was employed for the downstream routing of flow.

DTM derived flow fields define surface connectivity between any two points on the terrain. In a flow field, the general accumulation function can be defined as an integral of a weight - w(x), over a contributing area (CA).

$$A(\mathrm{x}) = \int_{CA} w(x)\ dx \qquad \text{Equation 4.10}$$

Where x represents the location of an arbitrary point in the flow field domain, A(x) is the accumulation function evaluated at the arbitrary point x. w(x) is the weighting field at point x. Typically, the weighting field is set at 1. A weighting value of 1 assumes no loss in volume of input flow as a result of hydrological processes such as evaporation or infiltration (Figure 4.2). However, the weighting field can be modified to reflect hydrodynamic processes such as infiltration, and, overland flow arising from excessive rainfall can be modelled with the weighting field set to be equal to rainfall intensity minus infiltration (Figure 4.3).

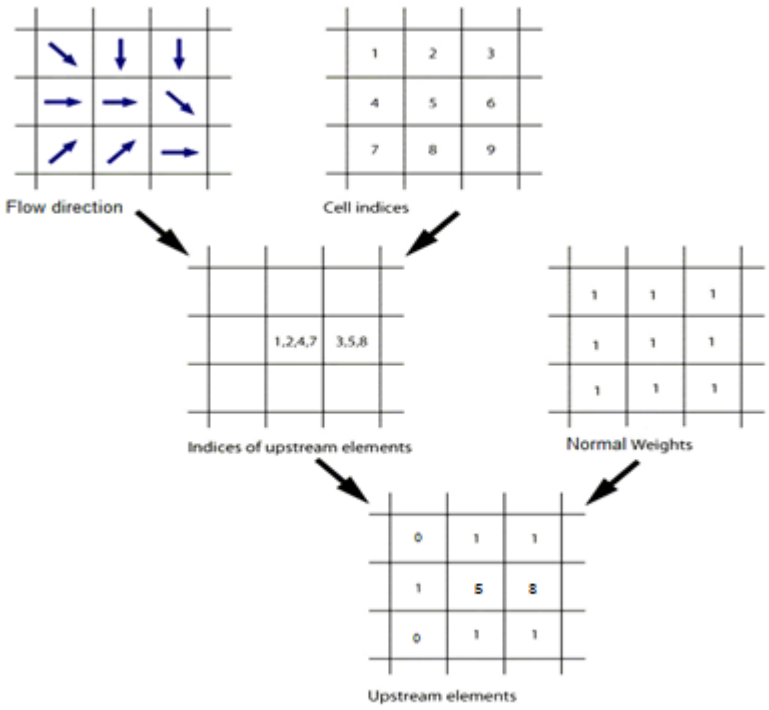

Figure 4.2: Typical flow accumulation grid with weight field set at 1 to reflect runoff depth without loss to evaporation and infiltration

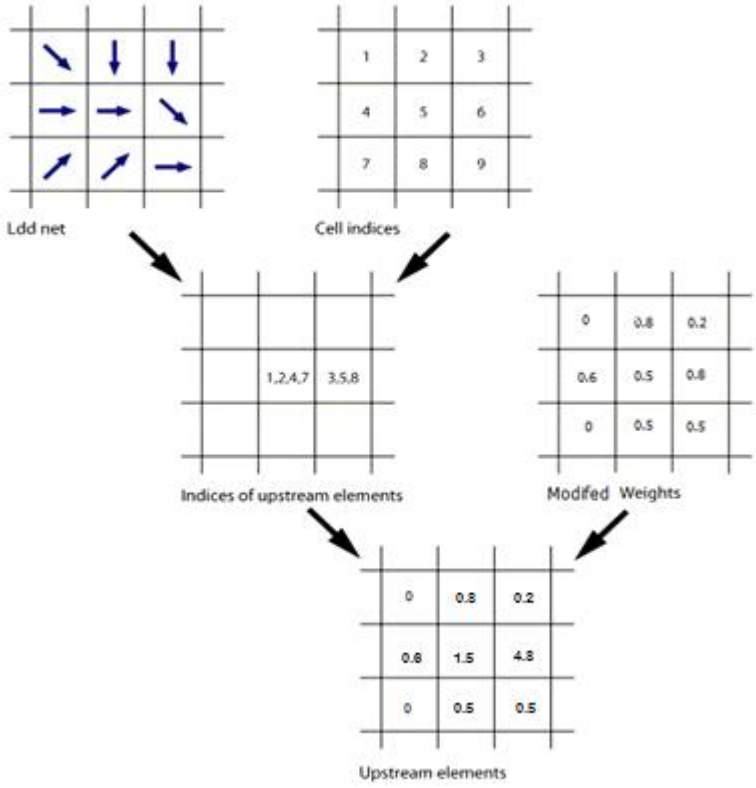

Figure 4.3: Flow accumulation calculation incorporating the influence of the weighted grid

Following Tarboton (1997), numeric flow accumulation using the D∞ algorithm can be evaluated recursively for each element as:

$$A = A(x_i) = w(x_i)\Delta + \sum_{\{k:P_{k_i}>0\}} P_{k_i} A(x_k) \qquad \text{Equation 4.11}$$

Where x_i is a location in the field represented numerically by a model element such as a grid cell in a DEM, A (x_i) represents the upslope accumulation at that particular grid. The grid cell area is represented by Δ, P_{k_i} is the proportion of flow from neighbour k grid cells contributing to the grid cell i and the notation ($k:P_{ki}>0$) denotes a summation over the set of k values such that $P_{ki} > 0$.

Flow accumulation at any particular grid cell is the sum of flow arising from that grid cell and the flow resulting from all other upslope topologically contributing cells, with grid cell weighted according to the proportion of flow it contributes. The flow accumulation calculation (Equation 4.11), allows for the incorporation of additional weights into the flow accumulation routine. Thus, other important parameters that affect runoff generation such as the spatial variation in infiltration rates or moisture retention capacity (soil properties) and the influence of vegetation cover on runoff volume and velocity can be incorporated. Runoff generation from upstream grid cells will naturally flow downslope as long as the infiltration capacity is exceeded along its flow route. The runoff generation for each grid cell can be represented as:

$$q_i = max(q_{in} + r_i - c_i, 0) \qquad \text{Equation 4.12}$$

Where q_{in} is the summed upslope runoff inflow, r_i is the input precipitation at grid cell i, q_i is the scalar at each grid cell i, and c_i is the infiltration capacity and the effect of evapotranspiration due to vegetation at grid cell i.

The recursive functionality in equation 4.11 enables local evaluation of flow quantities which are difficult to define using global weights, as these flow quantities are dependent on both recursive variables emanating from the flow field as well as simple local input variable values at the grid cell location.

$$A_i = max\left(\sum_{\{k:P_{k_i}>0\}} P_{k_i} q_k + r_i - c_i, 0\right)$$ Equation 4.13

The lumped effects of infiltration, antecedent evaporation and storage capacity can be represented by runoff coefficient (Viglione *et al.*, 2009). As such equation 4.13 can be rewritten as:

$$A_i = max\left(\sum_{\{k:P_{k_i}>0\}} P_{k_i} q_k + \alpha, 0\right)$$ Equation 4.14

The runoff coefficient for each grid can be represented a weighted grid in the flow accumulation routine to derive the contribution to flow for each cell. The modified TWI computation can be expressed as:

$$TWI = \ln\left(\frac{\left(\sum_{\{k:P_{k_i}>0\}} P_{k_i} q_k + \alpha, 0\right)}{\tan\beta}\right)$$ Equation 4.15

4.4.1.2 SCS-CN method

The SCS-CN method was used to estimate the relative change in runoff depth due to change in soil condition and vegetation cover. The method was implemented using the HEC-GeoHMS extension in ArcGIS 10.1. The HEC-GeoHMS extension provides a set of tools required for geospatial hydrological modelling. The SCS-CN approach requires information on land cover, soil type and a DTM. As reported in section 4.3.2, the land cover map of the transport corridor reflects the predominant land cover types within the transport corridor categorised in line with Soil Conservation Service Curve Number (SCS-CN) recommended categories to reflect potential evapotranspiration contributions based on vegetation growth cycle, rooting depth and crop coefficients (Holman *et al.*, 2004; USDA, 2004). Additional land use land cover information on the adjoining broader catchment was obtained from the land cover map (LCM 2007) for the UK. The LCM 2007 land cover

classification was aggregated into the 5 main land cover classes of the transport corridor and was rasterised. A merged land cover map of the transport corridor and adjoining fields was produced using the map algebra tool in ArcGIS. Additionally due to the limited coverage of the ALS data, a merged 2.5 m DTM was produced from the ALS and OS Landform elevation data in ArcGIS to enable the evaluation of the contribution of the wider catchment topography to the spatial distribution of surface runoff depth within the transport corridor.

Following Hess *et al.* (2010) and in line with the Hydrology of Soil Types (HOST) classes, the various soil types in the study area were classified into one of the four hydrological soil groups (A,B, C, D) as described in the SCS-CN method, with A and D representing the highest and lowest infiltration rate respectively (USDA, 2004). Group A soils are characterised by low runoff potential and high infiltration rates even when thoroughly wetted. They consist chiefly of deep, well drained sand or gravel and have a high rate of water transmission (greater than 7.6 mm/h). Group B soils have moderate infiltration rates when thoroughly wetted and consist chiefly of moderately deep, and moderately-to-well-drained soils with fine-to-moderately coarse textures. These soils (silt loam or loam) have a moderate rate of water transmission (3.8–7.6 mm/h). Group C soils have low infiltration rates when thoroughly wetted and consist chiefly of soils with a layer that impedes downward movement of water and soils with moderate to fine texture. These soils (sandy clay loam) have a low rate of water transmission (1.3–3.8 mm/h). Group D soils have high runoff potential with very low infiltration rates when thoroughly wetted. They consist chiefly of clay soils with a high swelling potential, soils with a permanent high water table, soils with a claypan or clay layer at or near the surface, and shallow soils over nearly impervious material. These soils have a very low rate of water transmission (0 - 1.3 mm/h).

To create the CN map, the hydrological soil group and land cover maps were uploaded to the ArcGIS 10.1 platform. The HEC-GeoHMS extension of ArcGIS 10.1 was used to generate the CN grid map. Prior to generating the CN grid map, the merged land cover map was converted into vector data to enable a union operation with the soil map merging both maps. The merged soil-land map included attributes from both layers of the merged dataset. A lookup table containing the land cover and soil type and curve numbers representing average conditions for the soil-land cover combination was also generated. The CN values

for different land cover and hydrological soil groups were adopted from a CN index table adapted to the UK soil conditions and weather (Hess *et al.*, 2010) was used in this study (Table 4.3) Hess *et al.* (2010) used five classes (Excellent' to 'Very Poor) unlike the conventional four employed in NRCS (1986) to describe soil-field conditions. These classes represent both the condition of the soil (as it affects runoff generation) and the presence of land management practices which increase or decrease the risk of runoff from the field. The representative soils were grouped according to soil hydrological group and allocated a CN for each soil–field condition and land cover (Table 4.4). The CN for Very Poor condition represents a soil whose hydrological response has been altered either as a result of trampling from grazing or heavy machinery to such an extent that it behaves as though it belongs to a soil hydrological group of higher runoff potential. However, for soil in hydrological group D characterised as Very Poor condition, the CN is not increased beyond the highest value given in NRCS (2002).

The CN grid was generated using HEC-GeoHMS with a 2.5m resolution hydrologically correct merged DTM of the study area, a lookup table and merged soil-land map as input data. The programme generates a raster CN grid and automatically adds a new CN field to the land cover/soil type attribute table and populates it with the computed curve number. The computed CN value for each pixel is for average conditions (i.e. antecedent moisture condition class II). The CN values for AMC II can be converted into CN values for AMC I (dry soils) and AMC III (saturated soils) by using the SCS (Soil Conservation Service) Standard Tables (USDA 2004) or computed using the following equations;

$$CN_I = \frac{(-75 \cdot CN_{II})}{(-175 + CN_{II})}, AMC\ I(dry\ soil) \qquad \text{Equation 4.16}$$

$$CN_{III} = \frac{(175 \cdot CN_{II})}{(75 + CN_{II})}, AMC\ III(saturated\ soil) \qquad \text{Equation 4.17}$$

Table 4.3: CN values used for runoff estimation in the study area. CN = 0 (maximum water storage in soil), CN = 100 (minimum water storage in soil). Adapted from Hess et al (2011) and USDA (2010)

Soils	Condition	Manmade surfaces (65% Impervious area)	Impervious area-dirt (Bare ground)	Grassland	Woodland
A	Very poor			78	45
	Poor			68	40
	Fair	77	72	58	35
	Good			49	30
	Excellent			39	
B	Very poor			86	66
	Poor			79	54
Alum,	Fair	85	82	66	42
Angelzarke,	Good			52	30
Ellerbeck,	Excellent			39	
C	Very poor			89	77
	Poor			86	75
Brickfields 3,	Fair	90	87	82	72
Dunkeswick,	Good			78	70
Enborne,	Excellent			74	
Nercwys,					
Salop, Wharfe					
D	Very poor			89	83
	Poor			89	81
Longmoss,	Fair	92	89	86	79
Wilcocks 1,	Good			83	77
Winter Hill	Excellent			80	

To determine which AMC Class is most appropriate in relation to the study area, the use of rainfall data is necessary. Daily precipitation data spanning a decade (2000-2010) as recorded at the weather station in Haltwhistle, UK, was used to identify storm events and in the computation of the required 5-day antecedent rainfall values (Antecedent Moisture Condition- AMC) based on three antecedent runoff conditions (see Table 4.4). After generating the CN map, the maximum potential retention (S) value which indicates the initial abstraction of rainfall by soil and vegetation were computed for each pixel using

Equation 4.8. Six storm events with varying precipitation intensity and AMC classes were evaluated. The runoff depth in mm was determined for each rainfall event by using Equation 4.7, and a runoff coefficient for each grid cell was computed using Equation 4.9. The runoff coefficient map was then used as a weight grid for down-the-slope propagation of the lumped effect of catchment properties (land cover and soil) into the calculation of flow accumulation and the modified TWI.

Table 4.4: Quantitative definition of antecedent runoff conditions (USDA 2010)

Antecedent runoff conditions	5-day antecedent rainfall values (mm)	
	Period without vegetation growth	Period with vegetation growth
Dry	Less than 12.7	Less than 35.6
Average	12.7 – 27.9	35.6 – 53.3
Wet	More than 27.9	More than 53.3

4.4.1.3 Terrain wetness index

The classic TWI was calculated as the natural logarithm of the ratio of the local upslope contributing area draining through a specific point and the local slope. The slope and upslope contributing area grids were generated from the merged 2.5 m grid DTM using the TauDEM ArcGIS plug-in (Tarboton, 2010). The TauDEM software accommodates the D ∞ procedure for representing flow direction and upslope contributing area (Tarboton, 1997; Hardy *et al.*, 2012). The D ∞ is a multiple flow direction algorithm that allows continuous flow angles and flow portioning between one or two neighbouring cells thereby minimizing the effect of over dispersion (Tarboton, 1997). In addition, D ∞ procedure can effective manage flow over relatively flat areas by a rule that forces flow in the direction of the nearest downslope cell (Wilson *et al.*, 2007). The first step in hydrological analysis is the removal pits. The presence of one or more grid cells surrounded completely by other cells of higher elevation usually results in artefacts that tend to interrupt the flow throughout the scene if unremoved. TauDEM uses a fill process to do this, raising the elevation of pits until they drain out (Tarboton, 2010). Flow direction and contributing area for each grid cell are then calculated from the DEM with filled pits using the D∞ procedure.

During flow direction computation, the D∞ algorithm assigns a single flow direction to each cell, which is represented as a continuous value between 0 and 2 π. This direction is defined as the steepest downward slope over eight triangular facets on a 3 x 3 pixel window centred on the cell of interest (Tarboton, 1997). Eight triangular facets are formed between the pixel and its eight neighbours. A downslope vector is calculated for each triangular facet which can lie within or outside a 45° angle range of the centre point of the facet. The flow direction for the central pixel is taken as the direction of the steepest downslope vector from all eight facets. This is advantageous as it avoids the approximation involved in locally fitting a plane and the counterintuitive influence of higher neighbours on downslope flow as is the case with the digital elevation model networks (DEMON) algorithm. Where it becomes impossible to allocate flow to one of the cardinal or diagonal directions a proportion of the flow is then assigned according to how close the flow direction angle is to the direct angle of the neighbouring cells (Figure 4.2).

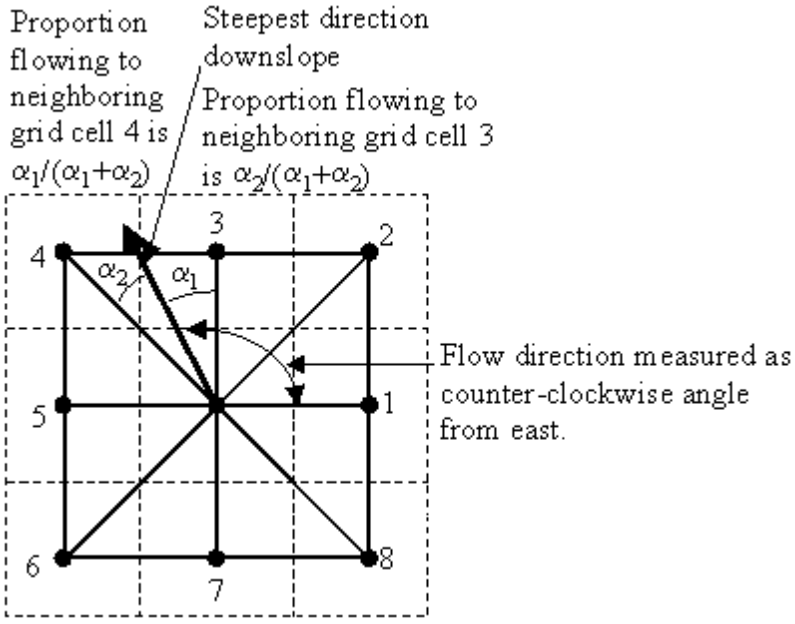

Figure 4.4: Diagram showing how flow direction is defined between two downslope grids based on proximity to the angle of steepest downslope on a triangular facet (After Tarboton 1997).

The routine has the option for inclusion of a weighting field grid. When the optional weight grid is used, the result is reported directly as a summation of weights, without any scaling

(Tarboton, 1997). The runoff coefficient grid was used as a weighting field incorporating the lumped effects of the spatial variability in soil and vegetation in the computation of flow accumulation. A modified TWI was computed and sensitivity testing was carried out to evaluate the robustness of the developed weighted grid and terrain flow model.
In addition to the modified TWI computation, the stream power index (SPI) which measures the erosive power of overland water flow was also computed. The SPI is based on the assumption that discharge is proportional to the specific catchment area. The SPI generally predicts the net erosion in areas with fairly steep slopes commonly associated with flow acceleration and convergence and net deposition in areas of reduced flow velocity as a result of flatten terrain or profile concavity. The erosive power of overland flow is often an important consideration in slope stability assessment where upland flow ingress slopes creating surface cuts or deposition of fines on slope drains along flow paths (Perry et al 2003). The SPI was calculated based on the formula developed by Moore *et al.* (1991)

$$SPI = A_S * \tan\beta \qquad \text{Equation 4.19}$$

Where A_S is the specific catchment area (the upslope area per unit width of contour (m^2/m)) and β is the local slope gradient (in degrees).

4.5 Geodatabase construction

The extracted slope stability variables of slope gradient, aspect, modified terrain wetness index (TWI), stream power index (SPI) and profile curvature derived from the ALS and Ordnance Survey DTM data (Sections 4.3.1.1 and 4.4.1.3) and land cover land use information of the transport corridor from the Compact Airborne Spectrographic Imager (CASI) imagery (Section 4.3.2) were compiled in a geodatabase in ArcGIS. Ten categories of slope gradients (5^o – 50^o) were identified from the ALS DTM to capture the upper and lower extremes of slope as well as the more typical cases found within the transport corridor. The Curvature grid is conventionally used to describe the physical characteristics of the slope face with respect to erosion and runoff processes. Various curvature components can be computed as the second derivative of the surface topography. In this study, profile curvature was employed as it provides an indication of curvature parallel to

the direction of the maximum slope. A negative value indicates that the surface is upwardly convex at that cell, while a positive profile indicates that the surface is upwardly concave at that cell, and a value of zero indicates a linear surface. Profile curvature influences the acceleration or deceleration of flow across the surface (Catani *et al.*, 2013). The profile curvature grid was reclassified into three classes; concave, flat, convex. The aspect grid represents the orientation of the gradient of each cell was also calculated. Aspects play a key role in landslide susceptibility as it may influence the exposure of the terrain to different amounts of rainfall and solar radiation, thus conditioning the terrain humidity and the vegetation growth (Dai and Lee, 2002; Catani *et al.*, 2013). The angular values of the aspect grid employed were typically reclassified on the basis of the facing direction with respect to the eight main cardinal directions (Burrough and McDonnell, 1998). The modified TWI and SPI grids were reclassified into ten classes using equal intervals.

Information on the underlying soils was extracted from the NATMAP vector data described in Section 3.4.3. Additional information on the distance to drainages was considered due to proximity to the South Tyne River of sections of the transport corridor. A shapefile of existing streams was extracted from the 1:2500 Ordnance Survey master map data and Euclidean raster of distance surface was created (ten buffer categories at 10m intervals) using the buffer tool in ArcGIS.

4.6 Evidential reasoning model

Evidential reasoning approach was employed to derive a spatial estimation of landslide susceptibility for the transport corridor. The approach requires the definition of basic probability assignment functions for the various landslide conditioning factors considered in the landslide susceptibility analysis. Following Carranza *et al.* (2005) a data driven approach was adopted for the estimation of evidential belief functions (EBFs) in this study. The data driven approach requires the transformation of thematic layers into evidential data layers based on the quantitative relationships between known past landslide occurrences and multiple landslide conditioning factors. This process entails an initial generation of evidential weights (basic probability assignment functions) for the various class attributes contained in the thematic layer. The evidential layers developed are then combined to generate the belief, disbelief and plausibility maps of the transport corridor.

To derive objective weights of the relative importance for each of the prepositions considered, techniques such as likelihood ratio function (Tien Bui *et al.*, 2012) and weight of evidence (Bonham-Carter, 1994; Lee *et al.*, 2013) are commonly employed in the derivation of basic probability assignment functions for landslide susceptibility assessment. Both techniques seek to highlight the contrast that may exist when two frequency distribution functions are compared, as is the case with landslide affected areas typically comprised of landslide prone and stable locations. The likelihood ratio technique was however chosen for this study owing to its relative simplicity to implement and is more frequently featured in literature as the means for evidential belief function derivation (Carranza *et al.*, 2005; Tien Bui *et al.*, 2012). The likelihood ratio is the ratio of occurrence probability to the non-occurrence probability for specific attributes (Park, 2011) and a brief overview of the procedure employed in this study is given below.

Eight causal factors (slope gradient, aspects, land-cover, zone of moisture accumulation (modified TWI), soil, SPI, distance from drainage channel and curvature) earlier identified from the field work and previous studies were considered in the landslide susceptibility assessment. Each of the eight thematic layers [A_i $(i = 1,2,\ldots,n)$] provided information on a cell by cell basis of the presence of landslide occurrence (T_p). 70% of the total landslide inventory was used as the training set for the determination of the relative contribution of each of the casual factors influencing slope instability in the study area. The frequency distribution functions showing the presence or absence of landslide cells for every class attribute in each of the evidences (factors influencing slope instability) was determined by overlaying the landslide inventory map on each of the eight maps of landslide conditioning factors. For example, given A_{ij} which is the jth class attribute (10^0-15^0 bin) of the evidence A_i (slope map), the likelihood ratio $\lambda(T_p)_{A_{ij}}$ indicating the degree of support for the occurrence of landslide is computed as defined by Equation 4.19:

$$\lambda(T_p)_{A_{ij}} = \frac{\frac{N(L \cap A_{ij})}{N(L)}}{\frac{N(A_{ij}) - N(L \cap A_{ij})}{N(F) - N(L)}} \qquad \text{Equation 4.19}$$

Where $N(L \cap A_{ij})$ is the number of landslide cells in class A_{ij}, $N(L)$ is the total number of landslide cell in the study area, $N(A_{ij})$ is the total number of pixels in class A_{ij}, and $N(F)$ is the total number of cells in the study area. The numerator is the proportion of landslides that intersect cells with an attribute value for a particular evidence A_{ij}. The denominator is the proportion of non-landslide cells in the given attribute class for a particular evidence A_{ij}.

The likelihood ratio of a non-landslide occurrence in a given attribute class for a particular evidence A_{ij} is defined by Equation 4.20:

$$\lambda(\bar{T}_p)_{A_{ij}} = \frac{\frac{N(L) - N(L \cap A_{ij})}{N(L)}}{\frac{N(F) - N(L) - N(A_{ij}) - N(L \cap A_{ij})}{N(F) - N(L)}} \qquad \text{Equation 4.20}$$

Where the numerator is the proportion of the landslides that did not occur in a given attribute class for a particular evidence A_{ij}. The denominator is the proportion of non-landslide areas in other attributes classes for the same evidence A_{ij}.

The likelihood ratio was computed for all the evidence layers. Likelihood ratio values can range from zero to infinity and as such, a standardization step is often required when deriving basic probability assignment functions from two likelihood ratios (Carranza *et al.*, 2005; Park, 2011). The standardisation procedure serves a dual purpose, firstly it allocates the weights of relative importance within class attribute values and secondly confines the mapping of the class attributes to the interval 0-1 (Park, 2011). Standardisation was achieved by dividing the individual class likelihood ratios by the sum of likelihood ratio values for all class attributes in a given thematic layer (See Equations 4.21, 4.22 and 4.23).

$$Bel(A_{ij}) = \frac{\lambda(T_p)_{A_{ij}}}{\sum_{j=1}^{n} \lambda(T_p)_{A_{ij}}} \qquad \text{Equation 4.21}$$

$$Dis(A_{ij}) = \frac{\lambda(\bar{T}_p)_{A_{ij}}}{\sum_{j=1}^{n} \lambda(\bar{T}_p)_{A_{ij}}} \quad \text{Equation 4.22}$$

$$Unc(A_{ij}) = 1 - \lambda(T_p)_{A_{ij}} - \lambda(\bar{T}_p)_{A_{ij}} \quad \text{Equation 4.23}$$

Though the approach is essentially data driven, some level of constraints becomes necessary when computing evidential belief functions (EBFs) from likelihood ratio (Carranza *et al.*, 2005; Park, 2011). Two key constraints as relating to landslide occurrences were observed independently during the computation of the evidential belief functions $Bel(A_{ij})$. Firstly, the absence of landslide incidence within a given class attribute of a particular evidence A_{ij} is indicative of the absence of belief ($Bel(A_{ij})$) but does not necessarily commit the belief function to disbelief ($Dis(A_{ij})$). In agreement with earlier studies (Carrranza et al 2005; Park 2011), these cases were regarded as one with only uncertainty and as such, $Dis(A_{ij})$ is 0 and Unc is set to 1. The second constraint had to do with locations that are naturally are not prone to landslide occurrences. Flat areas with zero slope values and water bodies are common examples. These areas were treated as areas of disbelief with $Bel(A_{ij})$ and $Unc(A_{ij})$ set to 0 for flat areas and water body, while $Dis(A_{ij})$ was set to 1.

4.6.1 Evidence aggregation

The Dempster's rule of combination was used in the aggregation of the EBFs derived for the eight landslide conditioning factors (Dempster, 1967). In accordance with the Dempster's rule of orthogonal sum of basic probability assignments, the EBF's were combined two at a time until all were aggregated. The formulae for the aggregation of evidential maps for two conditioning factors A_1 and A_2 was (Carranza et al 2005; Bui et al 2012):

$$Bel\ A_1A_2 = \frac{Bel\ A_1 Bel\ A_2 + Bel\ A_1 Unc\ A_2 + Bel\ A_2 Unc\ A_1}{1 - Bel\ A_1 Dis\ A_2 - Dis\ A_1 Bel\ A_2} \quad \text{Equation 4.24}$$

$$Dis\ A_1A_2 = \frac{Dis\ A_1A_2 + Dis\ A_1Unc\ A_2 + Dis\ A_2Unc\ A_1}{1 - Bel\ A_1Dis\ A_2 - Dis\ A_1Bel\ A_2}$$ Equation 4.25

$$Unc\ A_2A_2 = \frac{Unc\ A_2Unc\ A_2}{1 - Bel\ A_1Dis\ A_2 - Dis\ A_1Bel\ A_2}$$ Equation 4.26

Final combination maps of EBFs resulted in the integrated Bel, Dis, Unc and Pls maps for landslide occurrence based on given spatial evidences from the conditioning factors. The belief map is considered representative of the correlation between landslide location and each conditioning factor; as such the integrated belief map was used for deriving the landslide susceptibility index (LSI). In order to evaluate the contribution of the developed modified TWI computation to landslide susceptibility within the transport corridor slopes, two evidential belief models were developed. The two models were developed using the eight selected landslide conditioning factors with the essential difference being the use of the modified TWI in one and the classic TWI computation in the other.

4.6.2 Model validation

The landslide susceptibility maps were evaluated to access how well the model performed in classifying the landslide prone locations along transport corridor slope cuttings and embankments. Validation was achieved by comparing the developed landslide susceptibility maps with the existing landslide locations. The landslide inventory was first randomly partitioned into two mutually exclusive groups. The first group made up of 70% of the total landslide inventory was used as the training set employed in the construction of the landslide susceptibility map based on evidential belief function. The second group (remaining 30%) was used as a validation set to evaluate the predictive capability of the developed landslide susceptibility model based on the training dataset.

The success rate for the validation was determined by comparing the susceptibility map with the 30% validation set not considered during the susceptibility modelling. The success rate curve varies the decision threshold and plots the respective sensitivity against the total proportion of the study area in ranked susceptibility index (Brenning, 2005). Sensitivity is simply the proportion of known landslide cells correctly classified as susceptible (true

positive) and specificity is the proportion of catchment cells free of landslides that are correctly classified as stable (true negative). The relative ranks for each of the landslide susceptibility classes were obtained by sorting the calculated index values of all the cells in the study area in descending order and divided into 100 classes at 1% intervals. The area under the curve (AUC) is the average sensitivity of the classifier over the range of 1-specificity. The AUC provides a quantitative measure of the ability of the susceptibility model to fit known distribution of shallow landslides in the study area (Park, 2011; Lee *et al.*, 2013). The index ranges from 0.5 for models with no predictive capability, to 1 for models with perfect predictive power. For comparison purposes, the same validation procedure was applied on both EBF models (modified and classic TWI) in order to evaluate the predictive capability introduced into the EBF model with the inclusion of the lumped effects of land cover and soil into the characterisation of zones of moisture accumulation.

4.7 Summary

This Chapter details the methods employed in the development of a multi sourced multi scale geospatial model for recognition and prediction of slope instability in the transport corridor. The methodology includes the development of a scalable spatial geodatabase of factors responsible for slope instability in the transport corridor, the development of a surafce runoff model that incorporates the influence of underlying soils and vegetation cover to surface runoff generation as well as the broader catchment contributions to localised zones of moisture concentration within the transport corridor. The developed analytical framework efficiently integrates the various geospatial data and accounts for the ucertainties associated with the datasets and the landslide predictions. The integration of the SCS-CN method into the classic TWI computation enabled the incoporation of the influence of underlying soils and vegetation cover to surface runoff generation without the huge data requirements associated with earlier approaches (Quasi-TWI approach) developed to address the lack of integration of soil and vegetation cover in simulating spatial distibution of soil moisture and overland flow.

Eight landslide conditioning factors were identified as influential to landslide suceptibility in the transport corridor. Thematic maps of the various factor were transformed into evidential data layers based on the quantitative relationships between the inventory of past landslide and the various landslide conditioning factors. Evidential weights of the relative importance for each of the factors were generated and integrated using the evidential

reasoning approach. The results of the methodological procedures are presented in Chapter 5.

5 Results

5.1 Introduction

This chapter presents the results of the landslide susceptibility model for transport corridor environments. Section 5.2 covers techniques employed in the DTM generation and accuracy assessments. Section 5.3 details the processes and results associated with the development of the land cover map for the study area. Section 5.4 covers analysis aimed at integrating catchment contributions into the characterisation of zones of moisture accumulation within the transport corridor environment. Results obtained from the integration of multi-source and multiscale geospatial data approach for recognition and prediction of landslide susceptibility in transport corridors using evidential reasoning approach is reported in Section 5.5.

5.2 DTM interpolation

The global statistics for the DTM validation are presented in Table 5.1. Both interpolation techniques produced DTMs with mean errors in centimetre to sub-centimetre range. The results show very similar magnitude of mean error values for all IDW DTMs (1 mm). However, the size of the mean variance is shown to increase as the DTM grid sizes become larger. The mean absolute error values for the IDW DTMs indicate a slightly higher interpolation bias of a centimetre or less with each successive reduction in resolution. The root mean square error values indicate a general loss in DTM quality with reduction in spatial resolution. The RMSE increases from 2.3 to 3.5 for IDW DTM and 3.0 to 4.5 for ANUDEM DTMs as the cell size increases from 0.5 to 5 m. The 0.5m DTMs for both interpolation techniques provide more accurate representation of the of the transport corridor terrain as revealed in their lower average residues and RMSE values (1 mm for IDW and 4.6 cm for ANUDEM). Comparatively, the average residual and RMSE values show the IDW DTMs provide a better terrain representation for all ten grid resolutions assessed. Both interpolation techniques produced DTMs with very similar mean absolute error values, however, the error range (mean absolute error) in the ANUDEM DTM which increased from 16 to 24m as against 15 to 21m for the IDW DTMs. The slightly higher interpolation bias associated with the ANUDEM DTM is attributed to the drainage enforced algorithm employed. The drainage enforcement algorithm modifies the DEM by

the removal of spurious sinks and construction of relatively smooth surfaces (Hutchinson, 2008).

Table 5.1: Global statistics summarising errors for the IDW and ANUDEM interpolated DTMs compared against validation subset obtained from the original point cloud prior to DTM generation.

Interpolation method	Resolution (m)	Mean Error (m)	Min Error (m)	Max Error (m)	RMSE (m)	Mean Absolute Error (m)	Standard Deviation (m)
IDW	0.5	0.001416	-1.93	1.98	0.23	0.15	0.17
	1	0.001456	-2.85	6.83	0.24	0.15	0.18
	1.5	0.001116	-2.94	3.16	0.24	0.16	0.19
	2	0.002059	-3.22	7.37	0.26	0.16	0.21
	2.5	0.001133	-3.49	8.25	0.27	0.17	0.22
	3	0.001456	-3.80	7.92	0.29	0.18	0.23
	3.5	0.000991	-3.50	8.39	0.30	0.18	0.24
	4	0.000288	-4.41	7.00	0.32	0.19	0.25
	4.5	0.001098	-4.81	7.20	0.33	0.20	0.27
	5	0.001877	-4.94	7.35	0.35	0.21	0.28
ANUDEM	0.5	0.046156	-8.56	12.04	0.30	0.16	0.26
	1	0.046892	-8.35	10.96	0.31	0.16	0.26
	1.5	0.044477	-8.56	13.58	0.32	0.17	0.27
	2	0.044133	-7.17	8.81	0.32	0.18	0.29
	2.5	0.049933	-8.88	9.90	0.35	0.19	0.29
	3	0.043577	-10.16	10.96	0.37	0.20	0.31
	3.5	0.044921	-7.78	13.58	0.40	0.22	0.33
	4	0.045256	-4.59	6.14	0.40	0.23	0.33
	4.5	0.041857	-7.73	13.58	0.45	0.24	0.37
	5	0.041043	-9.87	13.83	0.45	0.24	0.37

Visual assessment of hillshade maps derived from IDW and ANUDEM interpolated DTMs of the ALS data of the transport corridor reveal a general trend of loss of topographic detail as the spatial resolution is reduced. The IDW DTMs seem to retain more fine-scale topographic details in contrast to the ANUDEM DTMs, where the smoothing effect of the drainage enforced ANUDEM interpolation is apparent (Figures 5.1 and 5.2). This is illustrated in transects taken across earthwork cutting and embankments within the transport corridor. An example is presented in Figure 5.3, which shows a maximum difference of 55 cm coinciding with the presence of a topographic depression on the south facing slope approximately 17 m from the point A. This topographic feature while

recognisable on the ANUDEM DTM transect is smoothened compare to the IDW. Both approaches work well in areas of relatively little topographic variation, for example, earthwork embankments largely covered by ballast that exhibit relatively uniform relief (Figures 5.4, 5.5 and 5.6). Overall, the IDW DTMs retain more information in situation where there is high frequency fine scale topographic variation in the earthwork infrastructure.

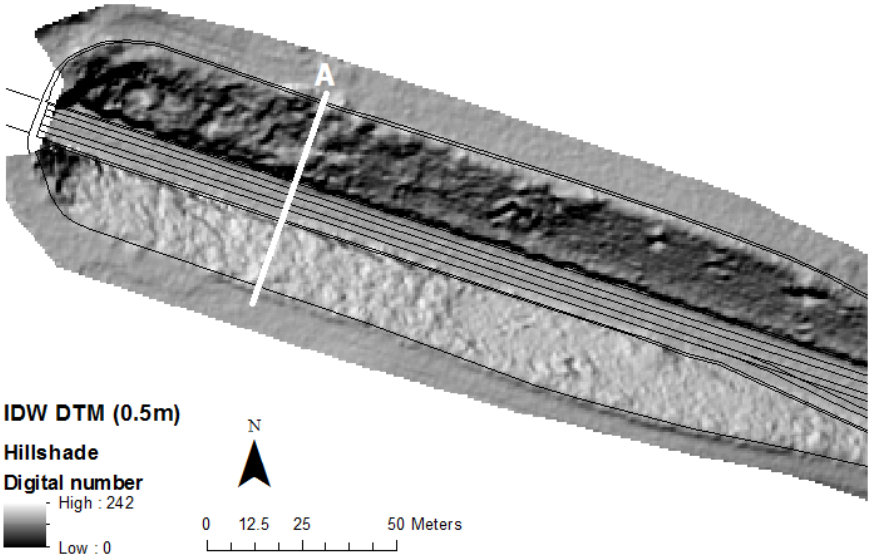

Figure 5.1: Hillshade of IDW interpolated DTM of earthwork cutting at Whitchester, showing location for transect plot in figure 5.

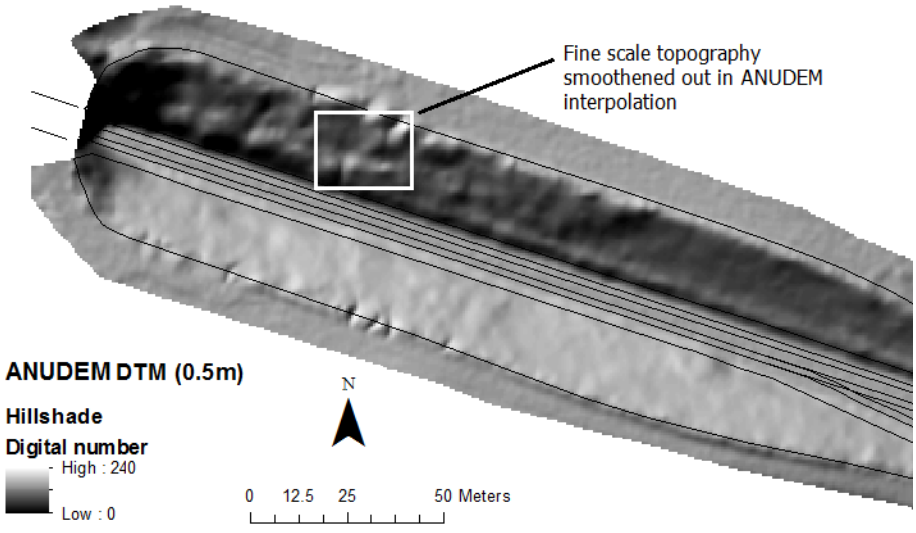

Figure 5.2: Hillshade of the ANUDEM interpolated DTM for earthwork cutting at Whitchester.

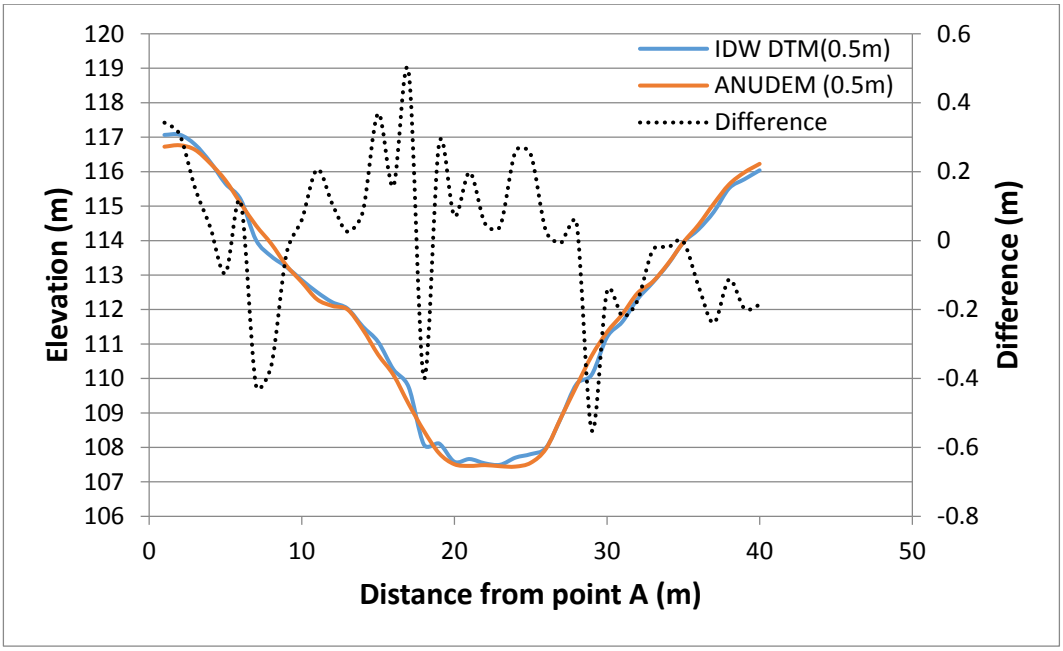

Figure 5.3: Elevation values along transect taken across an earthwork cutting in Whitchester. Transect location is as indicated in figure 5.2

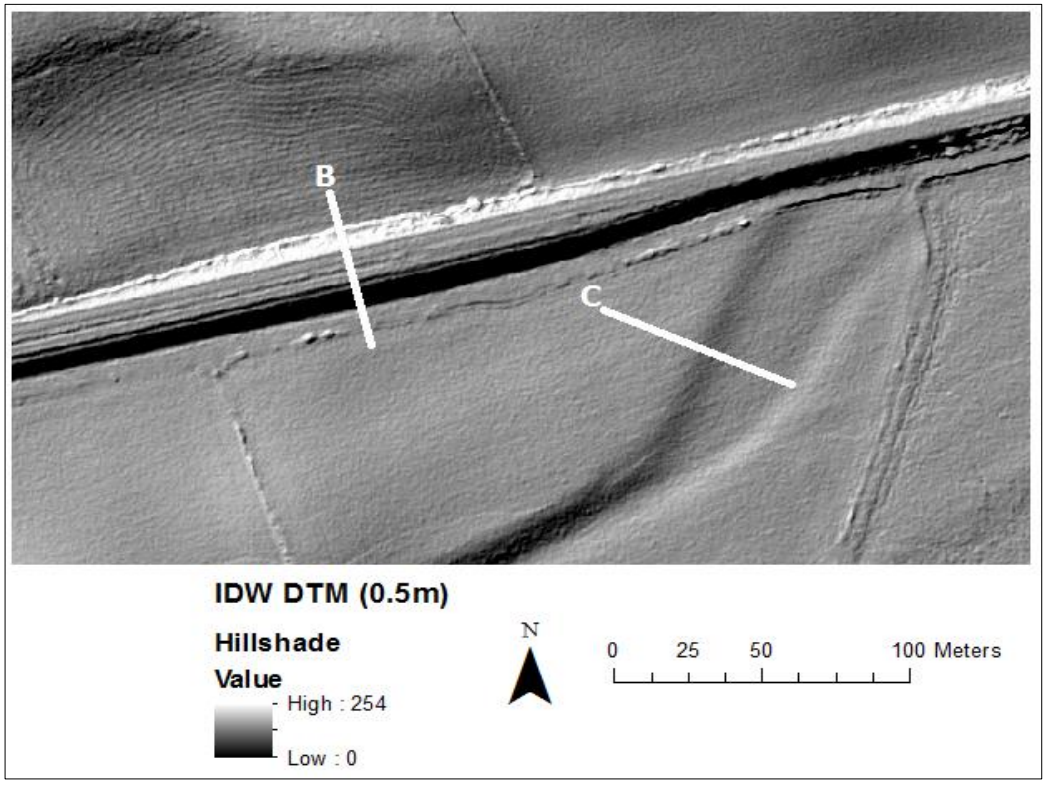

Figure 5.4: Hillshade of IDW interpolated DTM of earthwork embankment showing locations for transect plots in Figures 5.4 and 5.5

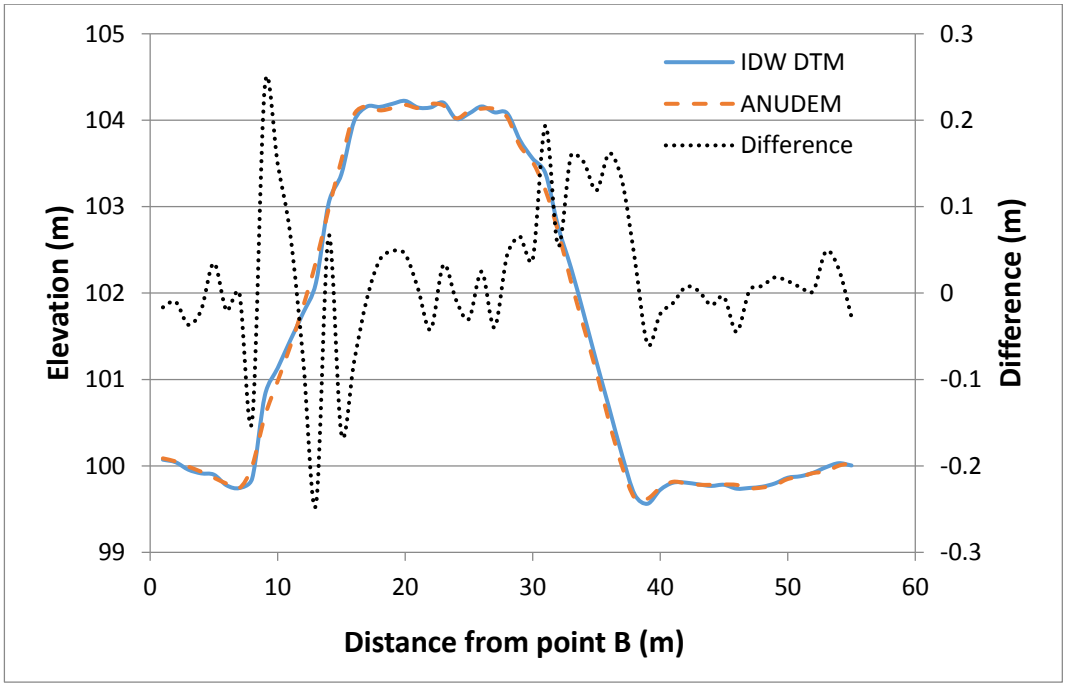

Figure 5.5: Elevation values along transect taken across an earthwork embankment at Melkridge for the IDW and ANUDEM interpolated DTMs.

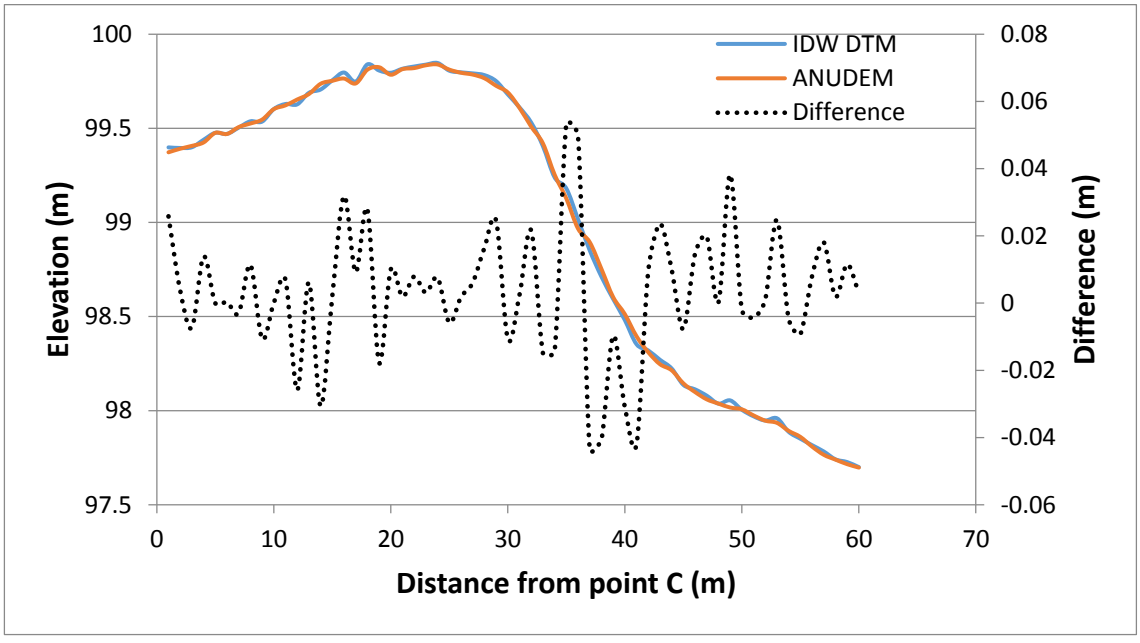

Figure 5.6: Transect of elevation values across a gently sloped terrain at Melkridge for the IDW and ANUDEM interpolated DTMs

5.2.1 Impact of interpolation technique and DTM resolution on terrain derivatives

In comparison with the elevation data, terrain derivatives provided better indications of statistically significant differences existing between the grid sizes and interpolation techniques. Analysis of first order derivatives (slope and aspect), second order derivative (curvature) and TWI, a compound derivative that combines local slope with upstream contributing area derived from interpolated IDW and ANUDEM DTMs are presented.

Typical slope gradients associated with earthwork cutting and embankments within the transport corridor ranges from 10^{o} and 49^{o}, although, near vertical gradients associated with retaining walls and rock gibbons are also present. Visually, in the IDW derived slope grids, the outline of the slope toe and crest are clearly discernible in the finer grid resolutions (0.5 and 1m) but become gradually blurred in coarser grid sizes. At 4.5 and 5 m resolutions, the overall shape of the earthwork boundaries with surrounding catchment slope becomes slightly fuzzy. The ANUDEM slope grids were visually smoother with the outlines of the embankment less distinct when compared at the same resolution as the IDW grids. Both interpolation techniques (IDW and ANUDEM) provided similar overall slope pattern for the 0.5 m DTMs (Figure 5.7). The plot of the IDW DTM generated slope values against the ANUDEM DTM slope values demonstrates a strong agreement (R^2 value of 0.8) in the general overall pattern of slope distribution (Figure 5.8). At the same resolutions, transects show the inclusion of more fine-scale topography in the IDW DTM than in the ANUDEM DTM. An example is presented in Figure 5.9, showing slope values for a transect across the Whitchester cutting. The gradient values for the topographic feature in the south facing slope of the Whitchester cutting 17 m from point A (presented earlier in Section 5.2) is 63^{o} for the IDW DTM but only 39^{o} for the ANUDEM DTM. The extreme gradient peaks are associated with variations in microtopography which are more prominently captured in the IDW DTM. In the ANUDEM algorithm the drainage enforcement algorithm imposes a global drainage condition that smoothens the general topographic trend in an attempt to maintain consistency with natural slopes resulting in the underestimation of the slope gradients (Hutchinson, 2008).

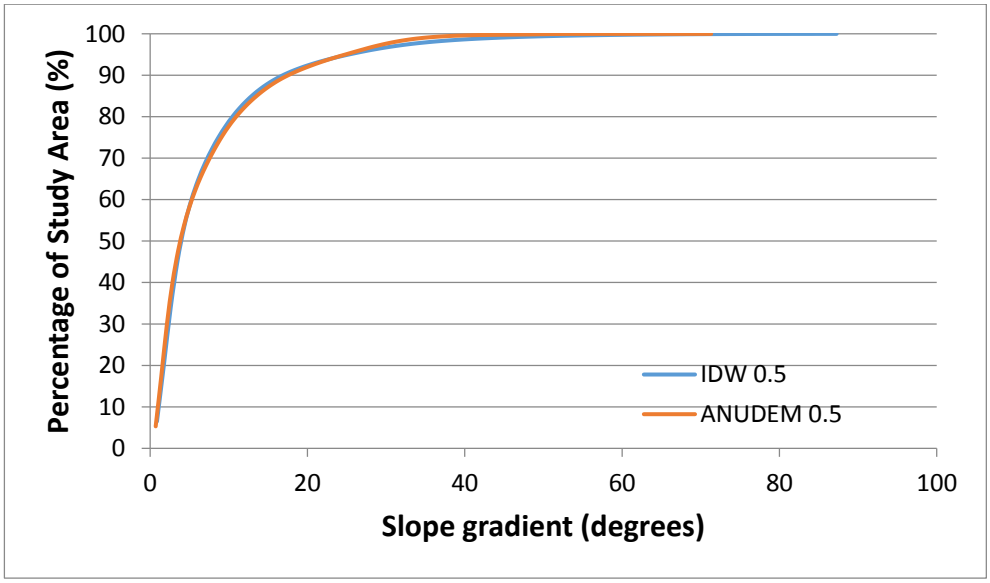

Figure 5.7: Cumulative frequency distributions for 0.5m IDW and ANUDEM DTM for the transport corridor slopes.

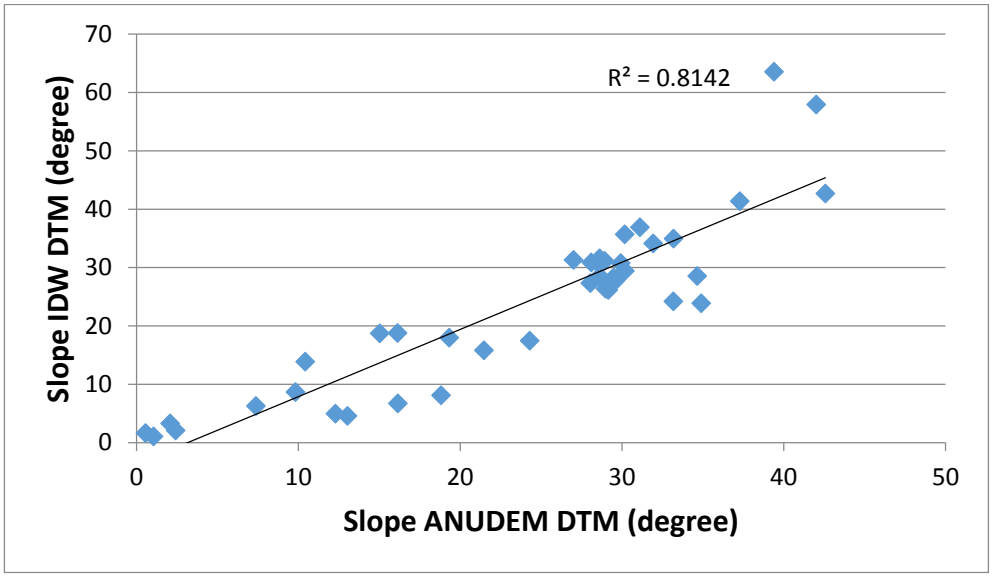

Figure 5.8: Correlation between IDW and ANUDEM DTM derived slope values for transport corridor slopes

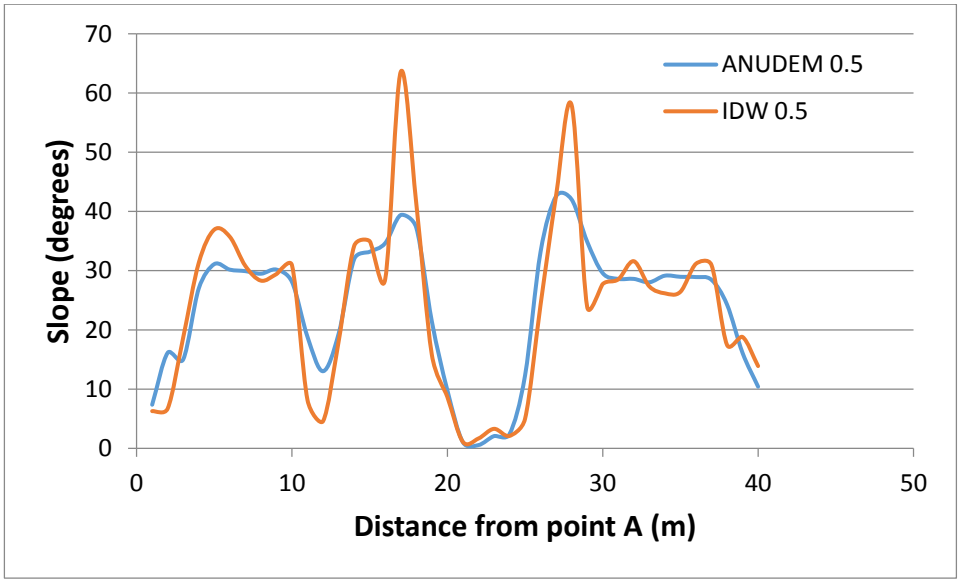

Figure 5.9: Slope values for IDW and ANUDEM DTMs along transect taken across an earthwork cutting in Whitchester. Transect location is as indicated in figure 5.1

A T-test of the sample means using the first to hundredth percentile values of the slope grids showed no significant difference ($p > 0.05$) in the means for slope grids derived from the IDW interpolated DTM. The obtained P-values for the ten DTMs per interpolation technique are presented in Table 5.2. However the plot of key percentile slope values against the grid resolutions for the IDW DTMs reveals the sensitivity of the distribution of slope values across the various grid sizes (Figure 5.10). The plot identifies the lower slope values as the least affected by increasing grid sizes. The 5^{th} percentile of gradients found in the transport corridor (corresponds to the 0 to 4^{o} slope class) is essentially unaltered as a result of reduced grid resolutions. Also, the median slope values for all resolutions are generally quite similar, though a slight underestimation of the median slope value in coarser grid resolutions. However, the 90^{th} and 99^{th} percentiles exhibit a discernible decrease in slope values with reduced grid resolution. A difference of 8^{o} and 9^{o} is recorded for the 90^{th} and 99^{th} percentile as DTM grid resolution reduced from 0.5 to 5 m.

Slope maps derived from the ANUDEM interpolated DTM exhibit the same general trend of decrease in slope variability with reduced DTM grid resolutions as observed for the IDW DTMs. However the smoothing effects of the ANUDEM algorithm is portrayed in the more pronounced drop in the maximum slope values with increasing grid cell sizes (Figure 5.11). The T-test showed significant difference ($p < 0.05$) in the sample means of the slope values

for the ten grid resolutions derived from the ANUDEM interpolated DTM. The p values obtained for the various ANUDEM slope grids is presented in Table 5.3. The results of the T-test and visual assessments suggest that the dominant slope gradients could be effectively characterised using any of the investigated grid resolutions of the IDW DTMs.

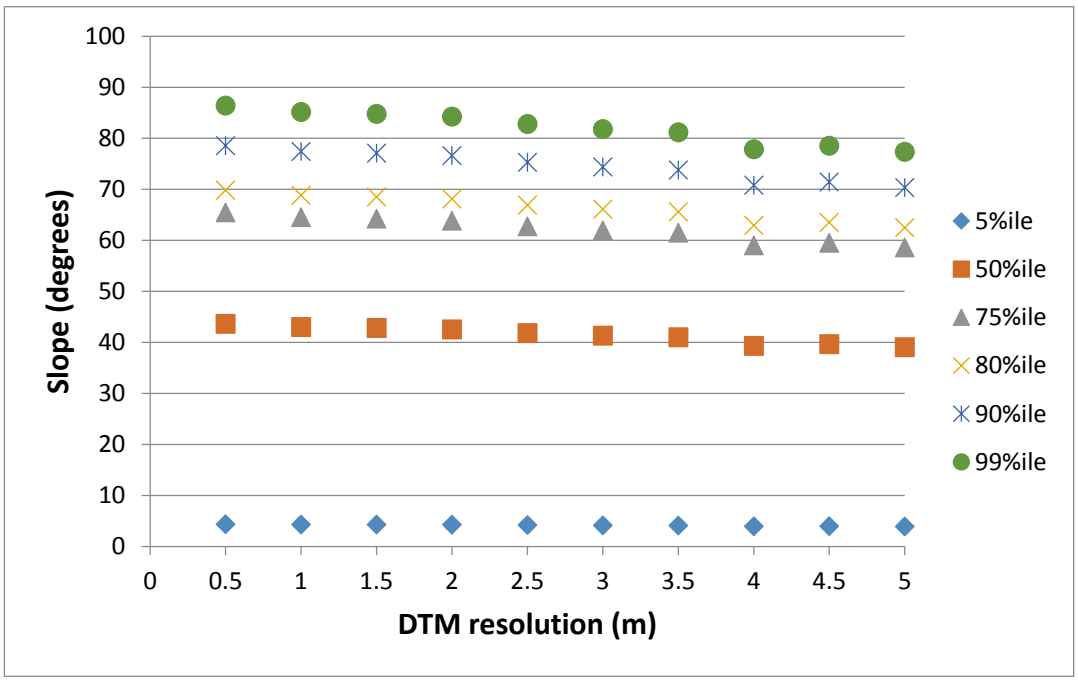

Figure 5.10: Figure 5.12: Key distribution values for transport corridor slopes derived from ten IDW DTMs resolutions.

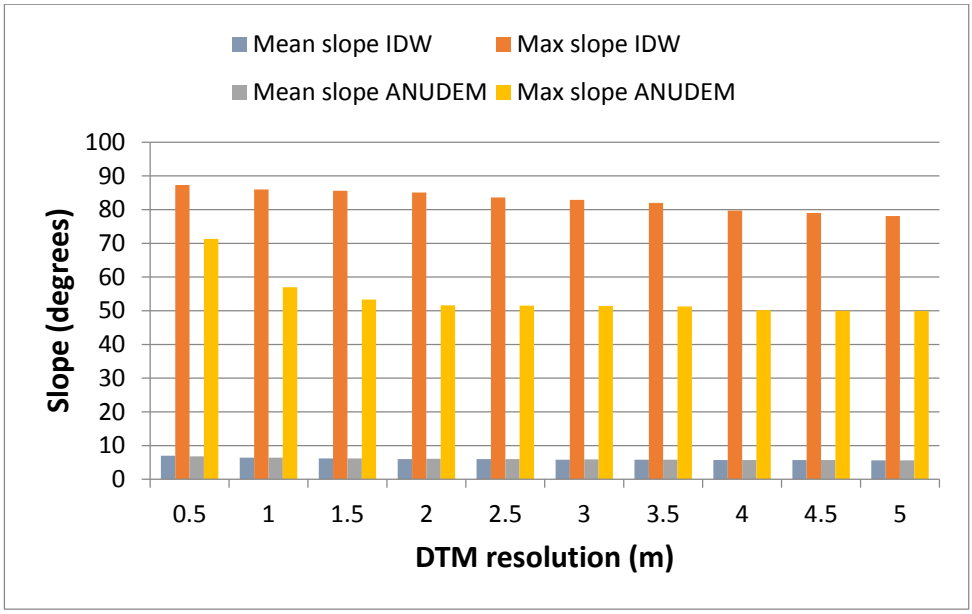

Figure 5.11: Variation in maximum and mean slope gradients for IDW and ANUDEM DTMs

Table 5.2: Summary statistics of T-test for IDW slope grids

	T-test for Equality of Means						
	t	Degree of freedom	P value Sig. (2-tailed)	Mean Difference	Std. Error Difference	95% Confidence Interval of the Difference	
						Lower	Upper
IDW1	0.18	197.96	0.86	0.63	3.56	-6.38	7.64
IDW1.5	0.23	197.93	0.82	0.83	3.55	-6.17	7.82
IDW 2	0.31	197.88	0.76	1.09	3.54	-5.88	8.07
IDW 2.5	0.52	197.64	0.60	1.84	3.51	-5.09	8.75
IDW 3	0.68	197.41	0.50	2.35	3.49	-4.52	9.23
IDW 3.5	0.77	197.23	0.44	2.68	3.47	-4.18	9.52
IDW 4	1.28	195.90	0.20	4.36	3.41	-2.37	11.08
IDW 4.5	1.17	196.23	0.24	4.01	3.42	-2.74	10.75
IDW 5	1.36	195.62	0.18	4.62	3.40	-2.08	11.32

Table 5.3: Summary statistics of T-test for ANUDEM DTMs

	T-test for Equality of Means						
	t	Degree of freedom	P value Sig. (2-tailed)	Mean Difference	Std. Error Difference	95% Confidence Interval of the Difference	
						Lower	Upper
ANUDEM1	2.73	188.80	0.01	7.24	2.65	2.02	12.46
ANUDEM1.5	3.53	183.25	0.00	9.12	2.58	4.02	14.21
ANUDEM 2	3.91	180.28	0.00	9.98	2.55	4.95	15.02
ANUDEM 2.5	3.97	179.79	0.00	10.13	2.55	5.10	15.16
ANUDEM 3	3.94	180.0	0.00	10.06	2.55	5.03	15.09
ANUDEM 3.5	3.94	180.0	0.00	10.06	2.55	5.03	15.09
ANUDEM 4	4.22	177.75	0.00	10.67	2.53	5.68	15.66
ANUDEM 45	4.28	177.22	0.00	10.81	2.53	5.83	15.79
ANUDEM 5	4.29	177.12	0.00	10.84	2.53	5.86	15.82

The CFDs computed for the aspect maps derived from all the IDW DTMs is presented in Figure 5.12. Very little variation exists between the different resolutions of the DTM grids. However, the better representation of the fine-scale topographic detail in the IDW DTMs translates into better representation of aspect. For example, Figure 5.13 shows the Whitchester cutting highlighting that the ANUDEM algorithm modifies the aspect of the slope in line with the dominant slope trend to ensue continuous flow.

The presence of fine scale topographic features is important to localised saturation, as variation in fine scale topography can result in differential soil moisture content or

prolonged wetting of a section the slope face. The limited ability of the ANUDEM to portray fine scale topography suggests the use of IDW DTM as better suited for the calculation of aspect over the transport corridor slopes. There was no significant impact in the representation of aspect due to resolution reduction for the IDW interpolation DTM at 5m. At a 1.5m resolution, the smoothing effect of the ANUDEM algorithm is seen to have readjusted aspect values at the base of the slope (approximately 20m from point A) in line with the predominant natural topography (Figure 5.14).

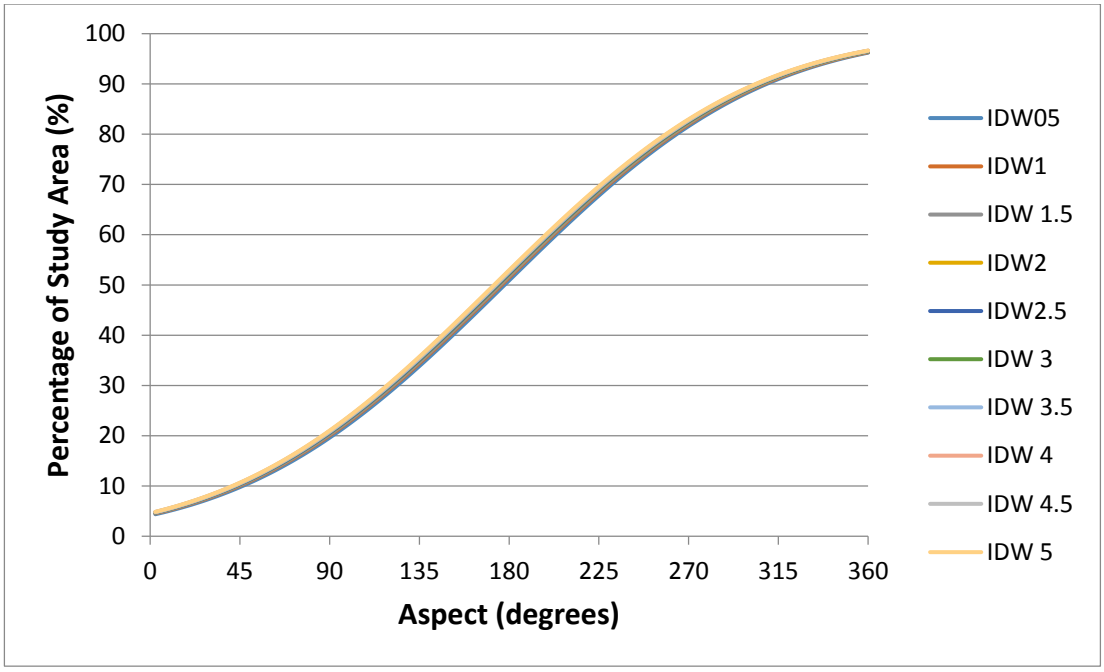

Figure 5.12: Cumulative frequency distribution curves of slope aspects for IDW DTMs

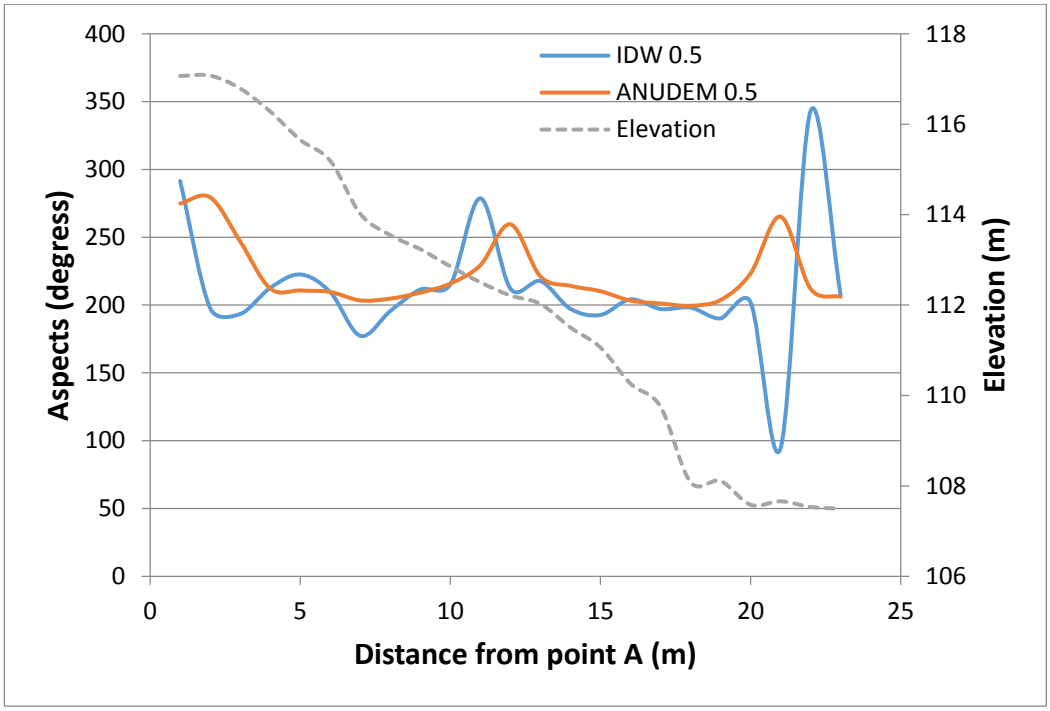

Figure 5.13: Variation in aspect values for transect taken across the south facing slope of the Whitchester embankment cutting. Location of transect is shown in Figure 5.4.

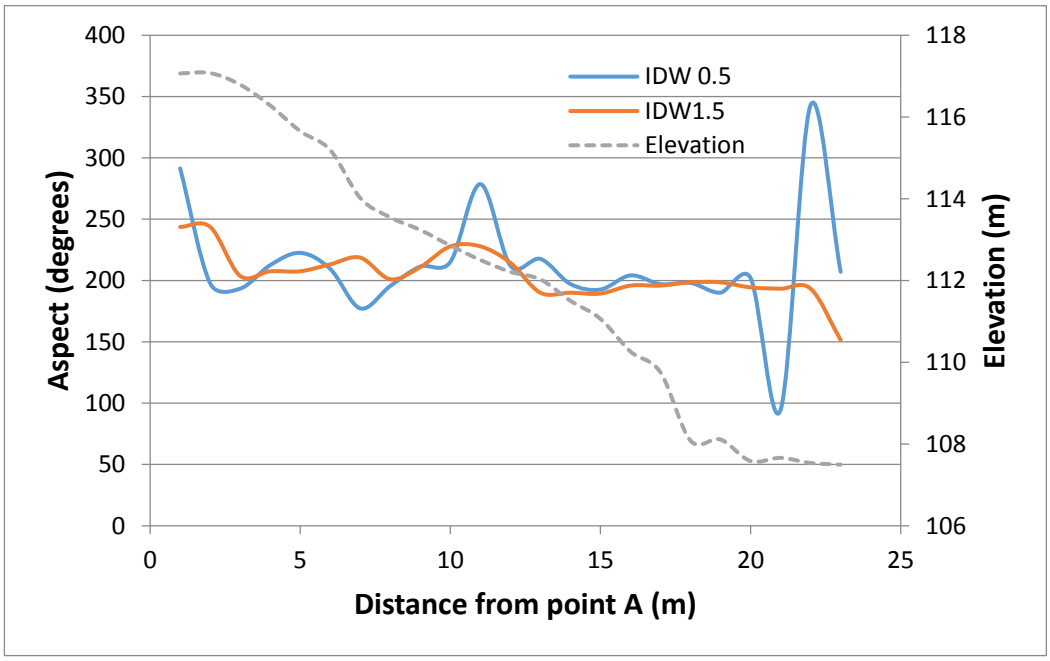

Figure 5.14: Figure 5.14: Plot of aspect values for transect across Whitchester cutting (south facing slope), showing loss of fine scale topography with resolution reduction from 0.5 to 1.5m. Location of transect is shown in Figure 5.4.

The curvature grids for all DTM resolutions was normalised to display curvature values within the range of -1 to 1 to allow for ease of comparison. The mean and standard deviation of the difference maps obtained by the subtraction of the 0.5 m DTM profile curvature values from the various grid resolutions indicated that no significant change occurred (Table 5.4). Transect across the Whitchester cutting show that concave profile curvature known to influence local accumulation of runoff on slope faces are better recognised by the IDW interpolated curvature grid (Figure 5.15). The curvature values from transect for the ANUDEM essentially plots in the negative domain of the overall curvature value range. This suggests a suppression of theses topographic features in the ANUDEM DTM.

Table 5.4: Summary statistics of difference maps obtained for profile curvature grids derived from IDW DTMs

Grid resolution	Mean	Standard Deviation
IDW 1	-0.05	0.008
IDW 1.5	-0.06	0.015
IDW 2	-0.08	0.012
IDW 2.5	-0.20	0.012
IDW 3	-0.17	0.014
IDW 3.5	-0.16	0.012
IDW 4	-0.15	0.018
IDW 4.5	-0.15	0.014
IDW 5	-0.28	0.016

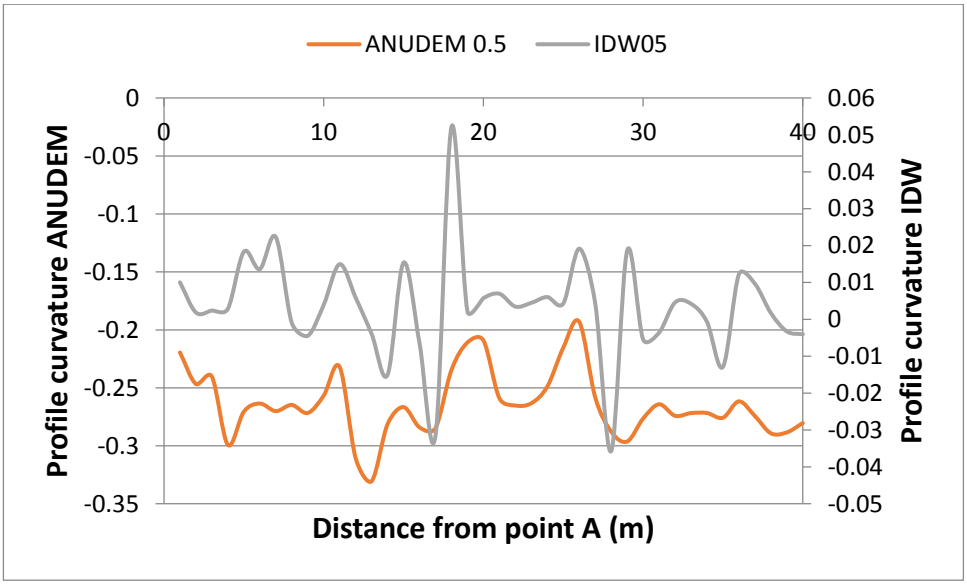

Figure 5.15: Variation in the representation of profile curvature for embankment cutting in Whitchester.

5.2.2 Impact of interpolation technique and DTM resolution on the calculation of the classic TWI

The classic TWI values for the transport corridor slopes were derived for the IDW and ANUDEM DTMS. The cumulative frequency distributions of the classic TWI values for the IDW and ANUDEM DTMs is presented in Figure 5.16. Higher classic TWI values translate into wetter soils and these values are generally seen to increase downslope culminating at the base of the slope. The marked increase in classic TWI values represented by seemingly random peaks in the IDW grids are in response to variation in slope values as theses point midway down the embankment cutting. For example on the north facing slope of the embankment cutting, the ANUDEM grid presents a near uniform downslope gradient of 30^{o} to 34^{o} ensuring continuous flow. This is reflected in the gradual downslope increase in the values of specific catchment area (Figure 5.17). The effect of microtopography is most pronounced in the IDW DTM as depicted in the number of upstream cells draining downslope. There appears to be a reset in the calculation of specific catchment area where the effects of microtopography is pronounced, resulting in an erratic increase and decrease in the number of cells draining downslope (Figure 5.18). The erratic nature of the spikes in the classic TWI value due to the presence of microtopography presents a challenge to the meaningful interpretation of the flow pattern. The sporadic increase and decrease in

computed specific catchment area values are responsible for the erratic nature of the IDW TWI results at finer resolutions. Generally, the classic TWI values increase at lower resolutions for both interpolated DTMs; thus, the effect of microtopography diminishes with increasing DTM grid size and the ANUDEM DTM seemingly providing a better representation of flow.

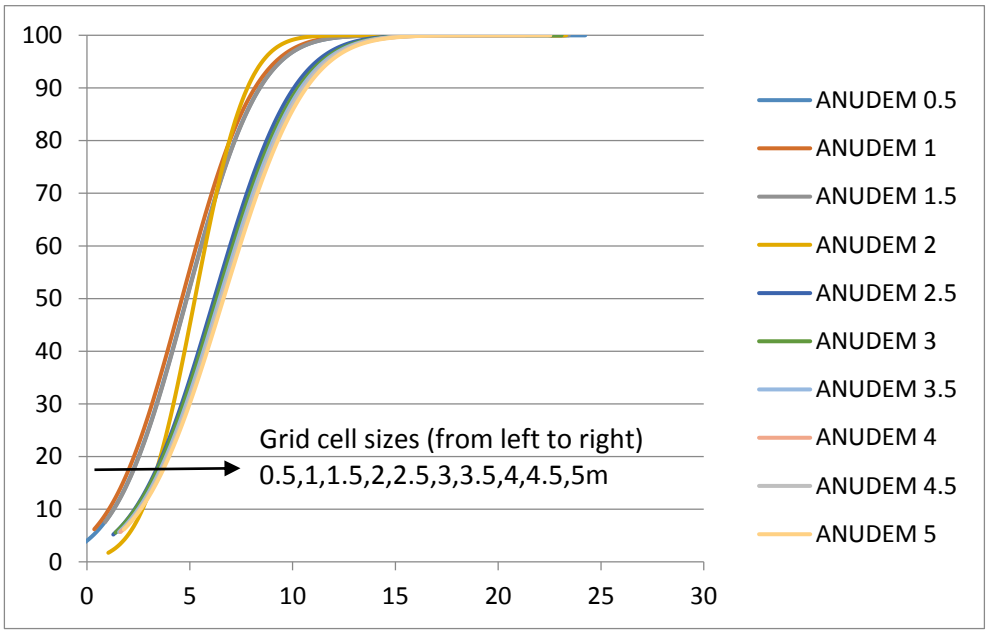

Figure 5.16: Cumulative frequency distribution of classic TWI values generated for all the evaluated ANUDEM DTM grid resolutions.

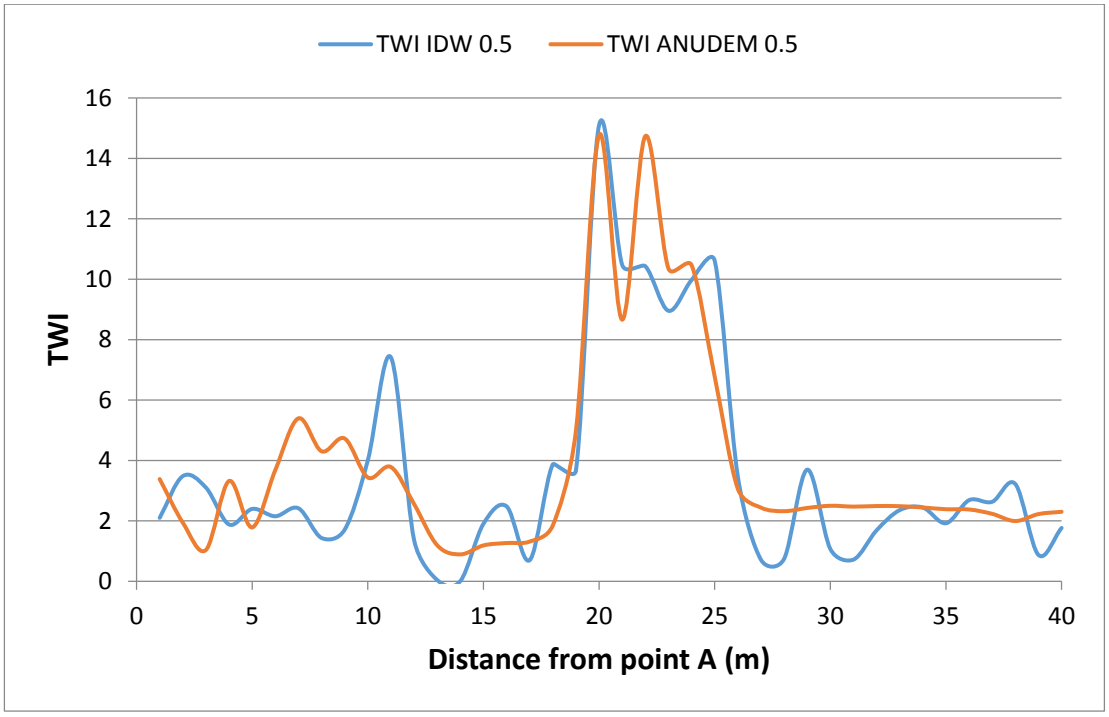

Figure 5.17: Plots of classic TWI values for 0.5 m IDW and ANUDEM DTMs across the Whitchester cutting

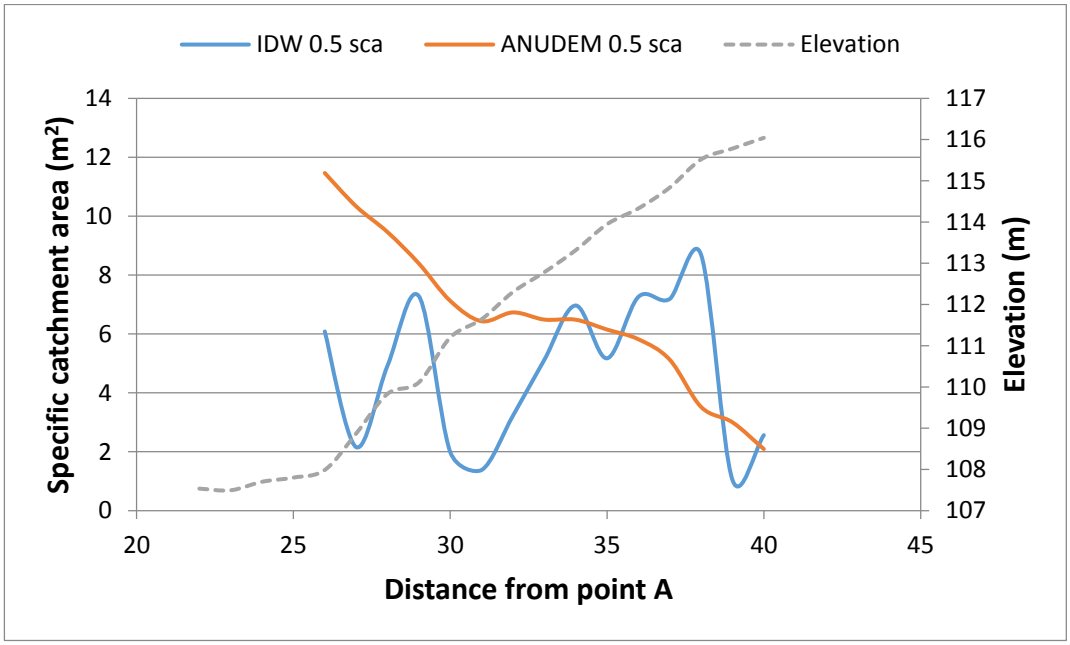

Figure 5.18: Plots of specific catchment area for ANUDEM and IDW DTMS for a north facing earthwork cutting at Whitchester.

Results of the Mann Whitney U statistics for the classic TWI grids at the various resolutions show no significant difference between the distributions of classic TWI values for all the grid resolutions Table 5.4. The Mann Whitney U test is a non-parametric test that allows for the comparison of two sets of independent data without the assumption of normal distribution. However, difference maps obtained by the subtraction of the 0.5 m DTM TWI values from the various grid resolutions indicated slight decrease in the mean values at the 2m resolution grid and thereafter the minimum and maximum classic TWI values between grids plateaued at 17 TWI units. This suggests a significant reduction in the contribution of the fine scale topographic features in the calculation of specific catchment area at 2m resolution. The summary statistics of the difference map obtained for the various grid resolutions are presented in Table 5.5. The 2.5m grid was used as the optimum grid size due to lengthy processing time required with the use of the 2m grid resolution.

Table 5.5 Summary statistics for the Mann Whitney U test for ANUDEM TWI grids

	TWI_1	TWI_15	TWI_2	TWI_25	TWI_3	TWI_35	TWI_4	TWI_45	TWI_5
Mann-Whitney U	4884.500	4826.500	4806.000	4925.000	4797.000	4883.000	4900.000	4824.000	4685.000
Z	-0.282	-0.424	-0.474	-0.183	-0.496	-0.286	-0.244	-0.430	-0.770
Asymp. Sig. (2-tailed)	0.778	0.672	0.635	0.855	0.620	0.775	0.807	0.667	0.441

Table 5.6: Summary statistics of difference maps obtained for the various ANUDDEM grid resolutions

Grid resolution	Mean	Standard deviation	Minimum	Maximum
ANUDEM 1	0.81	2.58	-20.24	18.56
ANUDEM 1.5	1.14	2.70	-19.02	19.99
ANUDEM 2	1.09	2.21	-18.06	16.97
ANUDEM 2.5	1.24	2.31	-17.23	17.71
ANUDEM 3	1.36	2.40	-17.57	17.96
ANUDEM 3.5	1.49	2.43	-17.03	17.82
ANUDEM 4	1.59	2.71	-17.81	17.82
ANUDEM 4.5	1.68	2.52	-17.56	17.57
ANUDEM 5	1.76	2.57	-17.30	17.51

5.3 Development of land cover map

The land cover map of the study area was generated from the CASI imagery in order to represent the influence of vegetation on the hydrological response of the land parcels in the subsequent modelling of overland flow of the broader catchment. The methods employed in the classification process are detailed in Section 4.3.2. In summary, supervised classification using the maximum likelihood classifier was carried out on the processed CASI image.

5.3.1 Simple band selection

For the nine land cover classes considered in the analysis, Table 5.6 lists the transformed separability values between the land cover classes recognised to be present in the study area. The lowest transformed divergence value of 1905 was observed for road-to-rail, road-to-building and shrubs-to-bare earth. Generally, the transformed divergence values for the classes show evidence of good separability (Table 5.7). The high separability between most of the land cover classes (see Table 5.7) is an indication of the ability of simple band selection approach to retain low variance information necessary for the characterisation of the various land cover types.

Table 5.8 shows the contingency matrix of the resulting classification. The highest numbers of misclassified pixels occurred between the road and rail classes with 19 pixels of the rail land cover class been wrongly classified as road. This was not surprising as low class separability has been reported to exist between roads, roof materials and bare soils due to their spectral similarity (Herold and Roberts, 2010). There are also indications of the existence of considerable overlap in the spectral signatures of several other land cover classes as indicated by the presence misclassified pixels. For example, the rail track-beds are essentially covered with ballast and as such exhibit a degree of spectral similarity with the road class (Table 5.7, transformed divergence of 1905). This is responsible for the high rate of misclassified pixels existing between the road and rail classes (Table 5.8). An error assessment based on 438 randomly located validation points of verified ground truth produced an overall accuracy of 80.59% with a kappa statistics of 0.75.

Table 5.7: Separability table for nine land cover classes in the study area

	River	**Woodland**	**Rail**	**Pasture**	**Managed pasture**	**Bare earth**	**Shrubs**	**Road**	**Buildings**
River	0	2000	2000	2000	2000	2000	2000	2000	2000
Woodland	-	0	2000	1916	2000	2000	1997	2000	2000
Rail	-	-	0	2000	2000	2000	2000	1905	1999
Pasture	-	-	-	0	2000	2000	2000	2000	2000
Managed pasture	-	-	-	-	0	2000	2000	1993	2000
Bare earth	-	-	-	-	-	0	1905	2000	2000
Shrubs	-	-	-	-	-	-	0	2000	2000
Road	-	-	-	-	-	-	-	0	1905
Buildings	-	-	-	-	-	-	-	-	0

Table 5.8: Contingency matrix for nine land cover classes in the study area

	River	Woodland	Rail	Pasture	Managed pasture	Bare earth	shrubs	Road	Building	Total	Producer's accuracy (%)	User's accuracy (%)
River	25	0	0	0	0	0	0	0	0	24	57.14	100.0
Woodland	1	39	0	6	0	0	8	2	0	56	90.70	69.64
Rail	0	0	21	0	0	0	0	2	0	23	52.50	91.30
Pasture	0	2	0	169	0	1	0	2	0	174	95.48	97.13
Managed pasture	0	0	0	1	7	2	0	0	0	10	100.0	70.0
Bare earth	0	0	0	0	0	21	0	0	0	21	84.0	100.0
Shrubs	0	1	0	1	0	1	13	0	0	16	61.90	81.25
Road	9	1	19	0	0	0	0	33	17	80	80.49	41.25
Buildings	7	0	0	0	0	0	0	2	25	34	59.52	73.53
Total	42	43	40	177	7	25	21	41	42			
Overall accuracy= 80.37							Overall Kappa statistics = 0.75					

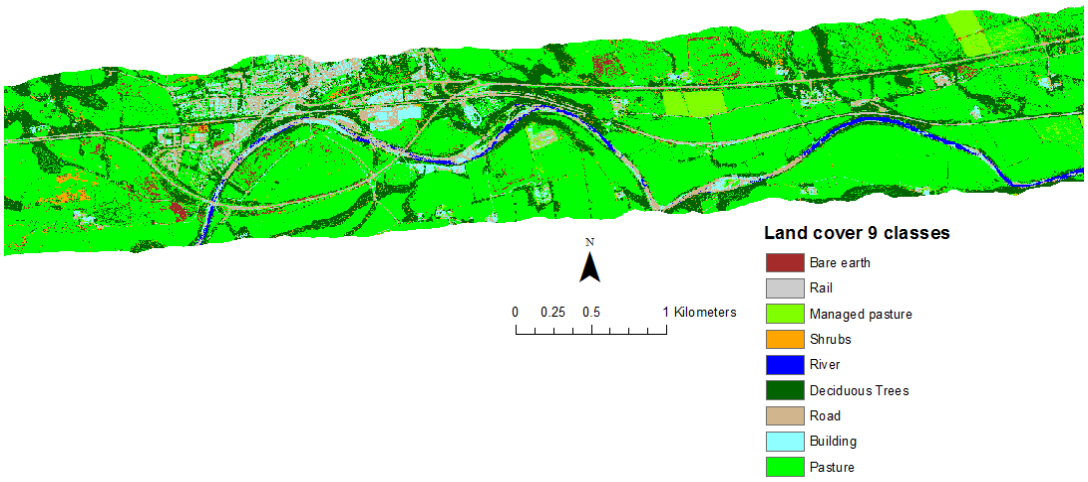

Figure 5.19: Land cover map of the transport corridor with nine land cover classes derived from the simple band selection image.

Land cover classes with considerable overlap in spectral space and of similar hydrological response to precipitation and surface runoff were merged to improve the overall classification accuracy. Table 5.9 presents the results of the transformed divergence analysis for eight land cover classes after the road and rail classes were merged. The divergence values reveal a good separability between the various land covers, with an average separability value of 1989. However, low separability values occur between shrubs-bare earth and building-manmade classes. A level of spectral overlap between the deciduous woodland, pasture and shrub classes is also shown to be present, as indicated by the overlap of those classes (Table 5.9). The deciduous land cover class is comprised of a mixture of deciduous woodland interspersed with coniferous trees. The mean reflectance values for coniferous and deciduous spectra are quite similar to each other and to typical green vegetation spectra like pasture and leafy green shrubs (Cipar *et al.*, 2004). Though, the deciduous and coniferous trees are easily distinguishable from one another by the higher near infra-red reflectance that characterises the deciduous trees, a decision was taken to group both tree species into a single land cover class on the basis of their closely related hydrological response to soil moisture and slope stability (Greenwood *et al.*, 2004; Glendinning *et al.*, 2009). As manmade and building land cover classes are essentially hydrological impervious surfaces they were also merged into a single class.

Table 5.9: Separability table for eight land cover classes in the study area

	River	Woodland	Pasture	Managed pasture	Bare earth	Shrubs	Manmade	Buildings
River	0	2000	2000	2000	2000	2000	2000	2000
Woodland	-	0	1916	2000	2000	1997	2000	2000
Pasture	-	-	0	2000	2000	2000	2000	2000
Managed pasture	-	-	-	0	2000	2000	1996	2000
Bare earth	-	-	-	-	0	1905	2000	2000
Shrubs	-	-	-	-	-	0	2000	2000
Manmade	-	-	-	-	-	-	0	1905
Buildings	-	-	-	-	-	-	-	0

In addition to the spectral similarity between the manmade and building land cover classes, the confusion matrix (Table 5.10) also shows significant number of misclassified pixels between manmade, building and the river classes resulting in low producer accuracy for the river class. Large boulders placed along the Tyne River bank for the purpose river bank erosion control were misclassified as building and manmade classes. The characteristic low level of the Tyne River at the time of the year the CASI image was acquired also exposed boulders on the river bed resulting in parts of the river being classified as building and manmade classes. This is responsible for the low producers accuracy recorded for the river class. There was also evidence that the CASI image was acquired during or immediately after some light showers as the road surface showed evidence of wetness as isolated specks of the river class on the pavement surfaces (Appendix 3). These isolated river pixels were later filtered out as no river class exists in areas where they were depicted. Overall, a higher classification accuracy of 83.79% with a kappa statistics of 0.75 was obtained for the eight class land cover classification. The land cover classification map is presented in Figure 5.20

Table 5.10: Contingency matrix for eight land cover classes in the study area

	River	**Woodland**	**Pasture**	**Managed pasture**	**Bare earth**	**shrubs**	**Manmade**	**Building**	**Total**	**Producers accuracy (%)**	**Users accuracy (%)**
River	24	0	0	0	0	0	0	0	24	57.14	100.0
Woodland	1	39	6	0	0	9	2	0	57	95.12	68.42
Pasture	0	1	170	0	1	0	2	0	174	95.51	97.70
Managed pasture	0	0	1	7	2	0	3	0	13	100.0	53.85
Bare earth	0	0	0	0	21	0	0	0	21	84.0	100.0
Shrubs	0	1	1	0	1	13	0	0	16	59.09	81.25
Manmade	7	0	0	0	0	0	64	14	85	79.01	75.29
Buildings	10	0	0	0	0	0	10	28	48	66.67	58.33
Total	42	41	178	7	25	22	81	42			
Overall accuracy= 83.56						Overall Kappa statistics = 0.79					

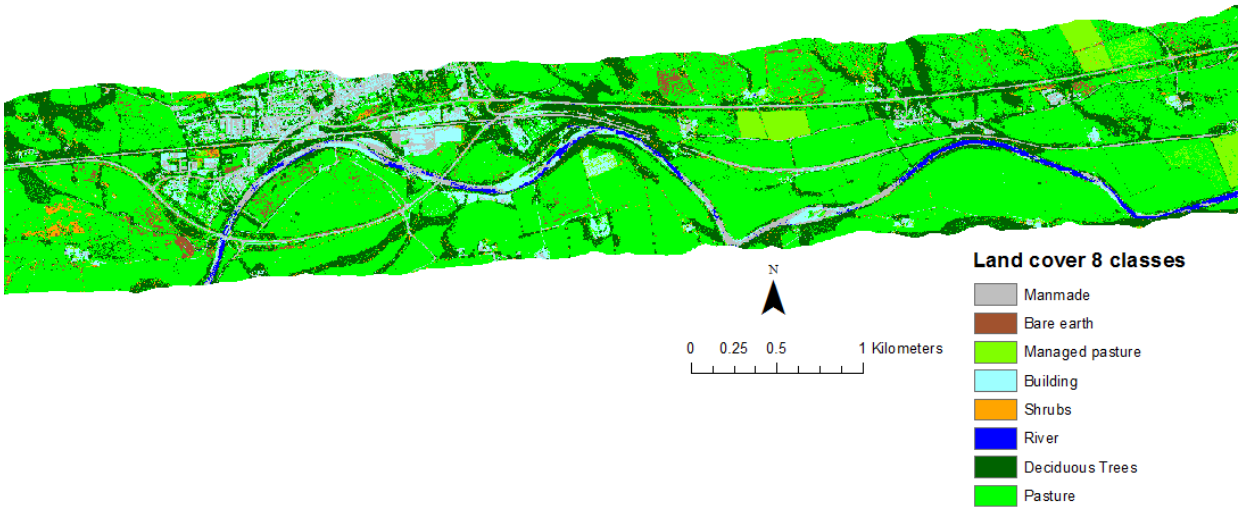

Figure 5.20: Land cover map of the transport corridor with eight land cover classes derived from the simple band selection image.

A relatively good separability (with average transformed separability value of 1990) exists between the seven land cover classes as shown in the transformed divergence values (see Table 5.11). The manmade and building classes were merged to reduce the error introduced by the spectral similarities between both land cover classes. An improved overall classification accuracy of 90.18% with a kappa statistics of 0.87 was also achieved, indicating a better classification map in comparison to the earlier land cover classification maps (Table 5.10). The merging of the rail, road and building classes to create an impervious class had improved the classification accuracy from an initial 80.37% with nine land cover classes to 90.18% with seven classes (Table 5.12). There is also considerable reduction of noise in the various land cover classes as shown by the decline in the number of misclassified pixels between classes (see Figure 5.21).

Figure 5.21: Land cover map of the transport corridor with seven land cover classes derived from the simple band selection image.

Table 5.11: Separability table for seven land cover classes in the study area

	River	**Woodland**	**Pasture**	**Managed pasture**	**Bare earth**	**Shrubs**	**Manmade**
River	0	2000	2000	2000	2000	2000	2000
Woodland	-	0	1916	2000	2000	1997	2000
Pasture	-	-	0	2000	2000	2000	2000
Managed pasture	-	-	-	0	2000	2000	1998
Bare earth	-	-	-	-	0	1905	2000
Shrubs	-	-	-	-	-	0	2000
Manmade	-	-	-	-	-	-	0

Table 5.12: Contingency matrix for seven land cover classes in the study area

	River	Woodland	Pasture	Managed pasture	Bare earth	shrubs	Manmade	Total	Producers accuracy (%)	Users accuracy (%)	Kappa
River	26	0	0	0	0	0	0	26	61.90	100.0	1
Woodland	1	39	6	0	0	9	2	57	95.12	68.42	0.65
Pasture	0	1	170	0	1	0	1	173	95.51	98.27	0.97
Managed pasture	0	0	1	7	2	0	1	11	100.0	63.64	0.63
Bare earth	0	0	0	0	21	0	0	21	84.0	100.0	1
Shrubs	0	1	1	0	1	13	0	16	59.07	81.25	0.80
Manmade	15	0	0	0	0	0	119	134	96.75	88.81	0.84
Total	42	41	178	7	25	22	123				
Overall accuracy= 90.18						Overall Kappa statistics = 0.87					

The pasture and shrubs classes were merged into a single class to account for error introduced by shrubs being misclassified as pasture. The resulting 5-class classification (Figure 5.22) had an overall accuracy of 87.21% with a Kappa statistic of 0.81 (Tables 5.13). The overall accuracy for the five land cover classification is slightly lower than the accuracy reported for the previous seven land cover classes map from which it was derived. The variation in the spectral characteristics among shrub species represented within the study area is thought to be the primary reason for the decline in the overall accuracy of the newly merged five land cover class map. The northern boundaries of the study area is characterised by heaths - low growing woody vegetation commonly associated with low quality acidic soils, which was generally brownish in colour at the time of validation sampling. The shrubs located around the flood plains of the Tyne River are within pasturelands and are essentially taller and leafy green in colour. This spectral variation within the shrub class is believed to be responsible for the spectral similarities revealed to exist between the shrub-bare earth class and between the shrub-pasture-woodland land cover classes. The merging of the pasture, managed pasture and shrub classes created a new composite class (pasture) characterised by large internal variability resulting in increased number of misclassified pixels between the pasture and woodland classes, which lead to a slight reduction in overall classification accuracy (Tables 5.12 and 5.13).

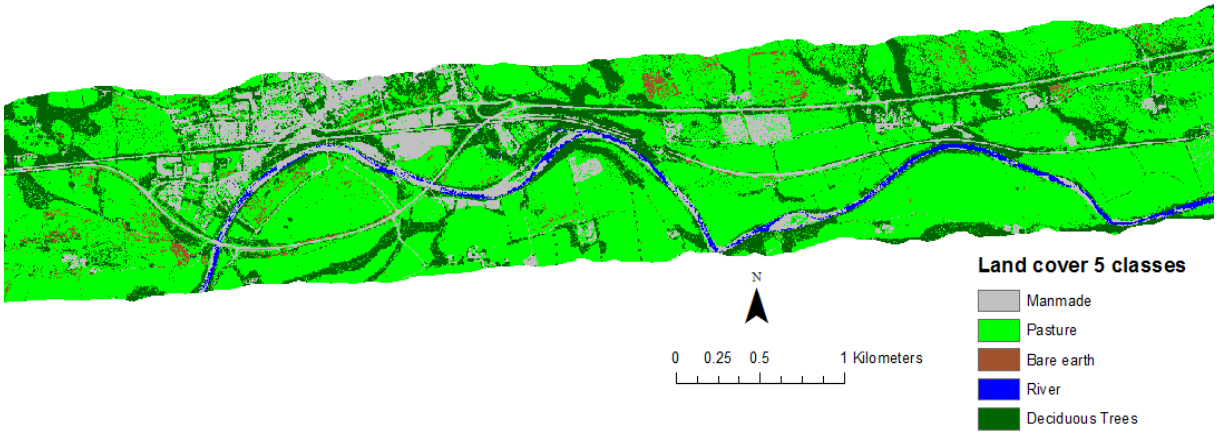

Figure 5.22: Land cover map of the transport corridor with five land cover classes derived from the simple band selection image.

The Tyne River was masked out using the Tyne river shapefile of the study area obtained from Ordnance Survey MasterMap data. This ensured a high degree of accuracy in the representation of the river class (Figure 5.23). The implementation of the mask also reduced the level of noise, with the elimination of all misclassified pixels occurring within the river class. The mask improved the overall classification accuracy of the 5 land cover class classification from 87.21% to 90.87% with a kappa of 0.87 (Table 5.14). The overall accuracy of the masked land cover map was further re-evaluated with the exclusion of the river class in the overall accuracy assessment. This was done to assess the overall map accuracy devoid of any improvement resulting from the introduced mask. An overall accuracy of 89.90% with a kappa statistics of 0.84 was recorded for the land cover classification map without the river class (Table 5.15). A fuzzy convolution filter was applied to the final masked land cover (five classes) map to reduce the speckled effect, which improved the overall classification accuracy of the 5-class masked land cover map to an overall accuracy of 91.10% and kappa statistics of 0.87 (Table 5.16) and an overall classification accuracy of 90.15% with kappa statistic of 0.85 for the masked land cover map without the river class (Table 5.17). The final land cover classification map derived from selected bands of the CASI imagery of the transport corridor is presented in Figure 5.24.

Table 5.13: Contingency matrix for the five land cover classification

	River	Woodland	Pasture	Bare earth	Manmade	Total	Producers' accuracy (%)	Users' accuracy (%)	Class kappa
River	26	0	0	0	0	26	61.90	100.0	1.00
Woodland	1	41	21	0	2	65	100.0	63.08	0.59
Pasture	0	0	179	7	3	189	86.47	94.71	0.90
Bare earth	0	0	7	18	0	25	72.0	72.0	0.70
Manmade	15	0	0	0	118	133	95.97	89.47	0.84
Total	42	41	207	25	123				
Overall accuracy= 87.21					Overall Kappa statistics = 0.81				

Table 5.14: Contingency matrix of the five land-cover classes with the river class masked.

	River	Woodland	Pasture	Bare earth	Manmade	Total	Producers accuracy (%)	Users accuracy (%)	Class kappa
River	42	0	0	0	0	42	100.0	100.0	1.00
Woodland	0	41	21	0	2	64	100.0	64.06	0.60
Pasture	0	1	179	7	3	189	86.89	94.71	0.90
Bare earth	0	0	7	18	0	25	72.0	72.0	0.70
Manmade	0	0	0	0	118	118	95.97	100.0	1.00
Total	42	42	207	25	123				
Overall accuracy = 90.87					Overall Kappa statistics = 0.87				

Table 5.15: Contingency matrix of the land-cover classes without the river class.

	Woodland	Pasture	Bare earth	Manmade	Total	Producers accuracy (%)	Users accuracy (%)	Class kappa
Woodland	41	21	0	2	64	100.0	65.06	0.60
Pasture	0	179	7	3	189	86.47	94.71	0.89
Bare earth	0	7	18	0	25	72.0	72.0	0.70
Manmade	0	0	0	118	118	95.93	100.0	1.00
Total	41	207	25	123				
Overall accuracy = 89.90				Overall Kappa statistics = 0.84				

Table 5.16: Contingency matrix of fuzzy convolution filter land cover classification map for five land cover classes

	River	Woodland	Pasture	Bare earth	Manmade	Total	Producers accuracy (%)	Users accuracy (%)	Class kappa
River	42	0	0	0	0	42	100	100	1.00
Woodland	0	41	20	0	2	64	100.0	65.08	0.62
Pasture	0	0	181	7	3	189	86.47	94.71	0.89
Bare earth	0	0	6	18	0	25	68.0	73.91	0.72
Manmade	0	0	0	0	118	118	95.93	100.0	1.00
Total	42	41	207	25	123				
	Overall accuracy = 91.10%				Overall Kappa statistics = 0.87				

Table 5.17: Contingency matrix of the final five land-cover classes, with application of fuzzy convolution filter and the exclusion of the river class

	Woodland	Pasture	Bare earth	Manmade	Total	Producers accuracy (%)	Users accuracy (%)	Class kappa
Woodland	41	20	0	2	64	100.0	65.08	0.61
Pasture	0	181	8	3	189	87.86	94.27	0.88
Bare earth	0	6	17	0	25	68.0	73.91	0.72
Manmade	0	0	0	118	118	95.93	100.0	1.00
Total	41	207	25	123				
Overall accuracy = 90.15%				Overall Kappa statistics = 0.85				

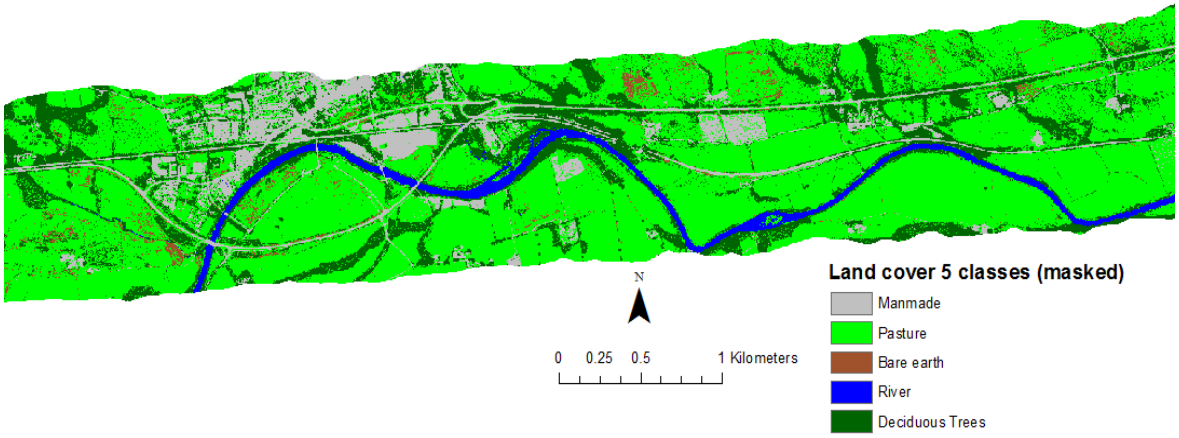

Figure 5.23: Land cover map of the transport corridor with five land cover classes with masked river class.

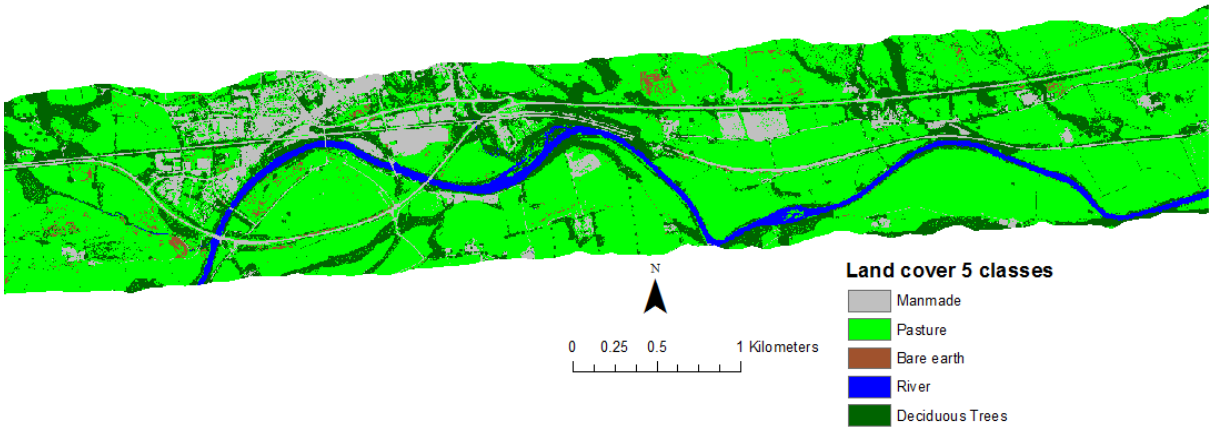

Figure 5.24: Final land cover classification map derived from selected bands of the CASI imagery of the transport corridor, with the application of fuzzy convolution to reduce the speckled effect and improve overall classification.

5.3.2 Spectral transformed (MNF) CASI image

The MNF image transformed divergence indicates a good separability between classes with the exception of the rail and road class (Table 5.18). The resulting contingency matrix of the classification also reveals a lower level of misclassification between some land cover classes and overestimation in others (see Tables 5.8, 5.19 and Figure 5.25) For example the transformed divergence value for the road and rail class in simple band selection image classification is 1905 while the separability value for the same classes in the transformed

image is 1768. This is expected as the MNF spectral transformation results in the distribution function of the different classes becoming more distinct due to the removal of random noise and low variance features (Bater and Coops, 2009). The resulting 9-class classification of the MNF image with an average transformed divergence value of 1938 as against 1989 for the simple band selection approach has an overall accuracy of 74.43% and a kappa statistic of 0.68 (Table 5.19). Similar results were obtained for the eight class land cover classification with good separability (Table 5.20), with an average transformed divergence value of 1998 but with poorer classification performance. The eight class land cover classification had an overall accuracy of 77.85% and a kappa statistics of 0.72 (Table 5.21) in comparison with the simple band section approach image with an overall accuracy of 83.56% and a kappa statistics of 0.79 (Table 5.10). The land cover classification map for eight land cover classes is presented in Figure 5.26.

Table 5.18: Separability table for nine land cover classes derived from the MNF transformed CASI image of the study area

	Woodland	**Rail**	**Road**	**Managed pasture**	**Buildings**	**Pasture**	**River**	**Bare earth**	**Shrubs**
Woodland	0	2000	2000	2000	2000	1996	2000	2000	2000
Rail	-	0	1768	2000	1998	2000	2000	2000	2000
Road	-	-	0	2000	1994	2000	2000	2000	2000
Managed pasture	-	-	-	0	2000	2000	2000	2000	2000
Buildings	-	-	-	-	0	2000	2000	2000	2000
Pasture	-	-	-	-	-	0	2000	2000	2000
River	-	-	-	-	-	-	0	2000	2000
Bare earth	-	-	-	-	-	-	-	0	1993
Shrubs	-	-	-	-	-	-	-	-	0

Table 5.19: Contingency matrix for nine land cover classes derived from the MNF transformed CASI image of the study area.

	River	**Woodland**	**Rail**	**Pasture**	**Managed pasture**	**Bare earth**	**shrubs**	**Road**	**Building**	**Total**	**Producers accuracy (%)**	**Users accuracy (%)**	**Class Kappa**
River	23	0	0	0	0	0	0	0	0	23	56.10	100.0	1.0
Woodland	1	39	0	5	0	0	5	2	0	52	90.70	75.0	0.72
Rail	0	0	24	0	0	0	0	0	0	24	60.0	100.0	1.0
Pasture	0	3	0	140	0	1	4	0	0	148	79.10	94.59	0.92
Managed pasture	0	0	0	0	7	0	0	1	0	8	100.0	87.50	0.5
Bare earth	0	0	0	30	0	23	4	1	0	58	92.0	39.66	0.36
Shrubs	0	1	0	1	0	0	8	0	0	10	38.10	80.0	0.90
Road	7	0	11	0	0	0	0	27	7	52	64.29	51.92	0.45
Buildings	9	0	5	1	0	1	0	11	35	63	83.33	55.56	0.51
Total	41	43	40	177	7	25	21	42	42				
Overall accuracy = 74.43							Overall Kappa statistics = 0.68						

Figure 5.25: Land cover map of the transport corridor with nine land cover classes derived from the MNF transformed CASI image.

Table 5.20: Separability table for eight land cover classes derived from the MNF transformed CASI image of the study area

	Woodland	**Managed pasture**	**Buildings**	**Pasture**	**River**	**Bare earth**	**Shrubs**	**Manmade**
Woodland	0	2000	2000	1996	2000	2000	2000	2000
Managed pasture	-	0	2000	2000	2000	2000	2000	2000
Buildings	-	-	0	2000	2000	2000	2000	1967
Pasture	-	-	-	0	2000	2000	2000	2000
River	-	-	-	-	0	2000	2000	2000
Bare earth	-	-	-	-	-	0	1993	2000
Shrubs	-	-	-	-	-	-	0	2000
Manmade	-	-	-	-	-	-	-	0

Table 5.21: Contingency matrix for eight land cover classes derived from the MNF transformed CASI image of the study area.

	River	Woodland	Pasture	Managed pasture	Bare earth	shrubs	Manmade	Building	Total	Producers' accuracy (%)	Users' accuracy (%)	Class Kappa
River	23	0	0	0	0	0	0	0	23	54.76	100.0	1.0
Woodland	1	39	5	0	0	5	2	0	52	90.70	75.0	0.72
Pasture	0	2	141	0	1	4	0	0	148	79.21	95.27	0.92
Managed pasture	0	0	0	7	0	0	1	0	8	100.0	87.50	0.87
Bare earth	0	0	30	0	23	4	1	0	58	92.0	39.66	0.36
Shrubs	0	0	1	0	0	9	0	0	10	40.91	90.0	0.90
Manmade	8	0	0	0	0	0	66	9	83	81.48	79.52	0.75
Buildings	10	0	1	0	1	0	11	33	56	78.57	58.93	0.56
Total	42	41	178	7	25	22	81	42				
Overall accuracy = 77.85%						Overall Kappa statistics = 0.72						

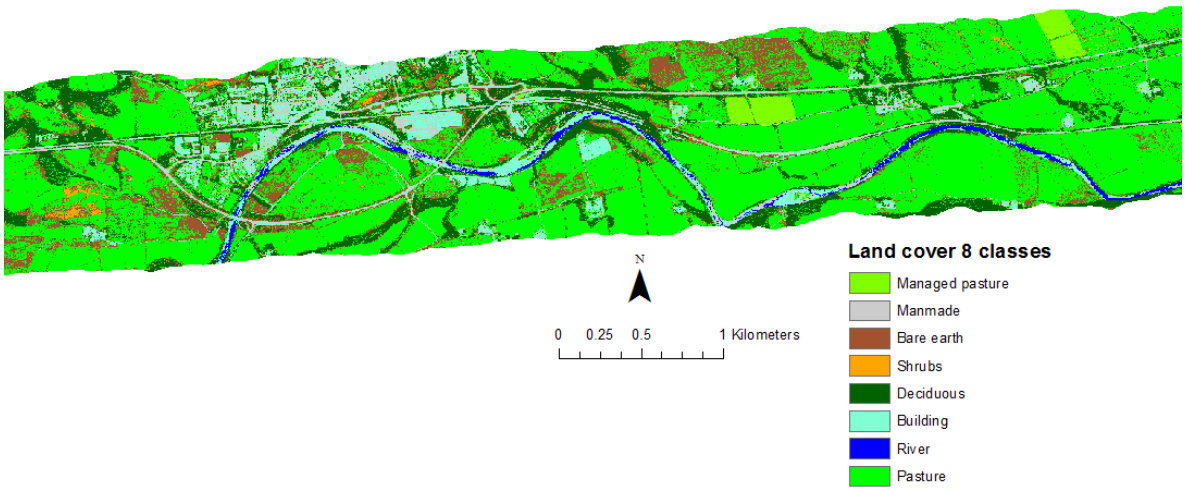

Figure 5.26: Land cover map of the transport corridor with eight land cover classes derived from the MNF transformed CASI image.

The poorer performance of the MNF images in terms of classification was also observed for the 5-class classification, with the application of the river mask and the subsequent fuzzy convolution filter. The final land cover map derived from the MNF transformed CASI image had an overall classification accuracy of 83.59% and kappa statistic of 0.76 (Table 5.22). The final land cover classification map derived from MNF transformation of the CASI imagery of the transport corridor is presented in Figure 5. 27.

Table 5.22: Contingency matrix for five land cover classes derived from the MNF transformed CASI image of the study area.

	River	Woodland	Pasture	Bare earth	Manmade	Total	Producers' accuracy (%)	Users' accuracy (%)	Class Kappa
River	26	0	0	0	0	26	61.90	100.0	1.0
Woodland	1	39	12	0	2	54	95.12	72.22	0.70
Pasture	0	2	150	4	2	158	72.46	94.94	0.89
Bare earth	0	0	45	21	1	67	84.0	31.34	0.27
Manmade	15	0	0	0	118	133	95.93	88.72	0.84
Total	42	41	207	25	123				
Overall accuracy = 80.82					Overall Kappa statistics = 0.73				

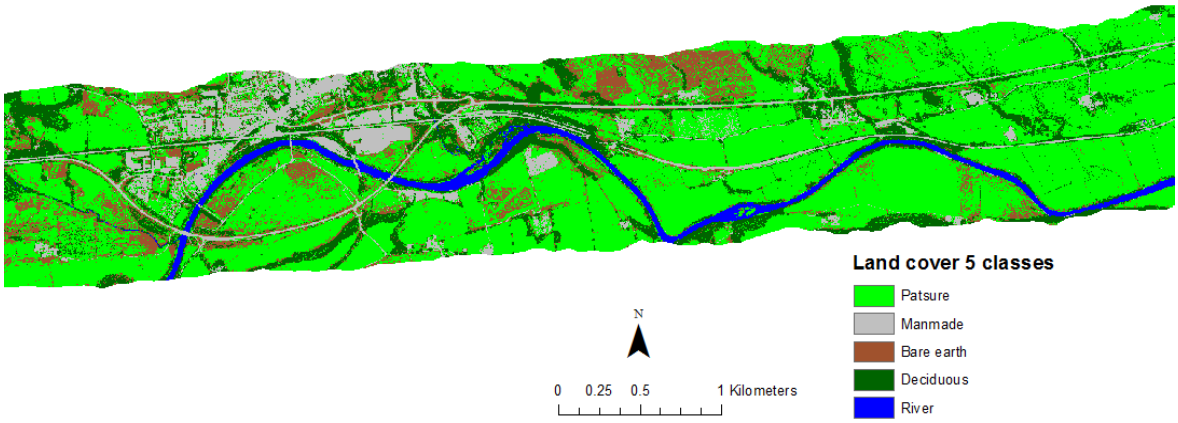

Figure 5.27: Land cover classification map derived from MNF transformed CASI image of the transport corridor, with the application of fuzzy convolution to reduce the speckled effect and improve overall classification

5.3.3 Comparison of the simple band selection and MNF transformed land cover maps

The accuracy assessments of the supervised maximum likelihood classification derived for the selected raw CASI bands and the MNF analysis images indicate higher classification accuracies for classification maps derived from the 'raw' selected band images (Table 5.23). Five broad land cover classes were recognised, these classes were categorised in line with anticipated hydrological response to overland flow and contributions to slope stability. An overall classification accuracy of 91.10% with a kappa statistics of 0.87 was recorded for the five-class land cover classification derived from the 'raw' selected band image, while an overall accuracy of 85.15% with kappa statistics of 0.80 was returned for the five class land cover classification from the MNF image . The producer and user accuracy obtained for the various land cover classes derived from the 'raw' selected band image suggests a high level of classification accuracy. Although the classified land cover maps derived from the MNF transformed image were characterised for some classes by fewer misclassified pixels, the maps show visible evidence of overestimation of the bare earth class and the under estimation of the shrub class. The overestimation of the bare earth class is reflected in the low user accuracy reported for the bare earth class in all of the MNF derived land cover classification contingency matrices. Adequate representation of the

various vegetation and non-vegetal cover types found within the transport corridor is critically important as differences in spatial coverage and hydrological properties will impact overland flow, moisture accumulation and slope stability. Essentially, vegetation exerts primary control on slope stability, with root systems contributing shear strength to slopes through root reinforcement. Also, vegetal processes like evapotranspiration can considerably modify soil water regime, reduce pore pressure and invariably enhance the stability of slopes. Based on better class coherency and higher overall classification accuracy, the five class land cover classification map acquired from the 'raw' selected band image was used as the input data for land cover related information in the modelling of slope stability within the transport corridor.

Table 5.23: Summary of the overall accuracy and kappa statistics obtained for the land cover classification

Land cover classes	Selected band image		PCA image	
	Overall accuracy (%)	Overall kappa statistics	Overall accuracy (%)	Overall kappa statistics
Nine	80.37	0.73	74.43	0.68
Eight	83.56	0.79	77.85	0.72
seven	90.18	0.87	83.11	0.78
Five	87.21	0.81	80.82	0.73
Five masked	90.87	0.87	84.47	0.79
Five masked (without river class)	89.90	0.84	82.83	0.75
Five masked (fuzzy convolution)	91.10	0.87	85.16	0.80
Five masked (fuzzy convolution without river class)	90.15	0.85	83.59	0.76

5.4 Integration of Catchment scale contributions

High infiltration is expected in permeable soils, with considerable runoff associated with less permeable soil types. The soil map shows that about 90 % of the agricultural field adjoining the transport corridor are underlain by slowly permeable seasonally waterlogged soils. Hence considerable amount of runoff generation are expected from the adjoining catchment areas. Runoff generation is a function of the underlying soil type and vegetation cover. High infiltration is expected in permeable soils, with considerable runoff associated

with less permeable soil types. A weighted grid was developed to incorporate the influence of soil and vegetation into the characterisation of soil moisture distribution in the study area.

5.4.1 Development of a weighted grid

Six storm events with varying precipitation intensity and AMC classes were evaluated. Storm intensity was defined based on the quantitative definition of antecedent runoff conditions as provided by USDA 2010 (discussed in detail in section 4.3.2.2). The rainfall data presented in Figure 5.28 corresponds to a storm in 26.10.2005 with depth of 22.8mm and a 5 day antecedent rainfall of 70.7 mm which corresponds to AMC 2. The runoff depth calculated for this storm is shown in Table 5.25 and varies 0.04 and 34.70.

Table 5.24: Storm categorisation showing precipitation intensity and antecedent moisture conditions prior the storm events.

Storms	Antecedent moisture condition (mm)	Precipitation intensity (mm)
2005-10-26	High (70.7)	Low (22.8)
2005-10-13	Low (2.55)	High (49.3)
2005-01-08	Medium (42.35)	High (70.5)
2007-06-17	High (74.7)	Medium (42.06)
2007-12-29	Medium (14.05)	Medium (34.7)
2008-09-06	Medium (12.7)	Low (10.95)
2010-10-23	Medium (40.73)	Medium (39.5)

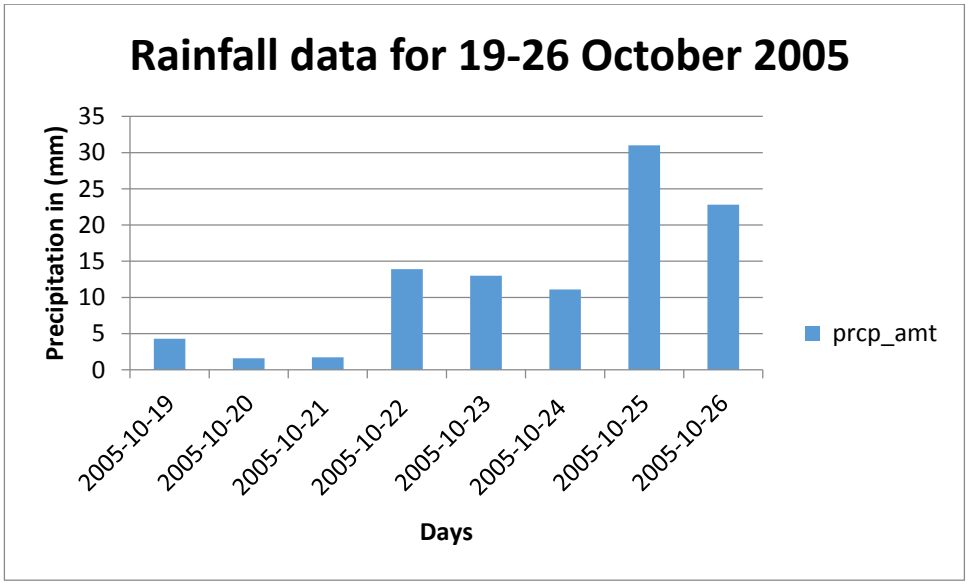

Figure 5.28: Storm event of 26-10-2005 with antecedent moisture condition of the study area.

Table 5.25 The generated runoff depth increases with increased antecedent moisture content and precipitation intensity. In compliance with equation 4.5, no runoff was generated when precipitation is lower than initial abstraction. Antecedent moisture condition is seen to exert more influence on runoff generation than rainfall intensity as evident in the storm events of 17.06.2007 and 09.06.2008. Lower runoff values are associated with permeable soil classes (Class A and B), while class D soils rich in clay fractions exhibited higher depths of surface runoff (Table 5.26). The woodlands exhibited lowest runoff values in comparison with other land cover classes. The weight grid engenders a more realistic spatial distribution of soil moisture that takes into cognisance the infiltration and evapotranspiration.

Table 5.25: Computed runoff depth for storm events and associated runoff coefficient values.

Storms	Runoff depth (mm)	Runoff coefficient	Mean (Runoff coefficient)	Standard deviation (runoff coefficient)
2005-10-26	0.04 – 34.74	0.01 -0.32	0.04	0.15
2005-10-13	0.02 – 49.3	0.03 – 0.44	0.09	0.15
2005-01-08	1.23 – 39.5	0.03 – 0.63	0.24	0.15
2007-06-17	0 – 70.5	0 – 0.77	0.42	0.14
2007-12-29	0.41 – 22.8	0.02 – 0.70	0.33	0.14
2008-09-06	0.8 – 42.06	0.11 – 0.82	0.52	0.13

Table 5.26: Runoff depths of some soil classes of the study area with varying rainfall intensity

Soil name	Soil class	Runoff depth(mm) for Storm 2008-09-06	Runoff depth(mm) for Storm 2007-12-29	Land cover
Ellerbeck	B	10.74	1.91	Grassland
Alun	B	10.74	1.91	Grassland
Nercwys	C	14.66	3.53	Grassland
Wharfe	D	22.53	7.64	Grassland
Brickfield 3	D	22.53	7.64	Grassland
Wilcock 1	D	22.53	7.64	Grassland

5.4.2 Sensitivity analysis of weight grid

The runoff coefficient map was generated from the estimated quantity of runoff depth and divided by the total rainfall. The precipitation value of the storm that occurred on 17.06.2007 was used for all other subsequent modelling. The land cover classes such as the woodland and the grasslands are products of aggregated of classes with similar hydrological responses. The sensitivity assessment was carried out on the developed weight grid with a view to evaluating the robustness of the grid to slight variations in data input. The runoff coefficient values for the various soil types and land cover combinations provided a range for the weights representing grasslands and woodlands. Sections of the weight grid representing grasslands were first clipped out and the highest and lowest grassland weights identified. A random raster was created with weights within the upper and lower limits randomly allocate within three standard deviations using normal distribution. The highest grassland weight was 0.62 representing grasslands overlying high runoff potential soils with low infiltration rates (Class D). The lowest grassland weight was 0.25 representing well to excessively drained sand or gravel and have a high rate of water transmission (greater than 7.6 mm/h). Three standard deviations was deemed appropriate as it represents 99.72 % possible variations that may exist within the weight range for grassland. The grassland was merged back with the original weight grid, such that only the weights of the grassland were adjusted. Five random normally distributed weight grids were computed for both grass and woodlands following the same procedure. The developed randomly distributed weights were used to compute the modified TWI maps of the transport corridor areas. The modified TWI values derived using random normally distributed weight for grassland is presented in Table 5.27. A Mann-Whitney U statistics test showed no significant difference between the medians of the modified TWI distributions generated with randomly distributed weight values for grassland. The adjusted weight values for woodlands did not result in any global alteration in the distribution pattern of generated surface runoff (Table 5.28). However, it is noteworthy that there were noticeable changes in flow pattern as indicated by difference in the values of specific catchment area computation at zones of flow convergence in the individual grids.

Table 5.27: Summary statistics of the modified TWI maps of the transport corridor and adjoining agricultural areas using randomly distributed weights for grasslands.

Grassland adjusted	Min	Max	Mean	standard deviation
TWI 1	0	21.93	5.17	1.95
TWI 2	0	21.93	5.17	1.95
TWI 3	0	21.93	5.17	1.95
TWI 4	0	21.93	5.17	1.95
TWI 5	0	21.93	5.17	1.95

Table 5.28: Summary statistics of the modified TWI maps of study area with randomly adjusted weights for woodlands

Woodland adjusted	Min	Max	Mean	standard deviation
TWI 1	0	20.07	5.32	1.96
TWI 2	0	20.07	5.32	1.96
TWI 3	0	20.07	5.32	1.96
TWI 4	0	20.07	5.32	1.96
TWI 5	0	20.07	5.32	1.96

5.4.3 Modified Terrain wetness index model

The modified TWI map predicts a general trend of increasing moisture with decreasing elevation with the south facing slopes exhibiting relatively wetter conditions in comparison with the north facing slopes (Figures 5.29 and 5. 30).

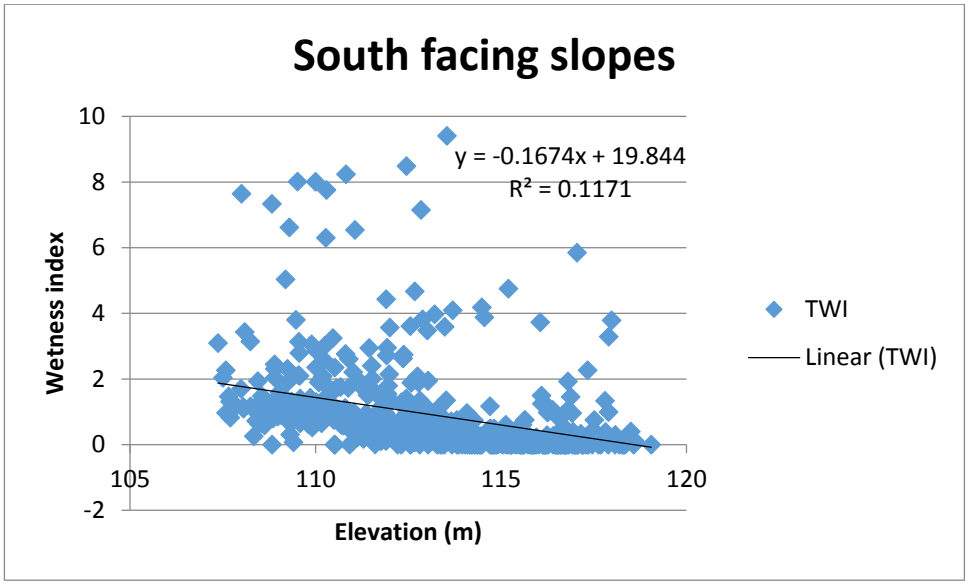

Figure 5.29: Scatter plot showing the relationship between elevation and terrain wetness index. The general trend in moisture content was obtained by fitting a linear regression trend line.

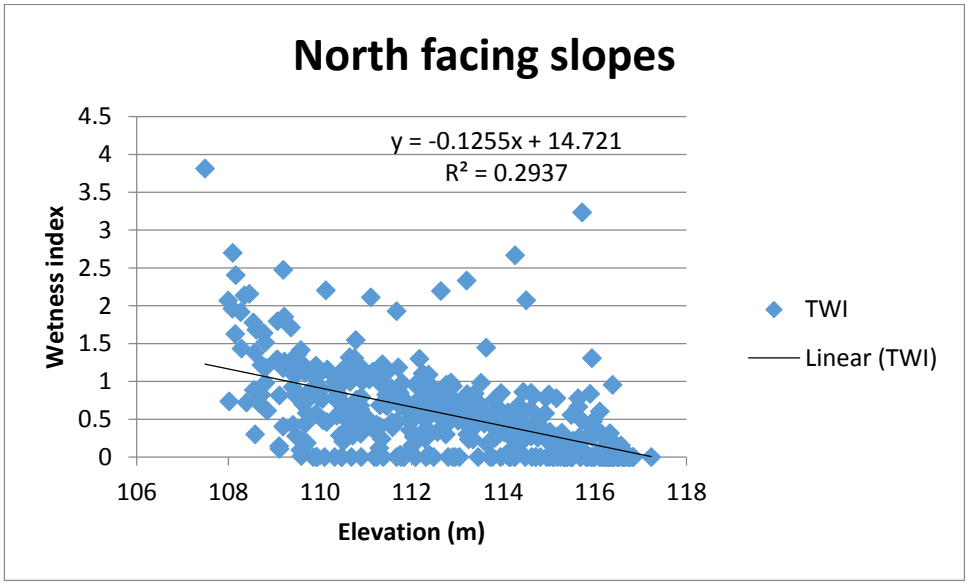

Figure 5.30: Scatter plot showing relationship between elevation and terrain wetness index for north facing slopes with a linear regression line depicting the general trend in predicted moisture content with increase in elevation.

The modified TWI map reveals considerable contribution from the surrounding broader catchment topography (Figure 5.31) to the localisation of zones of moisture accumulation along the transport corridor earthworks. This is clearly depicted by predicted ingress of

flow from the surrounding upland agricultural fields into the earthwork infrastructure of the transport corridor, with sections of the earthwork embankment serving as a barricade to upland overland flows. Figure 5.32 reveals points of predicted overland flow ingress into an earthwork cutting while Figure 5.33 illustrates the convergence of flow from surrounding upslope areas with the earthwork embankment acting as barriers to runoff draining towards the River South Tyne south of the corridor.

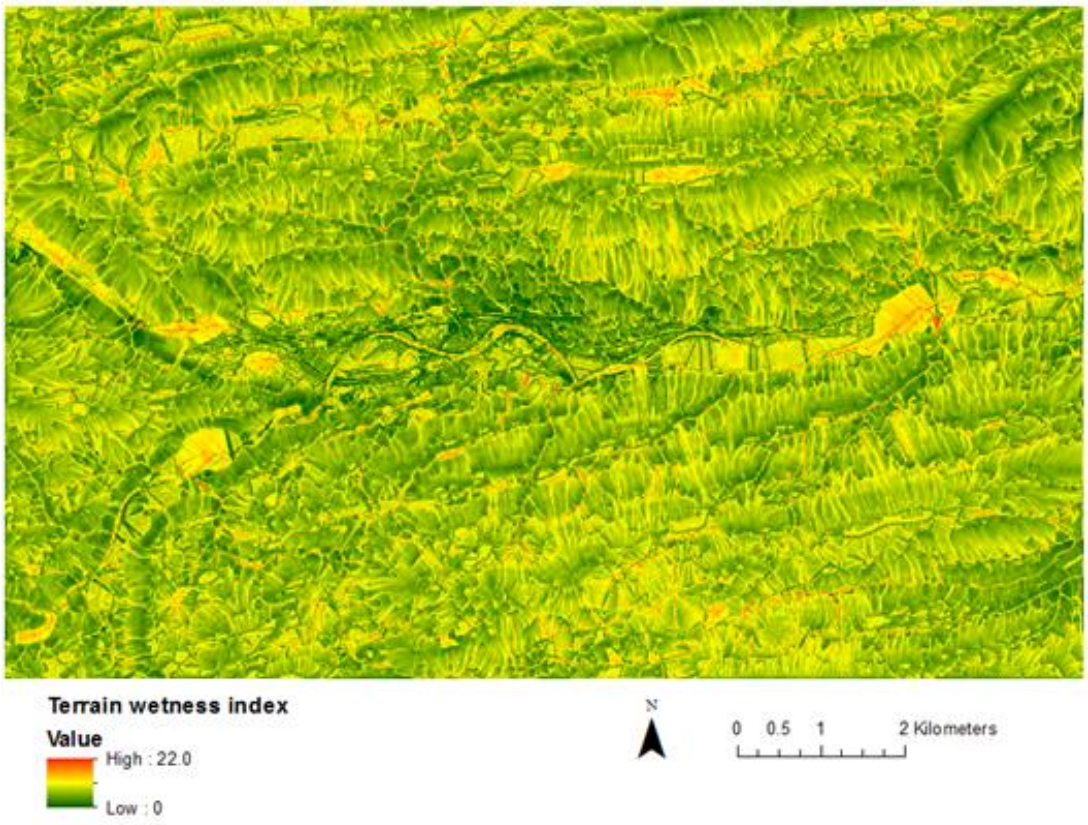

Figure 5.31: Modified terrain wetness index map of broader catchment area

The modified TWI map reveals high moisture concentrations towards the top and toe of the earthwork slopes, with lower soil moisture values half way down the slope. This is the general trend across the various earthwork cutting; however, there appears to be increased mid-slope concentration along sections of the slope face that coincides with areas of high concave curvature values. Increases in curvature in either direction can be significant influence the overall stability of a hillslope. Curvature affects the downslope movement of water in two notable ways (Ohlmacher, 2007). The existence of concave curvature increases the convergence of water flow into hollows thereby resulting in increased localise

saturation of those sections of the earthwork slope. Thus, while the rainfall amount and duration are equal, the fully saturated volume and average saturation of the earthwork slope is significantly different. In addition, these areas serve as miniature reservoirs retaining down-the-slope flow for longer durations. As a result these sections of the slope are typically characterised by higher pore-water pressure and experience higher shear stresses as a result of increased moisture content.

This phenomenon is clearly illustrated by a section taken across the Whitchester cutting earthwork of the corridor, where the presence of curvature is seen to coincide with increased wetness index values half way down the slope (see Figure 5.34). In Figure 5.34, the modified TWI values is seen to increase in response to the presence of microtopography. This trend is consistent across the various cutting earthworks within the transport corridor regardless of the soil type that constitutes the slope made-up material and height of the slope.

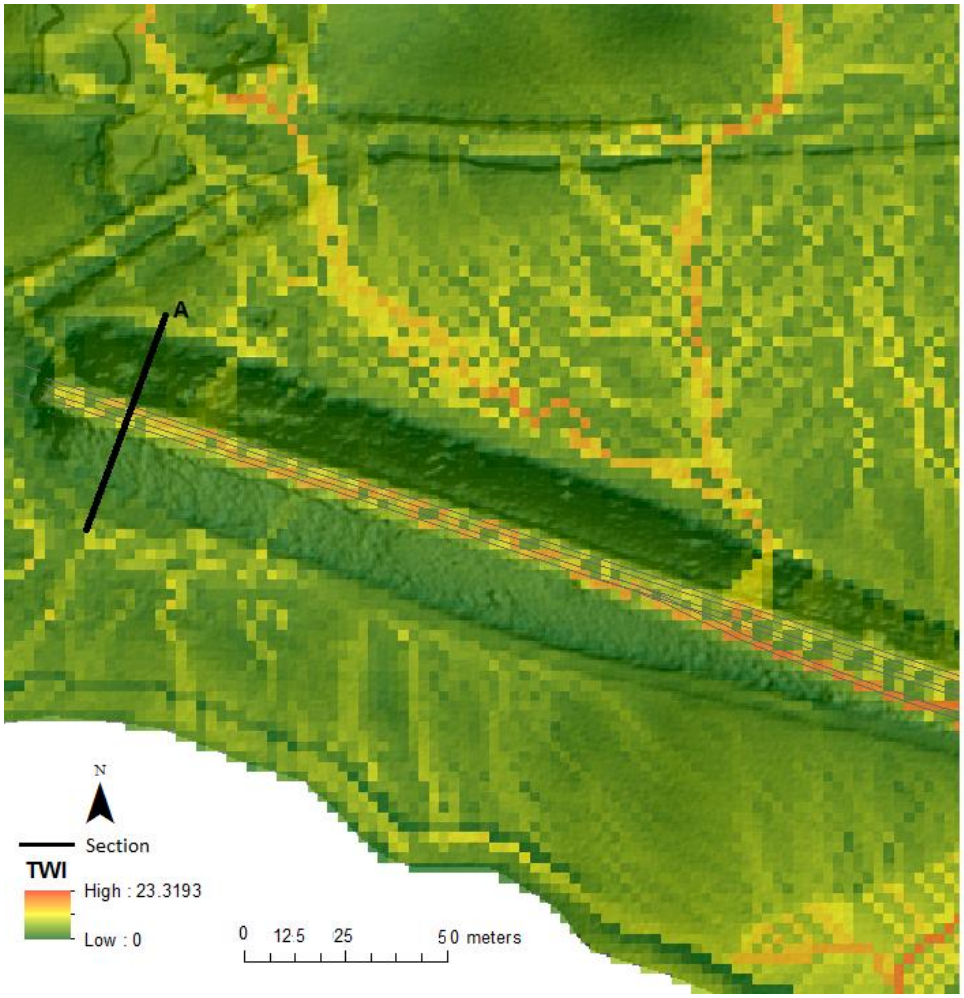

Figure 5.32: Modified TWI map of a section of the transport corridor revealing characteristic high moisture concentrations towards the top and toe of the earthwork slopes. Two points of predicted overland flow ingress into the cutting earthwork are clearly visible on the south facing slope.

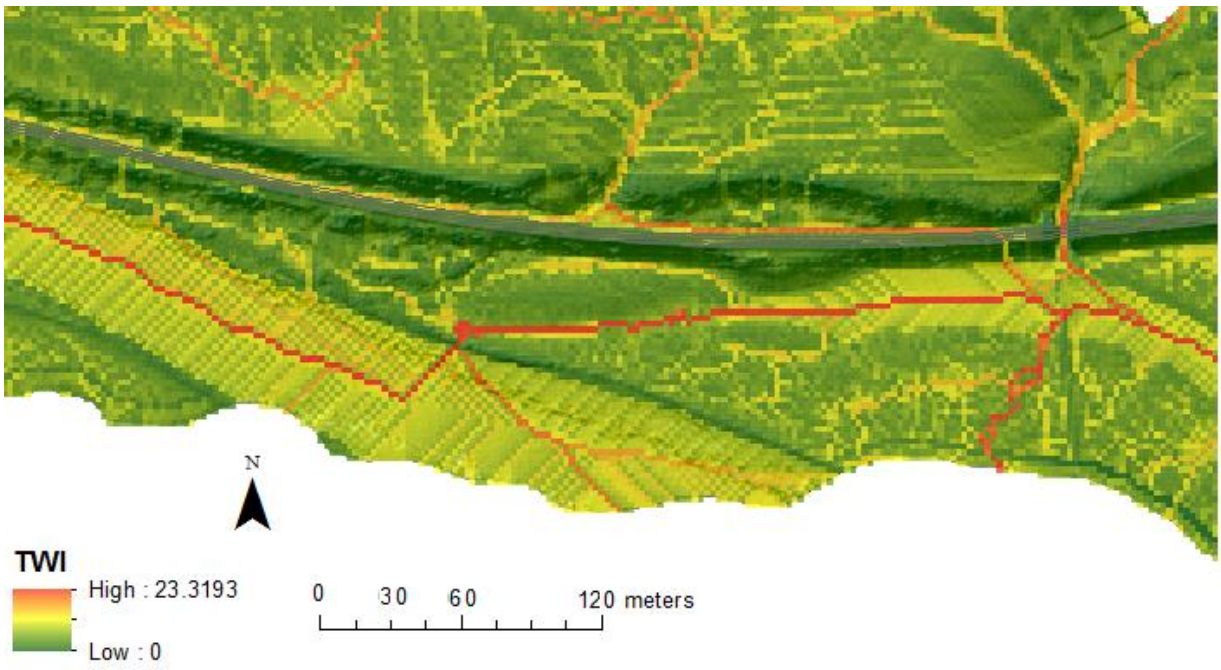

Figure 5.33: Modified TWI map revealing sections of earthwork embankment characterised by moisture accumulation as a result of flow convergence from surrounding upland topography.

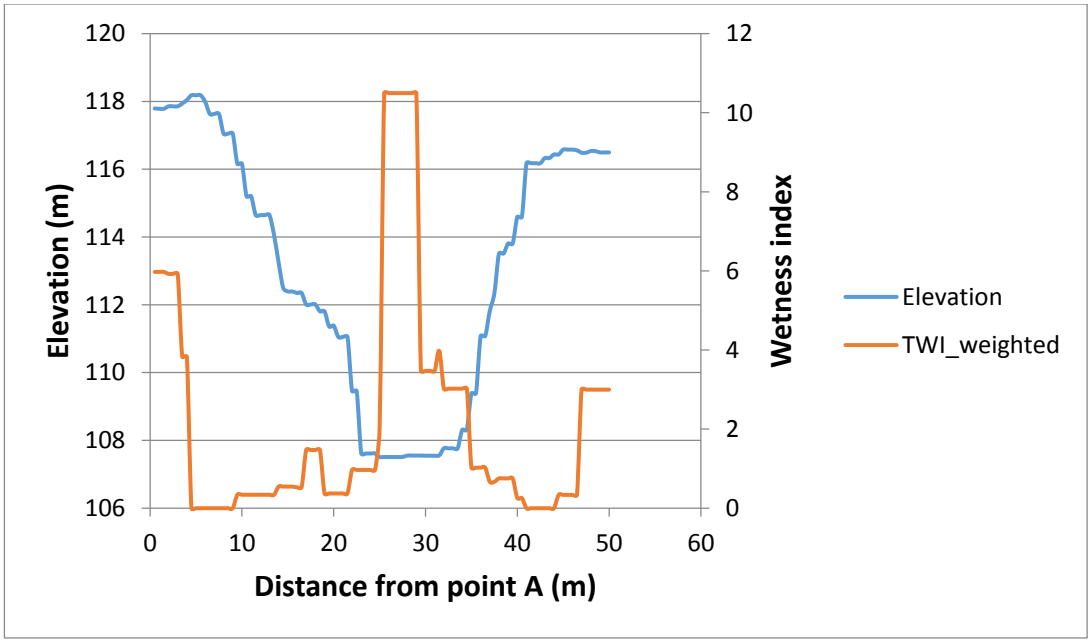

Figure 5.34: A transect of the modified TWI values across a slope cutting revealing zones high moisture concentration (towards the top and toe of the earthwork slopes) as surface runoff flows down the earthwork slope. Location of transect A is shown in figure 5.32.

5.5 Evidential reasoning model

The results of the transformation of the various thematic layers into evidential data layers are presented in tables 5.29 and 5.30. The tables show the derived weights and estimated Evidential Belief Functions (EBF) for the eight landslide conditioning factors. The magnitudes of positive weights show the relative importance of each variable class as a predictor of slope instability. The negative weights suggest relative stability within variable class range, high positive weights typically translate into higher belief functions signifying high susceptibility to slope instability.

The evidential belief layer for land cover shows landslide occurrence in all three predominant (grasses and shrubs, trees and man-made) land cover classes. The man-made land-cover class which is comprised essentially of ballast-lain earthwork embankments is seen to be associated with highest probability of landslide occurrences with a belief value of 0.5, followed by woodlands and then grassland. Half of the total number of landslide occurrence (50%) is believed to be associated with the man-made land cover class.

Table 5.29: Basic probability functions for slope, aspect, curvature and distance to drainage

Factor	Class	No. of pixels in domain	Landslide occurrence	W+	W-	Bel	Dis	Unc
Slope	5	188	4	0.331	1.011	0.044	0.101	0.855
	10	395	19	0.769	1.008	0.102	0.101	0.797
	15	845	41	0.777	1.017	0.102	0.102	0.796
	20	1421	78	0.884	1.015	0.117	0.102	0.782
	25	2052	137	1.089	0.982	0.144	0.098	0.758
	30	3128	235	1.237	0.922	0.163	0.092	0.744
	35	2731	184	1.100	0.972	0.145	0.097	0.757
	40	1204	56	0.743	1.028	0.098	0.103	0.799
	45	295	8	0.424	1.015	0.056	0.102	0.842
	>50	139	2	0.222	1.009	0.029	0.101	0.870
Aspect	Flat area	0	0	0	0	0	0	1
	N	3984	258	1.054	0.974	0.211	0.122	0.667
	NE	203	2	0.152	1.015	0.030	0.127	0.842
	E	41	2	0.781	1.001	0.156	0.126	0.718
	SE	332	20	0.976	1.001	0.195	0.126	0.679
	S	7105	455	1.042	0.944	0.208	0.119	0.673
	SW	518	24	0.740	1.012	0.148	0.127	0.725
	W	33	0	0	0	0	0	1
	NW	182	3	0.255	1.012	0.051	0.127	0.822
Curvature	concave(-)	5319	401	1.242	0.823	0.486	0.271	0.243
	Flat	265	8	0.474	1.012	0.186	0.333	0.481
	convex(+)	6814	355	0.837	1.204	0.328	0.396	0.276
Drainage	10	333	0	0	1.029	0	0	1
	20	604	13	0.335	1.036	0.012	0.092	0.896
	30	433	24	0.894	1.004	0.032	0.089	0.879
	40	627	67	1.822	0.958	0.064	0.085	0.851
	50	572	164	6.121	0.814	0.217	0.072	0.711
	60	540	166	6.759	0.809	0.239	0.072	0.689
	70	524	112	4.140	0.885	0.146	0.078	0.775
	80	418	101	4.852	0.892	0.172	0.079	0.749
	90	326	57	3.227	0.947	0.114	0.084	0.802
	100	8022	60	0.115	2.919	0.004	0.258	0.737

Table 5.30: Basic probability functions for soil, land cover, SPI and modified TWI

Factor	Class	No. of pixels in domain	Landslide occurrences	W+	W-	Bel	Dis	Unc
Soil	Brickfield 3	2645	0	0	1.294	0	0	1
	Ellerbeck	5624	490	1.453	0.642	0.316	0.109	0.575
	Wharfe	1692	257	2.726	0.757	0.593	0.128	0.279
	Nercwys	633	17	0.420	1.032	0.091	0.175	0.734
	Enborne	659	0	0	1.060	0	0	1
	Alun	1142	0	0	1.109	0	0	1
Landcover	Manmade	1756	171	1.642	0.899	0.507	0.180	0.313
	Grassland	2507	91	0.573	1.112	0.177	0.223	0.600
	Bare ground	183	0	0	1.016	0	0	1
	Water body	1	0	0	1.000	0	1	0
	Woodland	7948	502	1.026	0.953	0.317	0.191	0.492
SPI	1	3178	271	1.420	0.860	0.521	0.087	0.392
	2	6396	486	1.252	0.740	0.459	0.075	0.466
	3	1971	7	0.054	1.192	0.020	0.121	0.859
	4	500	0	0	1.045	0	0	1
	5	220	0	0	1.019	0	0	1
	6	91	0	0	1.008	0	0	1
	7	16	0	0	1.001	0	0	1
	8	9	0	0	1.001	0	0	1
	9	11	0	0	1.001	0	0	1
	>10	7	0	0	1.001	0	0	1
TWI modified	1	4893	368	1.239	0.848	0.067	0.085	0.848
	2	4579	215	0.750	1.150	0.041	0.115	0.844
	3	1525	68	0.711	1.041	0.038	0.104	0.857
	4	532	19	0.564	1.020	0.030	0.102	0.868
	5	230	6	0.408	1.012	0.022	0.101	0.877
	6	127	36	6.025	0.960	0.326	0.096	0.578
	7	164	19	1.996	0.987	0.108	0.099	0.793
	8	213	20	1.578	0.990	0.085	0.099	0.816
	9	39	9	4.569	0.991	0.247	0.099	0.654
	>10	97	4	0.655	1.003	0.035	0.100	0.864

These earthwork embankments are generally steep sloped (see Figure 5.5), sparsely vegetated and the presence of large amount of ballast permits high surface water

percolation. Rail ballast usually contains uniformly graded material with sufficiently large pore structure to facilitate rapid drainage. This attribute is in effect important in sustaining good track performance. However, in aging network infrastructure (like the one under investigation) and degraded ballast, the resistance to attrition and weathering is often lower than usual. This results in disintegration of some individual grains into finer particles and accumulates within the voids impeding drainage. This becomes particularly important when the track bed is underlain by slowly permeable to impermeable subgrade. Track stability is known be adversely affected by increase in the degree of saturation. Increased moisture influences track settlement, particle breakage and traffic ability problems arising from uneven track bed (Buddhima *et al.*, 2011). The belief function for the woodlands suggests that this land cover type is responsible for about 32% of the total landslide occurrences within transport corridor. The earthwork embankment and cuttings covered by grasses is seen to only explain 18% of the total landslide occurrence.

The computed belief functions for the various underlying soils in the transport corridor are presented in Table 5.30. The influence of underlying soils to landslide location reveals high values of belief for the relatively more permeable soils (Ellerbeck and Wharfe soil classes) in contrast to the loamy clayey seasonally waterlogged slowly permeable soils of the Alun, Nercwys and Brickfield series. This is not at all surprising as seasonally waterlogged clayey layered soils are often well compacted (National Soil Resources Institute, 2008), meaning most of the external surface moisture from precipitation ends up as runoff. Earthwork cuttings in these soils are stable with provision of sufficient drains. Baum *et al.* (2005) explains that percolating water is more impactful on slope instability as built up pore pressure known to reduce the stability of slopes when it accumulates above a less permeable intercalation. The Wharfe soil class which is essentially river alluvium made up of deep stone-less permeable fine loamy soils, variably affected by groundwater (Avery, 1980), is characterised by high occurrences of landslide and invariably assigned a higher belief function value. Though permeable and largely well drained, the presence of clay enrichment in the non-calcareous loamy or clayey alluvium (more than 30 cm thick) Wharfe soil class is known to sometimes result in winter flooding (Cranfield University, 2014). The relatively better drained Ellerbeck series is dominantly free draining loamy-gravely soils developed on very stony glaciofluvial or river terrace drift (Cranfield University, 2014), appears to be relatively more stable than the Wharfe soil class but less

stable in comparison to the loamy clayey seasonally waterlogged slowly permeable soils of the Alun, Nercwys and Brickfield series.

The proximity to river channel is known to adversely affect slope stability by eroding the slope or by base saturation that may result in elevated levels of the groundwater table (Pradhan *et al.*, 2010). The proximity of some sections the earthwork infrastructure of the transport corridor to the South Tyne River appears not to have noticeable effects on the location of slope instability. This may be as a result of strict guidelines enforcing sufficient provision of surface and slope drainage facilities to aid the reduction of groundwater levels within the earthwork cuttings and the collection of surface runoff at top of cuttings (Perry *et al.*, 2003b). With some stretches of the embankment earthworks located in close proximity of the river (approximately 15 meters), the belief values for proximity to drainage in Table 5.29 show that the degree of support for instability due to proximity to river for earthworks within 40m of the River Tyne is less than 7%.

The stream power index evidence layer exhibits an indirect relationship with landslide occurrence, with the belief values decreasing with increasing SPI values. The aspect map reveals predominantly north- and south-facing slope aspects due to the east-west orientation of the transport corridor. A belief value of 0.2 and disbelief value of 0.1 for north-facing and south facing slope aspect indicates the positive spatial association of these categories with landslide susceptibility (Table 5.29). The degree of belief for profile curvature indicates direct relationship with landslide occurrence. In the curvature map, concave surfaces which are generally associated with localised convergence of flow and at favourable slope gradients may develop shear surfaces, are characterised by relatively higher belief values of 0.5. Convex surfaces on the other hand are usually more exposed to the weather elements resulting in continuous expansion and contraction, which ultimately loosening up the soil. The convex surfaces explain about 33% of landslide occurrences.

The slope map reveals a curvilinear relationship with landslide susceptibility. Landslide frequency is seen to increases with slope gradient to a threshold above which the landslide density decreases. This is also reflected in a gradual rise in belief function with increasing slope gradient. Typical slope gradient values across the earthwork slope and embankment range from 11^0 to 49^0, with the steeper end of the interval generally associated with the earthwork embankments. The revealed threshold falls within an interval of slope angles

ranging from 25^0 to 35^0. This slope range is also seen to exhibit the lowest disbelief values of 0.09.

The result of the integrated maps of the various conditioning factors is presented in Figure 5.35, 5.36 and 5.37. Three maps representing the degree of belief, disbelief and uncertainty were derived. The belief function map reflects the distribution of slope instability across the transport corridor. The earthwork cuttings were identified as comparatively less susceptible to slope instability in contrast with the earthwork embankments, with the higher magnitude of earthwork embankment instability in the east end of the transport corridor. 5.1% of the earthwork cuttings were identified as relatively unstable in contrast to 47.5% for the earthwork embankment. Segments of the earthwork infrastructure built on the relatively more permeable soils of the Wharfe and Ellerbeck soil classes exhibited high belief values of 0.6 and 0.3 respectively accounts for over 80% of slope instability in the transport corridor (Table 5. 30). This indicates that infiltration processes may play a considerable role in the slope stability status within the transport corridor. Equally highlighted were sections of the embankment that served as barriers to converging upland flow from surrounding agricultural fields (see Figure 5.32).

The model identified as areas of low belief, areas where the classes provide weak support for landslide susceptibility such as in relatively flat transitional areas between earthwork cuttings and embankments. Low disbelief values also coincided with locations where there is strong support for instability. The uncertainty map identified locations along the transport corridor where the EBF model evaluated existing evidence as insufficient to conclusively map zones of slope instability. The uncertainty values were generally low across the corridor (0 to 0.2) with a mean uncertainty value of 0.04. The generally low uncertainty values indicates the appropriateness of datasets employed in modelling landslide susceptibility in the transport corridor and also low associated errors with regards to the prediction of locations with instability. However, the uncertainty map identified the well vegetated earthwork cuttings situated on the slowly permeable fine silty and clayey soils of the Brickfield 3 soil class west of the corridor as a location that might require additional information to ascertain its relative degree of stability.

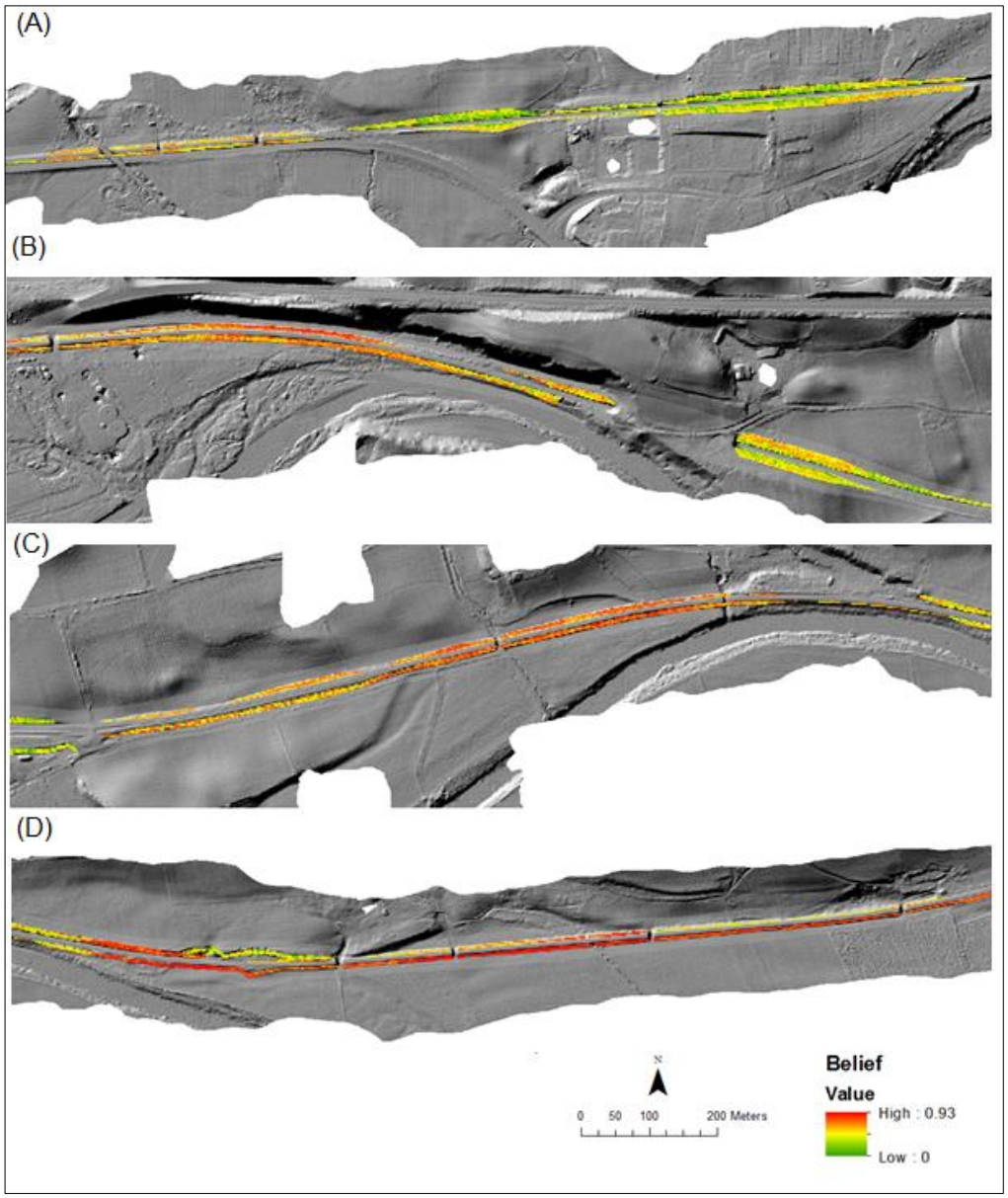

Figure 5.35: Integrated evidential belief map of the transport corridor earthworks

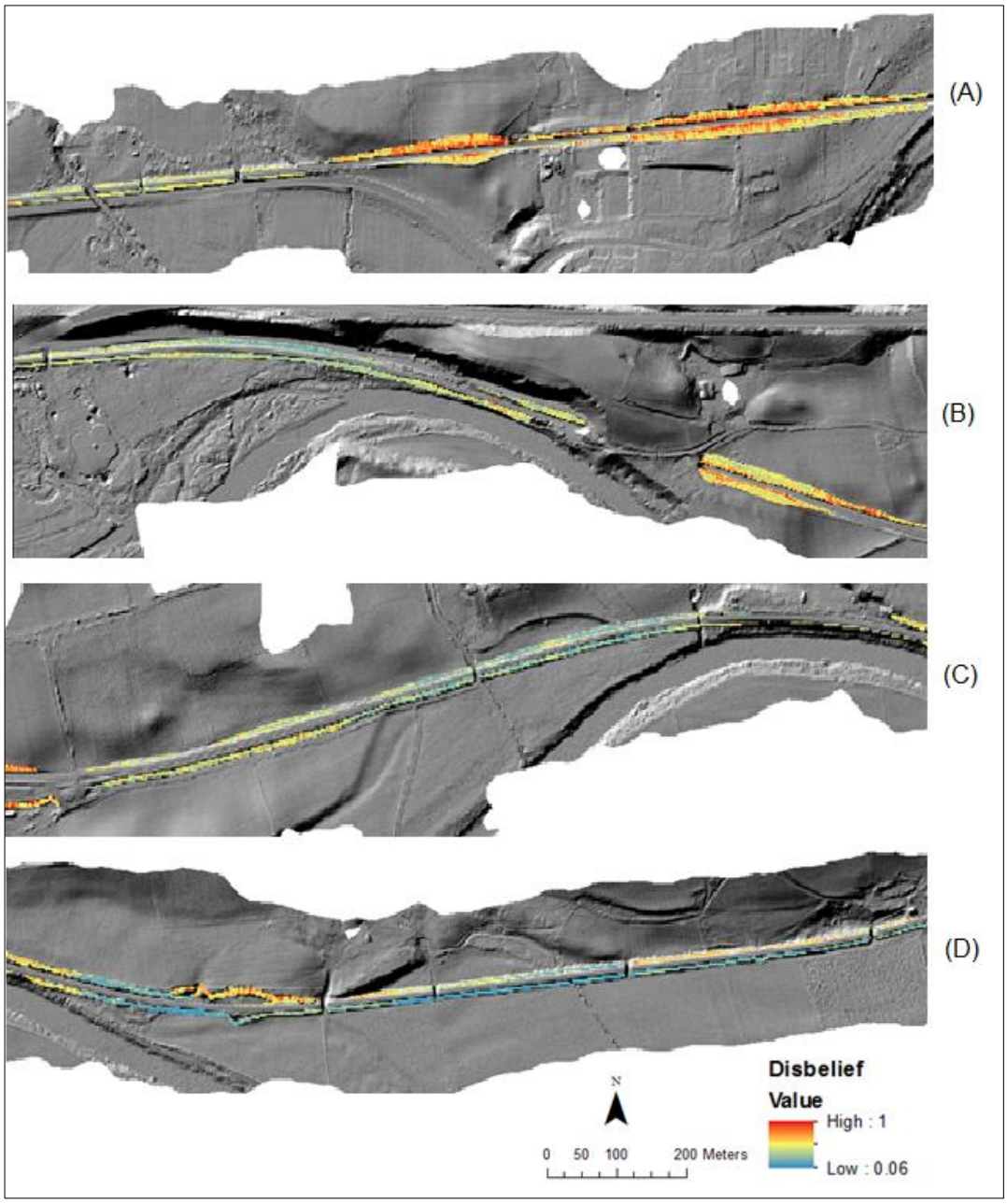

Figure 5.36: Integrated evidential disbelief map of the transport corridor earthworks

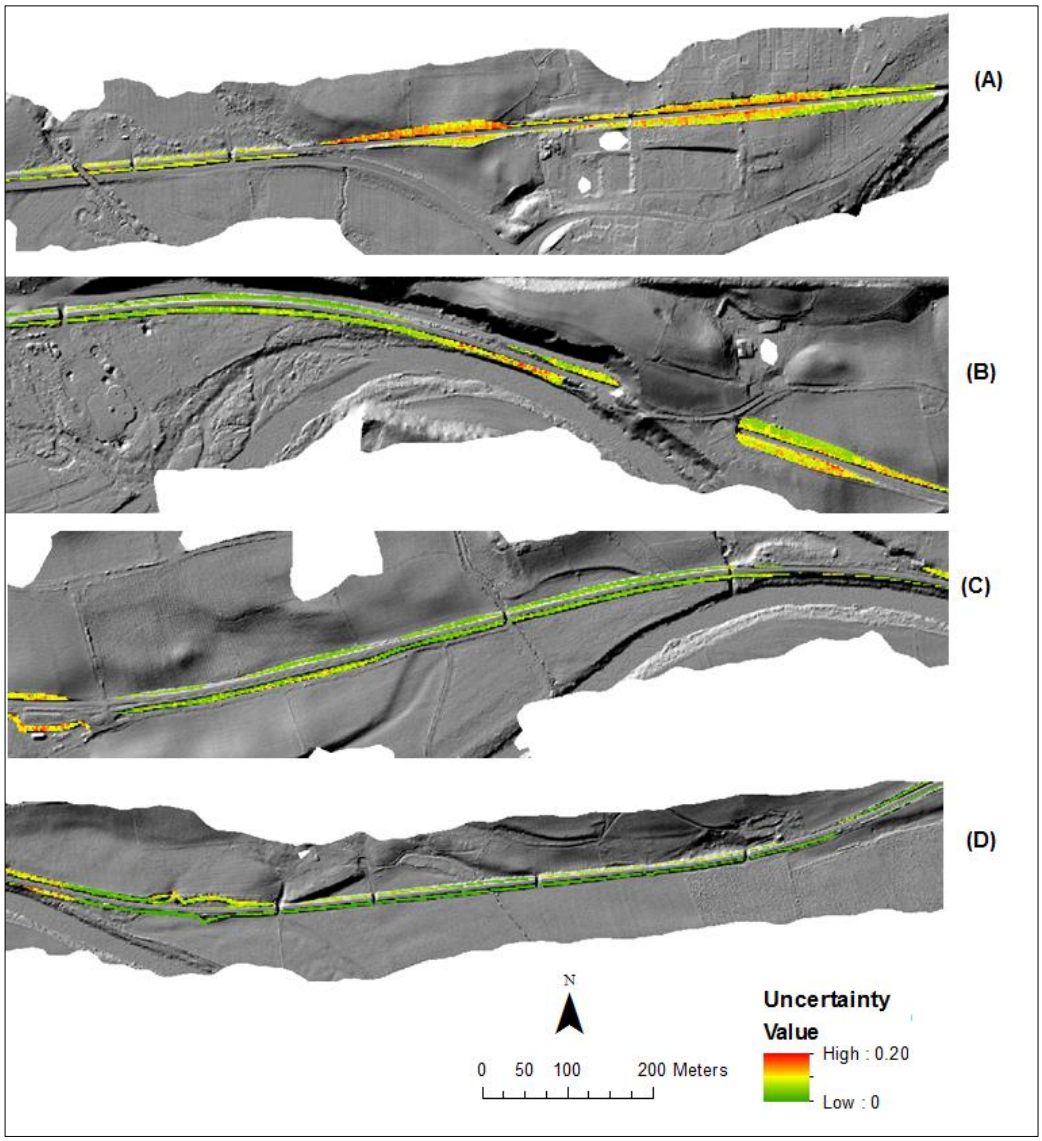

Figure 5.37: Integrated evidential uncertainty map of the transport corridor earthworks

5.5.1 Validation and model comparison

The classification results were first validated to evaluate how well the evidential belief function (EBF) models performed in rightly classifying the landslide locations with reference to available inventory records obtained from Network Rail. The success rate method provided an ample means of measuring the goodness of fit of the EBF landslide model to the training data. In addition to the provision of an overall model fit estimate for the models, the success rate technique also provides a detailed description of the model performance with respect to the susceptibility classes. The degree of model fit for the

modified TWI and the classic TWI evidential belief function (EBF) models is presented in Figure 5.38. The validation result shows a relatively equal goodness of fit for both EBF models with the area under the curve (AUC) value for the EBF model constructed using classic TWI computation (AUC= 89%) being slightly higher by less than 1% . Both models yielded high overall quantitative index of accuracy as indicated by the AUC values affirming the models high discriminative power in separating high instability susceptible areas from the relatively stable areas.

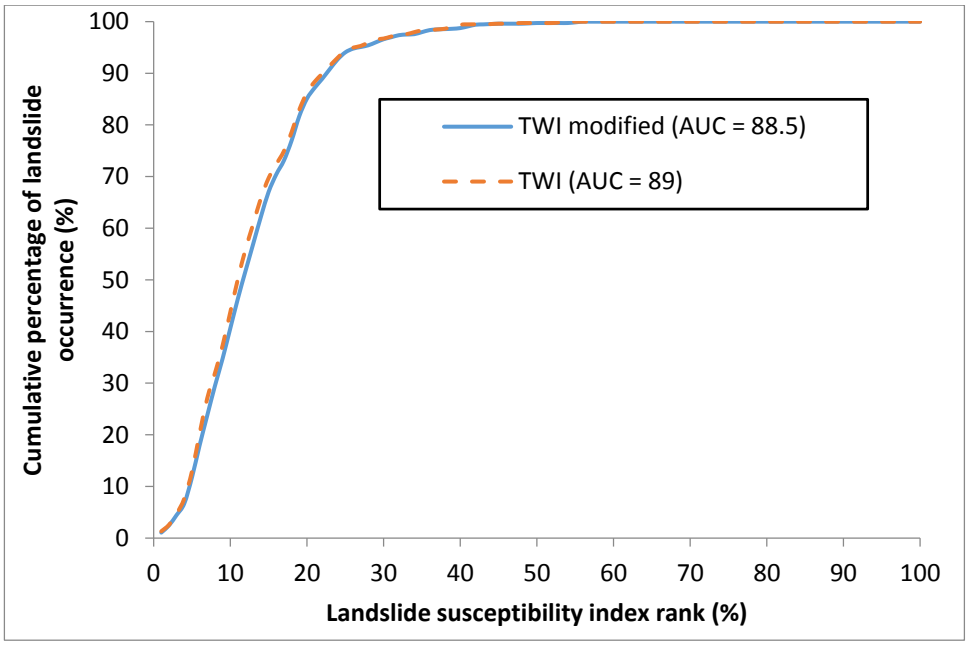

Figure 5.38: Analysis of model performance (goodness of fit) for the modified TWI and classic TWI EBF models, based on the comparison between the susceptibility map and landslide inventory used in the modelling (training set).

The success rate curve was also used to compare various cut-off combinations on the goodness of fit. Seven arbitrarily chosen ranks of landslide susceptibility index to be used as cut-off points (30%, 40%, 50%, 60%, 70%, 80% and 90%) were selected to further assess the reliability of model performance with respect to the susceptibility classes. Tables 5.31 and 5.32 show the percentage of correctly and incorrectly classified landslide pixels of the landslide inventory, as well as for the non-landslide areas at designated cut off points for the modified TWI and classic TWI EBF landslide susceptibility models. Both tables reveal an indirect relationship between sensitivity and specificity for both landslide and

non-landslide areas. With susceptibility threshold set at 70%, a total of 96.73% of the landslide inventory were correctly categorised while only 44.55% of the non-landslide were correctly identified. At the same threshold value of 70% the classic TWI EBF model is seen to be slightly more efficient (by a percent) in correctly classifying slopes that have landslides but less efficient in classifying stable slopes. This is particularly important as the magnitude of false negatives (mapping units free of landslides as unstable) classification by models reduces the reliability of results. The overestimation by the classic TWI model can be attributed to the higher TWI values and the broad generalisation associated with TWI computation as a result of the assumptions on which the calculation is based. Figures 5.39 and 5.40 suggest an optimum cut-off value of 80% for the classification of stable and unstable terrain within the transport corridor slope. The determination of optimum cut-off value is unique to the purpose of the susceptibility application. The selection is often tied to a target population been investigated, which in this case happens to be high risk landslide prone sites within the transport corridor. Sites identified by site inspectors of Network Rail as high risk landslide prone areas assisted in the decision for the choice of the optimum cut-off value. Figure 5.41 shows the variability in sensitivity and specificity with increase in cut-off value. The results show that at higher specificity the most susceptible sections of the earthworks are clearly highlighted. At a cut-off value of 80% most of the false positive cells present in the lower cut-off values were seen to have been classified into the stable terrain class and clearly identifying unstable regions on an earthwork cutting (see figure 5.41).

Table 5.31: Percentage of correctly and incorrectly classified landslides and non-landslide pixels based of seven arbitrarily selected cut-off values (thresholds at which assessment were carried out) from the success rate curve for the modified TWI EBF model.

Cut-off	Landslide		Non landslide	
	Present	Absent	Present	Absent
30	100	0	0.04	99.96
40	100	0	2.31	97.69
50	99.74	0.26	10.36	89.67
60	98.82	1.18	23.36	76.64
70	96.73	3.27	44.55	55.46
80	86.26	13.74	71.67	28.33
90	43.72	56.28	92.98	7.02

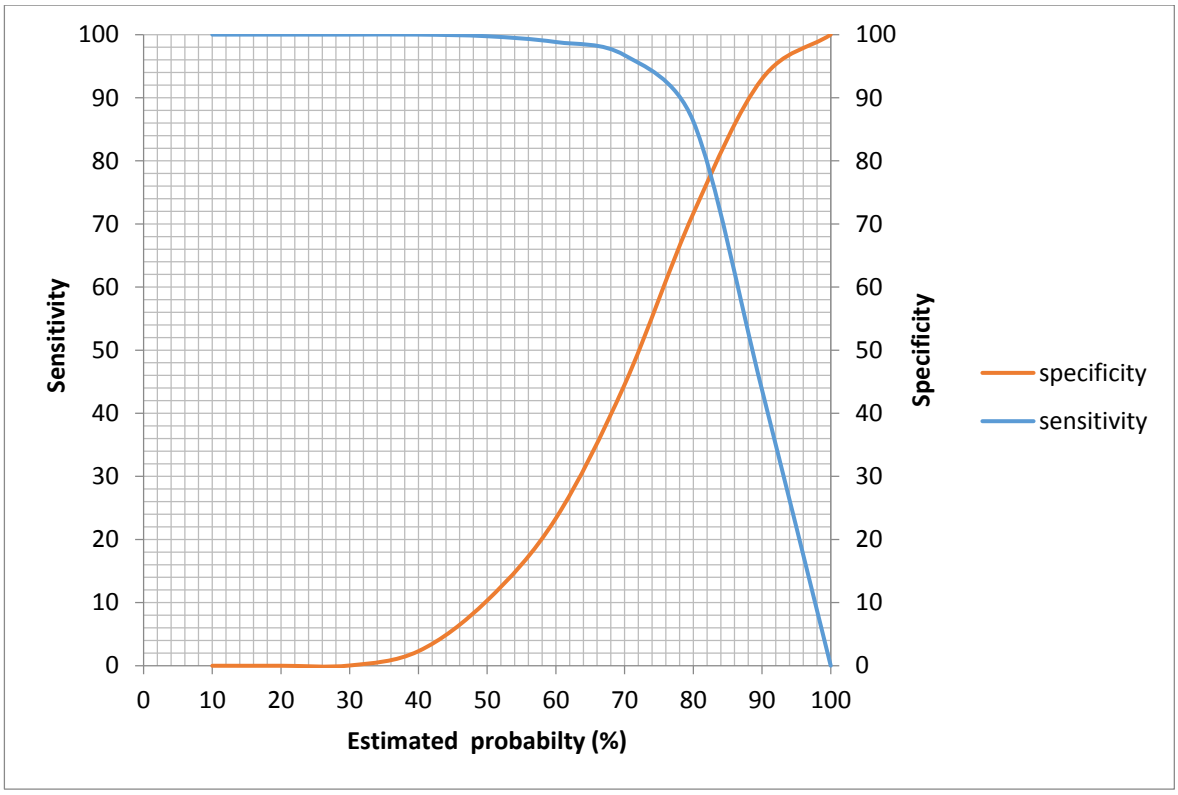

Figure 5.39: Cumulative frequency functions of sensitivity and specificity values for the TWI EBF model.

Table 5.32: Percentage of correctly and incorrectly classified landslides and non-landslide pixels based of seven arbitrarily selected cut-off values (thresholds at which assessment were carried out) from the success rate curve for ordinary TWI EBF model.

	Landslide		Non-landslide	
cut-off	Present	Absent	Present	Absent
30	100	0	0	100
40	100	0	0.02	99.98
50	99.83	0.17	9.03	90.97
60	99.67	0.34	22.06	77.94
70	97.85	2.15	42.77	57.23
80	91.92	8.08	69.29	30.71
90	65.09	34.91	92.01	7.99

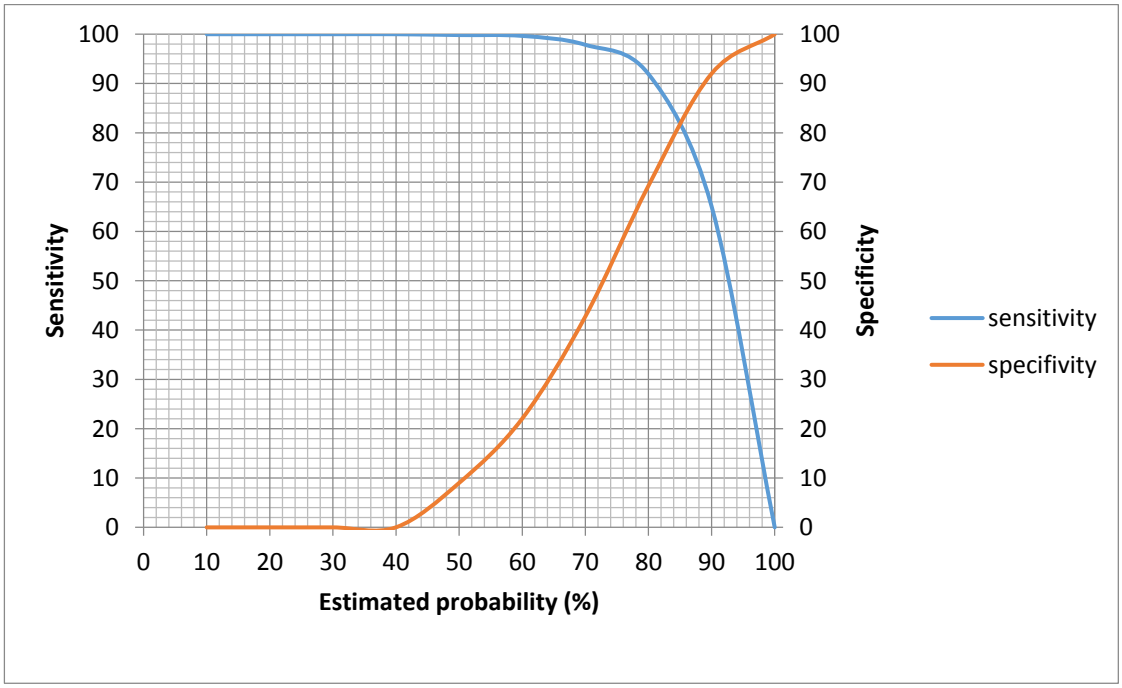

Figure 5.40: Cumulative frequency functions of sensitivity and specificity plotted against estimated probability (belief function).

However, a considerable amount of false positives still existed on the embankment earthworks thus necessitating a further upward review of the cut-off point to 90%. At the

90% cut-off point (classification accuracy of 42.72%) the model was able to effectively classify a considerable amount of the high risk areas on the embankment earthworks.

Since the success rate approach evaluates model performance based the training data employed during model construction, the approach is considered inadequate for measuring the predictive capability of the developed landslide susceptibility model. The prediction rate method provides validation for landslide predictions as predictions are based on the comparison between the susceptibility modelling results and independent (spatial, temporal or random) landslide dataset not employed during the stage of model construction (Chung and Fabbri 2003; Tien et al 2012; Park 2011). The predictive capability of the EBF models was assessed by comparing the landslide validation set (401 landslide grid cells) with the landslide susceptibility map. Figure 5.42 shows the predictive rate curves for the modified TWI and classic TWI EBF landslide susceptibility models. The results show both models to have reasonably good prediction capabilities. The models exhibited almost equal prediction proficiencies as reflected in the AUC values of 77.8% for the modified TWI and 77.5% for the classic TWI EBF model. Tables 5.33 and 5.34 demonstrate that the modified TWI model performed marginally better in the prediction of stable terrains. This is not at all surprising as the effects of vegetation cover, soil type and evapotranspiration were incorporated during model development. Adequate model prediction of stable slope will have considerable implication on the cost and overall planning process of the obligatory regular appraisal of earthwork stability as required by law in the UK.

A paired two sample t-test was carried out to verify the existence of statistically significant differences between the two EBF predictive models. The paired two sample t-test was performed on the number of correctly predicted landslide and non-landslide cells associated with selected cut-off values (95, 90, 85, 80, 75, 70, 65, 60, 55, 50, 45, 40, 35, 30, 25, 20, 15, and 10) derived from both predictions. The result of the t-test for the model predictions on correctly predicted landslide locations showed no significant difference between the two sample means (p value > 0.05). However a significant difference was observed between the sample means for the prediction of stable terrains. The t-test returned a p value of 0.008 at 95% confidence interval.

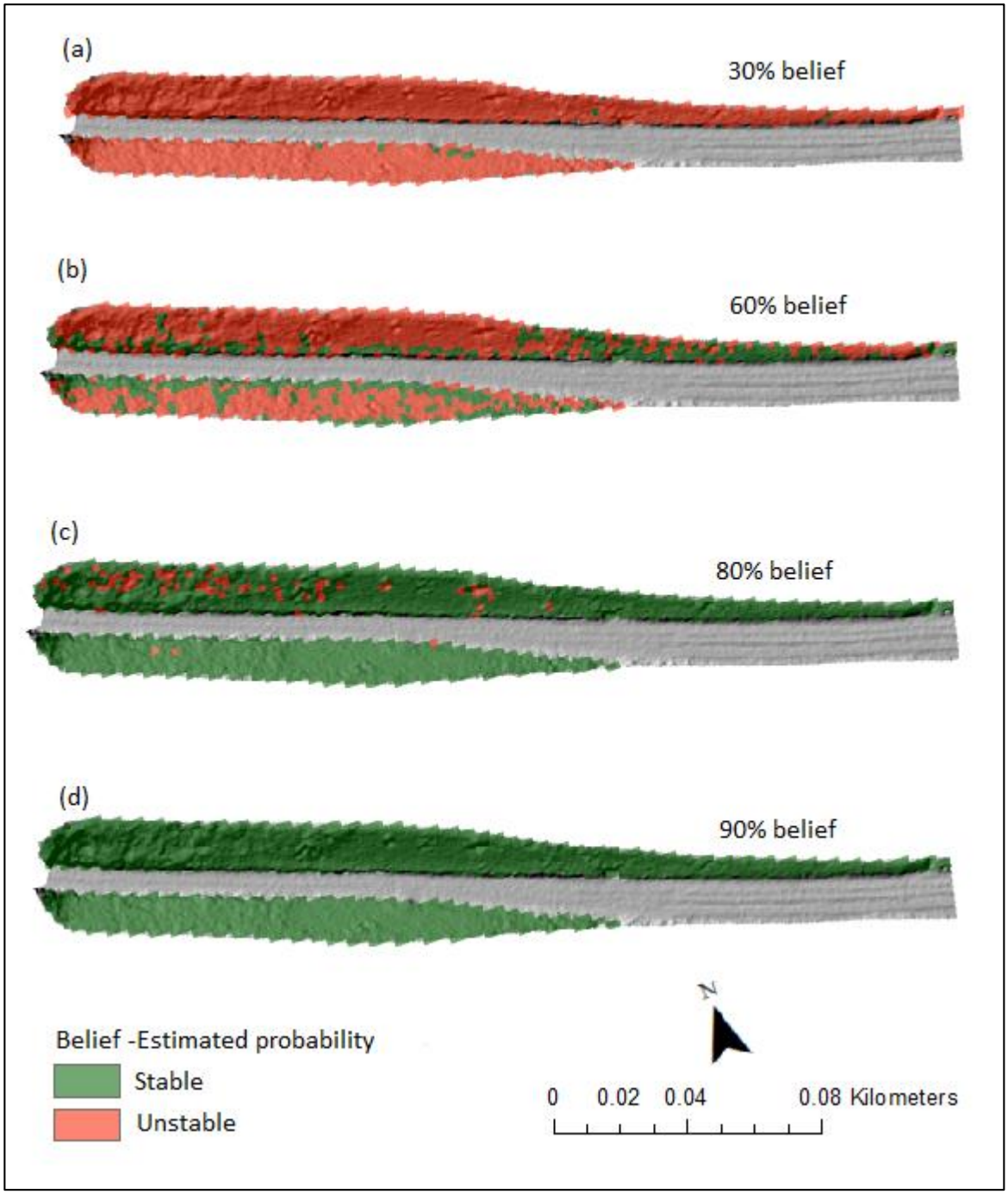

Figure 5.41: Landslide susceptibility maps of the Whitchester cutting at different cut-off values.

The landslide susceptibility map represents the spatial distribution of the degree of support to the presence or absence of slope instability based on available evidences. The relative susceptibility levels over the study area were visualised by means of five susceptibility

levels (very high, high, moderate, low and very low). An initial rank order transformation was applied to the integrated belief function map. The equal area classification method was used to classify susceptibility index values into 100 classes based on percentage area. The susceptibility class ranges were determined using results obtained from cut-off analysis and the susceptibility class breaks based on percentage of area as proposed by Pradhan and Lee (2010). The landslide susceptibility categorisation is presented in Figure 5.43 and final landslide susceptibility map is presented in Figure 5.44.

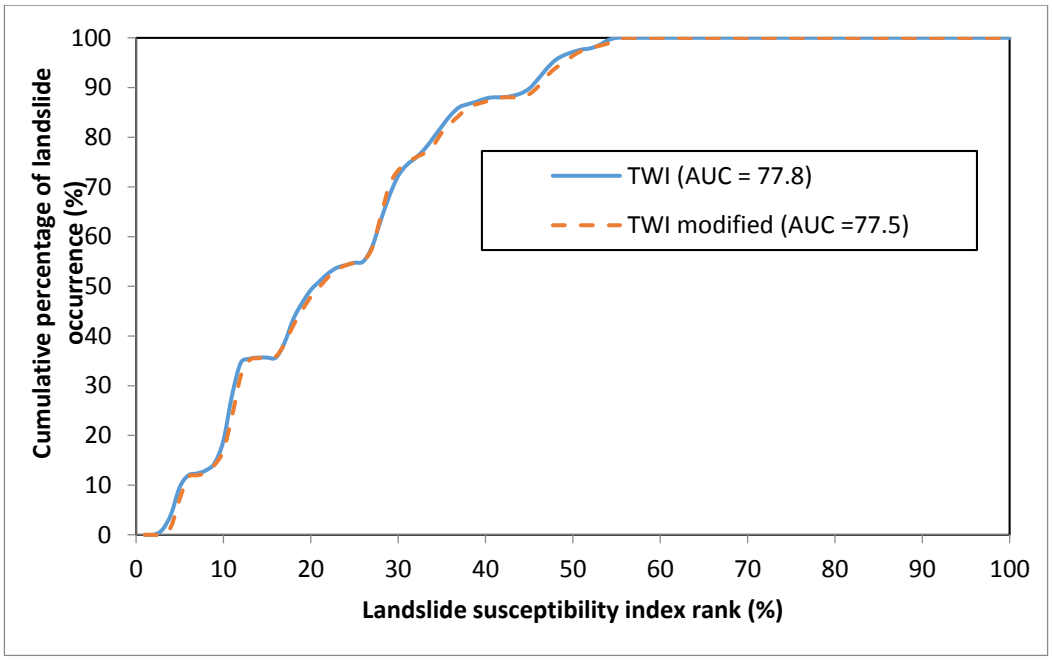

Figure 5.42: Prediction rate curves for the modified TWI and TWI EBF landslide susceptibility models.

Table 5.33: Percentage of correctly and incorrectly classified landslides and non-landslide pixels based of seven arbitrarily selected cut-off values from the predictive rate curve for the modified TWI EBF model.

	Landslide		Non-landslide	
Cut-off	Present	Absent	Present	Absent
30	100	0	0.05	99.94
40	100	0	2.39	97.61
50	95.76	4.24	9.90	90.10
60	87.03	12.97	22.29	77.71
70	72.57	27.43	42.49	57.51
80	46.88	53.12	68.60	31.40
90	15.21	84.79	90.91	9.09

Table 5.34: Percentage of correctly and incorrectly classified landslides and non-landslide pixels based of seven arbitrarily selected cut-off values from the predictive rate curve for TWI EBF model.

	Land cover		Non landslide	
Cut-off	Present	Absent	Present	Absent
30	100	0	0.04	99.96
40	100	0	2.39	97.61
50	96.76	3.24	8.66	91.34
60	87.53	12.47	21.01	78.99
70	70.57	29.43	40.70	59.30
80	48.13	51.87	66.24	33.76
90	15.71	84.29	89.79	10.21

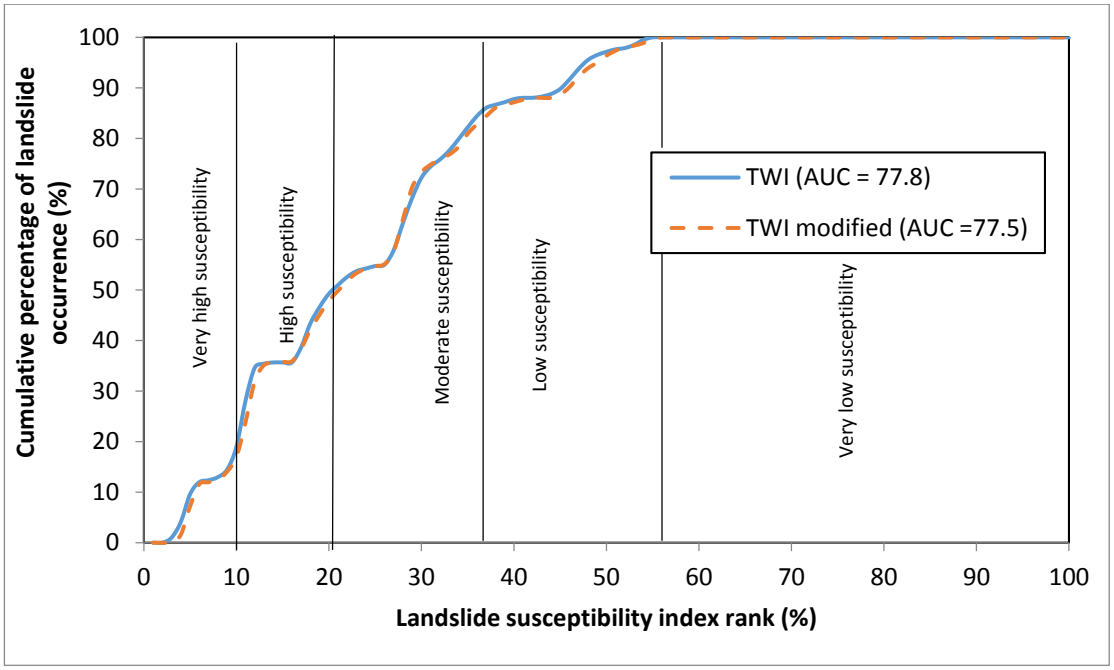

Figure 5.43 Cumulative frequency functions of landslide occurrences in the rank landslide susceptibility index values.

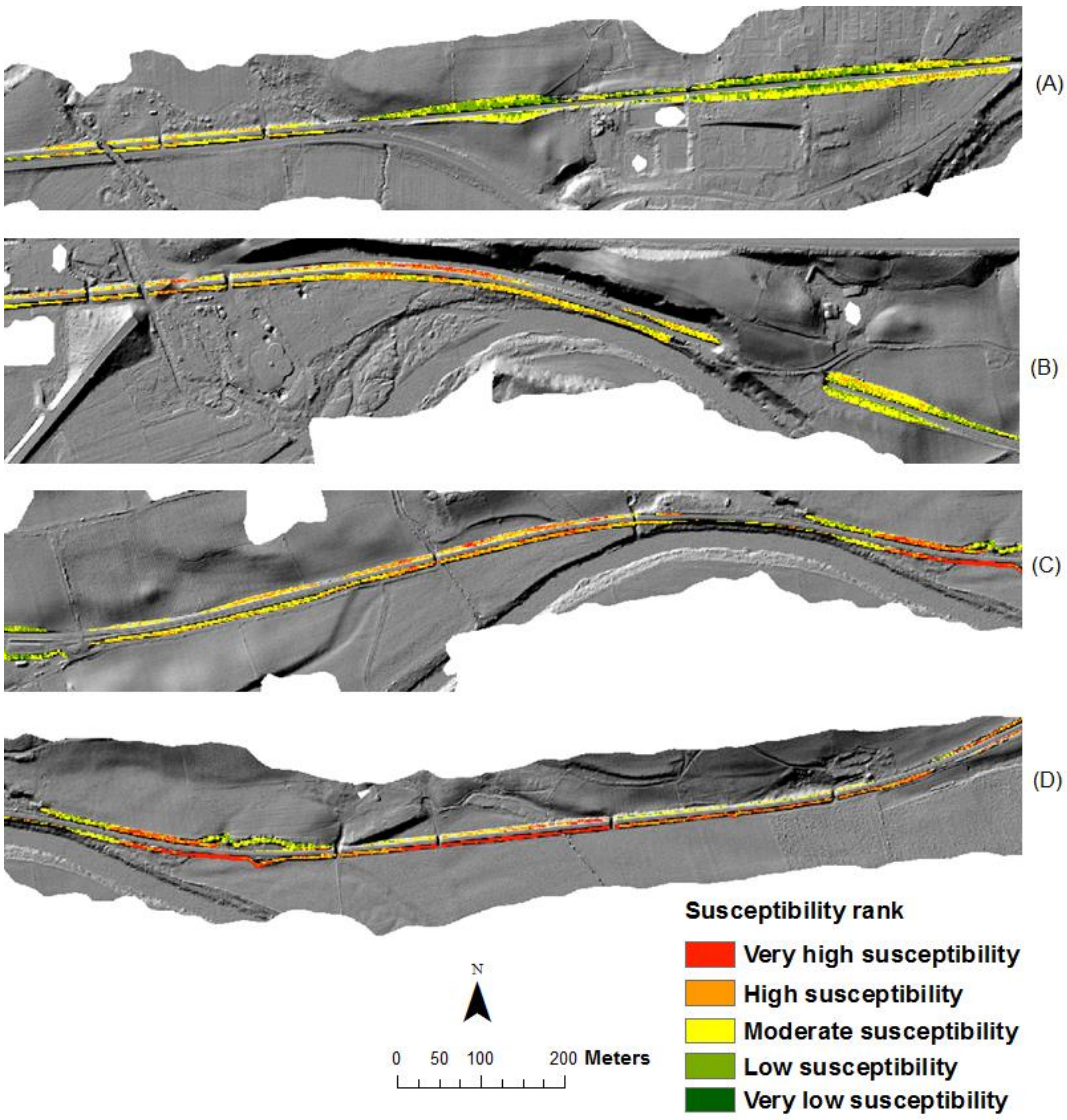

Figure 5.44: Landslide susceptibility zonation map of the transport corridor.

5.5.2 Model sensitivity

The sensitivity of the susceptibility model to variation in the proportion of training data was assessed. The training dataset was randomly subset into 30%, 40%, 50%, 60% and 80%. The various proportions were employed in the training of the evidential belief model and the final susceptibility maps were assessed. The frequency distribution of the resulting susceptibility models reveal that an increase in the number of training data results in a decrease of the median (50th percentile) and increase in variability (10th to 90th percentile range). The frequency distribution of map generated from 30% and 40% training data are characterised by outliers. (See Figure 5.45).

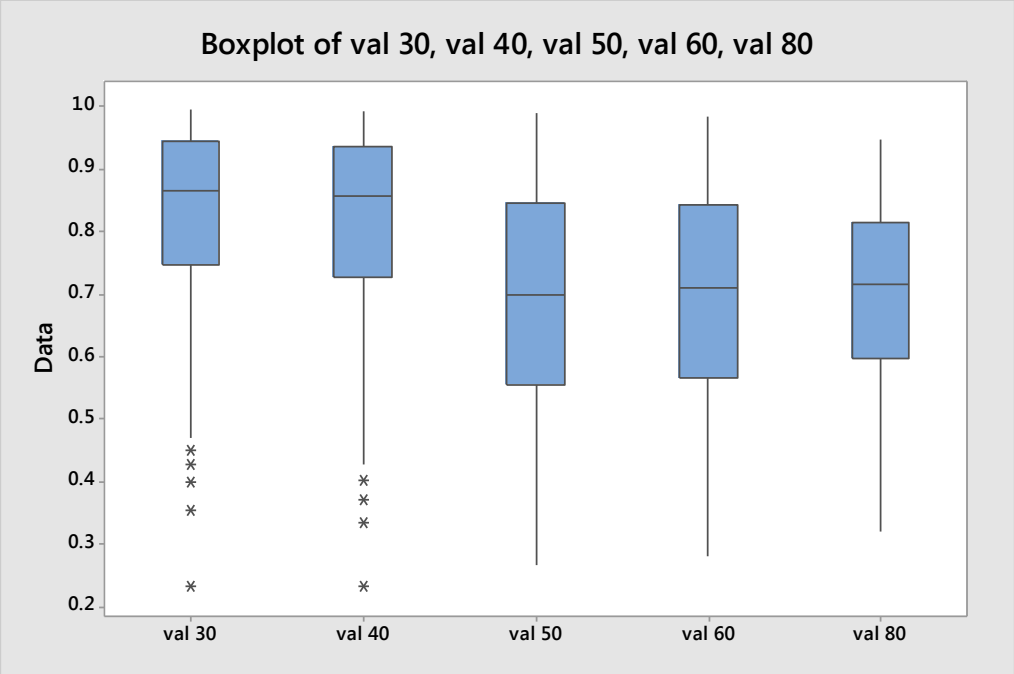

Figure 5.45: Box plot showing the effect of the amount of training data on the robustness of the EBF model.

This suggests that reduced number of training data affects the model's prediction and robustness as some of the landslide locations were considered outliers by the model parameterised with fewer proportions of training data. With increase in the proportion of training data the model variability is improved and consequently its goodness of fit to the training dataset. At 60% training data the median value is seen to have stabilised, thus implying that further increase in training data does not significantly improve the prediction capability of the model.

The uncertainty values associated with the produced susceptibility maps were characterised by a common trend of decreasing uncertainty with increase in goodness of fit (Figure 5.36). With regards the model's ability to correctly classify landslide prone areas with increasing training data, uncertainty associated with model predictions is seen to increase. The results also suggest that increase in the error associated with the percentage of rightly classified in the susceptibility prediction becomes marginal for percentages of training data exceeding 60%.

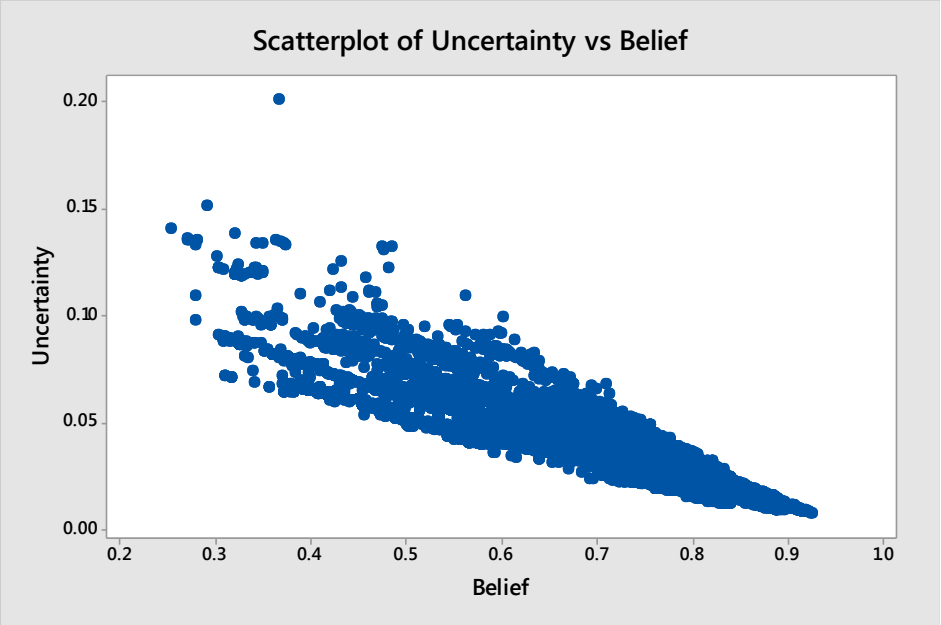

Figure 5.46: The relationship between uncertainty and improvement in the model's goodness of fit.

This finding underscores the proficiency of evidentially reasoning technique as an effective means of discriminating between stable and unstable slopes at an engineering scale slope assessment study.

5.6 Summary

Both interpolation techniques (IDW and ANUDEM) produced DTMs with similar margins of interpolation errors. The accuracy assessment of the various DTM resolutions assessed show apt representation of the overall landforms in the transport corridor. However, the IDW DTM is seen to retain more information on fine scale topography and less impacted by change in resolution, hence providing better representation of terrain derivative such as slope, aspect and curvature. The slightly higher interpolation bias associated the ANUDEM DTM is attributed to drainage enforced algorithm employed which modifies the DTM by constructing relatively smooth surfaces. Slope maps derived from both interpolation techniques exhibited the same general trend of decrease in the range of slope variability with increasing DTM grid size. The difference maps (IDW) reveal areas of the transport corridor characterised by lower slope gradients (0-4^{o}) as essentially unaltered with increasing DTM grid sizes, but a slight underestimation of higher slope values in coarser

grid resolution. This same pattern was observed in the aspect and curvature grids. The smoothing effect of the ANUDEM algorithm is portrayed in the more pronounced drop in the maximum values for slope, aspect and curvature, with increasing grid sizes. However, the ANUDEM interpolation technique reflects better gradual downslope increase in values of specific catchment area (flow) and smoothens out the effect of the presence of micro-topography commonly associated with the IDW DTM at similar resolutions. Hence, the ANUDEM interpolation routine enables better representation of flow and describes reasonably moisture distribution pattern in the transport corridor scale.

Land cover classification from a multispectral imagery show that better result were obtained from the simple band selection approach where retained low variance features of the original image is seen to enhanced the performance of image classifiers in the overall characterisation of land cover classes. The merged high resolution land cover map of the transport corridor and the relative coarser LCM 2007 of the broader catchment provided ample representation of the various land cover types and a means for the evaluation of their contributions on surface runoff generation from the broader catchment into the transport corridor. The integration of information on soil and land cover is seen to present more realistic spatial distribution soil moisture, with antecedent moisture shown to exert more influence on runoff generation than rainfall intensity. Lower runoff values were seen to be commonly associated with more permeable soil classes and woodlands. The weight grid for generated runoff depths developed from the runoff coefficient map of the transport corridor and adjoining catchment area for the various soil-land cover combinations, revealed higher weights for grasslands on impermeable soils in contrast to those on more permeable soils. The woodlands were generally characterised by low weights and the weights are lower when underlain by permeable soils.

The computed modified TWI grid indicates a general trend of increasing moisture with decreasing elevation and relatively wetter conditions for areas with considerable large upslope contributing area. Considerable catchment contributions to zones of moisture accumulation within the transport corridor from adjoining upland agricultural area were clearly visible. These are illustrated by points of ingress of flow into earthwork cuttings from the surrounding catchment and as zones of moisture accumulation along earthwork embankments.

The evidential reasoning approach enabled the integration of multiple spatial data for broad scale recognition of landslide prone earthworks. The degree of belief indicated the importance of slope with gradients between 25^{o} and 35^{o} and concave curvature. Permeable soils with intercalations accounted for over 80% of the existing slope instability, with proximity to river channel portrayed as not significantly contributing to the localisation of slope instability within the transport corridor. The ballast lain earthwork embankments were characterised by higher rates of instability with 47.5% of the embankments identified as relatively unstable in contrast to 5.1% of earthwork cuttings. The belief function for the woodlands suggests that this land cover type is responsible for about 32% of the total landslide occurrences within transport corridor. The earthwork embankment and cuttings covered by grasses accounted for only explain 18% of the total landslide occurrence.

The modified TWI model achieved reasonable characterisation of stable and unstable slopes with AUC value of 77.5. Comparatively the classic TWI EBF model is slightly more efficient at delineation of zones of slope instability but less efficient at rightly classifying stable slopes, casting doubts on the reliability of the model predictions. The overestimation by the classic TWI model can be attributed to the broad generalisation on which the classic TWI computation is based. The modified TWI model sensitivity test suggests that limited number of training data for model parameterisation can adversely affect the model prediction and robustness. However, at 60% training data, the prediction capability of the model is seen to have stabilised with further increase in the number of training data employed for model parameterisation having no significant improvement on the model predictions.

The implications of the results as it relates to the broader science and its contributions to susceptibility assessment of transport corridor slopes are discussed in detail in chapter 6.

6 Discussion

The analysis of the results presented in Chapter 5 is discussed in this chapter. The chapter is divided into five sections. Section 6.1 discusses the process of DTM creation and the impact of the interpolation techniques on the developed DTM and their derivatives. Section 6.2 outlines the important findings associated with the production of the land cover map of the transport corridor. In Section 6.3 the results of analyses integrating catchment contributions into the characterisation of zones of moisture accumulation within the transport corridor environment are discussed. Discussions on results obtained from the integration of multi-source and multiscale geospatial data approach for recognition and prediction of landslide susceptibility in transport corridors using evidential reasoning approach is reported in Section 6.4. A summary of the implications of the results obtained in this study is discussed in Section 6.5.

Slope instability within the transport corridor environment is largely associated with zones of flow accumulation and high soil moisture content. These hydrological processes are directly linked to terrain, land cover and underlying soil properties. High resolution datasets make available important terrain attributes such as slope and aspects which modulate solar insolation, evaporation and surface and sub-surface flow rates (Pack *et al.*, 1999; Fu and Rich, 2003; Ma *et al.*, 2010), curvature and specific catchment area that describe the accumulation of surface water (Sørensen *et al.*, 2006; Tarboton, 2010) necessary for hydrological terrain analysis and source of important input in slope stability assessment. The DTM provides the basis for the derivation of many these parameters. The accuracy assessment of the DTM (Bater and Coops, 2009), an optimum resolution for adequate representation of earthwork topography (Tenenbaum *et al.*, 2006; Miller *et al.*, 2012) and the non-inclusion of the microtopographic effects in relation to terrain wetness index (Miller *et al.*, 2012) are important considerations in the development of an efficient network-scale approach for remote assessment of hazards in the transport corridor environment. Other considerations include the capacity to sufficiently capture at fine scale, surface elements such as land cover and soil type known to significantly impact on slope stability. Unlike the land cover class that is seen to vary significantly over short distances in the transport corridor (Hardy *et al.*, 2012; Miller *et al.*, 2012), the underlying soil properties

have been shown to be relatively consistent over similar distances throughout the test corridor (Network Rail, 2005; Miller *et al.*, 2012).

6.1 The impact of interpolation technique on DTM generation

The results of errors associated with the accuracy of interpolated heights for the IDW and ANUDEM interpolated DTMs show that both interpolation technique produced DTMs with similar magnitude of mean error values with the IDW interpolated DTMs exhibiting slightly better error margins with coarsening grid resolution (see Chapter 5 and Table 5.1). There is a gradual loss in DTM quality with reduction in spatial resolution of DTM as indicated by the increasing RMSE. However, the rate of DTM deterioration with reduction in spatial resolution is more pronounced in ANUDEM DTMs. This is consistent with finding from similar studies (Aguilar *et al.*, 2005; Vaze and Teng, 2007; Bater and Coops, 2009). The slightly more conservative nature of the IDW DTMs means that greater detail of fine scale earthwork topography is retained at lower resolutions. This is particularly important in relation to the selection of an optimum DTM resolution, as TWI is better represented in coarser resolution so as to avoid the inclusion of the effects of microtopography (Sørensen *et al.*, 2006; Sørensen and Seibert, 2007).

The 0.5m DTMs for both interpolation techniques were found to provide the most accurate representation of the of the transport corridor terrain of all the DTM resolutions assessed as revealed in their lower average residues and RMSE values. Comparatively, the average residual and RMSE values show the IDW DTMs as providing better terrain representation for all ten grid resolutions assessed. Both interpolation techniques produced DTMs with very similar mean absolute error values. But the error range (mean absolute error) with increase in grid cell size is higher in the ANUDEM DTM. The mean absolute error increases from 16 to 24cm for the ANUDEM DTMs as against 15 to 21cm for the IDW DTMs. This marginally higher interpolation bias associated with the ANUDEM DTM is attributed to the drainage enforced algorithm employed (Hutchinson, 2013). Some authors have reported achieving DTMs of higher accuracy with other interpolation techniques such as kriging (Rees, 2000), and natural neighbour (Bater and Coops, 2009). Lloyd and Atkinson (2002) demonstrated that the derived benefit from using geostatistical approach over IDW is lost when densely populated data is available. The natural neighbour routine requires an initial creation of a TIN from source data for the identification of adjacent

points and Vornoi polygons used in the weighting of each point during the interpolation exercise (Bater and Coops, 2009) and as a result the interpolation technique handles poorly large datasets (Bobach *et al.*, 2009).

The IDW technique has been described as highly influenced by the user selected parameters by Bater and Coops (2009). It is sensitive to clustering and like all exert technique handles poorly summits not located on sample points. It also has a tendency of point isolation resulting in what is termed the "bulls eye". The IDW routine has however been shown to perform optimally (terrain representation) when the exponent of distance that controls the significance of surrounding points on the interpolated value is allocated a value of two (Yue *et al.*, 2007). The ANUDEM interpolation routine is characterised by a more homogenous behaviour even when point density is sparsely distributed or reduced as opposed to the IDW technique (Hutchinson, 2008).

Both interpolation routines are computationally efficient enabling the interpolation of over a million points within reasonable computational time and as such are well fitted for handling massive data commonly associated with the ALS dataset. This property is particularly important to the transport corridor project, where slope stability assessment requires high resolution terrain data covering linear tract that may extend for several kilometres. Both interpolation techniques delivered apt representation of the general landforms with the highest bias in elevation values found around landforms with steep gradients.

6.1.1 Impact of Interpolation on terrain derivatives

The shape and characteristics of fine-scale topographic features play an important role in the determining local patterns in aspects and potential incidence of solar radiation (Hardy *et al.*, 2012). These terrain features can influence local soil moisture and vegetation patterns (Moeslund *et al.*, 2013; Maynard and Johnson, 2014). The general pattern observed from the computed CFDs and extracted key percentile values of derived terrain attributes with change in grid resolution show that for the slope grids, a reduction in derived slope values with increasing grid cell size. The difference in estimated slope values with coarsening DTM resolutions is minimal in plains and landforms with relatively uniform relief and most pronounced in terrains with steep and highly undulating relief such as the earthwork cuttings (Figure 5.10). As earlier mentioned in Section 5.2.2, typical slope gradients

associated with earthwork cutting and embankments within the transport corridor range from 10^{o} and 49^{o}. This range of slope values is not significantly altered with change in grid resolution in the IDW DTMs with a maximum difference of 5^{o} existing between the 0.5 and 5 m DTMs across the 10^{o} and 50^{o} slope range. However, a significantly higher maximum difference of 16^{o} was recorded for the ANUDEM DTMs at the corresponding resolutions and slope range. The profile curvature is slightly underestimated with increasing grid cell sizes in the IDW DTMs (see Table 5.4). The profile curvature values obtained from ANUDEM DTM were largely underestimated with increasing grid cell sizes. The underestimation of profile curvature may adversely impact on the characterisation of concave and convex curvature information of fine scale features responsible for local dispersion and convergence zones on earthwork embankments and cuttings.

The erratic nature that characterises the calculated modified TWI values for the IDW interpolated DTM are essentially the responses to fine scale topographic features contained in the DTM. The erratic nature of these responses is seen to obscure the overall downslope flow trend. The general trend of surface flow pattern is, however, better captured in the ANUDEM interpolated DTMs that construct relatively smooth surfaces ensuring the calculation of continuous flow as revealed in the gradual downslope increase in specific catchment area values (see Figure 5.18). Moreover, steep slopes (greater than 50^{o}) are seen to be poorly represented in the ANUDEM interpolation routine (see Figure 5.11). This is because to ensure a smooth continuous surface alongside continuous first-derivative surfaces like slope gradient and direction, the ANUDEM routine computes minimum curvature for each grid cell which can significantly alter the values of first derivative occurring within the vicinity of the data points (Hutchinson, 2013). The consequence of the computed minimum curvature for each grid cell, is the significant averaging of values at these locations. As a result, a second derivative like curvature is grossly underestimated by the ANUDEM routine (ERSRI, 2010). In contrast, first and second derivative surfaces derived from the IDW interpolated DTMs present a consistent behaviour for values calculated for the various grid resolutions investigated.

The results also show that the attenuation of relief and systematic reduction in values of calculated terrain derivatives with increasing grid cell size from 0.5 to 5 m do not significantly alter the IDW DTM characteristics as portrayed by the lack of significant

difference between sample means (p values greater than 0.05 at 95% confidence level) obtained for the different resolutions of the IDW DTMs (see Table 5.2). This suggests that this range of DTM resolutions (0.5 – 5m) can provide a reliable basis for the extraction of slope stability terrain parameters. This fact is crucial to the development of an operational methodology. Though better terrain representation is generally achieved with higher resolution, issues of processing time and data storage capacity often associated with massive dataset usually necessitate an optimum resolution that provides adequate representation of the earthwork topography alongside reasonable processing cost. Sensitivity testing (discussed in section 5.2.5) indicated an optimum grid resolution of 2.5 m. This grid resolution ensured data processing at reasonable processing cost and provided adequate representation of first and second order terrain derivatives such as slope, aspect and curvature. Moreover, minimal inclusion of the effects of microtopography on the computation of TWI values was observed at this grid resolution (Table 5.6). Schmidt and Persson (2003) reported an optimum resolution of 2 m for a kriging interpolated DTM employed in the computation of TWI values. However Schmidt and Persson (2003) indicated the use of a filter with a radius of three cells which most likely aided in supressing small scale variation.

At detailed scale slope assessment, adequate representation of important terrain attributes known to exert considerable influence on soil moisture distribution and slope stability are better with specific interpolation techniques. The use of multiple interpolation routines in slope stability assessment is not common practice possibly due to the introduction of uncertainties as a result of interpolation bias, processing and data storage cost. However, meaningful consideration on the advantages and disadvantages of the various interpolation routines is required as the use of two interpolation techniques may be necessary for ample characterisation of the influences of various terrain attributes at engineering scale landslide susceptibility assessment.

6.2 Land cover map development

A cardinal aim of the development of a land cover map for the study area was for the categorisation of the various land cover types as represented in the CASI imagery in line with their hydrological responses and its subsequent integration into the modelling of overland flow from adjoining upland agricultural areas from the broader catchment. Land

cover type within the transport corridor is seen to vary quite considerably over relatively short distances (Miller *et al.*, 2012). The capacity to sufficiently capture at fine scale, surface elements that significantly impact on slope stability was the key motivation behind choice of dataset and classification approach. The multispectral aerial (CASI) imagery provided an ample source of information on vegetation cover with spectral signatures of individual plant species as well as more complex mixed pixel communities better differentiated by reason of its high spectral resolution. The selection of an optimal subset of bands tailored towards vegetation analysis proved an effective means of reducing data dimensionality (a pre-processing step to land cover classification) and produced land cover maps (Figure 5.19 and 5.20) with better classification accuracy as evident in the higher producer and user accuracies of the individual classes during the analysis in contrast to maps produced using spectral transformation MNF technique (Table 5.23).

Two trends common to both classification maps are the low producer and user's accuracies associated with land covers with significant spectral overlap and improvement in progression of class and overall accuracies with merging of classes with considerable spectral overlap. The preservation of all the low variance information from the original image in the simple band selection image ensures that discerning information on vegetation types as a result of variation in height of the reflectance curve are made available for the land cover classification routine (Van der Meer and de Jong, 2001). The presence of the low variance information generally had two implications on the overall classification. On one hand, it optimised the proficiency of the maximum likelihood classifier by making available subtle low variance information that effectively discriminate between land cover types with close proximity in their mean vector and covariance values (Tsai and Philpot, 2002). This is evident in the better class separation achieved for the pasture, woodlands and shrubs land-cover classes. On the other, the presence of correlated low variance information results in the widening of the class distribution and increases the level of overlap between classes. The confusion matrices obtained for land cover classification maps derived from the simple selected band approach reveal considerably higher rates of misclassified pixels for land cover classes with considerable spectral overlap, as revealed in low producers' accuracies for classes. (Tsai and Philpot, 2002).

Unlike the simple band selection approach, the MNF spectral transformation technique renders relationships between different groups of pixels representing the different land cover classes more distinctively by the removal of random noise or correlated lower variance features (Mather and Koch, 2011b). This effect is clearly evident in the lower number of misclassified pixels within the pasture land cover class in the contingency matrix of principal component image. However, the removal of random noise or correlated lower variance features was found to be counterintuitive with highly heterogeneous land cover classes (shrub) that display significant signature overlap in spectral space with other land cover classes. As a result, the considerable reduction in the number of misclassified pixels between classes in the classification maps as ensured in the principal component image, does not necessarily translate into higher overall classification accuracies as expected. But resulted in the over-estimation of the bare earth class and the underestimation of the shrub land cover class as shown by the low producers' accuracy recorded for these classes. Consequently, the reliability of modelling results obtained for both classes derived from MNF spectral transformation image may be inexact. This finding is consistent with similar studies (Tsai and Philpot, 2002) that show that image segmentation using principal component analysis often introduces the possibility of an over estimation due the absence of important low variance information that would have otherwise served as useful indicators in spectral segregation. It is however noteworthy that the bare earth land cover class is also one of the categories with relatively few available training pixels in a largely well vegetated transport corridor. As such, the overestimation may be a function of using training data that inadequately described the high-dimensional distribution of the land cover class. The overestimation of the bare earth class has important implications on the overall mapping of soil moisture in the transport corridor. As bare earth locations are generally characterised by high overland flow due to the absence of vegetation cover, thus its overestimation may largely undermine weights derived for locations during the modelling of catchment contribution to overland flow in the transport corridor. A number of advanced spectral processing techniques such as derivative analysis (Tsai and Philpot 2002) and continuum removal analysis (Mutanga *et al.*, 2005) that enables the capturing of low variance features and efficient discrimination between land cover classes are available. With derivative analysis, specific derivatives of spectral that characterise the desired information are identified and by adding these derivatives as features, the land cover

classification results are optimised (Tsai and Philpot, 2002). The continuum removal analysis involves isolating spectral features of interest, typical the red edge in vegetation analysis. A line of continuum which is defined as a hull over an absorption feature is removed by dividing the reflectance value at each wavelength along the line by the reflectance value of absorption feature (Mutanga *et al.*, 2005). These techniques were however not explored as the primary main of the use of the multispectral CASI imagery was simply for the development of a land cover map for the transport corridor.

6.3 Catchment contribution

Located entirely within the floodplains of the South Tyne River and bounded to the north and south by valley walls of the Tyne Gap, considerable amount of the overland flow responsible for localised saturation that characterise areas of topographic convergence within the transport corridor are believed to be generated from the surrounding upland agricultural areas of the adjoining broader catchment. A more holistic approach to the assessment of the spatial variability of hydrological influences on slope stability within the transport corridor required the inclusion of the contributions of the broader catchment. Unlike the oversimplification of overland flow in the classic TWI approach that assumes the entire upslope contribution in flow accumulation is relatively unaffected by processes of infiltration and evapotranspiration. A novel approach for the characterisation of soil moisture ensured that the influence of variability in soil hydrologic properties and vegetation cover are incorporated in providing a relative measure of terrain saturation across the transport corridor. With rainfall as the main trigger of slope instability in the UK and runoff generation as consequences of infiltration and saturation excesses, the SCS curve number method accounts for the contributions of infiltration and saturation in the computation of direct runoff as consequence of rain storms. The technique was originally advanced for use in the USA and is yet to be fully calibrated to reflect prevailing weather and soil conditions in the UK (Hess et al 2010). However the SCS CN approach is robust across a large range of climatic conditions, land cover land use and soil types and currently forms an essential part of the Catchment Flood Management Plan (CFMP) tool developed by the Environment Agency. The CFMP tool is used to evaluate the changes that may arise as a result of modifications in rural land management and land use activities and consequent impact on flood generation (Environment Agency 2009). The SCS CN model is an event model for prediction of direct runoff depths for individual storm events.

Evaluation of six separate storm events with varying precipitation intensity and antecedent moisture condition showed that the antecedent moisture condition plays a more significant role in the magnitude of runoff generated than rainfall intensity (Table 5.25). Lower runoff depths were associated with more permeable soil classes (Class B and C), while class D soils rich in clay fractions exhibited higher depths of surface runoff (Table 5.26).

With regards to the land cover types, the woodlands exhibited lowest runoff values in comparison with other land cover classes. The weight grid produced a more realistic spatial distribution of soil moisture that takes into cognisance the effects of infiltration and evapotranspiration. The uncertainty introduced into the computation of TWI by the introduction of the developed weight grid was found to be insignificant. The results of the sensitivity analysis from the evaluation of the robustness of the developed weights showed that the adjusted weight values for the grasslands and woodlands (discussed in Section 5.4.2) did not result in any global alteration in the distribution pattern of generated surface runoff (Table 5.27). However, the results suggest that the changes in the woodland distribution (TWI mean 5.32) will have more considerable effects on the soil moisture content in the test site than variation in grassland management (TWI mean 5.18).

The integration of the SCS curve number procedure into the traditional computation of TWI for estimation of direct runoff generation provided a more realistic representation of soil moisture estimation. The modified TWI technique utilised a weighted flow accumulation grid that incorporated the contributions of vegetation cover and soil type into the computation of the upslope contributing area, therefore enabling the local evaluation of the contributions emanating from the wider catchment flow field and the local input variables at each grid cell location. Topography wields primary control over the distribution of soil moisture in the study area. However, the weighted flow accumulation grid also outlines the influence of land cover and underlying soil type on computed TWI values. The modified TWI grid indicated that the highest runoff rates are associated with locations devoid of vegetation cover, while the woodlands are characterised by the least generated runoff depths. Overland flow is largely reduced in woodland as a result of inception, high infiltration rates and also near surface, field saturated hydraulic conductivities (Archer *et al.*, 2013). Thompson *et al.* (2010) showed that the internal drainability of soils (saturated hydraulic conductivity) are considerably improved by the

presence of high root densities and root diameters. Root activities enhance soil macroporosity and structure resulting in larger soil pore networks and increased soil permeability. Intrinsically, the permeability in woodlands is usually higher than that for same soil supporting other types of vegetation cover. In addition, the presence of trees on earthwork cutting and embankments have been shown to slightly improves the stability status of the infrastructure as these sections are relatively drier possibly due to increased evapotranspiration activities at depth (Miller *et al.*, 2012).

Generated runoff depths for the different soil types in the study area showed generally low values for (1) the well-drained stony loam over gravel of the Ellerbeck association, (2) the Alun and Wharfe series, comprised of deep well drained dominantly fine to coarse loamy typical brown alluvial soils extensively associated with river flood plains and (3) the deep stone less permeable loam of the Brickfield 3 group. While higher runoff generation were seen to have characterised the shallow peat on acidic igneous rocks of the Bangor group, the slowly permeable seasonally wet deep loam to clay, loam over sand, peat to loam, loam, bog peat and blanket peat of the Dunkeswick, Anglezarke, Wilcocks 1, Enborne, Longmoss and Winterhill groups respectively.

Predicted soil moisture patterns as depicted by the developed terrain based flow (modified TWI) model for the transport corridor are consistent with the general patterns reported in various studies (Tenenbaum *et al.*, 2006; Sørensen and Seibert, 2007; Hardy *et al.*, 2012), with moisture accumulation confined to zones of flow convergence (in concave and low gradient area) and increased propensity for runoff generation in steep convex terrains. The modelling results show evidences of points of ingress of flow of runoff from surrounding broader catchment topography into the transport corridor earthworks. The modified TWI model identified the predicted points of ingresses as zones of localised moisture accumulation. There are also evidences suggesting considerable flow incursion in sections of earthwork embankments from surrounding upland agricultural fields resulting in increased moisture accumulation along northern margins of embankment earthworks east of the corridor. These points of ingresses (described in Section 5.4.2) are characterised by relatively higher concentration of soil moisture as indicated in associated high TWI values.

In addition, the south facing earthwork slopes exhibit relatively higher soil moisture content owing to the relatively larger adjoining upland contributing area (Figure 5.22). Increased

pore water pressure, as a result of moisture accumulation at these zones of flow convergence, is expected to reduce effective stress of the slope make up material and increases the slope's susceptibility to instability (Iverson, 2005). Typically, around earthwork cuttings, high concentration of soil moisture was recorded for the top and toe of the earthwork with comparatively lower soil moisture values half way down the slope, as opposed to the gradual increasing downslope flow pattern described by Tenenbaum *et al.* (2006) for geomorphological slopes. A likely explanation for this may be the planar nature of the earthwork cutting that ensures increased downward flow of generated surface runoff. Furthermore, the earthwork cuttings also exhibit increased mid-slope concentration of soil moisture along sections of the slope face. The profile curvature grid shows that the points of increased soil moisture content coincided with areas of significant concave curvature values, an indication that the microtopography may influence considerably soil moisture distribution at this scale of modelling. The presence of curvature can provide local accentuation to pore water pressure which may adversely affect slope stability especially in well drained soils with intercalations where the occurrences of perched water tables are not uncommon (Baum *et al.*, 2005).

The earthwork embankments in the test corridor are large covered by ballast and in some sections sparsely vegetated but extensively bounded by a linear strip of a mixture of matured low and high water demand trees. The wetness index values obtained for the earthwork embankments are generally low describing drier conditions (Hardy *et al.*, 2012). Hence, mapping of soil moisture without due consideration to upland contributions can be misleading, as sections of the embankments east of the corridor may be considerably damper than indicated by TWI values owing to infiltrating water from adjoining zones of moisture accumulation (Figure. 5.25). Studies on slope stability assessment conducted on embankments and cuttings across the UK, have shown that infiltrating overland flow from areas bounding earthwork infrastructure can result in the cess-heaving process (Perry *et al.*, 2003b; Ridley *et al.*, 2004; Smethurst *et al.*, 2012), a process that significantly alters the strength characterisation of underlying clay foundations and eventually weaken the overlying soils (Briggs *et al.*, 2013). Though these studies reported findings for embankments founded on the plastic over-consolidated London clay deposit, similar conditions exist within the test corridor. As 27% of the earthwork infrastructure in the study area is underlain by slowly permeable seasonally waterlogged fine loamy fine loamy over

clay and clayey soils. A geotechnical survey report on a section of the transport corridor also revealed the presence of a clay layer incorporated at the toe of the earthwork embankments (Network Rail, 2005). Infiltrating water can increase existing pore water pressure distribution and therefore the effective stress of soil and invariably the slope stability (Smethurst *et al.*, 2012).

6.4 Evidential reasoning model

Evidential reasoning provides an efficient approach for the integration of multi-sourced, multi scale evidences (dataset) used in generating degrees of support required for the delineation of zones of instability. Cuttings and embankments are essential components of the transport corridor commonly spanning several kilometres. These infrastructures are usually under strict statutory safety obligations. The use of instrumentation for the diagnosing the propensity for instability in slopes and embankments has been very effective in providing better understanding on slope behaviour and evaluation of remedial techniques (Ridley *et al.*, 2004; Briggs *et al.*, 2013). Much of which involves monitoring and analysis of geotechnical properties of slopes make up materials, with measurements carried out over a number of years to capture temporal changes in the behaviour of the earthworks (Briggs *et al.*, 2013). However, the approach is expensive as such restricting its application to spatially limited high priority locations. Process based models are generally employed to facilitate instability assessment at engineering scale. Process based models can provide a clearer understanding of the physical processes and behaviour mechanisms at work within earthworks and how these infrastructures are influenced by extreme climate and vegetation (Clarke and Smethurst, 2010; Miller *et al.*, 2012; Smethurst *et al.*, 2012). These models are however specific to local meteorological, vegetation, hydrological, lithological and geo-mechanical conditions of individual slopes. Hence the extrapolation of results beyond the domain of acquisition is often challenging (Miller *et al.*, 2012). The high input data demand and parameter calibration are important concerns when considering a network scale application. Implementing numeric modelling on a network scale may require an extensive catalogue of site investigations providing details of geotechnical properties on a localised basis across the UK.

The developed methodology provided a probabilistic data driven approach for assessing slope failure hazard in the transport corridor environment. The probabilistic model

incorporated as input data key factors noted during detailed field work and duly investigated landslide triggering and conditioning factors reported for the UK transport corridor slopes (Perry *et al.*, 2003b; Ridley *et al.*, 2004; Hardy *et al.*, 2012; Miller *et al.*, 2012). Eight landslide conditioning factors namely slope gradient, aspect, profile curvature, distance to drainage, land-cover, TWI, SPI, soil and a triggering factor (precipitation) were utilised in the study. Underlying geology was not considered as the study site was essentially underlain by the same bedrock geology. The high spatial resolution of the input geospatial dataset ensured faithful representation of terrain features and the capturing of land cover variability which within the transport corridor varies quite substantially over short distances. The ALS data provided a reliable basis for extraction of terrain derivatives, while the multispectral aerial imagery enabled realistic mapping of vegetation cover variability at fine spatial scales.

Results of the basic probability assignment functions (evidential belief layer) computed for the various landslide conditioning factors considered in the study identified the ballast-lain earthwork embankments as highly susceptible to slope instability. The man-made land cover class that essentially covers the ballast-lain earthworks explains 50% of the total landslide occurrences in the transport corridor. The earthwork embankments are generally steep sloped, heavily to sparsely vegetated in places and the presence of large amount of ballast permits high surface water percolation. The earthwork embankments in Hardy *et al.* (2012) were portrayed as relatively drier by reason of the predicted low soil moisture content inferred from the TWI values obtained for these locations. The classic TWI approach that assumes zero infiltration was utilised in the study. The inferred moisture content can only hold for the modern well compacted highway embankments constructed to prevailing high industry specifications with provisions of adequate internal drains. But same cannot be said for the Victorian embankments test corridor constructed from poorly compacted soils and rock fragments (Network Rail, 2005) with predicted ingress of surface flow from surrounding zones of flow accumulation (Figure 5.25). Greenwood *et al.* (2004) noted the use of shrubs and trees in providing potential reinforcement to marginally stable embankments and cuttings within the transport infrastructure in the UK. This may explain the stretch of mature to semi matured trees at locations identified as zones of flow convergence in the modified TWI map. Studies have also shown that the pattern and extent of seasonal soil moisture content in embankments can be substantially influenced by the

tree species and root depth (Greenwood *et al.,* 2004; Briggs *et al.,* 2013). High water demand trees are often able to reduce excess soil moisture and sustaining the generated moisture deficits through the wet UK winter months (O'Brien, 2007). Thus, the belief function shows that woodlands are associated with about 32% of the total landslide occurrences within transport corridor, while embankment and cuttings covered by grasses is seen to only account for 18% of the total landslide occurrence.

The belief functions for the underlying soils in the transport corridor reveal high propensity for slope instability in the relatively more permeable soils (Alun, Ellerbeck and Wharfe soil classes) in contrast to the loamy clayey seasonally waterlogged slowly permeable soils of the Nercwys and Brickfield series. This is not at all surprising as seasonally waterlogged clayey layered soils are often consolidated (National Soil Resources Institute, 2008), occasioning most of the storm water from precipitation culminate in surface runoff. Earthwork cuttings in these soils are relatively stable with provision of sufficient drains. Baum *et al.* (2005) explains that percolating water is more impactful on slope instability as built up pore pressure known to reduce the stability of slopes when it accumulates above a less permeable intercalation. The Wharfe soil class which is essentially river alluvium made up of deep stone-less permeable fine loamy soils, variably affected by groundwater (Avery, 1980), is associated with high occurrences of landslide and invariably assigned a higher belief function value by the model. Though permeable and largely well drained, the presence of clay enrichment in the non-calcareous loamy or clayey alluvium (more than 30 cm thick) Wharfe soil class is known to sometimes result in winter flooding (National Soil Resources Institute, 2008). The relatively better drained Ellerbeck series is dominantly free draining loamy-gravely soils developed on very stony glaciofluvial or river terrace drift (National Soil Resources Institute, 2008), appears to be relatively more stable than the Wharfe soil class but less stable in comparison to the loamy clayey seasonally waterlogged slowly permeable soils of the Nercwys and Brickfield series.

6.4.1 Evidence integration

Unlike other spatial data integration models that produce a single landslide susceptibility map, the evidential belief model supports a series of basic probability assignment functions including belief, disbelief and uncertainty. This usually results in the production of three maps providing quantitative description of the relationships that exist between landslide

occurrences and the input multiple spatial layers. In this study, three basic probability assignment functions maps were produced. The belief map is considered representative of the correlation between landslide location and each conditioning factor; as such the integrated belief map served as the landslide susceptibility map used in deriving the landslide susceptibility index (LSI) of the study area. The disbelief map highlights locations where available evidences are not in support of the existence of instability. The uncertainty map indicates locations characterised by lack of information or where available evidences are insufficient to categorise as stable or unstable. A fourth map representing plausibility is sometimes produced by authors. The map presents the summed up degrees of belief and uncertainty on the existence of slope instability for each pixel location in the study area. The belief, disbelief and uncertainty function maps were produced for this study.

The integrated belief map showed the earthwork cuttings as relatively more stable with only 5.1% of the earthwork cuttings identified as unstable as against 47.5% for the earthwork embankments. The EBF model infers the presence of infiltrating surface moisture and fine scale microtopography as two important components seen to influence the localisation of sections of earthworks prone to failure. This is revealed in the high susceptibility to landslide occurrences associated with (1) earthwork cuttings on permeable and largely well drained soil formations with intercalations of clay materials, (2) presence of fine scale concave curvature responsible for localised soil moisture concentration mid-slope on earthwork cuttings and (3) ingresses of surface moisture into earthwork cuttings and embankments. The influence of underlying soil types to landslide location is underscored by the model's allocation of high values of belief to the relatively more permeable soils with variable intercalations of the Ellerbeck and Wharfe associations in contrast to the loamy clayey seasonally waterlogged slowly permeable soils of the Alun, Nercwys and Brickfield series (see Table 5.30). The well drained and permeable soils of Ellerbeck and Wharfe accounted for over 80% of slope instability in the earthwork infrastructure. Slope behaviour as it pertains to infiltrating rainwater is largely influenced by the hydraulic properties of the soils such as hydraulic conductivity and soil moisture characteristics (Reid, 1997). Variation in hydraulic properties of the soil can modify the distribution of pore water pressure and invariably the soil's effective stress field during rainwater infiltration (Reid, 1997; Cho and Lee, 2001).

Another variable that was identified by the EBF model as influential to the localisation of zones of slope instability is the presence of curvature. Concave features can serve as miniature reservoirs increasing local infiltration rates, retaining soil moisture for relatively longer periods and at favourable slope gradients may develop shear surfaces (Ohlmacher, 2007). The concave surfaces accounted for 49% of the total landslide while convex curvature accounted for 33% of the total landslide occurrences. The degrees of belief indicated the importance of slope with gradients between 25^0 and 35^0 as most influential to the incidence of slope instability in the transport corridor. Miller *et al.* (2012) reported a linear relationship between the increasing slope gradient and slope instability. However the EBF model reveals a curvilinear relationship with landslide frequency increasing with slope gradient to a threshold of 35^o above which landslide density decreases. Reasons for curvilinear behaviour are found in the relationship that exist between slope instability and competent geological formations (rocks and consolidated clays) in terrains where the steeper margins of the range of existing slope are represented by competent lithology (Iwahashi *et al.*, 2003; Ayalew *et al.*, 2004). The earthworks in the test site have a slope range of between 11 and 49 with mean slope gradient of 26^o. Slope gradients greater than 49^o are associated with retaining walls, rock gibbons and abutments which by nature are relatively stable. Thus at steeper gradients a reduction in landslide density is expected.

Relatively flat transitional areas between earthwork embankments and cuttings where the various evidences provide weak support to the incidence of slope instability were identified as areas of high degree of unbelief by the EBF model. Locations along the transport corridor where the EBF model evaluated existing evidence as insufficient to conclusively map zones of slope instability were characterised by high uncertainty values. The uncertainty map provides a measure of error (uncertainty) associated with the probability estimate per pixel in the landslide susceptibility map. The uncertainty values obtained were generally low across the corridor (Range = 0 – 0.2; mean = 0.04), a reflection of the degree of appropriateness of the selected landslide susceptibility conditioning factors (Figure 5.27). However the EBF model identified the well vegetated earthwork cuttings situated on the slowly permeable fine silty and clayey soils of the Brickfield 3 soil class west of the corridor as a location that requires additional information to ascertain its relative degree of stability. Generally the uncertainty values obtained for the earthwork infrastructure are higher for earthwork cuttings. This may be due to the nature of the landslide inventory data

used in training the EBF model. The inventory data is comprised of locations of failed slope and extent of work required. The spatial extent recorded for each location was not just the delineated extent of failure but extents recommended for remedial work which generally intrudes slightly into unaffected sections of the slope. The exert failure boundaries at the identified failed slope locations could not be verified during field work as remedial works had already been carried out by the Network Rail. The spatial heterogeneity in terms of land cover and soil type may also have contributed to the relatively higher uncertainty values cuttings in the western end of the corridor. The influence of fine scale microtopography in the localisation of zone of soil moisture accumulation on these cuttings is relatively concealed under a canopy of mature and semi mature trees on the cuttings.

6.4.2 Model validation and comparison

Model validation is an integral part of landslide susceptibility assessment and often carried out to analyse the degree of agreement between the results derived from modelling and the observed data. Landslide susceptibility maps are essentially comprised of information on the presence and absence of landslides within an area of interest. As such, accuracy can be easily assessed by comparison of inventory data with the susceptibility modelling outcome (Chung and Fabbri, 2003). Model predictions is generally tested against: (1) information used to parametrise the EBF model (goodness of fit) and (2) against an independent validation dataset. Model validation against an independent dataset provides insight on the predictive capability of the model. Generally a higher level of model fit is obtained in comparison to its predictive capability. Nonetheless, of the two model properties, the predictive capability is of primary concern, since goodness of fit only explains how well the model fits known landslide distribution used in its parametrisation.

6.4.2.1 Degree of model fitting

The success rate method provided a measure for the goodness of fit of the EBF model prediction to the training data, in addition to detailed description of the model performance with respect to the susceptibility classes. The modified and classic TWI EBF models results were validated against the test data used in parameterising both models (see Section 4.4.2 and 5.5.1). The success rate curve for the modified TWI EBF model (Figure 5.28) indicated that the most susceptible 10% class contains 44% of the landslide area, the most susceptible 20% class contains 86% of the total mapped landslides and the most 30% contains 97% of

the total mapped landslides. Both models suggest that a decision threshold set at 70% (the most susceptible 30%) will explain 97% of the total landslides in the study area. The modified TWI EBF model has an overall goodness of fit of 88.5 %, while the classic TWI EBF model exhibits a slightly better overall goodness of fit of 89%.

A contingency table of the models' misclassification rates showed the classic TWI EBF model as slightly more efficient (by a percent) in correctly classifying slopes that have landslides but less efficient in classifying stable slopes. For example, the classic TWI EBF model at a decision threshold of 70% of ranked landslide susceptibility, correctly classified 97% of landslide pixels (true positives) but could only identify 45% of pixels free of landside incidence (true negative). In contrast, the modified TWI EBF model was shown to have correctly classified 98% of landslide pixels and 43% of stable pixels (Table 5.31 and 5.32). The slight underestimation of the pixels free of landslide incidence by the classic TWI EBF model is attributed to the oversimplification of overland flow associated with the classic TWI computation. Both models exhibit high variability in sensitivity and specificity with increase in cut-off value. At higher specificity most of the earthworks are highlighted as highly susceptible to landslide and as sensitivity is increased a greater proportion of the earthwork is rightly classified. At a cut-off value of 80% most of the false positive cells present in the lower cut-off values were seen to have been classified into the stable terrain class while identifying the most susceptible 20% class which explains 86% of the total mapped landslides on the earthwork infrastructure (Figure 5.29).

This is particularly important as the magnitude of false negatives (earthworks free of landslides mapped as unstable) classification by models reduces the reliability of results. Figures 5.29 and 5.30 suggest an optimum cut-off value of 80% for the classification of stable and unstable terrain within the transport corridor slope. The determination of optimum cut-off value is unique to the purpose of the susceptibility application. The selection in this case was tied to high risk landslide prone sites within the transport corridor. Sites identified as high risk landslide prone areas by site inspectors of Network Rail were highlighted in the Merlin landslide inventory. The susceptibility maps show that at higher specificity the most susceptible sections of the earthworks are clearly highlighted. At a cut-off value of 80% most of the false positive cells present in the lower cut-off values

were seen to have been classified into the stable terrain class and clearly identifying unstable regions on the earthwork cutting (see Figure 5.29).

6.4.2.2 Comparison of model prediction

Testing for model prediction has been a controversial subject amongst researchers as to how best a model's predictive power can be assessed. It's generally agreed that landslide data employed for validation should be either temporal or spatially different from the training set. Some studies have employed the use of areas contiguous to the location where the training data were acquired (Zizioli *et al.*, 2013). The limitation to this approach is that landslides are inherently linked to local factors that can vary even with contiguous locations. Ideally a temporally different validation set presents the most logical approach, however, issues of storm intensity and duration usually for shallow landslides are normally not the same with each storm. Chung and Fabbri (2003) reinforced the use of the temporal validating set for assessing model prediction stating that landslide occurrences are more of exceeding an intricate threshold than of events of exert magnitude. However the use of spatially separate validation set model prediction assessment is the most reported model prediction validation approach in literature (Brenning, 2005; No-Wook, 2010; Tien Bui *et al.*, 2012).

Interpretation of model prediction for detailed scale assessment of landslide susceptibility can be tricky; hence performance indices such as predictive power, efficiency and reliability are usually employed to provide better understanding of the overall model performance (Beguería, 2006; Zizioli *et al.*, 2013). The predictive power of the model is given as a global accuracy generally represented by the AUC value, while model efficiency is taken as the proportion of correctly classified observations (Carrara *et al.*, 2008). Model reliability is the description of errors associated with model predictions. Reliability should reflect all sources uncertainty in relation to inventory compilation and thematic maps on conditioning factors considered in the study (Carrara *et al.*, 2008). The prediction rate curve was used to validate landslide predictions based on the comparison between the susceptibility modelling results and independent (spatial, temporal or random) landslide dataset not employed during the stage of model construction (Chung and Fabbri, 2003; Brenning, 2005).

The predictive capability of the EBF models was assessed against an independent validation set (401 landslide grid cells). The predictive rate curves for the modified TWI and classic TWI EBF landslide susceptibility models showed both models to possess reasonably good prediction capabilities (Figure 5.32). The AUC values of 77.8% for the classic TWI and 77.5% for the modified TWI EBF model suggest almost equal prediction proficiencies for both models. Analysis of the prediction results revealed the modified TWI mode as the slightly more conservative of both models. The prediction rate curve for the modified TWI EBF model (Figure 5.32) indicated that the model could predict 17% of unknown landslide at the most susceptible 10% class of the landslide area. In contrast, the classic EBF model predicted a slightly higher 18% of the most susceptible 10% landslide class. However, an evaluation of the percentage of correctly and incorrectly classified landslides and non-landslide pixels based on varying the decision thresholds indicated a higher percentage of misclassified stable slopes for the classic TWI EBF model. TWI EBF model is seen to be slightly more efficient in correctly classifying unstable slopes that but less efficient in classifying stable slopes (Table 5.33 and 5.34). The result of the t-test for the model predictions on correctly predicted landslide locations showed no significant difference between the two sample means (p value > 0.05). However a significant difference was observed between the sample means for the prediction of stable terrains, as the t-test returned a p value of 0.008 at 95% confidence interval. This implies that the modified TWI EBF model provides a better representation of stable slope locations within the transport corridor at the same landslide susceptibility prediction accuracy as the classic TWI EBF model. Adequate delineation of stable slope will have huge implication on the cost and overall planning process of the obligatory regular appraisal of earthwork stability as required by law in the UK.

The models exhibited equal levels of reliability as shown in the low uncertainty values associated with the model prediction (mean value of 0.04). Both models identified the heavily vegetated earthwork cutting in Haltwhstle (classic TWI = 0.19 and modified TWI = 0.2) as requiring additional information. This section of the corridor actually traverses part of the built area in Haltwhistle and is situated on the slowly permeable fine silty and clayey soils of the Brickfield 3 soil class. Clearly land cover and soil type has a major impact on the stability of earthwork cutting in transport corridor. The well vegetated earthwork

cutting remains relatively stable despite favourable slope gradient and the presence of varying degrees of curvature.

The classification requires a threshold or cut-off value that optimally discriminates between stable locations characterised by susceptibility values lower the cut-off and unstable locations with susceptibility values higher than the cut-off (Brenning, 2005). The optimum threshold value represents a point on the sensitivity and specificity graph that maximises the overall percentage of cases rightly classified. An evaluation of the percentage of correctly and incorrectly classified landslides and non-landslide pixels based on results obtained for the various decision thresholds suggest an optimum threshold value of 80% for the classification of stable and unstable terrain within the transport corridor slope.

However, the choice of an appropriate modelling cut-off value for the effective classification of stable from unstable slopes was govern by one of the objective of the study. The developed methodology is aimed at providing a means for identifying and prioritizing high risk sites for detailed engineering assessment. The results reveal need for a selection of high cut-off value (which in this study was set at 90%) to ensure the effective delineation of landslide locations limiting selection to most susceptible 10% class. These high risk sites are often characterised by low probability of occurrence but with highly impactful consequences and require the most urgent attention. Generally, there is always a competition for funding of maintenance project within the infrastructural network. Maintenance managers are required to prioritise funding of cutting renewal and maintenance programmes. The identification of these high risk sites will assist in ensuring that resource management is directed to key areas where the prospect of slope instability that may result in consequential disruption of traffic or even route closure is more eminent.

6.4.3 Model sensitivity

Having ascertained the capability of the evidential belief model to effectively discriminate between stable and unstable slopes of the earthworks in the transport corridor, the robustness and reliability of the developed models was assessed. The sensitivity of the susceptibility model to variation in the proportion of the training data was assessed. The training dataset was randomly subset into 30%, 40%, 50%, 60%, 80%, 90%. The frequency distribution of the resulting susceptibility models reveal that an increase in the number of training data results in a decrease of the median (50^{th} percentile) and in variability (10th to

90^{th} percentile range). The susceptibility maps exhibited better goodness of fit with less number of training data (mean = 0.83 at 30%) at the expense of model versatility as shown by the presence of outliers (Figure 5.35). The reduction in the model's goodness of fit as a result of increasing number of training data becomes negligible for percentages exceeding 60% of the training data. This suggests that the susceptibility model produced using 60% of the training data does not significantly defer from those produced using higher percentages of training data in terms of the model's goodness of fit. In addition, the above finding indicates the capability of the evidential reasoning model to cope with significant (up to 40%) random variation in the input data (Guzzetti *et al.*, 2006).

The uncertainty values associated with the produced susceptibility maps were characterised by a common trend of decreasing uncertainty with increase in goodness of fit (Figure 5.36). With regards the model's ability to correctly classify landslide prone areas with increasing training data, uncertainty associated with model predictions is seen to increase. The results also suggest that increase in the error associated with the percentage of rightly classified in the susceptibility prediction becomes marginal for percentages of training data exceeding 60%. This finding underscores the proficiency of the evidential reasoning technique as an effective means of discriminating between stable and unstable slopes at an engineering scale slope assessment study. A survey of literature reviews on allocation of 70% of landslide inventory data to susceptibility assessment for most statistical and probabilistic approaches (Ayalew and Yamagishi, 2005; Althuwaynee *et al.*, 2012; Tien Bui *et al.*, 2012; Lee *et al.*, 2013). This finding shows that the evidential reasoning model requires less training sites to achieve results commensurate to statistical models. The need to further investigate this finding using the extensive landslide inventory data is imperative, as the inventory data size used in this study is relatively small to conclude on the finding.

6.5 Summary

The discussions in earlier parts of this chapter covered the results obtained at various stages of the development of the evidential reasoning model for landslide susceptibility assessment of transport corridor slopes. In this section the implication of some of the findings to slope stability analysis in UK transport corridors and contributions to broader susceptibility assessment of transport corridor slopes is discussed.

The use of remotely sensed data in delivery and evaluation of terrain derivatives and land-cover information to slope stability assessment have been largely exploited for regional and catchment scale studies (Fell *et al.*, 2008). The use of remotely sensed geospatial data to detailed scale slope assessment has for some time been limited by resolution (Miller, 2011). To date, landslide susceptibility zonation within the transport corridor has been largely undertaken using geotechnical survey and monitoring approaches. However, increased availability of affordable very high resolution remotely sensed data set along with improved geospatial digital map data-sets, potentially allows the determination of key slope stability variables that are required to recognise vulnerable earthwork slopes (Miller, 2011; Hardy *et al.*, 2012).

In this study, a methodology for an analytical framework that allows for the integration of high resolution geospatial data in an objective manner to recognise slopes potentially susceptible to failure was developed. The methodology provided an effective means of appraising unstable and potentially unstable earthwork locations in transport corridor environments using an evidential reasoning multi-source geospatial integration approach. Evidential reasoning delivers a formal framework for weight allocation and spatial data integration of high resolution datasets normally required for detailed scale landslide susceptibility assessment. Alongside data representation and integration, evidential reasoning represents the degree of uncertainty associated with input geospatial data and developed susceptibility maps. The probabilistic approach is essentially data driven but with flexibility to reflect expert knowledge during the assignment of mass functions to reflect geomorphological realities like non-existence of landslides in flat plains and in areas of complex underlying geology (Park, 2011).

The potential of the evidential reasoning approach to transport corridor applications has been assessed in this study with modelling results illustrating the approach as copiously representing quantitative relationships, landslide occurrences and multiple geospatial data layers. Unlike other spatial data integration models, the evidential belief function model provides a series of mass functions including belief, disbelief, uncertainty and plausibility that allows for a more meaningful interpretation of landslide susceptibility and delineation of zones varying degree of susceptibility. The uncertainty map identifies locations in need of follow up studies and also helps in planning the nature of information required for the

assessment. This is particularly important in the transport corridor environment where actual failure is commonly preceded by signs that are picked up by site engineers during routine site investigation. Recent application of this technique to landslide susceptibility to small and catchment scale study has been reported (Park, 2011; Althuwaynee *et al.*, 2012; Lee *et al.*, 2013). However a survey of literature reveals no mention of the application of the technique at detailed scale as is the case with this study. This study has shown that the approach models parameter uncertainties, exhibits robustness and scales well to large data sets.

The application of ALS data for landslide susceptibility facilitated the creation of high resolution DTM which provides a 2.5D representation of the topography of the transport corridor (Jaboyedoff *et al.*, 2012). Given the densely vegetated nature of U.K. corridors, the ability of ALS to at least partially penetrate the vegetation canopy is crucial (Miller *et al.*, 2012). Equally important is the rapid development in the ALS technology has rendered high resolution point cloud acquisition relatively more affordable, ensuring that data acquisition over sizable spatial extent of transport corridor and adjoining terrain can be periodically captured. In the event of insufficient coverage of the adjoining broader catchment by ALS data, this study showed that the OS Landform DTM provides reasonable resolution for evaluation of catchment contribution to overland flow into the transport corridor. The real challenge with ALS is the cost of data processing and how to store the huge amount of data would be periodically collected, as computers will need to be more powerful to deal with the increasing data acquisition. Furthermore, ongoing development in mobile Lidar systems and its high data acquisition capacity (200 kHz) and holds promise for transport corridor application (Jaboyedoff *et al.*, 2012).

The TWI is frequently used to simulate soil moisture conditions in slope stability assessment. The index only explains the physical significance of terrain on runoff generation based on gravity. The modified TWI model developed in this study is unique in two ways, its takes the strength of both runoff estimation techniques and compensates for their weakness. For example, the modified TWI approach ensures the inclusion of the influence of catchment features, amount of rainfall and the antecedent moisture content of the soil in the estimation of direct runoff generation (a major criticism on the use of traditional TWI) and the downstream propagation of the contribution of the various soil-

land cover combinations to the estimation of runoff generation (a major limitation with the SCS curve number procedure). The modified TWI approach is simple and designed for single storm events. As such the propensity for saturation of transport corridor slopes with varying rainfall intensities can be assessed. The modified TWI grid provided a more realistic spatial distribution of soil moisture and showed that alongside topography the influence of near surface processes such infiltration and evapotranspiration explain the moisture distribution patterns of the transport corridor. Issues concerning the sensitivity of the method to Curve Number (CN) values originally developed the USA and the nonexistence of studies that have extensively reviewed calibration of CNs for UK conditions raises uncertainty with regards its use (O'Connell *et al.*, 2007). A measure of support for the use of the CN approach in the UK, particularly when relative change in runoff values is the main consideration have been provided by Holman *et al.* (2003). The study compared runoff estimates derived using the UK's Flood Estimation Handbook (FEH) methodology which accounted for climate, HOST class and weather with that of the uncalibrated CN method for four catchments that experienced flooding in 2000/2001. The results show similarities in runoff estimates increased rainfall amounts which are of particular interest in slope stability assessment. However, there are other issues that bother on the general CN technique such as fixing the initial abstraction ratio and lack of clear guidance on how to vary Antecedent Moisture Conditions (AMC) which are subjects many current ongoing researches and these areas remain a potential for future studies.

Numeric models are founded on a strong theoretic base and clearly describe the underlying physical processes leading to the instability being modelled when properly calibrated with an accurate landslide inventory. These models are employed for detailed scale slope stability assessment as results obtained are considered a closer representation of reality and more consistent in comparison with those of the heuristic and statistical models. However, concerns of high data demand, challenges with parameterization of heterogeneous variables and extrapolation of results confines these technique to spatially limited high priority sites and are very expensive when considered for detailed scale slope assessment over considerable expanse. The approach develop in this study employs a probabilistic approach to slope stability assessment. The probabilistic framework is simple, flexible and allows for integration of multiple data layers as such it can be extended and applied across broader spatial extent. The methodology provides a means of identifying and prioritising high risk

sites especially for earthwork structures difficult to access as is the case with rural railway networks where difficult terrain makes on site assessments strenuous and in some cases impossible. (Perry et al., 2003b).

7 Conclusions

7.1 Success of research aim and objectives

The aim of the research reported in this thesis was to develop a geospatial model integrating multi-scale multi-temporal data for the broad-scale recognition and prediction of the spatial landslide susceptibility faced by transport corridors. To achieve this aim the following research objectives were addressed:

1. Based on a critical review on the use of Geomatics in analysis and modelling of slope hazards, develop a conceptual framework for the integration of multi-scale multi-source geospatial data for the current and future evaluation of landslide susceptibility zonation and hazard assessment within transport corridor environments.
2. To develop a terrain-based flow model that addresses the effects of catchment-scale contributions, such as run-off, on the moisture concentration of engineered slopes within transport corridor environments.
3. To develop a multi-source, multi-scale approach that is based on evidential reasoning that incorporates the catchment contributions to a linear stretch of transport corridor earthworks and spatially quantify slope stability within transport corridor environments. In addition, the developed model performance is evaluated for a substantive section of a transport corridor.

7.1.1 Objective One

The first research objective was addressed by the review of literature in Chapter 2 and the development of a conceptual framework for the integration of multi-scale multi-temporal geospatial data in Chapter 4. The literature review identified increased moisture content resulting from excessive precipitation as being directly or indirectly responsible for most of the shallow landslides occurrence along transport corridor slopes (Jaiswal and van Westen, 2009; Jaiswal and van Westen, 2012). In the UK, these weather related slope instability occurrences are confined to periods of wet weather, particularly when the rate of transpiration is at its minimum and the effect of pore water pressure is at its peak. At relatively fine spatial scale, surface and near surface processes such as runoff generation, flow accumulation,

infiltration and evapotranspiration are vital to slope stability and are linked to terrain, soil characteristics, geology, hydrology and vegetation.

A conceptual framework pulling together the various processes and parameters identified from literature and during field visits was developed. The framework addressed three key areas: (1) the development of an integrated and scalable spatial geodatabase (addressed in Chapter four) that incorporates information on catchment contributions and the various precondition factors and triggers responsible for landslide incidence on earthwork cuttings and embankments in the study area. A raster-based geospatial database of identified slope stability parameters was constructed in ArcGIS 10.2. Importantly, a merged DTM developed from the high resolution ALS data of the transport corridor and relatively coarser Ordnance Survey Landform DTM data of the broader catchment facilitated the incorporation of catchment contribution to surface and near surface processes such as runoff generation and flow accumulation into the transport corridor earthwork, while retaining the high resolution spatial integrity of earthworks in the transport corridor. Slope stability variables namely slope gradient, aspect, terrain wetness index (TWI), stream power index (SPI) and profile curvature were derived from the merged DTM data (Sections 4.3.1 and 4.3.3).

A merged Land cover/land use map of the study area derived from land cover information on the transport corridor obtained from the Compact Airborne Spectrographic Imager (CASI) imagery (Section 4.3.2) and LCM 2007 dataset of the broader catchment provided the basis for the evaluation of the contribution of land cover to runoff generation, flow accumulation and evapotranspiration. Information on the underlying soils was extracted from the NATMAP vector data (Section 3.4.3). Additional information on distance to drainage was considered due to proximity to the South Tyne River of sections of the transport corridor. A shapefile of existing streams was extracted from the 1:2500 Ordnance Survey vector mapping dataset and a raster of distances from the drainage network was created. Landslide inventory prepared by Network Rail presented locations of recorded slope failures along the transport corridor and frequently maintained subsidence related areas along the rail route. These locations were acquired from Network Rail routine maintenance reports and Merlin dataset. The Merlin dataset identified eight locations on earthwork embankment and cuttings on the 8 kilometre-long test site at Haltwhistle where the research was implemented. (2) The development of a runoff model that integrates the upslope contribution of the adjoining

broader catchment to zones of moisture accumulation around earthwork cuttings and embankment within the corridor. The model incorporates the influence of infiltration, interception and modulation of overland flow due to variation in land cover type in the prediction of the spatial variability of soil moisture accumulation. This enables a more realistic prediction of the spatial variability of soil moisture accumulation reflecting contributions from adjoining catchment on a linear feature (earthwork embankment and cutting). (3) The development of a methodology for assessing the impact and influence of identified precondition factors and triggers in (1) on what is a complex system (landslide susceptibility). A formal framework for representing the contributions of the preceding two stages to landslide incidence and efficient integration of multi-source, multi scale geospatial data sets in mapping slope instability within transport corridor environment was achieved using the evidential reasoning approach.

7.1.2 Objective two

Objective two was addressed in Chapter 4 with the development of a novel approach for the characterisation of soil moisture distribution for the transport corridor which incorporates the effects of multi-scale catchment contribution to local zones of moisture concentration in earthworks. Unlike the classic TWI , the developed technique does not assume homogeneity of soil types and lack of vegetation cover (Barling *et al.*, 1994). Using the The SCS curve number procedure, the land cover information obtained from a merged land cover map of the transport corridor and adjoining fields and soil map of the wider catchment, an estimate of the spatial contribution of precipitation contributing to surface runoff was obtained. The developed weight grid was used to parameterise a weighted terrain accumulation flow model. The modified TWI technique, thus, enables the local evaluation of the contributions emanating from the wider catchment flow field and the local input variables at each grid cell location (Section 4.4.1.3). The predicted soil moisture pattern was consistent with the general patterns reported in various studies (Tenenbaum *et al.*, 2006; Sørensen and Seibert, 2007; Hardy *et al.*, 2012), with moisture accumulation confined to zones of flow convergence (in concave and low gradient areas) and an increased propensity for runoff generation in steep convex terrains. However, results of generated runoff estimations were seen to provide a more realistic representation of soil moisture estimation (Section 5.4), as lower soil moisture content were recorded for woodlands in contrast with other land cover types (Greenwood *et al.*, 2004). Permeable well drained soils were relatively drier and associated with lower

degrees of surface runoff as a result of infiltration (Bothma *et al.*, 2012). The modified TWI grid also identified zones of considerable ingress of flow into transport corridor earthworks from adjoining upland agricultural areas (Section 5.4.2). The developed modified TWI approach provides a surrogate means for soil moisture characterisation through remotely sensed data that takes into consideration the lumped effects of surface and near surface processes such as flow accumulation, infiltration and evapotranspiration.

7.1.3 Objective three

Deterministic models are generally considered as best suited for analysis of site specific slope studies with the quantitative information derived from these models directly applicable in the design of engineering works or in the quantification of risk (Van Westen *et al.*, 2006). Established on a strong theoretic base these models clearly describe the underlying physical processes leading to the slope instability with results obtained considered as a close representation of reality. However, concerns of high data demand, challenges with parameterization of heterogeneous variables and extrapolation of results render the technique very expensive when considered for studies that require detailed scale assessment of slope stability over considerable spatial expanse.

In this study, a probabilistic framework that considered parameter variability and the associated uncertainties (Van Westen *et al.*, 2008) in what is a complex system (landslides) was utilised. An evidential reasoning approach was employed in the multi-source geospatial data integration and quantitative evaluation of slope instability. The technique derived objective weights of the relative importance of each derived property to the final estimation of landslide susceptibility (Section 5.5), while providing a measure of the uncertainty of the properties to be taken into account (Carranza and Hale, 2003). In chapter 4, the evidential reasoning approach was shown to provide an efficient framework for the integration of multi-source multi-scale geospatial data. Eight slope stability variables extracted from topographic, soil and land use properties of the transport corridor were integrated within the evidential reasoning framework to characterise numeric measures of the belief, disbelief and uncertainty as to the existence of slope instability spatially within the transport corridor. The measure of computed belief based on the integration of the available evidence was in turn used for the broad-scale recognition and prediction of the spatial landslide susceptibility on earthworks of the Haltwhistle section of the Carlisle–Newcastle transport corridor.

The modified TWI evidential belief function model was implemented on an eight kilometre stretch of transport corridor slope at Haltwhistle, UK. The developed model had a goodness of fit of 88.5% with respect to the failed slopes used to parameterise the evidential reasoning model and an overall predictive capability of 77.75% based on independent validation dataset.

In summary, all the objectives of the research were successfully achieved. The result is a methodology that provides an efficient multi-source multi-scale approach to the quantitative evaluation of slope instability within transport corridor environments. Limitations remain with respect to the nature and size of the landslide inventory used and need for extensive calibration of CNs to better reflect UK conditions.

7.2 Research outcome

This research has successfully demonstrated the use of an evidential reasoning approach for the detailed assessment of slope stability in transport corridor environments. Using multi-source multi-scale geospatial data combined with a novel approach to the characterisation of soil moisture distribution, this work presents the first application of evidential reasoning to the detailed scale recognition of vulnerable earthwork slopes in transport corridor environments. High resolution ALS and CASI data were shown to provide adequate resolution for transport corridor slope stability analysis. DTM resolutions of between 0.5 to 5 m can provide suitable representations of transport corridor landforms with the choice of optimum resolution being a trade-off between adequate representations of transport corridor landform, drainage features and processing time. The developed methodology can be applied across broader spatial extents and in other transport corridors across the UK. The scalability of the model allows for periodic updates of temporal topographic, vegetation and landslide inventory data of the transport corridor, with the potential to improve the overall predictive performance of the model (Van Westen *et al.*, 2008). The developed methodology is particularly important as it allows for the estimation of slope instability predictions under extreme rainfall conditions. As increased duration and intensity of rainfall are expected under future climatic conditions in response to global climatic change (Ekström *et al.*, 2005) and prolong rainfall has been identified as the main trigger of many recent failures occurring across UK earthwork infrastructure (Ridley *et al.*, 2004; Miller *et al.*, 2012).

The model identifies surface processes (infiltration and surface runoff), topographic (gradient, soil properties and curvature) and land use properties (vegetation cover type) as having of a considerable influence on the vulnerability of earthworks to failure. This is revealed by high belief values associated with (1) earthwork cuttings on permeable and largely well drained soil formations with intercalations of clay materials, (2) presence of fine scale concave curvature responsible for localised soil moisture concentration mid-slope on earthwork cuttings and (3) points ingresses of surface moisture into earthwork cuttings and embankments. The influence of land cover type on slope behaviour was also captured, as heavily vegetated permeable earthwork cuttings west of the corridor were identified as relatively stable though with a corresponding high uncertainty (0.2), in contrast with the permeable relatively unstable sparsely vegetated earthwork cuttings east of the corridor. Permeable soils with variable intercalations accounted for over 80% of slope instability, with 5.1% of the earthwork cuttings identified as relatively unstable in contrast to 47.5% for the earthwork embankment. The modified TWI evidential belief function model is robust and provides a practical means for diagnosing slope instability and prioritising routine field inspection of vulnerable earthworks in transport corridor environments.

7.3 Beneficiaries and future work

The infrastructure management bodies of transport corridors will find the developed model insightful with respect to routine conditional appraisal of earthworks and long term strategic planning of earthwork sustainability. The developed methodology would assist in recognising and ranking spatially distributed high risk landslide prone sites within transport corridors. This in turn would potentially result in a cost effective allocation of scare resources, a reduction in the temporal frequency of routine site inspection and an increase in overall efficiency and manpower saving. The approach is simple, scalable and can be periodically updated to include new failure locations and additional causal factors not considered in earlier assessments.

The novel modified TWI approach to the characterisation of runoff generation and soil moisture distribution could potentially be applied in improving runoff estimation for Catchment Flood Management Plans (CFMPs) (Environment Agency, 2009). The UK's Flood Estimation Handbook (FEH) methodology (Reed, 1999; Hess *et al.*, 2010) currently employs the SCS CN method for runoff estimation. Runoff estimation derived using SCS

CN approach fails to incorporate in the contributions of broader catchment (Soulis and Valiantzas, 2012), but stimulates runoff generation based on interactions between land cover, soil-field conditions, weather and land management practice (Hess *et al.*, 2010). The modified TWI approach provides a potentially better runoff estimation.

7.4 Future research

The results in this study have indicated a number of directions for future research. A summary of these key areas are presented below.

- Given the limitations associated with the SCS CN approach, the need to investigate a means of calibrating the CNs values to reflect UK conditions is an important area of concern. Alternative approaches based on the modification of two indications of catchment hydrological response have been proposed by Packman *et al.* (2004). The use of base flow index and standard percentage runoff linked to the HOST classes holds great promise, but requires knowledge on the spatial influence of land cover (Hess *et al.*, 2010).
- The modified TWI evidential belief function model was characterised by a high rate of false positives as a result of the nature of landslide inventory employed in parameterization of the model. The inclusion of the substantial stable regions within the delineated failure boundaries was responsible for this occurrence. The need to develop a new system for mapping and recording the spatial boundaries of failure extent in the field prior to the remedial works is therefore imperative as the current Merlin database is deemed inadequate. Future work in partnership with Network Rail will consider improving the reliability of generated landslide inventory.
- Results of a preliminary assessment of the predictive capability of the developed methodology on adjoining highway cuttings and embankments have demonstrated a high proficiency in identifying landslide locations not included in the model parameterization. Future study will investigate the accuracy of predicted slope instability on the adjoining highway cutting and embankments in order to assess the broader applicability of the methods employed and developed in this research.
- Future studies will investigate ways on how the model could be extended in areas such as the inclusion of more qualitative information and considerations on obtaining better sets of weights for the evidential reasoning model through the incorporation of artificial intelligence such as generic algorithm and artificial neural networks.

- The results from this study show the developed model as an efficient means of recognizing and predicting slope instability in transport corridors. The approach is simple and a decision support tool can be developed by coding the entire process in python. With rainfall amount as the only input data required, the support tool would automatically identify high priority landslide risk sites, providing the needed information required for planning of routine site investigation and prioritizing of earthwork failure hazards

7.5 Conclusion

Detailed scale landslide susceptibility assessment had been largely restricted to process based models with high data demand and findings largely site specific, thus, imposing limitation on the validity of interpolating results over wider extents. In this study, a probabilistic data driven approach was developed using evidential reasoning as an efficient analytical framework for integrating multi source, multi scale geospatial data for the recognition of slopes potentially susceptible to failure. The novelty here is that evidential reasoning approach has not been reported applied at this scale of slope stability assessment. In addition, a novel approach to characterisation of soil moisture distribution was also developed. Land cover and soil type of the wider catchment were used to estimate the spatial contribution of precipitation to surface runoff, which in turn is used to parameterise a weighted terrain accumulation flow model. The technique developed essentially used geospatial information on soil and land cover unlike the earlier quasi and full dynamic wetness indices techniques that require information on physical geotechnical properties of soils, thus retracting from the original advantage of soil moisture characterisation by remotely sensed data through the use of surrogates.

The evidential reasoning approach to localisation of zones of slope instability can be easily developed into a decision support tool for automated recognition of recognise vulnerable earthwork slopes and applied over broader spatial extents.

References

Abramson, L.W. (2002) *Slope Stability and Stabilization Methods*. Wiley.

Acevedo, P. and Real, R. (2012) 'Favourability: concept, distinctive characteristics and potential usefulness', *Naturwissenschaften*, 99(7), pp. 515-522.

Aguilar, F.J., Agüera, F., Aguilar, M.A. and Carvajal, F. (2005) 'Effects of terrain morphology, sampling density, and interpolation methods on grid DEM accuracy', *Photogrammetric Engineering and Remote Sensing*, 71(7), pp. 805-816.

Akgun, A., Dag, S. and Bulut, F. (2008) 'Landslide susceptibility mapping for a landslide-prone area (Findikli, NE of Turkey) by likelihood-frequency ratio and weighted linear combination models', *Environmental Geology*, 54(6), pp. 1127-1143.

Aleotti, P. and Chowdhury, R. (1999) 'Landslide hazard assessment: summary review and new perspectives', *Bulletin of Engineering Geology and the Environment*, 58(1), pp. 21-44.

Althuwaynee, O.F., Pradhan, B. and Lee, S. (2012) 'Application of an evidential belief function model in landslide susceptibility mapping', *Computers and Geosciences*, 44, pp. 120-135.

Anderson, E.S., Thompson, J.A. and Austin, R.E. (2005) 'LIDAR density and linear interpolator effects on elevation estimates', *International Journal of Remote Sensing*, 26(18), pp. 3889-3900.

Anderson, M.G. and Kneale, P.E. (1980) 'Pore water pressure and stability conditions on a motorway embankment', *Earth Surface Processes*, 5(1), pp. 37-46.

Archer, N.A.L., Bonell, M., Coles, N., MacDonald, A.M., Auton, C.A. and Stevenson, R. (2013) 'Soil characteristics and landcover relationships on soil hydraulic conductivity at a hillslope scale: A view towards local flood management', *Journal of Hydrology*, 497, pp. 208-222.

Avery, B.W. (1980) *Soil Classification for England and Wales (Higher Categories)*. Soil Survey Technical.

Ayalew, L. and Yamagishi, H. (2005) 'The application of GIS-based logistic regression for landslide susceptibility mapping in the Kakuda-Yahiko Mountains, Central Japan', *Geomorphology*, 65(1-2), pp. 15-31.

Ayalew, L., Yamagishi, H. and Ugawa, N. (2004) 'Landslide susceptibility mapping using GIS-based weighted linear combination, the case in Tsugawa area of Agano River, Niigata Prefecture, Japan', *Landslides*, 1, pp. 73–81.

Baghdadi, N., Cavelier, S., Chiles, J.P., Bourgine, B., Toutin, T., King, C., Daniels, P., Perrin, J. and Truffert, C. (2005) 'Merging of airborne elevation data and radarsat data to develop a Digital Elevation Model', *International Journal of Remote Sensing*, 26(1), pp. 141-166.

Bajwa, S.G., Bajcsy, P., Groves, P. and Tian, L.F. (2004) 'Hyperspectral image data mining for band selection in agricultural applications', *Transactions of the American Society of Agricultural Engineers*, 47(3), pp. 895-907.

Bannari, A., Morin, D., Bonn, F. and Huete, A.R. (1995) 'A review of vegetation indices', *Remote Sensing Reviews*, 13(1-2), pp. 95-120.

Barla, G., Amici, R., Vai, L. and Vanni, A. (2004) 'Investigation, monitoring and modelling of a landslide in porphyry in a public safety perspective', in Lacerda, W., Ehrlich, M., Fontoura, S.A.B. and Sayao, A.S. (eds.) *Landslides: evaluation and stabilization. Ninth international symposium on landslides*. Leiden: A.A. Balkema Publishers, pp. 623–628.

Barling, R.D., Moore, I.D. and Grayson, R.B. (1994) 'A quasi-dynamic wetness index for characterizing the spatial distribution of zones of surface saturation and soil water content', *Water Resources Research*, 30(4), pp. 1029-1044.

Barnes, G.E. (2010) *Soil Mechanics: Principles and Practice*. Palgrave Macmillan.

Barredo, J.I., Benavides, A., Hervás, J. and Van Westen, C.J. (2000) 'Comparing heuristic landslide hazard assessment techniques using GIS in the Tirajana basin, Gran Canaria Island, Spain', *International Journal of Applied Earth Observation and Geoinformation*, 2000(1), pp. 9-23.

Bater, C.W. and Coops, N.C. (2009) 'Evaluating error associated with lidar-derived DEM interpolation', *Computers and Geosciences*, 35(2), pp. 289-300.

Bathurst, J.C., Burton, A., Clarke, B.G. and Gallart, F. (2006) 'Application of the SHETRAN basin-scale, landslide sediment yield model to the Llobregat basin, Spanish Pyrenees', *Hydrological Processes*, 20(14), pp. 3119-3138.

Baum, R.L., Coe, J.A., Godt, J.W., Harp, E.L., Reid, M.E., Savage, W.Z., Schulz, W.H., Brien, D.L., Chleborad, A.F., McKenna, J.P. and Michael, J.A. (2005) 'Regional landslide-hazard assessment for Seattle, Washington, USA', *Landslides*, 2(4), pp. 266-279.

Beguería, S. (2006) 'Validation and Evaluation of Predictive Models in Hazard Assessment and Risk Management', *Natural Hazards*, 37(3), pp. 315-329.

Berardi, R., Mercurio, G., Bartolini, P. and Cordano, E. (2005) 'Dynamics of saturation phenomena and landslide triggering by rain infiltration in a slope', *International conference on landslide risk management*. Taylor & Francis Ltd.,Vancouver, pp. 212–219.

Berman, M., Phatak, A. and Traylen, A. (2012) 'Some invariance properties of the minimum noise fraction transform', *Chemometrics and Intelligent Laboratory Systems*, 117, pp. 189-199.

Beven, K.J. (2000) *Rainfall-runoff modelling : the primer*. New York: John Wiley.

Beven, K.J. and Kirkby, M.J. (1979) 'A physically based, variable contributing area model of basin hydrology / Un modèle à base physique de zone d'appel variable de l'hydrologie du bassin versant', *Hydrological Sciences Bulletin*, 24(1), pp. 43-69.

Binaghi, E., Luzi, L., Madella, P., Pergalani, F. and Rampini, A. (1998) 'Slope Instability Zonation: a Comparison Between Certainty Factor and Fuzzy Dempster–Shafer Approaches', *Natural Hazards*, 17(1), pp. 77-97.

Birkinshaw, S.J., James, P. and Ewen, J. (2010) 'Graphical user interface for rapid set-up of SHETRAN physically-based river catchment model', *Environmental Modelling & Software*, 25(4), pp. 609-610.

Bobach, T., Farin, G., Hansford, D. and Umlauf, G. (2009) 'Natural neighbor extrapolation using ghost points', *CAD Computer Aided Design*, 41(5), pp. 350-365.

Bonham-Carter, G. (1994) *Geographic Information Systems for Geoscientists: Modelling with GIS*. Pergamon.

Boorman, D.B., Hollis, J.M. and Lilly, A. (1995) *Hydrology of Soil Types: a hydrologically-based classification of soils of the United Kingdom*. Wallingford, Oxfordshire.

Borga, M., Dalla Fontana, G. and Cazorzi, F. (2002) 'Analysis of topographic and climatic control on rainfall-triggered shallow landsliding using a quasi-dynamic wetness index', *Journal of Hydrology*, 268(1-4), pp. 56-71.

Borgatti, L., Corsini, A., Barbieri, M., Sartini, G., Truffelli, G., Caputo, G. and Puglisi, C. (2006) 'Large reactivated landslides in weak rock masses: A case study from the Northern Apennines (Italy)', *Landslides*, 3(2), pp. 115-124.

Bothma, C.B., van Rensburg, L.D. and le Roux, P.A.L. (2012) 'Rainfall intensity and soil physical properties influence on infiltration and runoff under in-field rainwater harvesting conditions', *Irrigation and Drainage*, 61(SUPPL.2), pp. 41-49.

Bott, M.P.H. (1987) 'Subsidence mechanisms of Carboniferous Basins of Northern England', in Miller, J., Adams, E.A. and Wright, V.P. (eds.) *European Dinantian Environments*. Chichester: John Wiley and Sons, pp. 21-32.

Bovolo, C.I. and Bathurst, J.C. (2012) 'Modelling catchment-scale shallow landslide occurrence and sediment yield as a function of rainfall return period', *Hydrological Processes*, 26(4), pp. 579-596.

Breiman, L., Friedmann, J.H., Ohlsen, R.A. and Stone, C.J. (1984) *Classification and regression tree*. 2nd edn. USA: Chapman and Hall /CRC.

Brenning, A. (2005) 'Spatial prediction models for landslide hazards: Review, comparison and evaluation', *Natural Hazards and Earth System Science*, 5(6), pp. 853-862.

Brenning, A. (2008) 'Statistical geocomputing combining R and SAGA: The example of landslide susceptibility analysis with generalized additive models', *Hamburger Beiträge zur Physischen Geographie und Landschaftsökologie*, 19 pp. 23-32.

Briggs, K.M., Smethurst, J.A., Powrie, W. and O'Brien, A.S. (2013) 'Wet winter pore pressures in railway embankments', *Proceedings of the Institution of Civil Engineers: Geotechnical Engineering*, 166(5), pp. 451-465.

Brovelli, M.A. and Lucca, S. (2012) 'Comparison of GRASS-LiDAR modules-TerraScan with respect to vegetation filtering', *Applied Geomatics*, 4(2), pp. 123-134.

Brown, K.M., Duncan, H., O'Dwyer, C., Davison, B., Hogarth, P., Butler, D. and Sampson, E. (2003) 'Geometric calibration of CASI imagery', *Remote Sensing and Photogrammetry Society Annual General meeting*. Nottingham, UK, September 2003. pp. 11 - 12.

Buddhima, I., Wadud, S. and Cholachar, R. (2011) *Advance Rail Geotechnology- Ballasted track*. CRC Press.

Burrough, P.A. and McDonnell, R.A. (1998) *Principles of Geographical Information Systems*. New York: Oxford University Press.

Butler, D. (2011) *Urban drainage*. 3rd edn. New York: Spon Press.

Caine, N. (1980) 'The Rainfall Intensity: Duration Control of Shallow Landslides and Debris Flows', *Geografiska Annaler. Series A, Physical Geography*, 62(1/2), pp. 23-27.

Cardinali, M., Reichenbach, P., Guzzetti, F., Ardizzone, F., Antonini, G., Galli, M., Cacciano, M., Castellani, M. and Salvati, P. (2002) 'A geomorphological approach to the estimation of landslide hazards and risks in Umbria, Central Italy', *Nat. Hazards Earth Syst. Sci.*, 2(1/2), pp. 57-72.

Carpentier, S., Konz, M., Fischer, R., Anagnostopoulos, G., Meusburger, K. and Schoeck, K. (2012) 'Geophysical imaging of shallow subsurface topography and its implication for shallow landslide susceptibility in the Urseren Valley, Switzerland', *Journal of Applied Geophysics*, 83, pp. 46-56.

Carranza, E., Owusu, E. and Hale, M. (2009) 'Mapping of prospectivity and estimation of number of undiscovered prospects for lode gold, southwestern Ashanti Belt, Ghana', *Mineralium Deposita*, 44(8), pp. 915-938.

Carranza, E.J.M. and Hale, M. (2003) 'Evidential belief functions for data-driven geologically constrained mapping of gold potential, Baguio district, Philippines', *Ore Geology Reviews*, 22(1–2), pp. 117-132.

Carranza, E.J.M., Woldai, T. and Chikambwe, E.M. (2005) 'Application of data-driven evidential belief functions to prospectivity mapping for aquamarine-bearing pegmatites, Lundazi district, Zambia', *Nat Resour Res*, 14, pp. 14–63.

Carrara, A. (1983) 'Multivariate models for landslide hazard evaluation', *Journal of the International Association for Mathematical Geology*, 15(3), pp. 403-426.

Carrara, A., Cardinali, M., Detti, R., Guzzetti, F., Pasqui, V. and Reichenbach, P. (1991) 'GIS techniques and statistical models in evaluating landslide hazard', *Earth Surface Processes and Landforms*, 16(5), pp. 427-445.

Carrara, A., Crosta, G. and Frattini, P. (2008) 'Comparing models of debris-flow susceptibility in the alpine environment', *Geomorphology*, 94(3-4), pp. 353-378.

Carrara, A., Guzzetti, F., Cardinali, M. and Reichenbach, P. (1999) 'Use of GIS Technology in the Prediction and Monitoring of Landslide Hazard', *Natural Hazards*, 20(2-3), pp. 117-135.

Casadei, M., Dietrich, W.E. and Miller, N.L. (2003) 'Testing a model for predicting the timing and location of shallow landslide initiation in soil-mantled landscapes', *Earth Surface Processes and Landforms*, 28(9), pp. 925-950.

Cascini, L. (2008) 'Applicability of landslide susceptibility and hazard zoning at different scales', *Engineering Geology*, 102(3–4), pp. 164-177.

Castellanos Abella, E.A. and Van Westen, C.J. (2008) 'Qualitative landslide susceptibility assessment by multicriteria analysis: A case study from San Antonio del Sur, Guantánamo, Cuba', *Geomorphology*, 94(3–4), pp. 453-466.

Catani, F., Lagomarsino, D., Segoni, S. and Tofani, V. (2013) 'Landslide susceptibility estimation by random forests technique: sensitivity and scaling issues', *Nat. Hazards Earth Syst. Sci.*, 13(11), pp. 2815-2831

Cen, H., Lu, R., Ariana, D.P. and Mendoza, F. (2013) 'Hyperspectral imaging-based classification and wavebands selection for internal defect detection of pickling cucumbers', *American Society of Agricultural and Biological Engineers Annual International Meeting 2013*. Kansas City, MO; United States. pp. 5187-5201. Available at: http://www.scopus.com/inward/record.url?eid=2-s2.0-84881641852&partnerID=40&md5=56db13c24710d424f92c866ea65abd4d (Accessed: 11/12/2013).

Çevik, E. and Topal, T. (2003) 'GIS-based landslide susceptibility mapping for a problematic segment of the natural gas pipeline, Hendek (Turkey)', *Environmental Geology*, 44(8), pp. 949-962.

Chang, H. and Kim, N. (2004) 'The evaluation and the sensitivity analysis of GIS-based landslide susceptibility models', *Geosciences Journal*, 8(4), pp. 415-423.

Chaplow, R. (1983) 'Engineering geomorphological investigations of a possible landslide, Killiecrankie Pass, Scotland', *Quarterly Journal of Engineering Geology*, 16(4), pp. 301-308.

Chauhan, S., Sharma, M., Arora, M.K. and Gupta, N.K. (2010) 'Landslide susceptibility zonation through ratings derived from artificial neural network', *International Journal of Applied Earth Observation and Geoinformation*, 12(5), pp. 340-350.

Chen, C. and Li, Y. (2012) 'A robust method of thin plate spline and its application to DEM construction', *Computers and Geosciences*, 48, pp. 9-16.

Chen, H., Dadson, S. and Chi, Y.-G. (2006) 'Recent rainfall-induced landslides and debris flow in northern Taiwan', *Geomorphology*, 77(1–2), pp. 112-125.

Chen, Y., Wilson, J.P., Zhu, Q. and Zhou, Q. (2012) 'Comparison of drainage-constrained methods for DEM generalization', *Computers and Geosciences*, 48, pp. 41-49.

Childs, C. (2004) 'Interpolation surfaces in ArcGIS spatial analyst', *ArcUser July-September*, pp. 32-35.

Cho, S.E. (2014) 'Probabilistic stability analysis of rainfall-induced landslides considering spatial variability of permeability', *Engineering Geology*, 171, pp. 11-20.

Cho, S.E. and Lee, S.R. (2001) 'Instability of unsaturated soil slopes due to infiltration', *Computers and Geotechnics*, 28(3), pp. 185-208.

Chowdhury, R.N. and Xu, D.W. (1995) 'Geotechnical system reliability of slopes', *Reliability Engineering & System Safety*, 47(3), pp. 141-151.

Chowdhury, R.N. and Zhang, S. (1993) 'Modelling the risk of progressive slope failure: A new approach', *Reliability Engineering & System Safety*, 40(1), pp. 17-30.

Chung, C.-J. and Fabbri, A. (1993) 'The representation of geoscience information for data integration', *Natural Resources Research*, 2(2), pp. 122-139.

Chung, C.-J. and Fabbri, A. (2003) 'Validation of Spatial Prediction Models for Landslide Hazard Mapping', *Natural Hazards*, 30(3), pp. 451-472.

Chung, C.J.F. and Fabbri, A.G. (1999) 'Probabilistic prediction models for landslide hazard mapping', *Photogrammetric Engineering and Remote Sensing*, 65(12), pp. 1389-1399.

Cipar, J., Cooley, T., Lockwood, R. and Grigsby, P. (2004) 'Distinguishing between coniferous and deciduous forests using hyperspectral imagery', *Geoscience and Remote Sensing Symposium, 2004. IGARSS '04. Proceedings. 2004 IEEE International*. 20-24 Sept. 2004. pp. 2348-2351 vol.4.

Clarke, D. and Smethurst, J.A. (2010) 'Effects of climate change on cycles of wetting and drying in engineered clay slopes in England', *Quarterly Journal of Engineering Geology and Hydrogeology*, 43(4), pp. 473-486.

Collins, B.D. and Znidarcic, D. (2004) 'Stability analyses of rainfall induced landslides', *Journal of Geotechnical and Geoenvironmental Engineering*, 130(4), pp. 362-372.

Congalton, R.G. (1991) 'A review of assessing the accuracy of classifications of remotely sensed data', *Remote Sensing of Environment*, 37(1), pp. 35-46.

Conte, O.A. and Coffman, R.A. (2013) *Geotechnical Special Publication*. Available at: http://www.scopus.com/inward/record.url?eid=2-s2.0-84887489143&partnerID=40&md5=5a36b66e24c8918101528ad0845a4a8d.

Costa-Cabral, M.C. and Burges, S.J. (1994) 'Digital elevation model networks (DEMON): a model of flow over hillslopes for computation of contributing and dispersal areas', *Water Resources Research*, 30(6), pp. 1681-1692.

Cranfield University (2014) *The Soils Guide.* Available at: www.landis.org.uk. (Accessed: Accessed 02/02/2014).

Crapper, M., Fell, M. and Gammoh, I. (2015) 'Earthworks risk assessment on a heritage railway', *Proceedings of the Institution of Civil Engineers: Geotechnical Engineering*, 167(4), pp. 344-356.

Crosta, G. (1998) 'Regionalization of rainfall thresholds: an aid to landslide hazard evaluation', *Environmental Geology*, 35(2-3), pp. 131-145.

Crozier, M.J., Deimel, M.S. and Simon, J.S. (1995) 'Investigation of earthquake triggering for deep-seated landslides, Taranaki, New-Zealand', *Quaternary International*, 25, pp. 65-73.

Crozier, M.J. and Glade, T. (2005) 'Landslide hazard and risk: issues, concepts, and approach', in Glade, T., Anderson, M.G. and Crozier, M.J. (eds.) *Landslide hazard and risk*. New York: Wiley, pp. 1–40.

Dai, F.C. and Lee, C.F. (2002) 'Landslide characteristics and slope instability modeling using GIS, Lantau Island, Hong Kong', *Geomorphology*, 42(3-4), pp. 213-228.

Dai, F.C. and Lee, C.F. (2003) 'A spatiotemporal probabilistic modelling of storm-induced shallow landsliding using aerial photographs and logistic regression', *Earth Surface Processes and Landforms*, 28(5), pp. 527-545.

Dai, F.C., Lee, C.F. and Ngai, Y.Y. (2002) 'Landslide risk assessment and management: an overview', *Engineering Geology*, 64(1), pp. 65-87.

Das, I., Stein, A., Kerle, N. and Dadhwal, V.K. (2011) 'Probabilistic landslide hazard assessment using homogeneous susceptible units (HSU) along a national highway corridor in the northern Himalayas, India', *Landslides*, 8(3), pp. 293-308.

De Vita, P., Agrello, D. and Ambrosino, F. (2006) 'Landslide susceptibility assessment in ash-fall pyroclastic deposits surrounding Mount Somma-Vesuvius: Application of geophysical surveys for soil thickness mapping', *Journal of Applied Geophysics*, 59(2), pp. 126-139.

Dempster, A.P. (1967) 'Upper and lower probabilities induced by a multivalued mapping.', *Ann Math Stat*, 28, pp. 325–339.

Dempster, A.P. (1968) 'A Generalization of Bayesian Inference', *Journal of the Royal Statistical Society. Series B (Methodological)*, 30(2), pp. 205-247.

Dietrich, W.E., Bellugi, D. and de Asua, R.R. (2001) 'Validation of the shallow landslide model, SHALSTAB, for forest management', in Wigmosta, M.S. and Burges, S.J. (eds.) *Land Use and Watersheds: Human Influence on Hydrology and Geomorphology in Urban and Forest Areas*. pp. 195-227.

Drakatos, G., Paradissis, D., Anastasiou, D., Elias, P., Marinou, A., Chousianitis, K., Papanikolaou, X., Zacharis, E., Argyrakis, P., Papazissi, K. and Makropoulos, K. (2013)

'Joint approach using satellite techniques for slope instability detection and monitoring', *International Journal of Remote Sensing*, 34(6), pp. 1879-1892.

Eberhardt, E. (2003) *Rock slope stability analysis - Utilization of advanced numerical techniques*. Vancouver: University of British Columbia Press.

Einstein, H.H. (1988) 'Landslide risk assessment procedure', *Proceedings of the fifth international symposium on landslides* pp. 1075-1090.

Ekström, M., Fowler, H.J., Kilsby, C.G. and Jones, P.D. (2005) 'New estimates of future changes in extreme rainfall across the UK using regional climate model integrations. 2. Future estimates and use in impact studies', *Journal of Hydrology*, 300(1–4), pp. 234-251.

Elith, J., Leathwick, J.R. and Hastie, T. (2008) 'A working guide to boosted regression trees', *Journal of Animal Ecology*, 77(4), pp. 802-813.

Endreny, T.A. and Wood, E.F. (2003) 'Maximizing spatial congruence of observed and DEM-delineated overland flow networks', *International Journal of Geographical Information Science*, 17(7), pp. 699-713.

Environment Agency (2009) *Catchment flood management plans*. [Online]. Available at: https://www.gov.uk/government/collections/catchment-flood-management-plans.

Ercanoglu, M. and Gokceoglu, C. (2002) 'Assessment of landslide susceptibility for a landslide-prone area (north of Yenice, NW Turkey) by fuzzy approach', *Environmental Geology*, 41(6), pp. 720-730.

Ercanoglu, M. and Gokceoglu, C. (2004) 'Use of fuzzy relations to produce landslide susceptibility map of a landslide prone area (West Black Sea Region, Turkey)', *Engineering Geology*, 75(3-4), pp. 229-250.

ERDAS (2008) 'Field guide', p. 370.

ERSRI (2010) 'ArcGIS Desktop help', *Available at: http://webhelp.esri.com*, Acessed 01-02-2013.

Favis-Morlock, D. and De Boer, D. (2003) 'Simple at heart? Landscape as a self-organizing complex system', in Trudgill, S. and Roy, A. (eds.) *Contemporary meanings in physical geography. Oxford University Press, USA, p. 127–172*. USA: Oxford University Press, pp. 127–172.

Feizizadeh, B. and Blaschke, T. (2013) 'GIS-multicriteria decision analysis for landslide susceptibility mapping: Comparing three methods for the Urmia lake basin, Iran', *Natural Hazards*, 65(3), pp. 2105-2128.

Felicísimo, Á., Cuartero, A., Remondo, J. and Quirós, E. (2012) 'Mapping landslide susceptibility with logistic regression, multiple adaptive regression splines, classification and regression trees, and maximum entropy methods: a comparative study', *Landslides*, 10(2), pp. 1-15.

Fell, R., Corominas, J., Bonnard, C., Cascini, L., Leroi, E. and Savage, W.Z. (2008) 'Guidelines for landslide susceptibility, hazard and risk zoning for land use planning', *Engineering Geology*, 102(3–4), pp. 85-98.

Fischer, L., Amann, F., Moore, J.R. and Huggel, C. (2010) 'Assessment of periglacial slope stability for the 1988 Tschierva rock avalanche (Piz Morteratsch, Switzerland)', *Engineering Geology*, 116(1–2), pp. 32-43.

Formetta, G., Rago, V., Capparelli, G., Rigon, R., Muto, F. and Versace, P. (2014) 'Integrated Physically based System for Modeling Landslide Susceptibility', *Procedia Earth and Planetary Science*, 9, pp. 74-82.

Fourie, A.B. (1996) 'Predicting rainfall-induced slope instability', *Proceedings of the ICE - Geotechnical Engineering*, 119, pp. 211-218.

Freeman, T.G. (1991) 'Calculating catchment area with divergent flow based on a regular grid', *Computers and Geosciences*, 17(3), pp. 413-422.

Fu, P. and Rich, P.M. (2003) 'A geometric solar radiation model with applications in agriculture and forestry', *Computers and Electronics in Agriculture*, 37(1-3), pp. 25-35.

Gallant, J.C. and Wilson, J.P. (1996) 'TAPES-G: A grid-based terrain analysis program for the environmental sciences', *Computers & Geosciences*, 22(7), pp. 713-722.

Galli, M., Ardizzone, F., Cardinali, M., Guzzetti, F. and Reichenbach, P. (2008) 'Comparing landslide inventory maps', *Geomorphology*, 94(3–4), pp. 268-289.

Gao, Y. and Mas, J.F. (2008) 'A comparison of the performance of pixel-based and object-based classification over images with various spatial resolutions.', *Online Journal of Earth Sciences*, 2(1), pp. 27-35.

Garbrecht, J. and Martz, L.W. (1997) 'The assignment of drainage direction over flat surfaces in raster digital elevation models', *Journal of Hydrology*, 193(1-4), pp. 204-213.

Glade, T. and Crozier, M.J. (2006) 'The nature of landslide hazard impact ', in Glade, T., Anderson, M.G. and Crozier, M.J. (eds.) *Landslide Hazard and Risk*. Chichester: John Wiley & Sons Ltd., pp. 43 -74.

Glendinning, S., Loveridge, F., Starr-Keddle, R.E., Bransby, M.F. and Hughes, P.N. (2009) 'Role of vegetation in sustainability of infrastructure slopes', *Proceedings of the Institution of Civil Engineers: Bridge Engineering*, 162(2), pp. 101-110.

Godt, J.W., Baum, R.L., Savage, W.Z., Salciarini, D., Schulz, W.H. and Harp, E.L. (2008) 'Transient deterministic shallow landslide modeling: Requirements for susceptibility and hazard assessments in a GIS framework', *Engineering Geology*, 102(3–4), pp. 214-226.

Goetz, J.N., Brenning, A., Petschko, H. and Leopold, P. (2015) 'Evaluating machine learning and statistical prediction techniques for landslide susceptibility modeling', *Computers and Geosciences*, 81, pp. 1-11.

Goetz, J.N., Guthrie, R.H. and Brenning, A. (2011) 'Integrating physical and empirical landslide susceptibility models using generalized additive models', *Geomorphology*, 129(3-4), pp. 376-386.

Gorsevski, P.V., Gessler, P.E. and Jankowski, P. (2003) 'Integrating a fuzzy k-means classification and a Bayesian approach for spatial prediction of landslide hazard', *Journal of Geographical Systems*, 5(3), pp. 223-251.

Gorsevski, P.V., Jankowski, P. and Gessler, P.E. (2005) 'Spatial Prediction of Landslide Hazard Using Fuzzy k-means and Dempster-Shafer Theory', *Transactions in GIS*, 9(4), pp. 455-474.

Green, A.A., Berman, M., Switzer, P. and Craig, M.D. (1988) 'A transformation for ordering multispectral data in terms of image quality with implications for noise removal', *IEEE Transactions on Geoscience and Remote Sensing*, 26(1), pp. 65-74.

Greenwood, J.R., Norris, J.E. and Wint, J. (2004) 'Assessing the contribution of vegetation to slope stability', *Proceedings of the Institution of Civil Engineers: Geotechnical Engineering*, 157(4), pp. 199-207.

Gritzner, M.L., Marcus, W.A., Aspinall, R. and Custer, S.G. (2001) 'Assessing landslide potential using GIS, soil wetness modeling and topographic attributes, Payette River, Idaho', *Geomorphology*, 37(1-2), pp. 149-165.

Grogan, K. and Fensholt, R. (2013) 'Exploring patterns and effects of aerosol quantity flag anomalies in MODIS surface reflectance products in the tropics', *Remote Sensing*, 5(7), pp. 3495-3515.

Gustavsson, M., Kolstrup, E. and Seijmonsbergen, A.C. (2006) 'A new symbol-and-GIS based detailed geomorphological mapping system: Renewal of a scientific discipline for understanding landscape development', *Geomorphology*, 77(1-2), pp. 90-111.

Guzzetti, F., Cardinali, M. and Reichenbach, P. (1996) 'The influence of structural setting and lithology on landslide type and pattern', *Environmental and Engineering Geoscience*, 2(4), pp. 531-555.

Guzzetti, F., Carrara, A., Cardinali, M. and Reichenbach, P. (1999) 'Landslide hazard evaluation: a review of current techniques and their application in a multi-scale study, Central Italy', *Geomorphology*, 31(1–4), pp. 181-216.

Guzzetti, F., Mondini, A.C., Cardinali, M., Fiorucci, F., Santangelo, M. and Chang, K.T. (2012) 'Landslide inventory maps: New tools for an old problem', *Earth-Science Reviews*, 112(1-2), pp. 42-66.

Guzzetti, F., Reichenbach, P., Ardizzone, F., Cardinali, M. and Galli, M. (2006) 'Estimating the quality of landslide susceptibility models', *Geomorphology*, 81(1-2), pp. 166-184.

Guzzetti, F., Reichenbach, P., Cardinali, M., Galli, M. and Ardizzone, F. (2005) 'Probabilistic landslide hazard assessment at the basin scale', *Geomorphology*, 72(1-4), pp. 272-299.

Haneberg, W. (2004) *Computational Geosciences with Mathematica*. Springer Berlin Heidelberg.

Hardy, A.J., Barr, S.L., Mills, J.P. and Miller, P.E. (2012) 'Characterising soil moisture in transport corridor environments using airborne LiDAR and CASI data', *Hydrological Processes*, 26(13), pp. 1925-1936.

Harp, E.L., Reid, M.E., McKenna, J.P. and Michael, J.A. (2009) 'Mapping of hazard from rainfall-triggered landslides in developing countries: Examples from Honduras and Micronesia', *Engineering Geology*, 104(3–4), pp. 295-311.

Haugerud, R.A. and Harding, D.J. (2001) 'Some algorithms for virtual deforestation (VDF) of LiDAR topographic survey data', *International Arch. Photogramm., Remote Sens. Spatial Inf. Sci.,*, 34((3/W4)), pp. 714-719.

He, B., Saassa, K., Nagai, O. and Takara, K. (2014) 'Simulation of a rapid and long travelling landslide using 2D-RAPID and LS-RAPID 3D models', in Sassa, K. (ed.) *Landslide Science for a Safer Geoenvironment, Volume 1: The International Programme on Landslides*. Springer

Heckerman, D. (1986) 'Probabilistic interpretation of MYCIN's certainty factors.', in Kanal, L.N. and Lemmer, J.F. (eds.) *Uncertainty in Artificial Intelligence*. Dordrecht: Kluwer Academic Publishers, pp. 167–196.

Herold, M. and Roberts, D. (2010) 'The spectral dimension in Urban Remote Sensing', in Rashed, T. and Jürgens, C. (eds.) *Remote Sensing of Urban and Suburban Areas*. Springer, pp. 47-66.

Hess, T.M., Holman, I.P., Rose, S.C., Rosolova, Z. and Parrott, A. (2010) 'Estimating the impact of rural land management changes on catchment runoff generation in England and Wales', *Hydrological Processes*, 24(10), pp. 1357-1368.

Hollaus, M., Wagner, W. and Kraus, K. (2005) 'Airborne laser scanning and usefulness for hydrological models', *Advances in Geosciences*, 5, pp. 57-63.

Holman, I.P., Hollis, J.M., Bramley, M.E. and Thompson, T.R.E. (2003) 'The contribution of soil structural degradation to catchment flooding: A preliminary investigation of the 2000 floods in England and Wales', *Hydrology and Earth System Sciences*, 7(5), pp. 754-765.

Holman, I.P., Quinn, J.M.A. and Knox, J.W. (2004) 'The development of the crop calendar dataset'.

Hsing-Chung, C., Linlin, G., Rizos, C. and Milne, T. (2004) *Geoscience and Remote Sensing Symposium, 2004. IGARSS '04. Proceedings. 2004 IEEE International*. 20-24 Sept. 2004.

Huang, Z., Law, K.T., Liu, H. and Jiang, T. (2009) 'The chaotic characteristics of landslide evolution: a case study of Xintan landslide', *Environmental Geology*, 56(8), pp. 1585-1591.

Hughes, D. (1998) 'Antecedent precipitation', in *Encyclopedia of Hydrology and Lakes*. Springer Netherlands, pp. 69-69.

Hungr, O., Evans, S.G., Bovis, M.J. and Hutchinson, J.N. (2001) 'A review of the classification of landslides of the flow type', *Environmental and Engineering Geoscience*, 7(3), pp. 221-238.

Hungr, O., Evans, S.G. and Hazzard, J. (1999) 'Magnitude and frequency of rock falls and rock slides along the main transportation corridors of southwestern British Columbia', *Canadian Geotechnical Journal*, 36(2), pp. 224-238.

Hungr, O., Leroueil, S. and Picarelli, L. (2014) 'The Varnes classification of landslide types, an update', *Landslides*, 11(2), pp. 167-194.

Hutchinson, M.F. (1989) 'A new procedure for gridding elevation and stream line data with automatic removal of spurious pits', *Journal of Hydrology*, 106(3-4), pp. 211-232.

Hutchinson, M.F. (2008) 'Adding the Z Dimension', in Wilson, J.P.a.F., A.S (ed.) *The Handbook of Geographic Information Science*. Oxford: Blackwell, pp. 144-168.

Hutchinson, M.F. (2013) 'ANUDEM Version 5.3'. 09/02/2013. Available at: http://fennerschool.anu.edu.au/research/software-datasets/anudem.

Iverson, R.M. (2000) 'Landslide triggering by rain infiltration', *Water Resources Research*, 36(7), pp. 1897-1910.

Iverson, R.M. (2005) 'Regulation of landslide motion by dilatancy and pore pressure feedback', *Journal of Geophysical Research: Earth Surface*, 110(2).

Iverson, R.M. and Reid, M.E. (1992) 'Gravity-driven groundwater flow and slope failure potential: 1. Elastic Effective-Stress Model', *Water Resources Research*, 28(3), pp. 925-938.

Ives, J.D. and Messerli, B. (1981) 'Mountain hazards mapping in Nepal: introduction to an applied mountain research project', *Mountain Research and Development*, 1(3-4), pp. 223-230.

Iwahashi, J., Watanabe, S. and Furuya, T. (2003) 'Mean slope-angle frequency distribution and size frequency distribution of landslide masses in Higashikubiki area, Japan', *Geomorphology*, 50(4), pp. 349-364.

Jaboyedoff, M., Oppikofer, T., Abellán, A., Derron, M.H., Loye, A., Metzger, R. and Pedrazzini, A. (2012) 'Use of LIDAR in landslide investigations: A review', *Natural Hazards*, 61(1), pp. 5-28.

Jackson, D.L. (2000) 'Guidance on the interpretation of the Biodiversity Broad Habitat Classification (terrestrial and freshwater types): Definitions and the relationship with other classifications ', *JNCC Report 307*, , p. 73.

Jaeger, J.C., Cook, N.G.W. and Zimmerman, R. (2009) *Fundamentals of Rock Mechanics*. Wiley.

Jaiswal, P. and van Westen, C.J. (2009) 'Estimating temporal probability for landslide initiation along transportation routes based on rainfall thresholds', *Geomorphology*, 112(1-2), pp. 96-105.

Jaiswal, P. and van Westen, C.J. (2012) 'Frequency-size relation of shallow debris slides on cut slopes along a railroad corridor: A case study from Nilgiri hills, Southern India', *Natural Hazards*, 61(3), pp. 1263-1275.

Jaiswal, P. and van Westen, C.J. (2013) 'Use of quantitative landslide hazard and risk information for local disaster risk reduction along a transportation corridor: A case study from Nilgiri district, India', *Natural Hazards*, 65(1), pp. 887-913.

Jaiswal, P., Van Westen, C.J. and Jetten, V. (2010a) 'Quantitative assessment of direct and indirect landslide risk along transportation lines in southern India', *Natural Hazards and Earth System Science*, 10(6), pp. 1253-1267.

Jaiswal, P., van Westen, C.J. and Jetten, V. (2010b) 'Quantitative landslide hazard assessment along a transportation corridor in southern India', *Engineering Geology*, 116(3-4), pp. 236-250.

Jaiswal, P., van Westen, C.J. and Jetten, V. (2011) 'Quantitative assessment of landslide hazard along transportation lines using historical records', *Landslides*, 8(3), pp. 279-291.

Jensen, J. (2004) *Introductory Digital Image Processing: A Remote Sensing Perspective*. 3rd edition edn. New Jersey: Prentice Hall, Upper Saddle River.

Johnson, G.A.L., Heard, A.J. and O'Mara, P.T.O. (1995) 'Carboniferous ', in Johnson, G.A.L. (ed.) *Robson's geology of Northeast England*. Newcastle upon Tyne: Transactions of the Natural History Society of Northumbria, pp. 249-265.

Jones, L.D. (2006) 'Monitoring landslides in hazardous terrain using terrestrial LiDAR: An example from Montserrat', *Quarterly Journal of Engineering Geology and Hydrogeology*, 39(4), pp. 371-373.

Kanungo, D.P., Arora, M.K., Sarkar, S. and Gupta, R.P. (2006) 'A comparative study of conventional, ANN black box, fuzzy and combined neural and fuzzy weighting procedures for landslide susceptibility zonation in Darjeeling Himalayas', *Engineering Geology*, 85(3–4), pp. 347-366.

Kanungo, D.P., Arora, M.K., Sarkar, S. and Gupta, R.P. (2009) 'Landslide Susceptibility Zonation (LSZ) Mapping – A Review', *Journal of South Asia Disaster Studies* 2(1), pp. 81-105.

Kanungo, D.P., Sarkar, S. and Shaifaly, S. (2011) 'Combining neural network with fuzzy, certainty factor and likelihood ratio concepts for spatial prediction of landslides', *Nat. Hazards Earth Syst. Sci.*, 59(3), pp. 1491–1512.

Kayastha, P., Dhital, M.R. and De Smedt, F. (2013) 'Application of the analytical hierarchy process (AHP) for landslide susceptibility mapping: A case study from the Tinau watershed, west Nepal', *Computers and Geosciences*, 52, pp. 398-408.

Kienzle, S. (2004) 'The effect of DEM raster resolution on first order, second order and compound terrain derivatives', *Transactions in GIS*, 8(1), pp. 83-112.

Krahn, J. (2004) *Stability modelling with SLOPE/W. AN Engineering Methodology*. GeoSlope Intrnational.

Lacerda, W. (2004) 'Behaviour of colluvial soils in a tropical environment', in Lacerda, W., Ehrlich, M., Fontoura, S.A.B. and Sayao, A.S.F. (eds.) *Landslides: Evaluation and Stabilization/Glissement de Terrain: Evaluation et Stabilisation, Set of 2 Volumes: Proceedings of the Ninth International Symposium on Landslides, June 28 -July 2, 2004*. Rio de Janeiro, Brazil: Taylor & Francis.

Lee, E.M. and Jones, D.K.C. (2004) *Landslide Risk Assessment*. London: Thomas Telford Publishing.

Lee, S. (2005) 'Application of logistic regression model and its validation for landslide susceptibility mapping using GIS and remote sensing data', *International Journal of Remote Sensing*, 26(7), pp. 1477-1491.

Lee, S. and Choi, J. (2004) 'Landslide susceptibility mapping using GIS and the weight-of-evidence model', *International Journal of Geographical Information Science*, 18(8), pp. 789-814.

Lee, S., Choi, J. and Min, K. (2002) 'Landslide susceptibility analysis and verification using the Bayesian probability model', *Environmental Geology*, 43(1-2), pp. 120-131.

Lee, S., Hwang, J. and Park, I. (2013) 'Application of data-driven evidential belief functions to landslide susceptibility mapping in Jinbu, Korea', *Catena*, 100, pp. 15-30.

Lee, S. and Pradhan, B. (2006) 'Probabilistic landslide hazards and risk mapping on Penang Island, Malaysia', *Journal of Earth System Science*, 115(6), pp. 661-672.

Lee, S., Ryu, J.-H., Won, J.-S. and Park, H.-J. (2004) 'Determination and application of the weights for landslide susceptibility mapping using an artificial neural network', *Engineering Geology*, 71(3–4), pp. 289-302.

Lee, S., Ryu, J.H., Min, K. and Won, J.S. (2003) 'Landslide susceptibility analysis using GIS and artificial neural network', *Earth Surface Processes and Landforms*, 28(12), pp. 1361-1376.

Leroueil, S., Locat, A., E, E. and N, K. (2012) 'Progressive failure in natural and engineered slopes', in Eberhardt E, Froese C, AK, T. and Leroueil, S. (eds.) *Landslides and Engineered Slopes, Proceedings, 11th International Symposium on Landslides*. Banff,: CRC Press, Boca Raton, pp. 1-31.

Leventhal, A.R. and Kotze, G.P. (2008) 'Landslide susceptibility and hazard mapping in Australia for land-use planning - with reference to challenges in metropolitan suburbia', *Engineering Geology*, 102(3-4), pp. 238-250.

Li, S., Wu, H., Wan, D. and Zhu, J. (2011) 'An effective feature selection method for hyperspectral image classification based on genetic algorithm and support vector machine', *Knowledge-Based Systems*, 24(1), pp. 40-48.

Lim, M., Mills, J.P., Barr, S.L., Barber, D., Glendinning, S., Parkin, G., Hall, J. and Clarke, B. (2007) 'High resolution earth imaging for transport corridor slope stability risk analysis', *Int. Arch. Photogramm., Remote Sens. Spartial Inf. Sci.*, 36(no. 1/W51), p. 6.

Lloyd, C.D. and Atkinson, P.M. (2002) 'Deriving DSMs from LiDAR data with kriging', *International Journal of Remote Sensing*, 23(12), pp. 2519-2524.

Lloyd, D.M., Anderson, M.G., Hussein, A.N., Jamaludin, A. and Wilkinson, P.L. (2001) 'Preventing landslides on roads and railways: a new risk-based approach', *Proceedings of the Institution of Civil Engineers-Civil Engineering*, 144(3), pp. 129-134.

Lobell, D. and Asner, G.P. (2002) 'Moisture effects on soil reflectance', *Soil Sci. Soc. Am. J.*, 66(3), pp. 722-727.

Lu, N. and Godt, J. (2008) 'Infinite slope stability under steady unsaturated seepage conditions', *Water Resources Research*, 44(11), p. W11404.

Ma, J., Lin, G., Chen, J. and Yang, L. (2010) 'An improved topographic wetness index considering topographic position', *18th International Conference on Geoinformatics, Geoinformatics 2010*.

Mackney, D., Hodgson, J.M., Hollis, J.M. and Staines, S.J. (1983) *Legend for the 1:250000 Soil Map of England and Wales. Soil Survey of England and Wales*. Harpenden.

Manley, G. and Harding, C. (2003) 'Soil slope hazard index as a tool for earthworks management', *Proc. 6th Int. Conf. Railway Engineering*. London, UK, April 30th - May 1st. Engineering Technics Press, p. 12.

Manning, L.J., Hall, J.W., Kilsby, C.G., Glendinning, S. and Anderson, M.G. (2008) 'Spatial analysis of the reliability of transport networks subject to rainfall-induced landslides', *Hydrological Processes*, 22(17), pp. 3349-3360.

Marjanović, M. and Caha, J. (2011) 'Fuzzy approach to landslide susceptibility zonation', *Proceedings of Dateo 2011 workshop*. Pisek, Czech Republic, 21-23 April 2011. pp. 181-195. Available at: http://www.scopus.com/inward/record.url?eid=2-s2.0-84868672714&partnerID=40&md5=65b2b1bfd1258f28f378fa9ffa7dd159.

Mather, P.M. and Koch, M. (2011a) *Computer processing of remotely-sensed images : an introduction*. Chichester, West Sussex, UK: Wiley-Blackwell.

Mather, P.M. and Koch, M. (2011b) 'Remote Sensing Platforms and Sensors', in *Computer Processing of Remotely-Sensed Images*. John Wiley & Sons, Ltd, pp. 29-66.

Mattia, C., Bischetti, G.B. and Gentile, F. (2005) 'Biotechnical characteristics of root systems of typical Mediterranean species', *Plant and Soil*, 278(1-2), pp. 23-32.

Maune, D.F. (2008) 'Aerial mapping and surveying.', in Dewberry, S. and Rauenzahn, L. (eds.) *Land Development Handbook*. Third edn. McGraw-Hill Professional,, pp. 877–910.

Maynard, J.J. and Johnson, M.G. (2014) 'Scale-dependency of LiDAR derived terrain attributes in quantitative soil-landscape modeling: Effects of grid resolution vs. neighborhood extent', *Geoderma*, 230–231, pp. 29-40.

Mezughi, T.H., Akhir, J.M., Rafek, A.G. and Abdullah, I. (2012) 'Analytical Hierarchy Process Method for Mapping Landslide Susceptibility to an Area along the E-W Highway (Gerik-Jeli), Malaysia', *Asian Journal of Earth Sciences*, 5(1), pp. 13-24.

Miller, A.J. (2011) 'Assessing landslide susceptibility by incorporating the surface cover index as a measurement of vegetative cover', *Land Degradation & Development*, pp. n/a-n/a.

Miller, P.E., Hardy, A.J., Mills, J.P., Barr, S.L., Birkinshaw, S.J., Parkin, G., Glendinning, S. and Hall, J.W. (2009) 'Intelligent integration of multi-sensor data for risk assessment in transport corridor environments', *International Arch. Photogramm., Remote Sens. Spatial Inf. Sci.*,, XXXVIII(1-4-7/W5), p. 6.

Miller, P.E., Mills, J.P., Barr, S.L., Birkinshaw, S.J., Hardy, A.J., Parkin, G. and Hall, J. (2012) 'A remote sensing approach for landslide hazard assessment on engineered slopes', *IEEE Transactions on Geoscience and Remote Sensing*, 50(4), pp. 1048-1056.

Mills, J.P., Buckley, S.J., Mitchell, H.L., Clarke, P.J. and Edwards, S.J. (2005) 'A geomatics data integration technique for coastal change monitoring', *Earth Surface Processes and Landforms*, 30(6), pp. 651-664.

Mishra, S.K. and Singh, V.P. (2003) *Soil conservation service curve number (SCS-CN) methodology*. Netherlands: Klumer Academic Publishers.

Moeslund, J.E., Arge, L., Bøcher, P.K., Dalgaard, T. and Svenning, J.-C. (2013) 'Topography as a driver of local terrestrial vascular plant diversity patterns', *Nordic Journal of Botany*, 31(2), pp. 129-144.

Montgomery, D.R. and Dietrich, W.E. (1994) 'A physically-based model for the topographic control on shallow landsliding', *Water Resources Research*, 30(4), pp. 1153-1171.

Moore, I.D., Grayson, R.B. and Ladson, A.R. (1991) 'Digital terrain modelling: A review of hydrological, geomorphological and biological applications', *Hydrological Processes*, 5, pp. 3-30.

Moore, P.L. and Iverson, N.R. (2002) 'Slow episodic shear of granular materials regulated by dilatant strengthening', *Geology*, 30(9), pp. 843-846.

Moreiras, S.M. (2004) 'Landslide incidence zonation in the Rio Mendoza valley, Mendoza province, Argentina', *Earth Surface Processes and Landforms*, 29(2), pp. 255-266.

Morton, D., Rowland, C., Wood, C., Meek, L., Marston, C., Smith, G., Wadsworth, R. and Simpson, I.C. (2011) 'Countryside Survey: Final report for LCM 2007- The new UK Land cover map', in *Technical Report Number 11/07*. Centre for Ecology and Hydrology, p. pp. 112.

Mutanga, O., Skidmore, A.K., Kumar, L. and Ferwerda, J. (2005) 'Estimating tropical pasture quality at canopy level using band depth analysis with continuum removal in the visible domain', *International Journal of Remote Sensing*, 26(6), pp. 1093-1108.

Muthu, K., Petrou, M., Tarantino, C. and Blonda, P. (2008) 'Landslide Possibility Mapping Using Fuzzy Approaches', *Geoscience and Remote Sensing, IEEE Transactions on*, 46(4), pp. 1253-1265.

Nandi, A. and Shakoor, A. (2010) 'A GIS-based landslide susceptibility evaluation using bivariate and multivariate statistical analyses', *Engineering Geology*, 110(1-2), pp. 11-20.

National Soil Resources Institute (2008) *The Digital Soil Map- NATMAP vector*. Cranfield, UK: Cranfield University.

Neaupane, K.M. and Piantanakulchai, M. (2006) 'Analytic network process model for landslide hazard zonation', *Engineering Geology*, 85(3–4), pp. 281-294.

Network Rail (2005) *Melkridge Embankment* (NEC2/WEM/34.0900/35.0747/DN).

Nichol, J.E., Shaker, A. and Wong, M.S. (2006) 'Application of high-resolution stereo satellite images to detailed landslide hazard assessment', *Geomorphology*, 76(1-2), pp. 68-75.

No-Wook, P. (2010) 'Evidential reasoning applied to GIS-based landslide susceptibility mapping with geospatial data', *Geoscience and Remote Sensing Symposium (IGARSS), 2010 IEEE International*. 25-30 July 2010. IEEE, pp. 2151-2154.

O'Brien, A.S. (2007) 'Rehabilitation of urban railway embankments: investigation, analysis and stabilisation', *Proceedings of the 14th Europian Conference on Soil Mechanics and Geotechnical Engineering*. Madrid, Spain, 24 - 27 Sep 2007. Millpress, Amsterdam, the Netherlands, pp. 125-143.

O'Callaghan, J.F. and Mark, D.M. (1984) 'The extraction of drainage networks from digital elevation data', *Computer Vision, Graphics, & Image Processing*, 28(3), pp. 323-344.

O'Connell, E., Ewen, J., O'Donnell, G. and Quinn, P. (2007) 'Is there a link between agricultural land-use management and flooding?', *Hydrology and Earth System Sciences*, 11(1), pp. 96-107.

Ohlmacher, G.C. (2007) 'Plan curvature and landslide probability in regions dominated by earth flows and earth slides', *Engineering Geology*, 91(2–4), pp. 117-134.

Ordnance Survey (2012) *Landform Profile User guide and technical specification*

Pack, R.T., Tarboton, D.G. and Goodwin, C.N. (1999) 'GIS-based landslide susceptibility mapping with SINMAP', *Engineering geology and geotechnical engineering. Proceedings of the 34th symposium, Logan, April 1999.*, pp. 219-231.

Packman, J., Quinn, P., Hollis, J. and O'Connell, P. (2004) *Review of Impacts of Rural Land Use and Management on Flood Generation, Short Term Improvement to the FEH Rainfall - Runoff Model: Technical Background*, pp. 1-66.

Pantelidis, L. (2011) 'A critical review of highway slope instability risk assessment systems', *Bulletin of Engineering Geology and the Environment*, 70(3), pp. 395-400.

Park, N.W. (2011) 'Application of Dempster-Shafer theory of evidence to GIS-based landslide susceptibility analysis', *Environmental Earth Sciences*, 62(2), pp. 367-376.

Pearl, J. (1990) 'Reasoning Under Uncertainty', *Annual Review of Computer Science*, 4(1), pp. 37-72.

Penna, D., Borga, M., Norbiato, D. and Dalla Fontana, G. (2009) 'Hillslope scale soil moisture variability in a steep alpine terrain', *Journal of Hydrology*, 364(3-4), pp. 311-327.

Perry, E. and Roberts, D. (2008) 'Sensitivity of narrow-band and broad-band indices for assessing nitrogen availability and water stress in an annual crop', *Agron. J.*, 100(4), pp. 1211-1219.

Perry, J., MacDonald, M., Pedley, M., Brady, K. and Reid, M. (2003a) 'Embankment cuttings: condition appraisal and remedial treatment', *Proceedings of the Institution of Civil Engineers-Geotechnical Engineering*, 156(4), pp. 171-175.

Perry, J., Pedley, M. and Reid, M. (2003b) 'Infrastructure embankments; condition appraisal and remedial treatment', *CIRIA*, pp. 47-73.

Petrie, G. and Toth, C.K. (2008) 'Introduction to laser ranging, profiling and scaning', in Shan, J., Toth, C.K. and Boca Raton, F.L. (eds.) *Topographic Laser Ranging and Scanning: Principles and processes*. CRC Press.

Petschko, H., Brenning, A., Goetz, J., Bell, R. and Glade, T. (2014) 'Spatially varying prediction uncertainties and their implications on landslide susceptibility maps', *EGU General Assembly 2014*. Vienna, Austria, 27 April - 2 May, 2014 EGU Geophysical research.

Phillips, J.D. (2003) 'Sources of nonlinearity and complexity in geomorphic systems', *Progress in Physical Geography*, 27(1), pp. 1-23.

Pierdicca, N., Pulvirenti, L. and Bignami, C. (2010) 'Soil moisture estimation over vegetated terrains using multitemporal remote sensing data', *Remote Sens. Environ.*, 114(2), pp. 440-448.

Porwal, A., Carranza, E.J.M. and Hale, M. (2003) 'Knowledge-driven and data-driven fuzzy models for predictive mineral potential mapping', *Natural Resources Research*, 12(1), pp. 1-25.

Pradhan, B. (2011) 'Manifestation of an advanced fuzzy logic model coupled with Geo-information techniques to landslide susceptibility mapping and their comparison with logistic regression modelling', *Environmental and Ecological Statistics*, 18(3), pp. 471-493.

Pradhan, B. and Lee, S. (2010) 'Landslide susceptibility assessment and factor effect analysis: backpropagation artificial neural networks and their comparison with frequency ratio and bivariate logistic regression modelling', *Environmental Modelling and Software*, 25(6), pp. 747-759.

Pradhan, B., Sezer, E.A., Gokceoglu, C. and Buchroithner, M.F. (2010) 'Landslide susceptibility mapping by neuro-fuzzy approach in a landslide-prone area (Cameron Highlands, Malaysia)', *IEEE Transactions on Geoscience and Remote Sensing*, 48(12), pp. 4164-4177.

Priemus, H. and Zonneveld, W. (2003) 'What are corridors and what are the issues? Introduction to special issue: the governance of corridors', *Journal of Transport Geography*, 11(3), pp. 167-177.

Pu, R., Gong, P., Tian, Y., Miao, X., Carruthers, R.I. and Anderson, G.L. (2008) 'Using classification and NDVI differencing methods for monitoring sparse vegetation coverage: A case study of saltcedar in Nevada, USA', *International Journal of Remote Sensing*, 29(14), pp. 3987-4011.

Quinn, P., Beven, K., Chevallier, P. and Planchon, O. (1991) 'The prediction of hillslope flow paths for distributed hydrological modelling using digital terrain models', *Hydrological Processes*, 5(1), pp. 59-79.

Quinn, P.F., Beven, K.J. and Lamb, R. (1995) 'The ln(a/tanβ) index: how to calculate it and how to use it within the TOPMODEL framework', *Hydrological Processes*, 9(2), pp. 161-182.

Raia, S., Alvioli, M., Rossi, M., Baum, R.L., Godt, J.W. and Guzzetti, F. (2014) 'Improving predictive power of physically based rainfall-induced shallow landslide models: A probabilistic approach', *Geoscientific Model Development*, 7(2), pp. 495-514.

Razak, K.A., Straatsma, M.W., van Westen, C.J., Malet, J.P. and de Jong, S.M. (2011) 'Airborne laser scanning of forested landslides characterization: Terrain model quality and visualization', *Geomorphology*, 126(1-2), pp. 186-200.

Reed, D. (1999) 'Flood estimation handbook', *Overview. Institute of Hydrology*, 1, p. 107.

Rees, W.G. (2000) 'The accuracy of Digital Elevation Models interpolated to higher resolutions', *International Journal of Remote Sensing*, 21(1), pp. 7-20.

Regmi, N.R., Giardino, J.R. and Vitek, J.D. (2010) 'Modeling susceptibility to landslides using the weight of evidence approach: Western Colorado, USA', *Geomorphology*, 115(1–2), pp. 172-187.

Reid, J.M. and Clark, G.T. (2000) *A whole life cost model for earthwork slopes* (Report 430). Crowthrone, UK: Crowthrone, T.L.

Reid, M.E. (1997) 'Slope instability caused by small variations in hydraulic conductivity', *Journal of Geotechnical Engineering*, 123(8), pp. 717-725.

Reid, M.E. and Iverson, R.M. (1992) 'Gravity-driven groundwater flow and slope failure potential: 2. Effects of slope morphology, material properties, and hydraulic heterogeneity', *Water Resources Research*, 28(3), pp. 939-950.

Ridley, A., McGinnity, B. and Vaughan, P. (2004) 'Role of pore water pressures in embankment stability', *Proceedings of the Institution of Civil Engineers-Geotechnical Engineering*, 157(4), pp. 193-198.

Rosen, P.A., Hensley, S., Joughin, I.R., Fuk, K.L., Madsen, S.N., Rodriguez, E. and Goldstein, R.M. (2000) 'Synthetic aperture radar interferometry', *Proceedings of the IEEE*, 88(3), pp. 333-382.

Rosso, R., Rulli, M.C. and Vannucchi, G. (2006) 'A physically based model for the hydrologic control on shallow landsliding', *Water Resources Research*, 42(6).

Roventa, E. and Spircu, T. (2009) 'Certainty Factors Theory', in *Management of Knowledge Imperfection in Building Intelligent Systems*. Springer Berlin Heidelberg, pp. 153-160.

Ruff, M. and Czurda, K. (2008) 'Landslide susceptibility analysis with a heuristic approach in the Eastern Alps (Vorarlberg, Austria)', *Geomorphology*, 94(3–4), pp. 314-324.

Rupke, J., Cammeraat, E., Seijmonsbergen, A.C. and Westen, C.J.V. (1988) 'Engineering geomorphology of the Widentobel catchment, Appenzell and Sankt Gallen, Switzerland. A geomorphological inventory system applied to geotechnical appraisal of slope stability', *Engineering Geology*, 26(1), pp. 33-68.

Safaei, M., Omar, H. and Huat, B.K. (2011) 'Deterministic rainfall induced landslide approaches; Advantages and limitations', *Electronic Journal of Geotechnical Engineering*, 16, pp. 1619-1650.

Santacana, N., Baeza, B., Corominas, J., De Paz, A. and Marturiá, J. (2003) 'A GIS-based multivariate statistical analysis for shallow landslide susceptibility mapping in La Pobla de Lillet Area (Eastern Pyrenees, Spain)', *Natural Hazards*, 30(3), pp. 281-295.

Sari, M. (2009) 'The stochastic assessment of strength and deformability characteristics for a pyroclastic rock mass', *International Journal of Rock Mechanics and Mining Sciences*, 46(3), pp. 613-626.

Sassa, K. (2014) *Landslide Science for a Safer Geoenvironment, Volume 1: The International Programme on Landslides (Ipl)*. Springer.

Savage, W. and Baum, R. (2005) 'Instability of steep slopes', in *Debris-flow Hazards and Related Phenomena*. Springer Berlin Heidelberg, pp. 53-79.

Savage, W.Z., Godt, J.W. and Baum, R.L. (2004) 'Modelling time dependent areal slope stability', in Lacerda, W., Ehrlich, M., Fontoura, S.A.B. and Sayao, A.S.F. (eds.) *Landslides: Evaluation and Stabilization/Glissement de Terrain: Evaluation et Stabilisation, Set of 2 Volumes: Proceedings of the Ninth International Symposium on Landslides,* . Rio de Janeiro, Brazil: Taylor & Francis.

Schmidt, F. and Persson, A. (2003) 'Comparison of DEM data capture and topographic wetness indices', *Precision Agriculture*, 4(2), pp. 179-192.

Schmugge, T.J., Kustas, W.P., Ritchie, J.C., Jackson, T.J. and Rango, A. (2002) 'Remote sensing in hydrology', *Advances in Water Resources*, 25(8), pp. 1367-1385.

Schulz, W.H. (2007) 'Landslide susceptibility revealed by LIDAR imagery and historical records, Seattle, Washington', *Engineering Geology*, 89(1-2), pp. 67-87.

Seibert, J. and McGlynn, B.L. (2007) 'A new triangular multiple flow direction algorithm for computing upslope areas from gridded digital elevation models', *Water Resources Research*, 43(4), p. W04501.

Shafer, G. (1976) *A mathematical theory of evidence*. Princeton: Princeton University Press.

Shahabi, H., Ahmad, B.B. and Khezri, S. (2013) 'Evaluation and comparison of bivariate and multivariate statistical methods for landslide susceptibility mapping (case study: Zab basin)', *Arabian Journal of Geosciences*, 6(10), pp. 3885-3907.

Shan, J. and Toth, K. (2008) *Topographic laser ranging and scanning: principles and processing*. LLC, UK: CRC Press,Taylor & Francis Group.

Simoni, S., Zanotti, F., Bertoldi, G. and Rigon, R. (2008) 'Modelling the probability of occurrence of shallow landslides and channelized debris flows using GEOtop-FS', *Hydrological Processes*, 22(4), pp. 532-545.

Smethurst, J.A., Clarke, D. and Powrie, W. (2006) 'Seasonal changes in pore water pressure in a grass-covered cut slope in London Clay', *Géotechnique*, 56(8), pp. 523-537.

Smethurst, J.A., Clarke, D. and Powrie, W. (2012) 'Factors controlling the seasonal variation in soil water content and pore water pressures within a lightly vegetated clay slope', *Geotechnique*, 62(5), pp. 429-446.

Smith, G.M. and Milton, E.J. (1999) 'The use of the empirical line method to calibrate remotely sensed data to reflectance', *International Journal of Remote Sensing*, 20(13), pp. 2653-2662.

Soeters, R. and Van Westen, C.J. (1996) 'Slope instability recognition, analysis, and zonation', *Special Report - National Research Council, Transportation Research Board*, 247, pp. 129-177.

Soininen, A. (2014) *Terrascan User's guide*. Terrasolid.

Sørensen, R. and Seibert, J. (2007) 'Effects of DEM resolution on the calculation of topographical indices: TWI and its components', *Journal of Hydrology*, 347(1-2), pp. 79-89.

Sørensen, R., Zinko, U. and Seibert, J. (2006) 'On the calculation of the topographic wetness index: Evaluation of different methods based on field observations', *Hydrology and Earth System Sciences*, 10(1), pp. 101-112.

Soulis, K. and Valiantzas, J.D. (2012) 'SCS-CN parameter determination using rainfall-runoff data in heterogeneous watersheds - the two-CN system approach', *Hydrol. Earth Syst. Sci.*, 16(3), pp. 1001-1015.

Sujatha, E.R., Victor Rajamanickam, G. and Kumaravel, P. (2012) 'Landslide susceptibility analysis using Probabilistic Certainty Factor Approach: A case study on Tevankarai stream watershed, India', *Journal of Earth System Science*, 121(5), pp. 1337-1350.

Takahashi, T. (2007) 'Progress in Debris Flow Modeling', in Sassa, K., Fukuoka, H., Wang, F. and Wang, G. (eds.) *Progress in Landslide Science*. Springer, pp. 60-77.

Tangestani, M.H. (2009) 'A comparative study of Dempster–Shafer and fuzzy models for landslide susceptibility mapping using a GIS: An experience from Zagros Mountains, SW Iran', *Journal of Asian Earth Sciences*, 35(1), pp. 66-73.

Tapete, D., Fanti, R., Cecchi, R., Petrangeli, P. and Casagli, N. (2012) 'Satellite radar interferometry for monitoring and early-stage warning of structural instability in archaeological sites', *Journal of Geophysics and Engineering*, 9(4), pp. S10-S25.

Tarboton, D.G. (1997) 'A new method for the determination of flow directions and upslope areas in grid digital elevation models', *Water Resources Research*, 33(2), pp. 309-319.

Tarboton, D.G. (2010) 'Terrain analysis using digital elevation models (TauDEM).', *Available at: http://hydrology.neng.usu.edu/taudem/ Accessed 01-03-2011*.

Tarboton, D.G., Schreuders, K.A.T., Watson, D.W. and Baker, M.E. (2009) 'Generalized terrain-based flow analysis of digital elevation models', *18th World IMACS/ MODSIM congress*. Cairns, Australia, 13-17 July, 2009. pp. 2000-2006. Available at: http://www.scopus.com/inward/record.url?eid=2-s2.0-80053022985&partnerID=40&md5=d736c1ab606c974cbca7a8186325b4f3.

Tenenbaum, D.E., Band, L.E., Kenworthy, S.T. and Tague, C.L. (2006) 'Analysis of soil moisture patterns in forested and suburban catchments in Baltimore, Maryland, using high-resolution photogrammetric and LIDAR digital elevation datasets', *Hydrological Processes*, 20(2), pp. 219-240.

Terlien, M.T.J. (1998) 'The determination of statistical and deterministic hydrological landslide-triggering thresholds', *Environmental Geology*, 35(2-3), pp. 124-130.

Thompson, S.E., Harman, C.J., Heine, P. and Katul, G.G. (2010) 'Vegetation-infiltration relationships across climatic and soil type gradients', *Journal of Geophysical Research: Biogeosciences*, 115(G2), pp. 1-12.

Tien Bui, D., Pradhan, B., Lofman, O., Revhaug, I. and Dick, O.B. (2012) 'Spatial prediction of landslide hazards in Hoa Binh province (Vietnam): A comparative assessment of the efficacy of evidential belief functions and fuzzy logic models', *Catena*, 96, pp. 28-40.

Tiwari, R. and Rao, K.S. (2006) 'Deformability characteristics of a rock mass under true-triaxial stress compression', *Geotechnical & Geological Engineering*, 24(4), pp. 1039-1063.

Tsai, F. and Philpot, W.D. (2002) 'A derivative-aided hyperspectral image analysis system for land-cover classification', *IEEE Transactions on Geoscience and Remote Sensing*, 40(2), pp. 416-425.

USDA (2004) *National Engineering Handbook. Part 630 Hydrology. Chapter 10 Estimation of direct runoff from storm rainfall.* United States Department of Agriculture,.

Van Asch, T.W.J., Buma, J. and Van Beek, L.P.H. (1999) 'A view on some hydrological triggering systems in landslides', *Geomorphology*, 30(1-2), pp. 25-32.

Van Asch, T.W.J., Malet, J.P., Van Beek, L.P.H. and Amitrato, D. (2007) 'Techniques, issues and advances in numerical modelling of landslide hazard.', *Bull. Soc. géol. France* 178(2), pp. 65-88.

Van Den Eeckhaut, M., Hervás, J., Jaedicke, C., Malet, J.P., Montanarella, L. and Nadim, F. (2012) 'Statistical modelling of Europe-wide landslide susceptibility using limited landslide inventory data', *Landslides*, 9(3), pp. 357-369.

Van Den Eeckhaut, M., Poesen, J., Verstraeten, G., Vanacker, V., Moeyersons, J., Nyssen, J. and van Beek, L.P.H. (2005) 'The effectiveness of hillshade maps and expert knowledge in mapping old deep-seated landslides', *Geomorphology*, 67(3–4), pp. 351-363.

Van Den Eeckhaut, M., Reichenbach, P., Guzzetti, F., Rossi, M. and Poesen, J. (2009) 'Combined landslide inventory and susceptibility assessment based on different mapping units: An example from the Flemish Ardennes, Belgium', *Natural Hazards and Earth System Science*, 9(2), pp. 507-521.

Van der Meer, F. and de Jong, S.M. (2001) *Imaging spectrometry : basic principles and prospective applications*. Dordrecht, The Netherlands: Kluwer Academic Publishers.

Van der Meer, F., de Jong, S.M. and Bakker, W. (2006) 'Imaging Spectrometry: Basic analytical techniques', in van der Meer, F. and de Jong, S.M. (eds.) *Imaging Spectrometry:: Basic Principles and Prospective Applications*. Dordrecht, Netherlands: Springer, pp. 17 - 61.

Van Westen, C.J., Castellanos, E. and Kuriakose, S.L. (2008) 'Spatial data for landslide susceptibility, hazard, and vulnerability assessment: An overview', *Engineering Geology*, 102(3-4), pp. 112-131.

Van Westen, C.J., Rengers, N. and Soeters, R. (2003) 'Use of geomorphological information in indirect landslide susceptibility assessment', *Natural Hazards*, 30(3), pp. 399-419.

Van Westen, C.J., Soeters, R. and Sijmons, K. (2000) 'Digital geomorphological landslide hazard mapping of the Alpago area, Italy', *International Journal of Applied Earth Observation and Geoinformation*, 2000(1), pp. 51-60.

Van Westen, C.J., Van Asch, T.W.J. and Soeters, R. (2006) 'Landslide hazard and risk zonation - Why is it still so difficult?', *Bulletin of Engineering Geology and the Environment*, 65(2), pp. 167-184.

Vaze, J. and Teng, J. (2007) 'impact of den resolution on topographic indices and hydrological modelling results ', in Oxley, L. and Kulasiri, D. (eds.) *MODSIM 2007 International congress on modelling and simulation*. Modelling and Simulation Society of Australia and New Zealand, pp. 706-712.

Viglione, A., Merz, R. and Blöschl, G. (2009) 'On the role of the runoff coefficient in the mapping of rainfall to flood return periods', *Hydrology and Earth System Sciences*, 13(5), pp. 577-593.

Vorpahl, P., Elsenbeer, H., Märker, M. and Schröder, B. (2012) 'How can statistical models help to determine driving factors of landslides?', *Ecological Modelling*, 239, pp. 27-39.

Wan, S., Lei, T. and Chou, T. (2010) 'A novel data mining technique of analysis and classification for landslide problems', *Natural Hazards*, 52(1), pp. 211-230.

Wang, H., Liu, G., Xu, W. and Wang, G. (2005) 'GIS-based landslide hazard assessment; an overview', *Progress in Physical Geography*, 29(4), pp. 548-567.

Waters, C.N., Browne, M.A.E., Dean, M.T. and Powell, J.H. (2007) *Lithostratigraphical framework for Carboniferous successions of Great Britain (Onshore)*. Survey, B.G.

Waters, C.N. and Davis, S.J. (2006) 'Carboniferous: extensional basins advancing deltas and coal swamps', in Brenchley, P.J. and Rawson, P.F. (eds.) *The Geology of England and Wales*. Geological Society, pp. 173-224.

Wati, S.E., Hastuti, T., Widjojo, S. and Pinem, F. (2010) 'Landslide susceptibility mapping with heuristic approach in mountainous area: a case study in Tawangmangu Sub-District, Central Java, Indonesia.', *International Arch. Photogramm., Remote Sens. Spatial Inf. Sci.,*, XXXVIII(Part 8), pp. 248-253.

Western, A.W., Grayson, R.B., Blöschl, G., Willgoose, G.R. and McMahon, T.A. (1999) 'Observed spatial organization of soil moisture and its relation to terrain indices', *Water Resources Research*, 35(3), pp. 797-810.

Wilson, J.P. and Gallant, J.C. (2000) *Terrain Analysis: Principles and Applications*. New York: John Wiley and Sons.

Wilson, J.P., Lam, C.S. and Deng, Y. (2007) 'Comparison of the performance of flow-routing algorithms used in GIS-based hydrologic analysis', *Hydrological Processes*, 21(8), pp. 1026-1044.

Wolock, D.M. and McCabe, G.J. (1995) 'Comparison of Single and Multiple Flow Direction Algorithms for Computing Topographic Parameters in TOPMODEL', *Water Resources Research*, 31(5), pp. 1315-1324.

Wood, E.F., Sivapalan, M., Beven, K. and Band, L. (1988) 'Effects of spatial variability and scale with implications to hydrologic modeling', *Journal of Hydrology*, 102(1-4), pp. 29-47.

Wu, M.J., Li, Z.C., Yuan, P.J. and Jiang, Y.H. (2008a) 'Twenty years of safety monitoring for the landslide of Hancheng PowerStation', *Proceedings , 10th International Symposium on Landslides and Engineered slopes*. Xian, China. pp. 1335-1341. Available at: <Go to ISI>://WOS:000266239200179.

Wu, S., Li, J. and Huang, G.H. (2008b) 'A study on DEM-derived primary topographic attributes for hydrologic applications: Sensitivity to elevation data resolution', *Applied Geography*, 28(3), pp. 210-223.

Yager, R.R., Fedrizzi, M. and Kacprzyk, J. (1994) *Advances in the Dempster-Shafer Theory of Evidence*. New York: Wiley.

Yalcin, A. (2008) 'GIS-based landslide susceptibility mapping using analytical hierarchy process and bivariate statistics in Ardesen (Turkey): Comparisons of results and confirmations', *Catena*, 72(1), pp. 1-12.

Yalcin, A., Reis, S., Aydinoglu, A.C. and Yomralioglu, T. (2011) 'A GIS-based comparative study of frequency ratio, analytical hierarchy process, bivariate statistics and logistics regression methods for landslide susceptibility mapping in Trabzon, NE Turkey', *Catena*, 85(3), pp. 274-287.

Yesilnacar, E. and Süzen, M.L. (2006) 'A land-cover classification for landslide susceptibility mapping by using feature components', *Int J Remote Sens*, 27(2), pp. 253-275.

Yilmaz, I. (2009) 'Landslide susceptibility mapping using frequency ratio, logistic regression, artificial neural networks and their comparison: A case study from Kat landslides (Tokat-Turkey)', *Computers and Geosciences*, 35(6), pp. 1125-1138.

Yin, Y., Wang, H., Gao, Y. and Li, X. (2010) 'Real-time monitoring and early warning of landslides at relocated Wushan Town, the Three Gorges Reservoir, China', *Landslides*, 7(3), pp. 339-349.

Yoshimatsu, H. and Abe, S. (2006) 'A review of landslide hazards in Japan and assessment of their susceptibility using an analytical hierarchic process (AHP) method', *Landslides*, 3(2), pp. 149-158.

Yue, T.X., Du, Z.P., Song, D.J. and Gong, Y. (2007) 'A new method of surface modeling and its application to DEM construction', *Geomorphology*, 91(1-2), pp. 161-172.

Zhang, Q., Wang, L., Zhang, X.Y., Huang, G.W., Ding, X.L., Dai, W.J. and Yang, W.T. (2008) 'Application of multi-antenna GPS technique in the stability monitoring of roadside slopes', in *Landslides and Engineered Slopes. From the Past to the Future, Two Volumes + CD-ROM*. CRC Press, pp. 1367-1372.

Zhang, W. and Montgomery, D.R. (1994) 'Digital elevation model grid size, landscape representation, and hydrologic simulations', *Water Resources Research*, 30(4), pp. 1019-1028.

Zhao, H.F. and Zhang, L.M. (2014) 'Instability of saturated and unsaturated coarse granular soils', *Journal of Geotechnical and Geoenvironmental Engineering*, 140(1), pp. 25-35.

Zheng, L., Li, M., Sun, J., Tang, N. and Zhang, X. (2005) 'Estimation of soil moisture with aerial images and hyperspectral data', *International Geoscience and Remote Sensing Symposium (IGARSS), 2005*. IEEE, pp. 4516-4519.

Zhou, C.H., Lee, C.F., Li, J. and Xu, Z.W. (2002) 'On the spatial relationship between landslides and causative factors on Lantau Island, Hong Kong', *Geomorphology*, 43(3–4), pp. 197-207.

Zhou, Y.F., Tham, L.G., Yan, W.M., Dai, F.C. and Xu, L. (2014) 'Laboratory study on soil behavior in loess slope subjected to infiltration', *Engineering Geology*, 183, pp. 31-38.

Zhu, A.X., Wang, R., Qiao, J., Qin, C.-Z., Chen, Y., Liu, J., Du, F., Lin, Y. and Zhu, T. (2014) 'An expert knowledge-based approach to landslide susceptibility mapping using GIS and fuzzy logic', *Geomorphology*, 214(0), pp. 128-138.

Zizioli, D., Meisina, C., Valentino, R. and Montrasio, L. (2013) 'Comparison between different approaches to modeling shallow landslide susceptibility: a case history in Oltrepo Pavese, Northern Italy', *Natural Hazards and Earth System Sciences*, 13(3), pp. 559-573.

Appendix 1: Flow diagrams of methods

This appendix provides the reader a more detailed coverage of the various components of the developed methodology. This include; Stage1- Processing of ALS data, DTM generation and extraction of slope stability parameters and the development of the land cover map of the transport corridor. Stage 2- The development of a weighted grid and stage 3 landslide susceptibility assessment using evidential reasoning.

Stage 1.

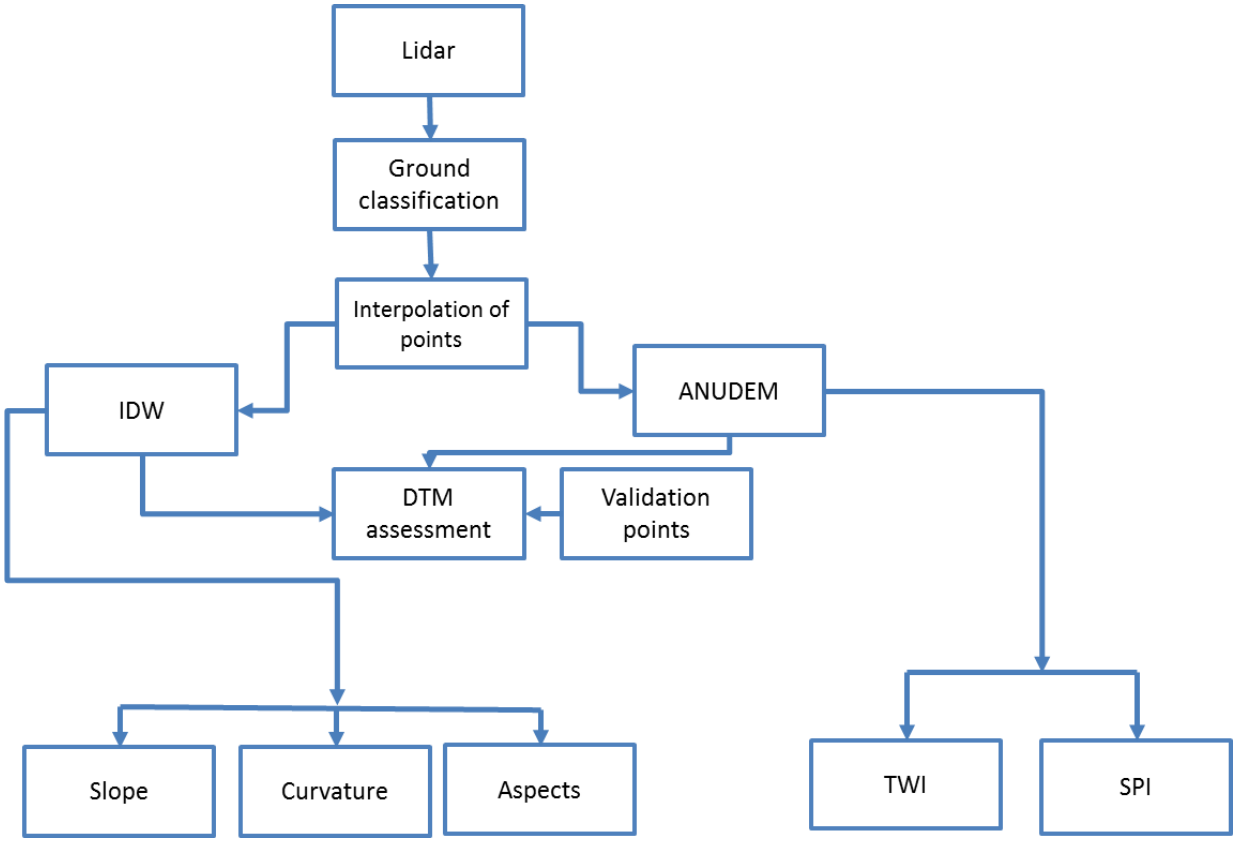

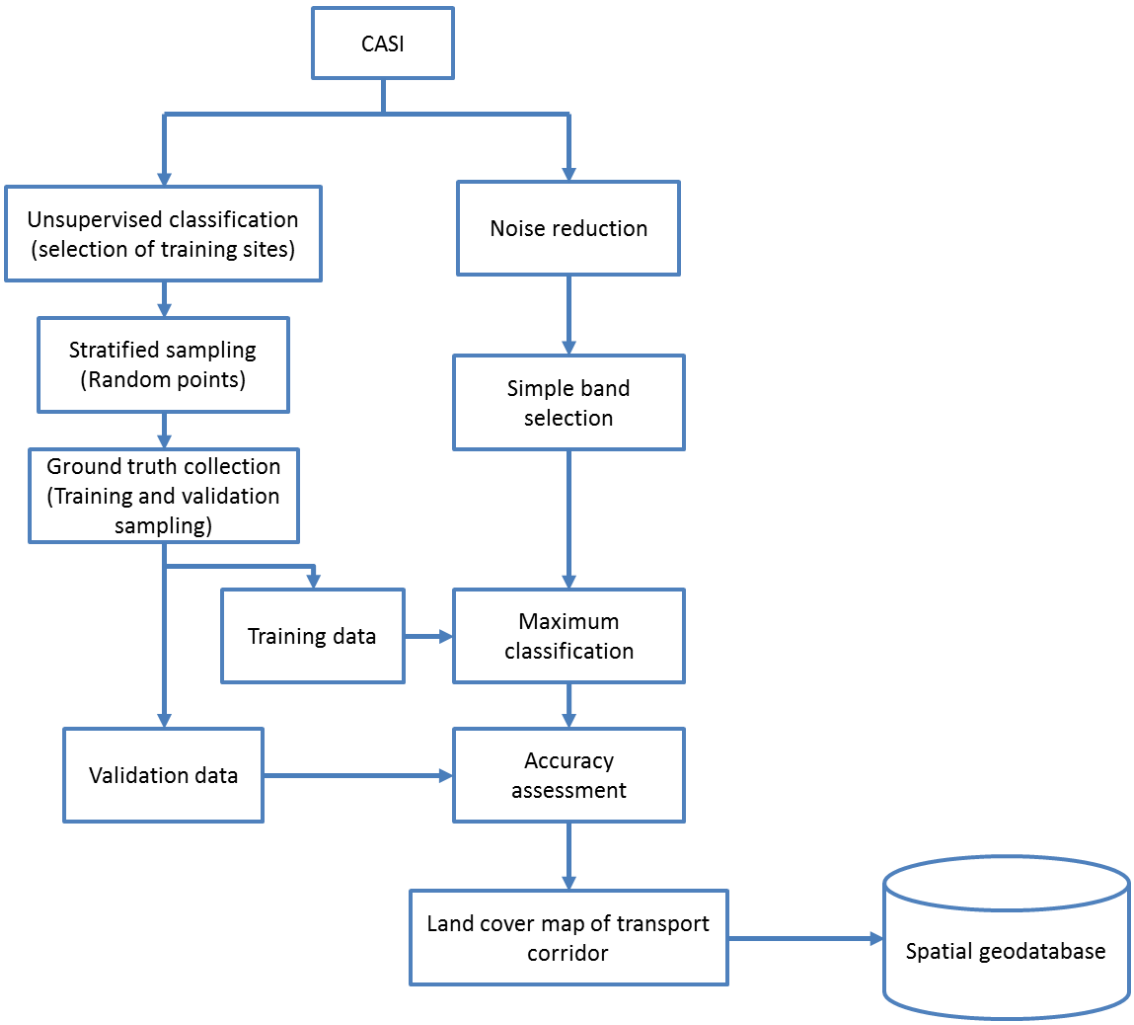
CASI
Unsupervised classification (selection of training sites)
Noise reduction
Stratified sampling (Random points)
Simple band selection
Ground truth collection (Training and validation sampling)
Training data
Maximum classification
Validation data
Accuracy assessment
Land cover map of transport corridor
Spatial geodatabase

Stage 2:

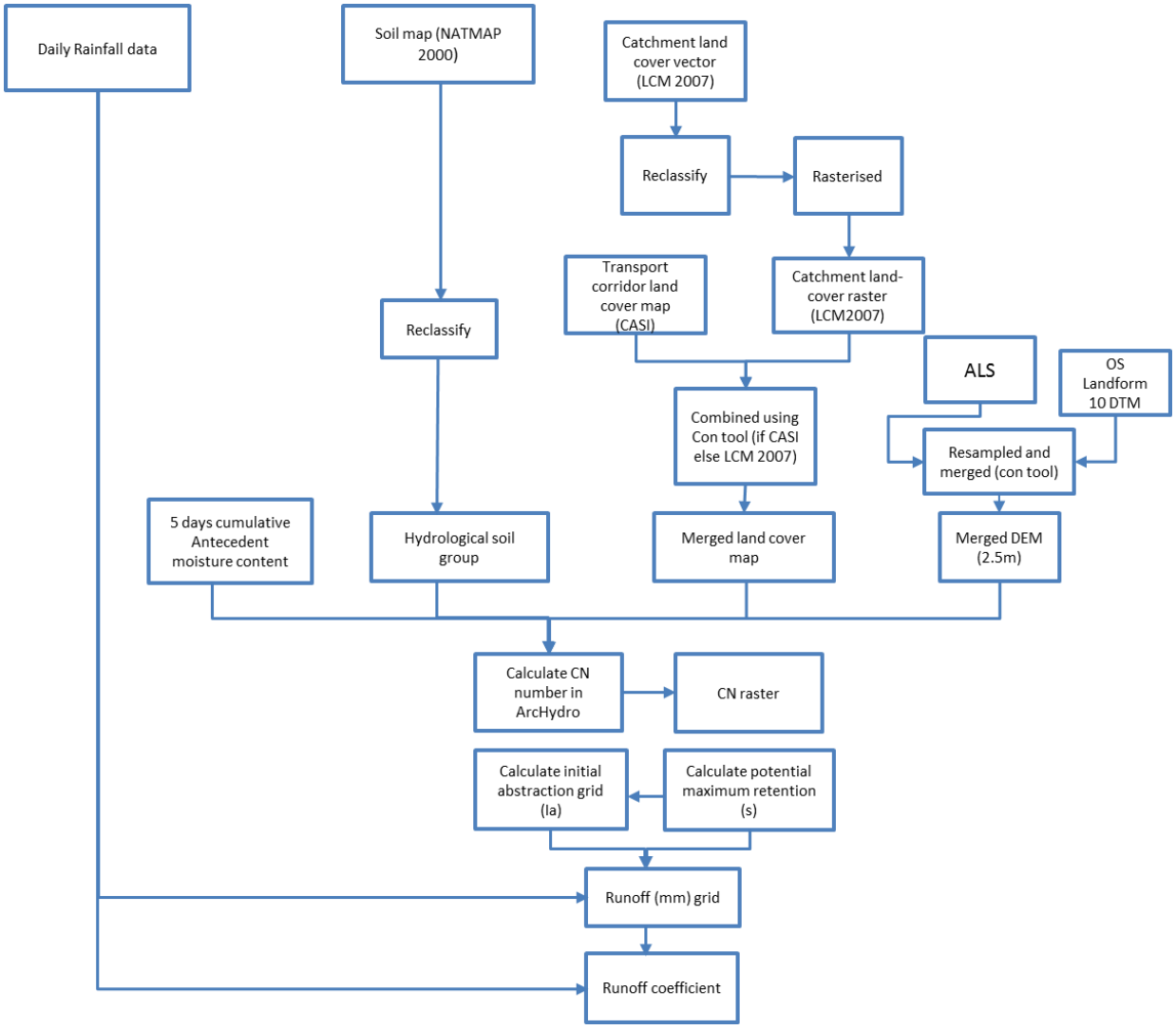
Daily Rainfall data
Soil map (NATMAP 2000)
Catchment land cover vector (LCM 2007)
Reclassify
Rasterised
Transport corridor land cover map (CASI)
Catchment land-cover raster (LCM2007)
Reclassify
ALS
OS Landform 10 DTM
Combined using Con tool (if CASI else LCM 2007)
Resampled and merged (con tool)
5 days cumulative Antecedent moisture content
Hydrological soil group
Merged land cover map
Merged DEM (2.5m)
Calculate CN number in ArcHydro
CN raster
Calculate initial abstraction grid (Ia)
Calculate potential maximum retention (s)
Runoff (mm) grid
Runoff coefficient

Stage 3

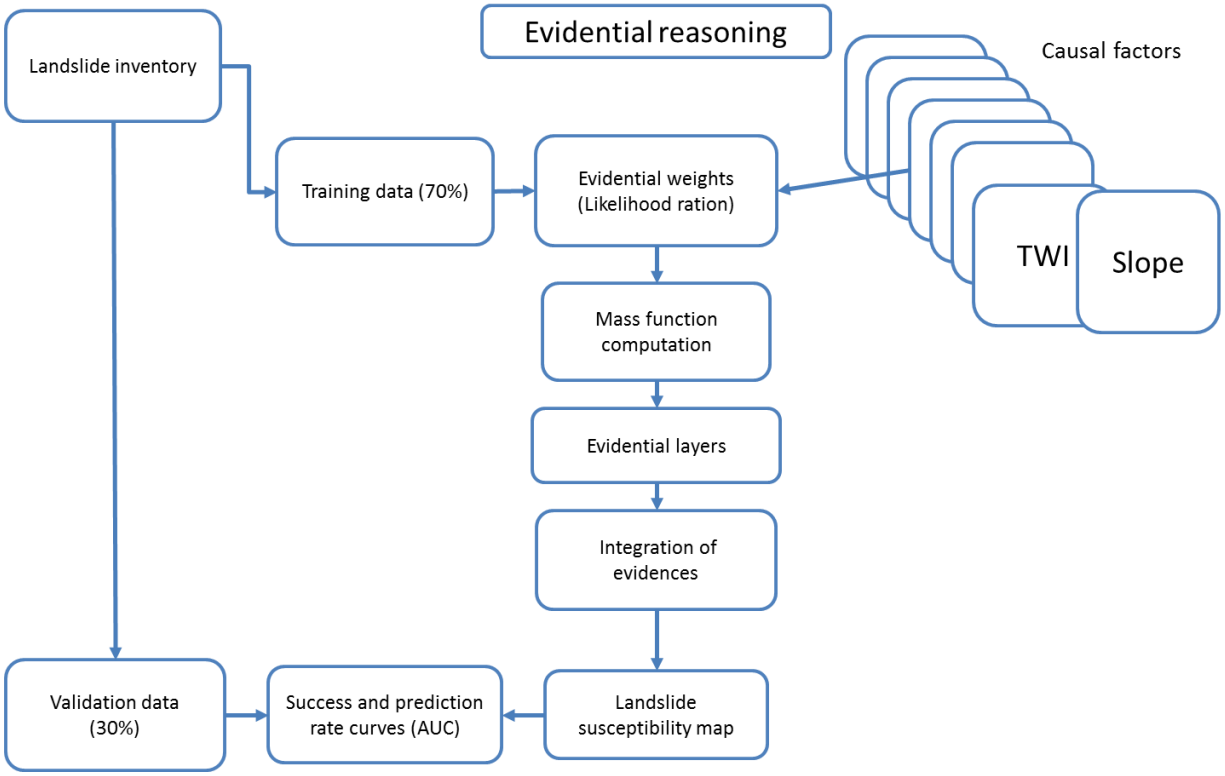
Evidential reasoning
Causal factors
Landslide inventory
Training data (70%)
Evidential weights (Likelihood ration)
TWI
Slope
Mass function computation
Evidential layers
Integration of evidences
Validation data (30%)
Success and prediction rate curves (AUC)
Landslide susceptibility map

Appendix 2: The regression equations generated for each of the 32 bands with relative R^2 correlation coefficient derived using the empirical line method after Smith and Milton (1999)

The empirical line method after Smith and Milton (1999) was employed in the radiometric calibration of CASI imagery by Hardy 2010.

CASI Band	Central wavelength (nm)	Regression equation	R^2 correlation coefficient
1	398	y = 0.0072x - 5.7759	1
2	405	y = 0.0075x - 2.7677	0.9994
3	413	y = 0.0094x - 4.0857	0.9993
4	420	y = 0.0109x - 6.2091	0.9999
5	428	y = 0.0126x - 5.5489	0.9993
6	435	y = 0.0124x - 5.0131	1
7	444	y = 0.0113x - 4.6365	0.9994
8	452	y = 0.01x - 3.0913	0.9999
9	462	y = 0.0103x - 3.8989	0.9999
10	471	y = 0.0105x - 3.0749	1
11	482	y = 0.0105x - 3.0558	0.9998
12	493	y = 0.0108x - 3.128	0.9999
13	504	y = 0.011x - 2.7955	0.9997
14	517	y = 0.0112x - 2.4983	0.9997
15	530	y = 0.0109x - 2.4335	0.9996
16	544	y = 0.011x - 2.6015	0.9997
17	559	y = 0.0112x - 2.326	0.9999
18	575	y = 0.0118x - 2.2385	0.9998
19	592	y = 0.0122x - 2.1158	0.9999
20	610	y = 0.0122x - 2.0664	0.9998
21	630	y = 0.0126x - 1.6787	0.9999
22	652	y = 0.0132x - 1.6441	0.9996
23	675	y = 0.0131x - 1.4088	0.9997
24	700	y = 0.0149x - 1.6909	0.9998
25	728	y = 0.0163x - 2.7653	0.9997
26	758	y = 0.0157x - 3.6425	0.9998
27	790	y = 0.0143x - 3.7689	0.9997
28	824	y = 0.018x - 4.1063	0.9997
29	862	y = 0.0164x - 4.0208	0.9998
30	901	y = 0.0224x - 3.9166	0.9997
31	943	y = 0.051x - 4.7153	0.9996
32	988	y = 0.0254x - 4.5207	0.9997

Appendix 3: Supervised classification of CASI imagery

The CASI image was characterised by closely related land cover types with significant spectral overlap which made the land cover classification both challenging and interesting. For example, large boulders placed along the Tyne River bank for the purpose of river bank erosion control had similar spectral characteristics as building and manmade classes. The characteristic low tide of the Tyne River at the period of acquisition of the CASI image resulted in the exposure of boulders on the river beds. These were largely responsible for the low producers accuracy recorded for the river class. There were also evidences that the CASI image was acquired during or immediately after some light showers, as the road surfaces show evidence of wetness depicted as isolated specks of the river class on pavement surfaces. These isolated river class pixels were later filtered out as no river class existed as depicted in these areas. There were also significant numbers of misclassified pixels between the man-made and building land cover classes around built up areas and bridges in the land cover classification map.